UNIVERSITÀ DEGLI STUDI DI MILANO

PhD course in Environmental Sciences
XXXIII cycle

Effect of sterols and sphingolipids deprivation on pollen tube growth in *Nicotiana tabacum* (L.).

BIO/01

Candidate

Nadia Stroppa

R11841

Tutor: Prof.ssa Morena Casartelli

Co-Tutor: Prof.ssa Alessandra Moscatelli

Head of the PhD course: Prof. Francesco Ficetola

A.A. 2019-2020

INDEX

PART I

Chapter 1

INTRODUCTION

Unifying principles of membrane organization through evolution

The organization of eukaryotic cells is mainly determined by their biological membranes, which constitute a physical boundary of hydrophobic nature between different aqueous environments; they separate the intracellular from the extracellular space and define distinct functional compartments within the cell: the organelles. The structures and functions of biological membranes strongly depend on the lipids that constitute the bilayer as well as the proteins residing in the membrane. The physical basis for the spontaneous formation of the lipid bilayer of the cell membrane is the propensity of the hydrophobic moieties of lipids to self-associate and the tendency of their hydrophilic moieties to interact with aqueous environments and with each other. The amphipathicity of lipids is the chemical property that enables cells to segregate their internal constituent from the external environment and, at the subcellular level, it is through this property that the membrane surrounding each cellular compartment is assembled. This compartmentalization enables the segregation of specific chemical reactions to increase the cell's biochemical efficiency and restrict dissemination of reaction products. The lipid bilayer of most biological membranes is composed of three major classes of lipid molecules: glycerophospholipids, sterols and ceramide-based sphingolipids. Of these, phospholipids are the most abundant and can spontaneously form lipid bilayers in aqueous solutions: their hydrophilic head groups face the aqueous surrounding and their hydrophobic fatty acyl chains form the hydrophobic core of the membrane.

According to the fluid mosaic model, postulated by Singer and Nicolson in 1972, lipids of biological membranes form a homogeneous fluid-like or liquid-disordered (L_d) phase in which proteins and lipids are randomly distributed and move freely (Edidin, 2003). In this model, membrane proteins are like icebergs floating in a sea of lipids. However, in recent years, numerous studies have provided evidence of the existence of highly structured microdomains within this ocean of lipids, called lipid rafts, that impose organization on the distribution of proteins in the bilayer and exhibit a specific molecular composition. These domains are enriched in sterols and sphingolipids and depleted in unsaturated phospholipids. The lipid rafts hypothesis is experimentally supported by studies on model membranes which demonstrated that a mixture of lipids normally found in biological membranes spontaneously undergo a "phase separation" leading to the formation of liquid-ordered domains (L_o) that are segregated from the surrounding phospholipids (Schroeder et al., 1994; Ahmed et al., 1997; Dietrich et al., 2001; Silvius 2003). The formation of this more organized phase, that coexists with the L_d phase in the same membrane, depends on the association between sterols and highly saturated hydrocarbon chains of sphingolipids (Brown and London, 1997; Edidin 2003). This

close lateral association is responsible for the most distinctive biochemical characteristic of membrane rafts: their insolubility in the presence of non-ionic detergent such as Triton X-100 at low temperatures (Brown and London, 1997). Thus, the isolation of detergent-insoluble membranes (DIMs) is one of the most widely used methods for the biochemical study of lipid rafts.

In various studies there is a consensus in defining membrane rafts as small (10-200nm), heterogeneous, highly dynamic, sterols and sphingolipids-enriched domains that compartmentalize cellular processes (Pike, 2006).

The existence of specific domains is an important aspect of membrane organization; although lipids themselves are a prerequisite for phase partition, it is established that proteins are equally important for regulating these structures (Lingwood and Simons, 2010). Proteins, with different affinities for the L_d or L_o phase, may become enriched in, or excluded from, the liquid ordered domains. Recruitment of proteins to lipid rafts likely affects their function in several ways. Firstly, the concentration of different proteins in rafts could facilitate and optimize protein-protein interactions and maximize signaling processes. Secondly, the ordered lipid environment may directly modulate the activity of protein complexes, e.g., by modification and/or stabilization of their conformation (Operakarova and Tanner, 2003).

Early evidence supporting the existence of membrane microdomains came from studies by Simon and van Meer (1988) on the polarized distribution of sphingolipids in MDCK cells (Madin-Derby Canine Kidney). MDKC cells are highly polarized with a strong differentiation between apical and basolateral surfaces. The apical surface of a typical epithelial cell is chemically and functionally distinct from the basolateral surface, the former is enriched in sphingolipids (glycosphingolipids and sphingomyelin) and cholesterol, while the latter is enriched in glycerophospholipids and phosphatidylcoline. This different composition is consistent with the observation that apical membranes of MCDK cells are relatively rigid while basolateral membranes are more fluid (Le Grimellec et al., 1988). Cell polarity and demarcation between the two domains are maintained by the tight junctions connecting adjacent cells in the epithelial sheet, thus lipids in the apical membrane cannot freely diffuse to the basolateral membrane. This difference in composition was shown to be attributable to the sorting of proteins and lipids in the Golgi complex and *trans*-Golgi membranes, and to the direct trafficking of these molecules to the cell surface (Simon and van Meer, 1988). Several studies showed that, in MDCK cells, sorting of fluorescently labeled glycosphingolipids takes place in the trans-Golgi network (TGN) and that these lipids are asymmetrically transported to the apical cell membrane, suggesting that sphingolipids are critical for the membrane distribution of proteins (van Meer and Simons, 1988).

Despite the abundance of information on the composition and structure of lipid rafts, the precise functional roles of these lipid microdomains are still subject to debate. It has been suggested that they might induce lateral compartmentalization of membrane proteins, thereby providing a dynamic scaffold to organize certain cellular processes (Simons and Toomre, 2000; Rajendran and Simons, 2005). In animals, the association of particular proteins with these specialized microdomains has emerged as an important regulator of crucial physiological processes, such as signal transduction, hormone signaling, polarized secretion, cytoskeletal organization, apoptosis, generation of cell polarity and the entry of infectious organisms into living cells. The recruitment and concentration of various receptors and signaling components within DIMs has led to hypothesize that sterol-rich domains have a role in transmembrane signal transduction, thus lipid rafts may represent "signaling platforms" in which different components of a signal transduction cascade are locally concentrated (Simons and Toomre, 2000; Okamoto et al., 1998; Hoessli et al., 2000). In several studies in mammalian cells, SNARE proteins involved in membrane fusion events at the plasma membrane (PM) have been reported to be localized in DIMs, suggesting a potential role of lipid rafts in exocytosis. Moreover, depending on the cell type, localization of SNARE proteins in PM microdomains may have either a stimulatory or inhibitory effect on secretion (Salun et al., 2004). Another function attributed to lipid rafts is their potential involvement in cytoskeleton organization by association with actin-rich regions of the cells (Falk et al., 2004; Wickström et al., 2003). Many cell death receptors and their ligands were reported to be enriched in DIMs. It has been suggested that, in this case, lateral association of lipid rafts can concentrate receptors and ligands to trigger a potent apoptotic response (Garcia, 2003). In addition, lipid rafts are involved in the entry of infectious organisms into living cells by acting as a portal for pathogen entry and on the other side, providing functional platforms for signaling events in order to regulate a defensive response at the cell periphery (Rosenberger et al., 2000; Shin and Abraham, 2001).

Lipid rafts in plants

Over the past twenty years, lipid rafts have also been extensively studied in higher plants, and DIMs have been characterized for their protein and lipid composition.

The presence of lipid rafts in plants was initially identified by analyzing a low-density, Triton X-100 insoluble fraction isolated from tobacco somatic cells (*Nicotiana tabacum*), which exhibited a specific protein composition, different from that of the general PM and enriched with signaling proteins such as heterotrimeric G-proteins and glycosylphosphatidylinositol(GPI)-anchored proteins (Peskan et al., 2000; Mongrand et al., 2004). In addition, Borner et al. (2005) isolated and analyzed DIMs from somatic cells of *Arabidopsis thaliana.* They found that DIMs fraction was enriched in sterols and

sphingolipids, whereas typical structural glycerophospholipids were drastically reduced, thereby confirming they could be considered the biochemical counterpart of membrane rafts (Mongrand et al., 2004).

The chemical structure of plant sphingolipids and sterols associated with plant DIMs are significantly different from their counterpart in animals. While ergosterol and cholesterol are the major sterols in fungi and animals respectively, higher plants contain a vast array of sterols, with sitosterol, stigmasterol and 24-methylcholesterol predominant. Moreover, phytosterols are often glycosylated to form sterylglucosides (SG) and acylated sterylglucosides (ASG). In several studies these conjugated sterols are found to be enriched in plant DIMs (Lefebvre et al., 2007; Furt et el., 2010; Laloi et al., 2007). Phytosterols appear as key compounds for the formation of membrane rafts domains. Depletion of sterols induced by methyl-β-cyclodextrin (MBCD) leads to an overall increase in acyl chain disorder and a reduction of the liquid-phase heterogeneity of the isolated PM. The fact that such a treatment also prevented DIMs recovery reinforces the link between the sterol-driven lateral segregation of raft domains in the PM and resistance to solubilization by non-ionic detergent (Roche et al., 2008). Recovery of DIMs also strongly depends on the unsaturation degree of fatty acyl chains. Strong evidence came from the dramatic decrease in the total amount of DIMs isolated from *Arabidopsis thaliana fad2* and *Fad3*$^{+}$ mutants, affected in their fatty acid desaturases (Laloi et al., 2007). Moreover, the unsaturation degree of lipid acyl chains of plant cell membranes plays a crucial role in the ability of lipid species to partition into lipid rafts (Laloi et al. 2007).

The major plant sphingolipids are glycosyl inositol phospho ceramides (GIPCs) and glucosylceramides. GIPCs contain saturated or mono-unsaturated very long chain fatty acids with 22-26 carbon atoms, mostly hydroxylated in position 2. The chain length and the hydroxyl group at the interface between polar heads and acyl chains contribute to reinforcing lipid-lipid interactions in plant rafts. The sphingolipid content of the rafts differs markedly between tobacco and *Arabidopsis*; in the former glucosylceramides are predominant, while *Arabidopsis* is dominated by GIPCs (Mongrand et al., 2004; Borner et al., 2005; Cacas et al., 2012). Although sphingolipid-enrichment of plant DIMs appears not to be as great as that of sterols, sphingolipid depletion has negative effects on plant development; *Arabidopsis* plants, which are deficient in Serine palmitoyltransferase, the first enzyme of sphingolipid biosynthesis, showed reduced growth (Chen et al., 2006). Indeed downregulation of LCB1 or LCB2 subunit of Serine palmitoyltransferase, in Arabidopsis, resulted in a severe reduction in plant growth (Chen et al., 2006). Sphingolipid biosynthesis is essential throughout multiple stages of plant development, as shown by defects in gametophyte development in *Atlcb2* mutants (Dietrich et al., 2008). In addition, downregulation of LCB2 in Arabidopsis leads to a lack of the deposition of intine layer in pollen, which is correlated with a destructuring of the ER and Golgi membranes in

mutant pollen (Dietrich et al., 2008). Moreover, it has been demonstrated that sphingolipid inhibitors affects the secretory pathway and induces structural changes in the endomembrane of plant somatic cells (Melser et al., 2010; Melser et al., 2011; Markham et al., 2011).

Analyses have shown that the major structural glycerophospholipids, such as phosphatidylcholine (PC), phosphatidylethanolamine (PE), phosphatidylinositol (PI), phospatidylserine (PS) and phosphatidic acid (PA) are largely depleted from DIMs when compared to PM lipid content. Moreover, glycerolipids of plant DIMs contain more saturated fatty acyl chains and contribute to the rigidity of the liquid ordered phase of lipid rafts (Peskan et al., 2000; Mongrand et al., 2004; Borner et al., 2005).

Polar heads of phospholipids are very similar to those of animal phospholipids. However, the former lipids exhibit shorter acyl chains (<20 carbon atoms) and less unsaturation (from 1 to 3 vs 4-6 double-bonds) compared to the latter. Phospholipids can interact with sterols through van der Waals, as well as hydrophobic and hydrophilic forces. However, interactions between phospholipids and sterols are weaker than those reported between sphingolipids and sterols. This is partially explained by the fact that fatty acid chains of sphingolipids are longer than those of phospholipids, thereby allowing stronger hydrophobic forces (Cacas et al., 2012).

Interestingly, polyphosphoinositides, a class of minor phospholipids involved in signaling, were found to be enriched in DIMs of tobacco cells (Mongrand et al., 2004; Furt et a., 2010). Polyphosphoinositides are phosphorylated derivatives of phosphatidylinositol (PtdIns) implicated in many cellular processes. In animal and yeast cells, they control numerous cell functions, such as exo and endocytosis, cytoskeletal adhesion, and signal transduction as second messenger precursors and/or as signaling molecules by interacting with different protein partners. In the pollen tube and root hairs, which are characterized by an extreme form of polar growth, highly localized phosphatidylinositol 4,5-bisphosphate (PtdIns(4,5)P_2) has been evidenced at the membrane tip (Kost et al. 1999). It functions as an effector of small G proteins at the apex of cells influencing membrane fusion events (Monteiro et al., 2005). Furt et al. (2010) showed that polyphosphoinositides, in particular phosphatidylinositol 4-phosphate (PtdIns4P) and PtdIns(4,5)P_2, were enriched in DIMs fraction isolated from tobacco leaves and BY-2 cells, whereas, phosphatidylinositol, the biosynthetic precursor, was largely depleted from this fraction. In addition, fatty acid composition analysis revealed that this enrichment in polyphosphoinositides was accompanied by their association with more saturated fatty acids. Along with their classical role as second messenger in signal transduction at the cell surface, phosphorylated products of PtdIns play critical roles in the regulation of membrane trafficking, as regulators for the recruitment or the activation of proteins essential for cytoskeletal dynamics or vesicular transport (Janmey et al., 1999; Martin, 2001). Local changes in the

concentration of polyphosphoinositides, and in particular of PtdIns(4,5)P_2 in the PM could also represent cell signals. It can be assumed that rafts domains could serve to properly localize PtdIns(4,5)P_2 and/or to organize PtdIns(4,5)P_2 binding proteins partners into signaling complexes. The formation of PM microdomains might facilitate the interaction of PtdIns(4,5)P_2 with some binding partners, while excluding others. PtdIns(4,5)P_2-dependent signaling in plants, as well as in animals, could be achieved by its compartmentalization in microdomains (Furt et al., 2010). (See below for signaling phospholipids in pollen tubes).

An asymmetric distribution of lipid rafts in PM has been demonstrated to promote cell polarity, which mediates cell migration in a wide range of cells, including leukocytes, carcinomas, and epithelial cells (Manes et al., 2003). In *Candida albicans* recent evidences suggest that lipid rafts contribute to hyphal morphogenesis. Interestingly, staining with filipin, a molecule which stains membrane sterols in a wide range of cell types, revealed that sterols localization pattern is highly polarized towards the leading edge during all stages of hyphal growth (Martin and Konopka, 2004). Moreover, blocking either sphingolipid biosynthesis or sterol biosynthesis resulted in a loss of ergosterol polarization and caused abnormal hyphal morphogenesis. In the same study, lipid rafts have been correlated with cytoskeleton dynamics since polymerization of actin filaments and rafts integrity seem to be interdependent (Martin and Konopka, 2004). The cytoskeleton is actually involved in the polarized growth of many cell types, including root hairs and pollen tubes (Hazan and Liu, 2002; Moscatelli and Idilli 2009; Rounds and Bezanilla, 2013).

In root apex cells of *Arabidopsis thaliana* structural sterols are abundant in the PM. They accumulate in trichoblasts during the pre-bulging and bulge stages, showing a polar accumulation in the tip during root hair elongation but they are also present in mature root hairs. Local accumulation of structural sterols represents one of the early polarity markers that determine the bulging site in root hair initiating trichoblasts. Furthermore, it has been shown that structural sterols are involved in vesicular recycling and endocytosis, emerging as important regulating players in the tip growth of Arabidopsis root hairs (Ovečka et al., 2010).

The requirement for the polarized distribution of sterols and membrane microdomains has also been recently investigated in Angiosperm pollen tubes, another tip-growing plant cell. In particular, in *Nicotiana tabacum* pollen tubes, which this thesis is concerned with, two different experimental approaches showed a polarized distribution of sterols and higher ordered membranes from the tip to the shank. Staining with filipin made it possible to visualize sterol-rich domains present on the PM, with a ring-like distribution (Fig. 1 a,c, arrows) and especially concentrated in the PM of the whole apex (Fig. 1 a,c asterisks) and in vesicles accumulating in the clear zone (Fig. 1 b,d, arrows),

suggesting that sterol-rich membrane domains could be involved in polarized secretion and in asymmetric distribution of proteins and lipids along the pollen tube. (Moscatelli et al., 2015).

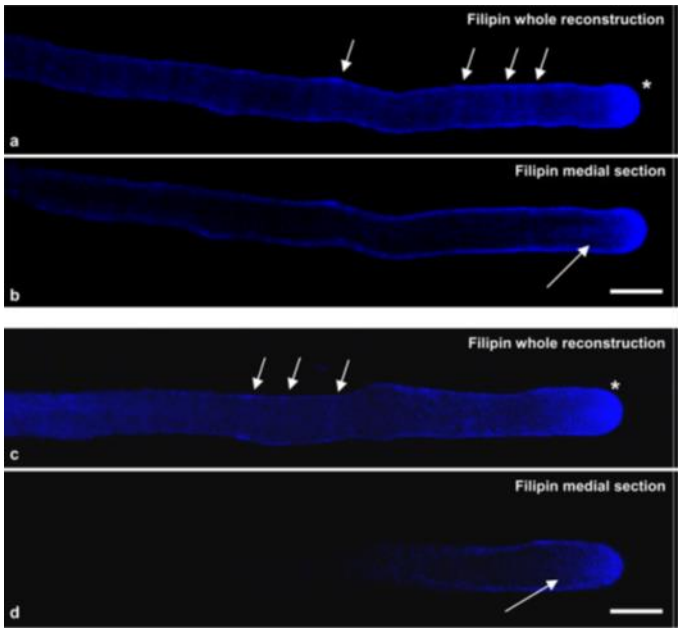

Fig. 1. Sterol localization. (a,c) Whole reconstructions. Sterols are present on the PM, in a ring-like distribution (arrows), and sterol-rich domains are especially concentrated in the apex (asterisks). (b, d) Medial sections. Sterols are observed in vesicles in the clear zone (arrows). Scale bars: 10 μm. (Moscatelli et al., 2015).

The use of the styryl dye di-4-ANEPPDHQ allowed to study the relationship between sterol distribution and the presence of membrane microdomains. The ratiometric live imaging of di-4-ANEPPDHQ detected the membrane order level and thus highlighted the asymmetric distribution of the two phases along growing pollen tubes, with a significantly higher ordered membrane in the apical region than in the shank. Moreover, live cell imaging showed that the polarized distribution of high ordered membrane domains in the tip was abolished when cells were incubated with β-cyclodextrin (BCD), which is known to extract sterols from membranes and destroy lipid rafts in different cell types (Moscatelli et al., 2015; Ohtani et al., 1989; Ilangumaran and Hoessli, 1998; Roche et al., 2008). The asymmetric distribution of lipids on PM, together with that of proteins that are specifically recruited to the lipid microdomains, is a distinctive feature and a fundamental requirement for the growth of the pollen tube tip (Moscatelli and Idilli, 2009).

In addition, DIMs were purified from tobacco pollen microsomes and biochemically characterized. Lipid analysis showed that, like DIMs isolated from animals (Simons and Sampaio, 2011) and from plant somatic and cultured cells (Cacas et al., 2012), DIMs of tobacco pollen tubes were characterized by a high sterol content, an increased content of hydroxylated very long chain fatty acids (VLCFA) sphingolipids and phospholipids enriched with saturated fatty acids. This

suggested that the physical/chemical basis for membrane raft formation (London, 2002) is maintained in the pollen tubes (Moscatelli et al., 2015).

Protein analysis of pollen tube DIMs revealed that they specifically displayed proteins that were not identified in DIMs isolated from somatic cell PM (Mongrand et al., 2004; Borner et al., 2005; Lefebvre et al., 2007). Protein identification revealed that actin, prohibitins and proteins involved in methylation reactions and in phosphoinositide pattern regulation are specifically present in pollen tube DIMs. Although this could reflect the peculiarity of tip- versus isodiametric-growing cells, it cannot be excluded that these proteins are derived from endomembrane DIMs. They also showed proteins that have been identified in DIMs isolated from plant somatic cell PM, such as tubulins, voltage dependent anion channels (VDACs), and proteins involved in membrane trafficking (Moscatelli et al., 2015).

Pollen is the male gametophyte

Sexual reproduction is a key step in the life cycle of plants which has undergone several modifications through evolution. Alternating generations of gamete-producing multicellular gametophytes and spore-producing sporophytes characterizes the aplo-diploid life cycle of land plants. Over the course of evolution, the gametophytic phase has been reduced in terms of both size and lifespan compared to the sporophyte generation (Heslop-Harrison, 1975). Changes have also involved the fertilization process; pluricellular gametophytes of Bryophytes and Pteridophytes deliver a high number of flagellated sperm cells in the environment where they need water to swim in order to reach the egg cells for fertilization. In seed plants, male and female gametophytes are reduced to microscopic structures and are dependent on the sporophytic tissues for their development. In particular, the flower of angiosperms has specialized structures, the anthers and the pistils, in which male and female gametophytes are formed respectively. The fertilization process of seed plants, especially of angiosperms, does not involve the high risk of male gamete delivery in the environment; it is the whole male gametophyte, called pollen grain, that is released from the anthers and transported on a compatible pistil both by wind or by specialized insects. This innovation allows sperm cells to be transported for longer distances from the mother plant, promoting an increase of the species' genetic variability. Moreover, in this way, the fertilization process of angiosperms becomes independent from water. Therefore, pollen grains play a major role in conveying the male genetic material toward the female gametophyte in plant sexual reproduction.

The adaptation of plants to different environmental conditions also implies that delivered pollen grains may develop specific survival strategies before reaching the stigma of compatible

flowers. Pollen dehydration before the anthesis allows male gametophytes of many species to persist in a quiescent state in the environment until they reach the right pistils. This condition is typical of bicellular pollen which is delivered from the anthers when the generative cell (GC) still has to divide into two sperm cells (SCs). Other species deliver pollen grains in which the GCs had already produced two SCs during the microgametogenesis; in this case the pollen dehydration is less pronounced and pollen grains must reach a compatible pistil in a shorter time for successful pollination and fertilization. In extreme cases of recalcitrant pollen, it was observed that pollen grains germinate within the anthers and here the pollination time is even shorter (Franchi et al., 2002; Franchi et al., 2011; Firon et al., 2012; Franchi et al, 2014; Onelli et al., 2020).

Once a pollen grain lands on the surface of a compatible stigma it hydrates, becomes metabolically active and starts to build a cell protrusion, called pollen tube, which grows on the stigma and is guided through the style transmission tissue to reach the ovary. Pollen tubes can be considered a safe route to transport sperm cells, which have lost flagella, in the proximity of the female gametophyte and the correct growth of the pollen tubes also represents a prerequisite for fertilization and species conservation.

Pollen tube growth

The pollen tube is a highly specialized cell which grows at the apex through an extreme form of polar growth known as tip growth (Hepler et al., 2001). Golgi-derived secretory vesicles are transported by the acto-myosin system to the apical region where they fuse with a restricted area of the PM, reversing outside cell wall material and providing new segments of PM (Hepler et al., 2001). This polarized secretion defines an apical growth PM domain and allows a specific protein/lipid composition with respect to the subapical areas (Kost et al., 1999; Potocky et al., 2003; Helling et al., 2006).

Ultrastructural studies have shown that the distribution of organelles is not uniform along the tube; vesicles accumulate in the tip or clear zone of the pollen tube, while larger organelles are retained in the shank (Hepler et al. 2001; Cheung and Wu, 2008). Four functional zones can be distinguished along pollen tubes: an apical region or clear zone (5-10 μm from the tip) characterized by numerous vesicles organized into a typical V-shaped aggregate, a subapical organelles-rich zone, a nuclear region with a vegetative nucleus and generative cell and a vacuolated zone (Li et al., 1997). As the pollen tube grows, periodic callose plugs are formed to block off the older parts of the tube and maintain the cytoplasm near the growing tip (Hepler et al., 2001).

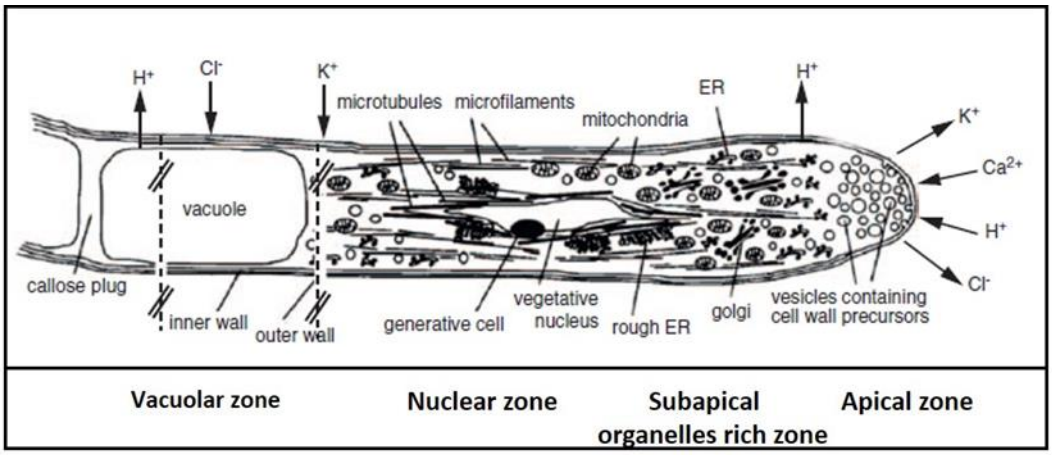

Fig.2 The panel shows a diagrammatic representation of a pollen tube with the typical zonation, including the clear zone, subapical, nuclear and vacuolar regions (Konrad et al., 2011).

The polar growth of this highly elongated cell relies on the coordinated action of different cellular processes, such as cell wall formation, turgor pressure, ion fluxes, organization and dynamics of cytoskeletal elements, and membrane trafficking (Heslop-Harrison, 1987; Steer and Steer, 1989; Holdaway-Clarke and Hepler, 2003; Chebli and Geitmann, 2007; Krichevsky et al., 2007; Cheung and Wu, 2008).

Cell wall components and deposition

In general, plant cell expansion depends on the interplay between intracellular driving forces and the controlled extensibility of the cell wall. Growth is driven by internal turgor pressure and is restricted by the ability of the cell wall to extend under this pressure. The apical cell wall is crucial in regulating tip growth since it has to provide enough plasticity to allow the incorporation of new membrane and cell wall material in order to support the growth process, but, at the same time, it has to be strong enough to withstand the internal turgor pressure and prevent the cell bursting (Steer and Steer, 1989).

During the elongation process there is an intense secretory activity that contributes to the continuous depositing of new cell wall material (Steer and Steer, 1989). The wall in the apical region is almost exclusively composed of a pectic network (Ferguson et al. 1998). Pectins are complex polysaccharides that are constituted by homogalacturonan (HGA) as the major component, composed of α-(1,4)-linked D-galacturonic acid residues (GalA residues), rhamnogalacturonan I (RG-I) and rhamnogalacturonan II (RG-II). Pectins are synthesized in the Golgi apparatus in a highly methyl-esterified form, packaged into secretory vesicles and delivered to the tip where they fuse reversing outside new cell wall material. In a very narrow region just behind the apical domain, esterified pectins are converted by PME (pectine methyl-esterase) enzyme into molecules with a lower degree

of esterification. Free carboxyl residues are crosslinked by Ca^{2+}, thus pectin backbone gains strength behind the tip. (Bosch and Hepler, 2005; Palin and Geitmann, 2012). Therefore, in the shank, the cell wall consists of de-esterified pectins along with callose and cellulose, which are synthesized - not secreted - by transmembrane enzyme complexes integrated into the PM (Ferguson et al., 1998; Hepler et al., 2001; Li et al., 2002; Chebli et al., 2012).

Pectin de-esterification, cellulose and callose deposition enhance the stiffness and stability of the pollen tube cell wall behind the tip and in the shank so that these cell wall regions do not expand in response to turgor pressure and the cylindrical shape of pollen tube is maintained. This controlled spatial distribution of components of the pollen tube cell wall contributes to maintaining the pollen tube shape during its growth, mainly in the hard journey through the style (Fayant et at., 2010). Two monoclonal antibodies, JIM7 and JIM5 (Knox et al., 1990) have been particularly useful in resolving the pattern of esterification in different species, such as *Nicotiana tabacum* (Bosch et al., 2005), *Solanum chacoense* (Parre and Geitmann, 2005), and *Arabidopsis thaliana* (Dardelle et al., 2010; Chebli et al., 2012). JIM7 binds to methyl-esterified GalA residues and therefore indicates the presence of highly methyl-esterified pectin epitopes, while JIM5 binds preferably to at least four contiguous unesterified residues and labels the relatively de-esterified pectins (Clausen et al., 2003; Bosch and Hepler, 2005b). Immunofluorescence localization of cell wall pectins has shown that the esterified form is most abundant in the apical region, while de-esterified pectins are more concentrated in areas behind the tip, nevertheless, some variation in labeling pattern may occur, depending on the species and experimental conditions used (Stepka et al., 2000; Parre and Geitman, 2005).

The balance between secretion and PME activity thus yields a gradient at the pollen tube apex with highly esterified pectins at the extreme pole and a progressively less esterified mix of polymers at increasing distances from the apex (Hepler et al., 2013). Further evidence supporting a role of PME in pollen tube growth involved the application of pollen tube growth media supplemented with orange peel PME. Exogenous PME inhibits in vitro growth (Bosch et al., 2005; Parre and Geitmann, 2005) resulting in thickening of the apical cell wall due to an early conversion of apical methyl-esterified pectins into de-esterified pectins by this enhanced extracellular PME activity. In addition, a concomitant dissipation of the intracellular tip-focused Ca^{2+} gradient is observed (Bosch et al., 2005). These data show that PME-mediated configuration of pectins at the apex is an important component in controlling pollen tube growth. Genetic proof for the critical role of PME activity in the regulation of pollen tube growth came from a study in which an *Arabidopsis* pollen-specific PME, VGD1, was functionally interrupted by the insertion of a transposon (Jiang et al., 2005). VGD1 is a PME isoform with one of the highest levels of expression in pollen (Pina et al., 2005). Functional interruption of

VGD1 reduces PME activity in the pollen to 82% of the wild type and pollen tube growth in the style and transmitting tract is greatly retarded, resulting in reduction of male fertility (Jiang et al., 2005; Rockel et al., 2008). Only few tubes can reach ovules, resulting in successful fertilization only in the upper part of the silique. In addition, the *vgd1* pollen tubes are unstable and frequently burst when germinated and grown in an *in vitro* culture medium, compared with wild-type pollen tubes, suggesting that the decrease in overall PME activity leads to an imbalance of the apical wall dynamics and a failure to resist the internal turgor pressure. Mutant pollen tubes grown *in vivo* may perceive enough structural support from the surrounding female sporophytic tissues. These findings indicate that the VGD1 product might be involved in the interaction between pollen tubes and female floral tissues via modification of cell walls and that this interaction may be important for the stabilization of the pollen tubes (Jiang et al., 2005).

In *Nicotiana tabacum* the pollen specific NtPPME1 is secreted into the pollen tube apical apoplast where it catalyzes de-methylesterification of pectins and silencing of NtPPME1 leads to retarded growth of tobacco pollen tube (Bosch et al., 2005; Bosch and Hepler, 2005). Recent studies have shown that in growing tobacco pollen tubes, polar targeting of NtPPME1 to the pollen tube apex depends on an apical F-actin mesh network, called actin fringe (Wang et al., 2013). Disruption of the spatial organization of apical actin fringe by wortmannin, results in the failure of exocytic trafficking and targeting of NtPPPME1 to the surface of the pollen tube apex, leading to an alteration of cell wall construction and rigidity in the pollen tubes. The single layer of the methyl-esterified pectins is completely abolished after wortmannin treatment, consistent with the wortmannin-induced abolition of tip-localized NtPPME1. These data demonstrate that the exocytic trafficking of NtPPME1 to the apical region of the pollen tube is responsible and essential for maintaining the proper pectin cell wall composition and cell wall rigidity in growing pollen tube. In addition, Wang et al. (2016) demonstrated, for the delivery of NtPPME1, a polar exocytic process which is distinct from the conventional Golgi-trans Golgi network (TGN)-PM exocytosis pathway in pollen tube. They identified a Golgi-derived secretory vesicle (GDSV) for the polar secretion and targeting of NtPPME1 to the cell wall that bypasses the TGN during cell polarization. This observation suggests that while pectins could be delivered to PM through the sorting activity of TGN, secretion of PME could not involve the TGN.

PME activity can be regulated by PME Inhibitors (PMEIs; Giovane et al., 2004), secreted to the apex of the pollen tube (Li et al., 2002; Chebli et al., 2013). PMEIs are small proteins that inhibit PME activity through the formation of a reversible 1:1 complex the stability of which is pH dependent, being higher in acidic conditions that are typical of an apoplastic environment (D'avino et al., 2003).

PME is also subjected to intramolecular regulation. In addition to the catalytic PME domain and the N-terminal signal peptide, which is required for protein targeting to the endoplasmatic reticulum, most of the isoforms of PME present in the Arabidopsis genome encode a pro-region downstream of the signal peptide, with a predicted molecular mass of 15 to 25 kDa. Interestingly, this region shares some homology with PMEIs. Recent localization studies on the tobacco pollen specific PME, NtPPME1, revealed that the full length product fused to GFP is secreted, whereas NtPPME1 lacking the pro-region is not, suggesting that the pro-region participates in the correct targeting of the mature PME (Bosch et al., 2005). In addition, whereas overexpression of the whole NtPPME1 protein - including its pro-region - does not affect *in vitro* pollen tube growth, transient expression of the PME domain alone reduces the growth rate dramatically. The expression of the PME domain also leads to the accumulation of de-esterified pectins in the apical pollen tube wall, which appears to alter the rheological properties of the apical cell wall with the concomitant cessation of growth (Bosch et al., 2005). Importantly, the inhibitory effect caused by the PME domain can be partially rescued by co-expressing the pro-region. These experiments not only show that the PME domain alone is sufficient for exerting its enzymatic activity but also support the idea that the pro-region acts as an intramolecular inhibitor of PME activity, thereby preventing premature de-esterification of pectins prior to secretion. The predicted structural similarity between the pro-region and PMEIs (Bateman et al 2004) substantiates this idea. Similarly, PMEIs appear to inhibit the activity of PMEs lacking the autoinhibitory pro-region (Rockel et al., 2008). Both PME and PMEI were found to be preferentially distributed to the apical cell wall (Bosch et al., 2005; Rockel et al., 2008; Wang et al., 2013); it was proposed that in tobacco pollen tubes, different endocytic pathways at the flanks of the tip region may contribute to the maintenance of the apical distribution of PMEI (Rockel et al., 2008). Nevertheless it is not fully understood how PME and PMEI maintain their high distribution at the tip and how the highly methylesterified and demethylesterified pectins are differentially distributed to the apex and the shank. Moreover, PME activity is modulated by the chemical characteristics of the environment, especially by changes in pH. The de-esterification of pectins by PME can have an opposite consequence for the plasticity of the cell wall. PMEs produce acidic pectins, which can crosslink Ca^{2+} ions, reinforcing the cell wall structure and at the same time, the protons produced by the hydrolysis decrease the local pH and can consequently promote the activity of cell wall hydrolysis resulting in cell wall extension and growth (Gaffe et al., 1994; Bordenave, 1994 Catoire et al., 1998). An additional mechanism for the regulation of PME activity at the tip involves a negative feedback, in which the local decrease in pH generated by protons released during the de-esterification reduces PME activity (Moustacas et al., 1991). The combined effect of inactivating PME and activating polygalacturonase and pectate lyase would loosen the cell wall and facilitate the pulsed growth.

However, the subsequent dilution of negative charges would increase the pH and cause a reactivation of PME activity and inactivation of cell wall hydrolysis, leading to an apical wall stiffening and a decrease in growth rate. Thus the PME together with other pectin-associated enzymes could play a key role in controlling oscillations in pollen tube growth.

Whereas the apical region of pollen tubes is characterized by the pectin layer that extends for the entire tube length and forms the outer cell wall layer, just behind the apex pollen tubes are stabilized by the deposition of cellulose and callose. Cellulose is normally present in smaller quantities than callose in pollen tubes and at the apex of pollen tubes it is probably important in maintaining the hemispherical shape, rather than counterbalancing the turgor pressure (Aouar et al., 2010; Wang et al., 2011). Callose is synthesized by the enzyme callose synthase (CalS) (Turner et al., 1998; Brownfield et al., 2007) and is very abundant in pollen tubes except in the apical area suggesting that it will help to strengthen the cell wall in non-growing regions.

Cellulose is synthesized at the PM by transmembrane cellulose synthase (CesA) complexes (CSCs), which are assembled in either the endoplasmic reticulum (ER) or Golgi (McFarlane et al., 2014), and subsequently delivered to the plasma membrane (Lerouxel et al., 2006). Therefore, efficient transport of the CSCs to and from PM is important for cellulose synthesis (Sampathkumar et al., 2013; McFarlane et al., 2014). Once the CesAs are assembled, they may be directed to the PM, possibly via the trans-Golgi network (TGN) and small vesicle compartments, the so called Microtubule-Associated Cellulose Synthase Compartments (MASCs) or Small CesA Compartments (SmaCCs) and they are typically delivered to the PM in close proximity to cortical microtubules (MTs) (Crowell et al. 2009; Gutierrez et al., 2009). It has been shown that long range transport Golgi and SmaCCs require actin filaments (AFs). Actin filament depolymerizing drugs disrupt the correct distribution of Golgi bodies and SmaCCs, leading to altered distribution of CSCs on the PM (Gutierrez et al., 2009). However, although AFs play a major role in cell distribution of Golgi, once SmaCCs are released in the cell cortex, they are captured by the plus end of cortical MTs and transported by a mechanism involving MT dynamics (MT depolymerization) until the site where they have to be incorporated with the PM (Gutierrez et al., 2009). Here the CesA complexes are activated - likely by phosphorylation of CesAs - and begin to track along microtubules to produce cellulose microfibrils (Chen et al., 2010; Chen et al., 2016).

On the PM, CSCs synthesize unbranched glucan chains that assemble into para-crystalline cellulose microfibrils using UDP-glucose as substrate. Once the CesA complex has produced a cellulose microfibril it needs to be removed from the PM and it seems that CSCs could be internalized via clathrin mediated endocytosis, a mechanisms which also removes lipids, other proteins, and

probably cell wall constituents from the PM and the apoplast (Bashline et al., 2013; Gadeyene et al., 2014; Bashline et al., 2015).

Recent evidence suggested that the lipid environment of the CSCs is crucial for its proper structural organization and function at the PM and notably, its activity has been identified in DIMs, in hybrid aspen cells (Bessueille et al., 2009). However, the CesA proteins were not identified in other proteomic studies of DIMs (Borner et al., 2005, Lefebvre et al., 2007), probably due to the different plant species and different extraction methods used. Indeed, the large size of the CSCs makes them difficult to isolate and identify by mass spectrometry, even in enriched total membrane fractions, where they are abundant (Alexandersson et al., 2004). Therefore, although this remains controversial, it is hypothesized that the CSCs are delivered to DRM microdomains.

Callose is a polysaccharide made up of a β-1,3-linked glucose residue with some β-1,6 branches, and is synthesized by callose synthase (CalS), a protein localized in the PM, which use UDP-glucose as a substrate (Ferguson et al., 1998). Thus, callose deposition depends on the activity of CalS, which is secreted at the pollen tube tip (Cai et al., 2011). It is plausible that CalS complex is assembled in the ER, as shown in tobacco pollen tubes (Cai et al., 2011), and delivered to the PM, via the TGN (Cai et al., 2011; Drakakaki et al., 2015). Similarly to CesAs, CalS is integrated into the PM, with a preference for detergent resistant membrane microdomains, as reported in proteomic analysis of DIMs isolated from poplar, tobacco and *Medicago truncatula* (Besseueille et al., 2009; Morel et al., 2006; Lefebvre et al., 2007). In control pollen tubes, time course experiments showed that the localization of CalS changes as the tube elongates; after 30 min in a growth medium, CalS was more concentrated in the tip PM, with respect to the shank and distal regions. In longer pollen tubes (grown for 90 min), immunofluorescence experiments revealed a different localization in the three distinct regions of the tube: a strong, punctate staining was maintained in the apex, a slighter staining was observed in the intermediate region and a stronger signal was seen again in the distal region (Cai et al., 2011).

The equilibrium between the cell's turgor and the secretion of pectin has to be accurately balanced to maintain proper tip growth (Grebnev et al., 2017), and the pollen tube must be able to redirect its growth direction in response to external guidance cues (Adhikari et al, 2020). Consequently, a plethora of signaling networks and factors are involved in the regulation of pollen tubes, including ion gradients, small GTPases and signaling phospholipids (Heilmann and Ischebeck, 2016; Guo and Yang, 2020; Ischbeck et al., 2010; Michard et al., 2017; Scheible and McCubbin, 2019; Steinhorst and Kudla, 2013; Vogler et al., 2019; Zang et al., 2020).

Ion gradients in growing pollen tubes

Pollen tubes exhibit markedly polarized internal gradients and fluxes of regulatory ions, such as, Ca^{2+}, protons and chloride, which appear to be implicated in the regulation of polarized growth (Hepler et al., 2001). Functions of Ca^{2+} in pollen tubes range from key roles in the prevention of self-fertilization, regulation of the cytoskeleton, influence on secretion, vesicle dynamics and membrane trafficking, to its role as a constituent of the cell wall. It has been demonstrated that a tip-focused calcium gradient is essential for pollen germination and tube growth (Hepler et al., 2001; Robinson and Messerli, 2002; Holdaway-Clarke and Hepler, 2003; Feijo et al., 2004). In all species investigated, the cytosolic concentration of Ca^{2+} is highest in close proximity to the PM at the tip of the pollen tube, ranging from 2-10 μM in the first 20 μm of the apical region to 20-200 nM in the shank of the tube (Steinhorst and Kudla, 2013; Pierson et al., 1994; Malho et al., 2000). The dissipation of this Ca^{2+} gradient inhibits pollen tube growth, and alterations of site of the apical Ca^{2+} peak determines reorientation of growth direction (Pierson et al., 1994; Malho et al., 2000). In contrast extracellular Ca^{2+} concentrations vary in a range of 10–10000μM.

Apical influx of Ca^{2+} ions from the extracellular space - through stretch-activated Ca^{2+} channels during the extension phase of growth - is the major source establishing the gradient, together with subapical Ca^{2+} pumps that lower cytosolic Ca^{2+} immediately behind the tip (Holdaway-Clarke et al. 1997; Pierson et al., 1996; Messerli et al., 2000; Dutta and Robinson, 2004). A mechanism of Ca^{2+} release from internal stores can also contribute to controlling cytosolic ion levels; for example, inositol 1,4,5 trisphosphate (IP3) receptors are present (Franklin-Tong et al. 1996, Malh´o 1998), and phosphatidyl inositol 4,5, bisphosphate ($PtIns4,5P_2$) is enriched at the PM of pollen tubes (Kost et al. 1999); it is plausible, therefore, that IP3 derived from the hydrolysis of $PtIns4,5P_2$ releases Ca^{2+} from internal stores, conceivably from vesicles or ER in the apical clear zone.

Pharmacological approaches resulting in the inhibition of Ca^{2+} channels have demonstrated a direct relationship between ion concentration and oscillatory growth (Geitman and Cresti, 1998). Some observations have also shown that the Ca^{2+} gradient at the tip determines where SVs fuse with the PM. A high concentration of Ca^{2+} also helps to maintain dynamic AFs in this area and inhibits cytoplasmic streaming of SVs in the tip, allowing them to fuse with the apical PM (Taylor and Hepler 1997; Hepler et al., 2001; Camacho and Mahlo, 2003; Cardenas et al., 2008). When Ca^{2+} gradient is dissipated, AFs extend to the apex and acquire the ability to transport large organelles in the clear zone, leading to growth inhibition (Pierson et al., 1994). Furthermore, experiments with Latrunculin B (LatB) - which prevents actin polymerization - revealed a connection between actin dynamics and the Ca^{2+} gradient in lily pollen. Application of LatB to growing tubes leads to growth retardation, followed by growth arrest and simultaneously the Ca^{2+}gradient dissipates.

In addition, the stability of MTs has also been shown to be dependent on Ca^{2+} concentration in a calmodulin-dependent manner (Fisher et al., 1996).

Besides this essential Ca^{2+} gradient, there are other ionic gradients existing in a growing pollen tube, such as K^+, Cl^- and H^+. The latter gradient creates a constitutive cytoplasmic alkaline band immediately behind the clear zone, while the pollen tube apex appears to be slightly acidic, since cytosolic pH is generally one unit lower than that of the alkaline zone (Feijo et al., 1999). Proton gradient is maintained by an influx in the apical region together with a proton efflux in the subapical region (Feijo et al., 1999). Localized ion fluxes imply restricted localized presence of proteins involved in their transport. Pollen tubes expressing GFP-H^+ATPase revealed that this pump is mainly localized in the flanks of the tip, supporting the idea that a proton influx occurs in the tip, while a proton efflux is maintained in subapical regions (Certal et al., 2008). In addition, an influx of K^+ ions at the tip has been observed and an analysis of *Arabidopsis* mutants has led to hypothesize a role for K^+ fluxes in pollen tube growth and in the efficiency of male gamete transport (Fan et al., 2001). Furthermore, tightly regulated fluxes of anions, including most notably Cl^-, appear to be crucial for pollen germination and pollen tube growth. Interestingly, the chloride anion has a reversed direction of flow compared to cations as it was observed leaking out at the tip and entering the tube at the shank (Zonia et al., 2002).

The interplay between Rho small GTPases and signaling phospholipids is essential for tip growth

Small GTPases of the Rho family are important signaling proteins found in all eukaryotic cells that regulate and coordinate a variety of cellular processes, including reorganization of the actin cytoskeleton and membrane trafficking (Etienne-Manneville and Hall, 2002). While animal Rho GTPases family comprises Rho, Rac and CDC42 proteins, yeast cells exclusively express Rho and CDC42 isoforms (Takai et al., 2001). In plants, Rho GTPases are represented by a much smaller subfamily of proteins that are most closely related to animal Rac, and are referred to as Rac-Rop (Rho of plants) GTPases (Winge et al., 1997; Vernoud et al., 2003). Spatially restricted signaling by Rho GTPases is essential for the polarization of eukaryotic cells, which is in turn required for the morphogenesis, mobility and division of single cells, and for the development of multicellular organisms.

sGTPases belonging to the Rac-Rop are involved in tip growth and participate in a wide variety of processes. Active Rac-Rop GTPases are locally confined to the pollen tube tip, where they can act as molecular markers for polarized secretion (Kost et al., 1999; Klahre et al., 2006; Bloch et al., 2016). In addition, Rac-Rop GTPases are involved in the organization of the actin cytoskeleton

as well as in membrane trafficking and control of vesicle fusion with tip PM (Gu et al., 2005; Chen et al., 2003; Lee et al., 2008).

Rho-GTPases are active as signaling molecules in the GTP-bound conformation and interact with multiple effectors in this state. They are regulated by further proteins like GTPase-activating proteins (RhoGAPs) that inactivate the signaling function of Rho GTPases by stimulating their intrinsic GTPase activity, which converts them to the inactive GDP-bound conformation. Guanine nucleotide-exchange factors (RhoGEFs), usually associated with the plasma membrane, promote the exchange of GDP for GTP and activate the signaling function of Rho GTPases. With the possible exception of the Arabidopsis protein SPIKE1, which shows some homology to an animal family of RhoGEFs and is required in cell-shape development (Qiu, et al., 2002), there are no plant homologs of animal RhoGEFs. Only recently, a small family of plant proteins has been identified that contains a conserved PRONE (plant-specific Rop nucleotide exchanger) domain conferring Rac-Rop-specific RhoGEF activity (Berken et al., 2005; Gu et al., 2006). Association of most Rho-GTPases with the PM depends on their post-translational modification by C-terminal prenylation. Guanine nucleotide dissociation inhibitors (RhoGDIs) can remove the prenylated GTPases from the membrane and sequester them in the cytoplasm to form heterodimers. RhoGDIs are most commonly considered negative regulators of Rho GTPases (Etienne-Manneville and Hall, 2002), despite recent indications of their possible function in promoting Rho activation (Court and Sudbery, 2007; Lin et al., 2003; Del Pozo et al., 2002). In physiological conditions Rac/Rop-GTPases in pollen tubes are localized in a restricted area of the apical membrane, a region which has long been considered as the growth domain, and are key regulators of polar cell expansion (Kost et al., 1999; Zheng and Yang, 2000; Fu et al., 2001).

Overexpression of wild-type or constitutively active Rac-Rop depolarizes pollen tube tip growth (Kost et al., 1999; Li et al., 1999), presumably, because it causes an extension of the area of the PM at the tip that is associated with activated Rac-Rop and results in the ectopic fusion of secretory vesicles and a marked swelling of the apical region. By contrast, the elongation of the pollen tube is strongly inhibited by the expression of dominant-negative Rac-Rop (Kost et al., 1999; Li et al., 1999), which seems to block the apical secretion. These evidences suggest an essential role for Rac-Rop in determining growth polarity and apical secretion.

In *Nicotiana*, pollen tube growth is controlled by the Rac/Rop-GTPase Nt-Rac5, which is associated with the PM at the apex (Klahre and Kost, 2006). Nt-RhoGAP1, which enhances the GTPase activity of Nt-Rac5 *in vitro*, is expressed in tobacco pollen tubes and strongly inhibits the growth of these cells when overexpressed. Nt-RhoGAP1 does not accumulate at apex, but rather at the flanks of the tip when expressed at low levels, which do not interfere with cell growth. These

evidences suggest that Nt-RhoGAP1 has a role in restricting Nt-Rac5 activity to the apex by promoting its GTPase activity at the flank of the pollen tube tip, where its signaling function is inactivated (Klahre and Kost, 2006). Nt-RhoGDI2 is specifically expressed in tobacco pollen tubes at high levels (Klahre et al., 2006). Overexpression of Nt-RhoGDI2 fused to yellow fluorescent protein shows that it accumulates in the pollen tube cytoplasm and transfers co-expressed fluorescent Nt-Rac5 fusion proteins from the PM to the cytoplasm, thereby strongly inhibiting tobacco pollen tube growth (Klahre et al, 2006). This observation is in line with the idea that RhoGDIs proteins have a role as negative regulators of Rho signaling by transfer RhoGTPases from the plasma membrane to the cytoplasm, where they form inactive heterodimers (DeMardirossian and Bokoch, 2005).

However, several studies demonstrate that interaction with Nt-RhoGDI2 is required for normal intracellular localization and activation of Nt-Rac5. A mutant form of Nt-Rac5, in which a conserved arginine residue required for RhoGDI interaction (Gibson and Wilson-Delfosse, 2001; Lin et al., 2003), is replaced by alanine (Nt-Rac5R69A), displays reduced binding to Nt-RhoGDI2, although it interacts normally with effector proteins and Nt-RhoGAP1. In addition, it hydrolyzes GTP at the same rate as Nt-Rac5. Finally, while Nt-Rac5 fusion proteins show membrane association specifically at the apex, fluorescent Nt-Rac5R69A fusion proteins accumulate at the highest levels laterally at the tip PM of tobacco pollen tubes. Nt-Rac5R69A does not induce the massive depolarization of pollen tube tip growth as caused by the overexpression of Nt-Rac5. All these results on the function of Nt-RhoGAP1 and Nt-RhoGDI2 demonstrate that these two regulatory proteins are involved in a constant Nt-Rac5-recycling mechanism, which is necessary for the maintenance of the polarized localization and activity of Nt-Rac5 at the plasma membrane at the pollen tube apex. The constant membrane recycling, which is necessary to balance the massive incorporation of secretory vesicles at the apex (Picton and Steer, 1983; Moscatelli et al., 2007), presumably transports active Nt-Rac5 to the flanks of the pollen tube tip, where it is inactivated by Nt-RhoGAP1-stimulated GTP hydrolysis. Inactive Nt-Rac5 then seems to be transferred from the PM to the cytoplasm and transported back to the apex by Nt-RhoGDI2. To complete the recycling, RhoGEFs and factors with RhoGDF activity promote the release of Nt-Rac5 from Nt-RhoGDI2 to enable Nt-Rac5 reassociation with the PM at the apex, and its reactivation at this location (DeMardirossian and Bokoch, 2005). In plants a small family of proteins - which is not found in animals or fungi - with a conserved PRONE (plant- specific Rop nucleotide exchanger) domain conferring Rac-Rop specific RhoGEF activity has only recently been identified. When members of the *Arabidopsis* RhoGEF family are expressed in tobacco pollen tubes, they accumulate at tip PM inducing a depolarized isotropic growth (Gu et al., 2006; Zhang and McCormick, 2007).

Besides the elaborate functional interactions that occur among distinctly localized regulatory proteins directly interacting with the sGTPases, such as RhoGAPs, RhoGDIs and RhoGEFs, additional mechanisms contribute to the maintenance of polarized Rac/Rop signaling in tip growth. Lipid signals act with the mentioned regulatory proteins in the regulation of Rac/Rop GTPases (Ishbebeck et al., 2011; Kost et al., 1999).

Phosphatidylinositol monophosphate kinases, which synthesize PtdIns(4,5)P_2, have been identified as Rac/Rho effectors in animal cells (Hartwig et al., 1995). In pollen tubes a Rac/Rop-associated lipid kinase activity seems to be responsible for the generation of the signaling lipid PtdIns(4,5)P_2 in the PM at the apex of elongating tobacco pollen tubes, which is where Rac/Rop activity accumulates (Kost et al., 1999). It was postulated that PtdIns(4,5)P_2 functions as a Rac/Rop effector in pollen tubes, which might promote the fusion of secretory vesicles with the PM (Kost et al., 1999) as it does in other cell types (Hay et al., 1995; Cremona and Camilli, 2001). Synthesis of PtdIns(4,5)P_2 allows Rho-GTPase to control targeted exocytosis by regulating membrane trafficking and to modify the AF organization by interacting with actin-binding proteins (Van Aeltys and D'Souza-Schorey 1997, de Curtis 2008). Hay et al. (1995) suggested that PtdIns(4,5)P_2 regulates the organization of AFs and polarized exocytosis by altering the lipid composition of membrane microdomains and/or by recruiting proteins that mediate membrane fusion. PtdIns(4,5)P_2 might not only function as an effector of Rac/Rop GTPases, but also as a positive regulator of pollen tube Rac/Rop GTPases. In addition, it has been shown that PtdIns(4,5)P_2 can act as a RhoGDF by destabilizing the interaction between RhoGTPases and RhoGDIs, stimulating membrane association and activation of GTPases activity (Faurè et al., 1999). Pollen tube phosphoinositide specific phospholipase C (PtdIns-PLC) activity contributes to maintaining the polarized distribution of PtdIns(4,5)P_2 and the spatial control of Rac/Rop signaling.

A specific isoform of PLC, Nt-PLC3, has been identified in tobacco pollen tubes. It appears to be constantly targeted at the tip flanks and never accumulates at the extreme apex, in a pattern that is complementary to the distribution of PtdIns(4,5)P_2, with some overlap with the PLC3-PtdIns(4,5)P_2 localization at the flanks of the tip. Dominant negative expression of PLCs mutated in their active site and chemical inhibition of Nt-PLC3 activity cause a depolarization of tip growth and swollen tube tips. In addition, PtdIns(4,5)P_2 visualized by a lipid sensor was observed spreading in a much larger area of plasma membrane at the tip of pollen tubes upon PLC inhibition. (Helling et al., 2006). Hydrolysis of PtdIns(4,5)P_2 by phospholipase C, which results in the formation of IP3 and diacyl glycerol (DAG), followed by IP3-dependent Ca^{2+} release from internal stores, plays a crucial role in regulating Ca^{2+} homeostasis (Yang and Kazanietz 2003). DAG was detected at the tip of growing tobacco pollen tubes, and accumulation of DAG in these cells depends on PtdIns-PLC activity

(Helling et al., 2006). DAG is presumably generated at the flanks of the pollen tube tip, where PLC activity and PtdIns(4,5)P_2 distribution overlap; it is continuously retrieved from subapical regions of the PM by endocytic membrane recycling and reinserted in the apical domain (Helling et al., 2006). Recent studies have shown that PtdIns(4,5)P_2 and PLCs maintain a differential position in the PM as the pollen tube grows and that endocytosis and membrane recycling play a central role in regulating their targeted localization. In animal cells, it was established that DAG, the second product of PLC activity, acts as a second messenger and activates protein kinases C (PKC) (Nishizuka, 1988; Valverde et al., 1994). However, so far, no plant orthologue of these protein kinases has been identified (Islas-Flores et al., 2015). Consequently, the role of DAG in plant cell signaling is under debate and it was suggested that DAG might not function as a signaling molecule and may instead be rapidly converted to phosphatidic acid (PA) by diacylglycerol kinase (Meijer and Munnik, 2003). Phosphatidic acid has been shown to participate in the regulation of exocytosis and endocytosis. This phospholipid, which can also arise as a product of phospholipase D (PLD), promotes membrane curvature and the formation of secretory vesicles, while playing a crucial role in the structural integrity of the Golgi (Sweeney et al., 2002) and in cytoskeleton reorganization (O'Luanaighet al., 2002). In pollen tubes, PA accumulated in the shank PM (Potocky et al., 2003) and it was found that antagonists of PA accumulation and inhibitors of PLC and PLD reversibly haltered polarity, disrupting Ca^{2+} gradient and influencing the transport and accumulation of vesicles in the apical regions. Maintenance of asymmetrical distribution of these lipid signaling molecules is due to coordination of exocytic/endocytic processes, and at the same time, the concerted action of PtdIns(4,5)P_2, IP3 and PA modulates the tip-focused Ca^{2+} gradient, membrane secretion, and cytoskeleton organization, thereby playing a key role in the establishment and maintenance of polarity.

Pollen tube growth is a delicate equilibrium between secretory and endocytic pathways

The purpose of the intense vesicle trafficking through the apical region is the delivery of cell wall precursors, membrane material, enzyme and signaling molecules by exocytosis. As suggested by the apical accumulation of secreted esterified pectins and PMEIs, the classical model of tip growth proposes that exocytosis occurs at the pollen tube apex. To provide sufficient material for cell wall construction, secretory vesicles need to fuse with the plasma membrane at a higher rate than is required for PM extension (Picton and Steer, 1983; Derksen et al., 1995; Bove et al., 2008). Therefore, the maintenance of pollen tube tip architecture requires internalization of excess membrane by endocytosis in order to regulate membrane internal economy, ensuring at the same time the correct localization of polarized distributed proteins/lipids and regulating factors in the PM as the pollen tube

elongates. Pollen tube growth can be considered the result of a delicate equilibrium between exocytosis and endocytosis.

The efficiency of tip growth is maintained by accumulation of SVs in the clear zone of the tip region: a substantial portion of these vesicles is captured and maintained in the apical region, where it is generally accepted that only Brownian movement of vesicles is observed (de Win et al., 1999). The distribution of secretory vesicles and the specific site of secretion are correlated with the distribution of actin filaments (AFs) (Kroeger et al., 2009; Lovy-Wheeler et al., 2005). SVs that do not fuse with PM are driven towards the apex by the actomyosin-dependent reverse fountain-like cytoplasmic streaming (Hepler et al., 2001) that it is thought to be responsible for the typical V-shaped vesicle accumulation in the tip. Movement of vesicles toward the apex occurs in the cortical region of the tube and up to 7-10 μm from the tip, where some of the vesicles invert their trajectory and are transported towards the grain by streaming in the central zone of the tube cytoplasm (Hepler et al., 2001; Parton et al., 2001; Wang et al., 2005). In the apical flanks (2–5 μm from the apical plasma membrane) a dynamic actin fringe defines the region where secretory vesicles preferentially fuse with the plasma membrane (Kost et al., 1999; Fu et al., 2001). SVs are delivered to a position that corresponds exactly to the proximal end of the actin fringe, where, in very close proximity to the plasma membrane, SVs increases their chance to release their content in this area (Bove et al., 2008; Kroeger and Geitmann, 2012). Movement of vesicles in the cone-shaped region is not actin-myosin dependent (Kroeger et al., 2009).

Drugs interfering with AFs dynamics at the tip lead to the formation of long actin filaments in this region, resulting in growth inhibition and loss of cytoplasmic zoning (Pierson et al., 1994); thus, the absence of stable actin bundles in the apex seems to be required for fusion of SVs with the apical PM domain. The alkaline band is involved in enhancing the activity of actin depolymerization factors to shift actin towards its monomeric form; together with the steep-focused Ca^{2+} gradient, the alkaline band is therefore a critical determinant of AFs polymerization state and reverse streaming (Cardenas et al., 2008). Studies using pollen specific *Arabidopsis thaliana* Rac/Rop1 expressed in tobacco pollen tubes showed that this protein localizes in the apical dome of the PM where it acts as a central switch in the control of tip growth. Expression of a dominant inactive Rac/Rop1 mutant blocked tip-localized Rop signaling and inhibited pollen tube growth, whereas the constitutive expression of an active form of *Arabidopsis thaliana* Rac/Rop5 in tobacco pollen tubes apparently induced actin polymerization and actin bundle formation in the tip, inducing pollen tubes to form balloons and suggesting a complete loss of polarity (Kost et al., 1999). By contrast, AFs in pollen tubes expressing a dominant negative form of Rac/Rop5 were finer and less organized and pollen tube growth was strongly inhibited (Kost et al., 1999). Moreover, when overexpressed, Rac/Rop1

leads to a depolarized growth as a consequence of fusion of SVs with a wider area of plasma membrane. Conversely, expression of a null mutant of Rac/Rop1 strongly inhibits growth and apical secretion (Fu et al. 2001). All these observations provide evidence linking Rho-GTPases to actin organization in the control of cell polarity and secretion in plants. In addition, Rac/Rop-GTPases regulate AF dynamics by acting on formins, which are actin-nucleating proteins (Pollard, 2007; Goode and Eck, 2007). Formins (FH) are known to regulate actin-related processes and coordinate actin and microtubule function in HeLa cells. It has been suggested that formins could functionally connect the sGTPases to the actin cytoskeleton; in fact, in HeLa cells it was observed that mDia1, a member of the formin-homology family of proteins and an effector of the sGTPases Rho, enables MTs to align with actin bundles, through interaction with members of the Rho family (Ishizaki et al., 2001). Close association between MTs and AFs has been observed in the subapical regions of pollen tubes after rapid freeze fixation and substitution (Lancelle et al., 1987; Lancelle and Hepler, 1992) and MT organization seems to depend on correct organization of the actin cytoskeleton (Idilli et al., 2012). When actin polymerization is inhibited by low concentrations of LatB, a dramatic reorganization of the MT cytoskeleton occurs, leading to the formation of MT bundles, often organized in rings, in the apex and shank of tobacco pollen tubes (Idilli et al., 2012). In pollen tubes, FH3 and FH1 stimulate actin bundle formation and actin assembly along the shank, where AFs are responsible for cytoplasmic streaming. Overexpression of these proteins induces cell membrane deformation, suggesting a role in polar growth (Cheung and Wu, 2004; Ye et al., 2009). In *Arabidopsis*, FH5 is associated with the apical membrane just behind the apical flanks of pollen tubes and plays a role in the organization of subapical actin mesh-like structure. RNAi experiments or antisense transgenes against Nt-FH5 have shown that actin polymerization stimulated by FH5 is important for maintaining the polarized distribution of vesicles and organelles (Cheung et al., 2010). Since pollen tube elongation is closely linked with actin polymerization, it has been suggested that properly regulated membrane-associated actin polymerization induced by formin could contribute to protrusive growth at the tip.

The exact sites of exocytosis at the pollen tube apex have been investigated using fluorescent dyes or expressing (GFP)-fused secretory vesicle markers. The accumulation of exocytic vesicles at the pollen tube apex suggests that exocytosis occurs at the extreme apex and studies on the secretion of new cell wall material also favor tip localization of exocytosis (Hepler and Whinship, 2015; Rounds et al., 2014). Direct evidence for apical secretion in pollen tubes derives from FRAP analysis of a GFP labeled pollen specific receptor-like kinase AtPRK1 which localizes to the apical PM (Lee et al., 2008). Treatment with Brefeldin A, an inhibitor of secretion (Nebenführ et al., 2002), abolished PM labeling by AtPRK1-GFP and arrested this fusion protein in the endoplasmic reticulum,

confirming that AtPRK1-GFP is inserted into PM via exocytosis. To identify the exact site of secretion, Lee et al. (2008) selectively bleached AtPRK1-GFP in the PM either at the apex or in an adjacent lateral region. Rapid fluorescence recovery was observed at the apex, demonstrating that secretion occurs in this region. No fluorescence recovery was observed after bleaching lateral PM regions, suggesting that these regions are devoid of detectable exocytic activity. In the same work it is also suggested that depolymerization of apical AFs seems to be necessary for vesicle docking and fusion to the PM for exocytosis (Lee et al., 2008). Similar experiments were also performed using GFP fused to the pollen specific *N. tabacum* PME, NtPPME1. NtPPME1-GFP exclusively labeled the apical cell wall of pollen tubes (Bosch et al., 2005; Wang et al., 2013) and FRAP analysis revealed that after bleaching the recovery of NtPPME1-GFP fluorescence first occurred in the center of the apex, from where it spread distally (Wang et al., 2013).

Observations carried out by staining pollen tubes with lipophilic styryl FM dyes and FRAP analysis suggest another site of exocytosis at the shoulder of the apex (Bove et al., 2008; Zonia and Munnik, 2008, Moscatelli et al., 2012). FRAP experiments in different regions of the apex of tobacco pollen tubes stained with FM4-64 demonstrated that exocytosis actually occurs in both the very apex and apical flanks. While fast secretion occurs in the apical flanks, slower exocytosis has been observed in the central part of the apex (up to 2 μm from the apical plasma membrane) (Moscatelli et al., 2012), suggesting that secretion in different domains of the clear zone relies on distinct mechanisms and probably accomplishes different functions. Moreover, it was demonstrated that fast secretion in the apical flanks depends on actin fringe structure, since low concentrations of LatB affect the speed of fluorescence recovery in the apical flanks and not in the apex (Moscatelli et al., 2012).

In addition, pharmacological analysis further indicated that exocytosis in the subapical region also occurred and was actin-dependent, whereas exocytosis in the extreme apex was actin-independent (Rounds et al., 2014; Moscatelli et al., 2012).

Evidence that secretion as well as endocytosis occurs during pollen tube growth came from studies in which the amount of membrane material supplied by fusion of secretory vesicles was quantitatively compared to the amount of membrane material required for PM extension. It was determined that membrane material deposited to the PM exceeds that needed for pollen tube growth, and it is estimated that nearly 80% of the secreted membrane is retrieved by endocytosis during pollen tube growth (Picton and Steer, 1983; Steer and Steer, 1989; Derksen et al., 1995; Bove et al., 2008). Derksen et al. (1995) revealed the presence of coated vesicles in tobacco pollen tubes - presumed to be an early stage of endocytosis - in regions just behind the clear zone. This observation, together

with data proving the existence of sequences coding for a clathrin heavy chain-like polypeptide (Blackbourn and Jackson, 1996), suggested that clathrin-dependent endocytosis functions in recycling excess PM secreted at the tip during pollen tube growth (Derksen et al., 1995). A more recent analysis in pollen tubes of different species, using the FM dye FM4-64, showed that most of the internalized plasma membrane of pollen tubes accumulates at the tip in the V-shaped fluorescent area, suggesting that most of the internalized PM is recycled into the secretory pathway (Parton et al., 2001; Moscatelli et al., 2007) and that V-shaped accumulation of vesicles in the clear zone includes newly internalized endocytic vesicles besides secretory vesicles (Bove et al., 2008; Moscatelli et al., 2007; Zonia and Munnik, 2008). Since FM dyes insert homogeneously into the PM and do not make it possible to distinguish between different patterns of endocytosis, electron dense gold particles referred to as Nanogold, which were either negatively ($^{-}$Ng) or positively charged ($^{+}$Ng), were used to resolve endocytic processes. In tobacco pollen tubes, negatively and positively charged Nanogold, along with studies on internalization of the lipophilic dye FM4-64 showed two different sites of endocytosis: in the apical dome and along the shank. Time lapse experiments using FM4-64 showed that internalization in the apex was significantly lower than in the shank, suggesting for the first time that exocytosis, as well as endocytosis, occur in the tip region and that the clear zone could represent the site of accumulation of transport vesicles and not just secretory vesicles. Experiments of endocytosis dissection with charged nanogold confirmed the presence of distinct endocytic pathways in pollen tubes. Positively and negatively charged nanogold particles bind negatively and positively charged residues on the PM respectively, showing, at the ultrastructural level, the fate of internalized PM segments in different regions of the pollen tube. The results revealed that positively charged nanogold was internalized in the shank of tobacco pollen tubes, whereas negatively charged nanogold was internalized in the tip region of the cell. $^{+}$Ng was internalized in the pollen tube shank and delivered to the TGN, which can be considered the plant counterpart of animal early endosome compartments (EEs), and from TGN $^{+}$Ng could be sorted for degradation or recycling. After internalization, endocytic vesicles destined for degradation or recycling to the plasma membrane could therefore be sorted through distinct TGN subdomains. The degradation pathway involves multivesicular bodies/late endosomes (MVBs) and lytic vacuoles. Cargoes destined for degradation are trapped in the internal vesicle system of MVBs; delivery of plasma membrane proteins/lipids to vacuoles requires previous ubiquitination, which is the signal for ESCRT-dependent sorting to the degradation pathway (Herbert et al., 2012). The pattern of $^{+}$Ng internalization suggests that, as in somatic cells, even in pollen tubes TGN represents a first sorting station for MVBs and vacuoles (Moscatelli et al., 2007). Moreover, most vesicles internalized in the shank are recycled to the apex of the pollen tube through the Golgi apparatus. The probe was observed in cis and medial Golgi stacks

and was recycled to the plasma membrane by exocytosis. Thus, the plasma membrane internalized in the pollen tube shank is largely reused for secretion and pollen tube growth (Bove et al., 2008; Moscatelli et al., 2007). In addition, $^{+}$Ng has been observed in vesicles containing fibrillar material similar to cell wall component outside the protoplast, suggesting that the removal and recycling of elements of the cell wall could be involved in the regulation of mechanical properties of pollen tube during the elongation process, along with cell wall loosening enzymes.

$^{-}$Ng is internalized in the apical dome of the pollen tube and is found in a limited number of vesicles in the tip region and in vacuoles. Sometimes $^{-}$Ng particles were observed in vesicular tubular elements related to trans face of Golgi, but not in cis or medial cisternae. Most internalized particles are delivered to degradation pathways through the TGN. Moreover, pulse-chase experiments clearly showed a recycling pathway confined to the tip region. This pathway could not involve TGN function (Moscatelli et al., 2007), since secretory carrier membrane proteins (SCAMPs), which characterize TGN in tobacco BY-2 cells (Lam et al., 2007), were mostly localized in small apical vesicles and secondarily in TGN and vacuoles in lily pollen tubes (Wang et al., 2010). While these proteins characterize EEs, it may be hypothesized that an early sorting stationcould exist in the apex before the TGN and enable faster recycling of internalized plasma membrane limited to the tip. This tip-limited recycling process may not be involved in pollen tube growth but could be involved in the redistribution of protein complexes or lipids between different membrane domains in order to maintain functional specialization in the apical plasma membrane.

Despite clathrin-dependent endocytosis in plants probably accounting for most endocytic processes into the cell, evidence of clathrin-independent endocytosis in plant cells has recently emerged (Onelli et al., 2008; Baluska et al., 2004; Bandmann and Homann, 2012). In animal cells, clathrin-independent endocytosis may occur in lipid raft domains (Simons and Gerl, 2010). Lipid-dependent endocytosis follows the pattern of internalization described for clathrin-dependent endocytosis and probably also involves the ER (Ewers and Helenius, 2011). In plants, knowledge of the existence of raft domains has progressively increased during recent years along with attempts to investigate their functions. Proteins associated with these lipid platforms are involved in signaling, trafficking and cell wall metabolism (Morel et al., 2006; Lefebvre et al., 2007; Men et al, 2008). In plants, little is known about lipid raft involvement in endocytosis. Li et al. (2012) showed that the protein flotillin 1 (Flot1), a component of lipid rafts in plants, participates in clathrin-independent endocytosis. In animals it has been demonstrated that flotillins are involved in membrane curvature and plasma membrane invagination during internalization processes (Frick et al., 2007). In *Arabidopsis* root cells, Flot1 partially colocalizes with the endocytic marker FM4-64 and is observed

in plasma membrane invaginations, where it leads to large vesicle formation, TGN, endosomes, and ER (Li et al., 2012). Endocytic processes depending on Flot1 appear to require the integrity of sterol-rich membrane microdomains and cytoskeleton: AF and MT depolymerizing drugs have shown that MTs are required for efficient distribution/dynamics of microdomains containing Flot1. This data suggests that clathrin-independent endocytosis involving Flot1 and probably sterol-rich membrane microdomains occurs in Arabidopsis root cells (Li et al., 2012).

The use of Ikarugamicina (Ika), a drug affecting clathrin-dependent endocytosis, made it possible to distinguish different internalization mechanisms in pollen tubes. It has been demonstrated that both clathrin-dependent and clathrin-independent endocytic processes are involved in recycling different PM proteins/lipids in the apex and in regulating pollen tube growth (Moscatelli et al., 2007) and that clathrin-dependent and clathrin-independent endocytosis occur in different regions of pollen tubes and are involved in different internalization pathways (Moscatelli et al., 2007). Ika showed clathrin-dependent and clathrin-independent internalization of $^{+}$Ng in the shank: clathrin-dependent endocytosis is involved in recycling internalized plasma membrane through the secretory pathway, whereas clathrin-independent endocytosis conveys the internalized material to vacuoles. The dimension of coated endocytic vesicles 10–15 μm from the tip suggests that clathrin-dependent endocytosis occurs in this pollen tube area (Derksen et al., 2005; Zonia and Munnik, 2008). $^{-}$Ng detects a second clathrin-dependent endocytic process occurring at the tip, whereby internalized material is sorted to vacuoles without intersecting the secretory pathway. $^{-}$Ng has been observed in TGN but not in Golgi stacks, suggesting another degradation pathway that is dependent on the formation of clathrin-coated vesicles (Moscatelli et al., 2007). Thus, clathrin-dependent and clathrin-independent degradation pathways coexist and are localized in different areas of the pollen tube plasma membrane. Time-lapse experiments using FM4-64, with or without Ika, show only partially reduced internalization in the tip and shank. Pulse-chase experiments using $^{-}$Ng suggest that some vesicles are recycled in the apical region without leaving the clear zone. Since Ika treatment impairs uptake of the probe destined to the degradation pathway, it is still not clear whether the endocytic pathway involved in relocalizing apical plasma membrane proteins/lipids is also affected by the clathrin-dependent inhibitor (Moscatelli et al., 2007). It has been shown that in animals synapses, PtdIns4,5P_2 is involved in exo- and endocytic cycling of presynaptic vesicles and secretory granules and plays a role in regulating clathrin-mediated endocytosis. Evidence of the involvement of this polyphosphoinositide in endocytic processes in plant cells comes from observation of salt-stress-induced association of PtdIns4,5P_2 with clathrin-coated vesicles in *Arabidopsis* (König et al., 2008). Moreover, it is known that a proper balance between phosphatidylinositol 4-monophosphate (PtIns4P) and PtdIns4,5P_2 is required for clathrin-dependent endocytosis in pollen tubes (Zhao et al.,

2010). Overexpression and silencing of kinase PIP5K6, which is necessary for PtdIns4,5P_2 synthesis, show that this phosphoinositide is important for the activation of the early stages of clathrin-dependent endocytosis, by promoting formation and invagination of clathrin-coated pits in the apical plasma membrane; PtdIns4P functions in later stages of clathrin-coated vesicle formation in tobacco pollen tubes (Zhao et al., 2010). In addition, since PtdIns4,5P_2 seems to be involved in regulating actin cytoskeletal dynamics (Stevenson et al., 2000; Dowd et al., 2006), the interaction between PtdIns4,5P_2 and actin could be a factor affecting clathrin-coated vesicle formation. In fact, results using low concentrations of latrunculin B are of further importance as they showed that clathrin-dependent and clathrin-independent endocytosis along the shank require actin, whereas the clathrin-dependent degradation pathway at the tip does not (Moscatelli et al., 2012). Moreover, it seems that internalization in the tip is also partially impaired by LatB and an actin-dependent clathrin-independent internalization pathway could therefore be active in the tip of pollen tubes, in repositioning/recycling plasma membrane proteins/lipids in the clear zone. The hypothesis that some vesicles in the clear zone do not enter in cytoplasmic streaming but remain in the tip and eventually re-fuse with the plasma membrane, has been put forward by studies carried out in lily and *Petunia inflata* (Bove et al., 2008; Guo and McCubbin, 2012). The combination of FRAP and STICS (SpatioTemporal Image Correlation Spectroscopy) analysis in lily pollen tubes showed that, once they arrived in the flanks, many secretory vesicles detached from actin filaments and failed to fuse with plasma membrane. Therefore, they are recycled by the forward stream to the flanks region (Bove et al., 2008). Alternatively, it has been proposed that the apex could be a site of "kiss-and-run" endocytosis (Bove et al., 2008). This type of endocytosis has been described in synapses as a clathrin-independent internalization process involved in fast, apical recycling mechanism (Saheki and Camilli, 2012), but experimental evidence for this mechanism in pollen tubes remains elusive.

There is evidence that a kinesin-like protein is associated with vesicles in the tip region and that these vesicles are associated with short MT strands in the clear zone (Tiezzi et al., 1992; Cai et al., 1993). Although kinesin is known to play a role in driving the movement of organelles along MTs in *in vitro* assays, the identity of these organelles is still unknown (Romagnoli et al., 2003; Cai and Cresti, 2012). Clathrin-dependent and clathrin-independent degradation pathways could therefore be regulated by different mechanisms involving MTs instead of AFs in the tip region and the putative microtubular motor proteins observed in this area suggest that MTs could play a role in the apex localized vesicle trafficking.

The cytoskeletal apparatus in the pollen tube

The functions of the cytoskeleton in plant cells have been well characterized, mostly based on studies that employed a variety of single-cell model systems (Kost et al., 1999). Aside from being required for basic cellular processes, such as nuclear division, organelle positioning, cytokinesis, membrane trafficking and cell expansion, the plant cytoskeleton plays a key role in cellular events that are thought to be important for the development of multicellular organs. The plant cytoskeleton comprises actin filaments (AFs) and microtubules (MTs) that are highly dynamic through their interaction with various actin- and microtubule-associated proteins (Erhardt and Shaw, 2006; Hussey et al., 2006). Cytoskeletal proteins are structural proteins that constitute AFs and MTs (namely actin and tubulin, respectively), whereas cytoskeletal-associated proteins comprise proteins that regulate AF and MT architecture or functions and motor proteins to promote organelles/vesicles translocation along them. AFs and MTs are filamentous structures that form spontaneously under physiological conditions as the result of the polymerization of G-actin monomers or of alfa/beta- tubulin heterodimers, respectively. Both these structures are extremely dynamic and undergo constant assembly and disassembly at their ends (Chen et al., 2000; Joshi et al., 1998; Margolis and Wilson, 1998; Schoenenberger et al., 1999), allowing cells to rapidly reorganize their cytoskeleton in response to environmental or developmental signals.

The cytoskeleton in pollen tubes has been intensively studied. Rapid and directional tip growth of pollen tubes requires an intense intracellular trafficking of vesicles and organelles in order to redistribute membrane-bound structures and enables the accumulation of secretory vesicles at the pollen tube apex sustaining highly polarized growth of the cell. The intense movement of organelles and vesicles is dependent on the dynamics of the cytoskeleton and occurs along specific tracks defined by the organization of the cytoskeletal elements, which can be able to reorganize in response to external signals and to coordinate membrane trafficking with the growth rate of pollen tubes (Cai et al., 2015).

The actin cytoskeleton has been shown to be crucial for pollen tube growth (Taylor and Hepler, 1997; Gibbon et al., 1999; Hepler et al., 2001; Vidali et al., 2001; Hussey et al., 2006; Chen et al., 2009; Fu, 2010). It is regarded as one of the most critical components in controlling exo/endocytic vesicles trafficking and protein targeting in the growing pollen tubes since organelles movement, vesicles trafficking and signaling networks are all dependent on the spatial organization and dynamics of actin (Vidali and Hepler, 2001; Vidali et al., 2001; Chen et al., 2003, Cheung et al., 2008, Fu, 2010).

During pollen tube growth the actin cytoskeleton represents the intracellular transport system that carries Golgi-derived vesicles containing the materials required for cell wall synthesis and

membrane fusion to the tip (Pierson and Cresti, 1992; Hepler et al., 2001; Vidali and Hepler, 2001) and it has also been viewed as a structural element supporting the turgor pressure needed to drive and maintain rapid pollen tube growth (Picton and Steer, 1982; Steer and Steer, 1989; Derksen et al., 1995). Additionally, actin polymerization has also been shown to be important for pollen tube growth (Gibbon et al., 1999; Vidali et al., 2001)

Pharmacological approaches and various staining methods in fixed cells, combined with techniques for visualization of actin in living cells (especially the latest Lifeact-mEGFP) (Lovy-Wheeler et al., 2005; Vidali et al., 2001), have revealed multiple forms of actin filaments in pollen tubes. It is now clear that the pollen tube is characterized by at least three different arrangements of actin filaments that are consistent with the zonation of the cytoplasm. In the shank, AFs are arranged in longitudinal thick AFs bundles responsible for transporting organelles or vesicles from the grain to the tip along the cell cortex. In the subapical region AFs form a highly dynamic structure described as "collar" (Gibbon et al., 1999, Fu et al., 2001), "fringe" (Lovy-Wheeler et al., 2005), "mesh" (Geitmann et al., 2002; Chen et al., 2002) or "funnel" (Vidali et al., 2001) in pollen tubes from different species. The sub-apex of the pollen tube is where organelles reverse their movement and turn back toward the base along the longitudinal actin cables in the center of the tube, giving rise to the typical reverse-fountain cytoplasmic streaming pattern (Hepler et al., 2001). This region therefore has a critical role because it is very likely that the assembly of new actin filaments or the elongation of existing actin filaments occurs here (Cheung and Wu, 2004; Hepler and Winship, 2015). Large organelles do not enter the apical region and instead it is small vesicles that enter and become accumulated in the apical zone.

The visualization of the actin fringe has been optimized with the development of improved methods of fixation (Lovy-Wheeler et al., 2005) or by using transformed cells expressing actin-binding protein fused with fluorescent markers (Vidali et al., 2009). Using rapid freeze fixation of lily (*Lilium formosanum*) pollen tubes, together with staining with anti-actin antibody, the structure appears as a dense fringe of longitudinally oriented microfilaments, beginning 1 to 5 μm behind the tip and extending up to 5 to 10 μm basally. The AFs are positioned in the cortical cytoplasm close to the plasma membrane (Lovy-Wheeler et al., 2005). More recently, Lifeact-mEGFP has become the actin marker of choice in growing pollen tubes. Lifeact-mEGFP contains an actin-binding site of 17 amino acids derived from yeast ABP-140 fused with mEGFP. This probe has been employed to visualize the organization and dynamics of AFs in growing tobacco, Arabidopsis and lily pollen tubes (Vidali et al., 2009; Qu et al., 2013; Dong et al., 2012). Even though its precise structure and composition has not yet been clearly defined, the subapical actin fringe is thought to participate in vesicle trafficking in the apex and in controlling formation and maintenance of the apical clear zone

(Qin et al., 2011; Vidali et al., 2009; Hepler and Whinship, 2015). The actine fringe can be seen as a kind of turning point in the cell because most of the larger organelles stop and reverse their movement in proximity to the actin fringe, while secretory vesicles can usually cross the actin fringe and reach the apex. The actin fringe is likely to be a dynamic structure whose extension is closely related to the rate of pollen tube growth (Dong et al., 2012). The assembly of the actin fringe is likely the result of a balanced process of assembly/disassembly regulated by many factors and proteins. It is reported that highly dynamic AFs that are constantly generated from the apical PM are required for the construction of the subapical actin fringe and that this process is most likely mediated by formins, such as AtFH5 (Cheung et al., 2010).

In the apical region, the third type of AFs arrangement is represented by less abundant, fine and highly dynamic short AFs (Qu et al., 2013; Fu et al., 2001). This form of AFs is distinguished from the subapical actin fringe, and it is the precise dynamics of these AFs that is crucial for tip growth. The nucleation factor for these apical AFs has yet to be identified, and it is proposed that the nucleation is probably mediated by formins (Qu et al., 2013; Cheung et al., 2010). On the other hand, calcium-responsive actin depolymerization promoting factors, such as villin2 (VLN2) and VLN5, play an important role in the rapid turnover of AFs in the apical region of the pollen tubes through their Ca^{2+}-dependent AF-severing activity (Qu et al., 2013). In addition, it has been shown in *in vitro* assays that MAP18 (Zhu et al., 2013) and MDP25 (Qin et al., 2014) are able to sever actin filaments in a calcium-dependent manner, thus both proteins may coordinate with villins to regulate actin dynamics in pollen tubes. The involvement of these highly dynamic actin filaments in the final step of vesicle trafficking has not yet been established and, consequently, we need more information on their possible interaction with vesicles during secretion and endocytosis. The apical plasma membrane and the cytoplasmic region immediately beneath the tip contain a myriad of regulatory factors that are necessary for the growth of the pollen tube (calcium, phospholipids, sGTPases, reactive oxygen species, actin-binding proteins, etc,), therefore, actin filaments in the tip are expected to be highly dynamic in order to adapt quickly to new growth conditions.

As minimal quantities of latrunculin B stop tube growth without apparently affecting organelle motility in the shank (Vidali et al., 2001), a sensitive sub-population of actin filaments in the apex or subapex is evidently involved in growth. Considering the distribution of actin filaments at the pollen tube apex and sub-apex, the actin fringe and the short dynamic actin filaments are both potential candidates for this function.

Unlike what happens in animal cells, the movement of organelles in plant cells is predominantly based on actin filaments and, despite increasing knowledge on the role of MTs in

membrane trafficking, growth and morphogenesis in somatic cell division, very little is known about their role in cells with polarized growth, such as pollen tubes. In the pollen tube, the role of actin filaments is clearly related to the transport of organelles and vesicles while the role of microtubules is not well defined (Cheung et al., 2008). MTs are thought to be a target for self-incompatibility signaling (Poulter et al., 2008), and may be involved in the movement of the generative cell and vegetative nucleus in pollen tubes (Laitiainen et al., 2002). Moreover, new evidence suggests that MTs could be involved in exocytosis and endocytosis (Cai et al., 2015; Idilli et al., 2013; Onelli et al., 2015) and in the short-lived movement and fine positioning of organelles in pollen tubes (Romagnoli et al., 2003; Idilli et al., 2013; Onelli et al., 2018).

Using immunofluorescence microscopy, the distribution of MTs was investigated in several species of Angiosperm (Lancelle and Hepler, 1992; Pierson et al., 1986; Del Casino et al., 1993; Derksen et al., 2002; Gossot and Geitmann, 2007). In *Nicotiana tabacum* long and longitudinal oriented MT bundles occur centrally in the cytoplasm in the distal region of the pollen tube, while the cortical region close to the apical PM contains randomly oriented short MT segments, suggesting the existence of more stable MT bundles in the shank compared to the apical and subapical regions. A similar pattern was also revealed in living tobacco pollen tubes by transiently expressing the Arabidopsis plus-end tracking microtubule-binding protein AtEB1 (Cheung et al., 2008). In the sub-apical and apical regions of pollen tubes, the organization of microtubules is less certain. In these regions MTs are likely to be dynamic and therefore standard techniques of chemical fixation could easily misrepresent their arrangement. It was hypothesized that post-translational modifications of tubulin could be involved in MTs stabilization and in functional diversification of MTs (Hammond et al., 2008). Most post-translational modifications occur on the microtubular polymer rather than on soluble tubulin and it has long been known that, compared to dynamic MTs, stable MTs accumulate more post-translational modifications which are correlated to specific functions of MTs (Hammond et al., 2008). Dynamic MTs are usually tyrosinated, while the more stable ones are detyrosinated, acetylated or both (Bulinski and Gundersen 1991, Gelfand and Bershadsky, 1991, Piperno et al., 1987). In pollen tubes, most MTs contain tyrosinated α-tubulin and are mainly localized at the apical and subapical regions of *Nicotiana tabacum* pollen tubes. These observations have led to hypothesize that these regions could be the zone where dynamic MTs are found.

Recently, Idilli et al. reported that both endocytosis and exocytosis in the apex were affected by Nocodazole (Noc), an anti-tumor agent that affects MT dynamic instability, leading to MT depolymerization in vitro and in vivo (DeBrabander et al., 1976; Hoebeke et al., 1976; Samson et al., 1979). Low concentrations of Noc only affects short MTs in the pollen tube tip and proximal shank, but not distal MT bundles (Idilli et al., 2013), indicating distinct features and functions of different

subsets of MTs in pollen tubes. In addition, the treatment increases the rate of apical exocytosis, but inhibits PM internalization in the apex. The researchers postulated that MT polymerization could facilitate PM invagination and subsequent conveyance to degradation pathways in the pollen tube tip. The Noc treatment also revealed a role for MTs in the control of pollen tube diameter (Idilli et al., 2013), thus MT-dependent exocytosis or endocytic recycling are hypothesized to affect the secretion and function of PME and PMEI and subsequently modulate the pectin deposition and de-esterification in the tip in order to control pollen tube growth (Idilli et al., 2013; Rockel et al., 2008; Derksen et al., 2011).

As already discussed, plasma membrane internalized in the shank is mostly sent to the Golgi apparatus to be reused in the secretion pathway and in part conveyed to vacuoles through the trans-Golgi network (TGN) (Moscatelli et al., 2007). Conversely, PM internalized in the apex mostly goes to the degradation pathway, bypassing the Golgi/TGN apparatus (Moscatelli et al., 2007). Specific drugs affecting actin filament and microtubule integrity have further defined these degradation pathways: PM internalized in the shank is delivered to multivesicular bodies (MVBs)/prevacuolar compartments (PVCs) and then to vacuoles in an AF-dependent way (Moscatelli et al., 2012), while PM endocytosed in the tip is conveyed to vacuoles by bypassing the Golgi/TGN, in a MT-dependent manner (Idilli et al., 2013).

In tobacco pollen tubes, acidic vesicles concentrated in the clear zone have been identified using Lysosensor confirming that at least part of these vesicles could represent an EE-like compartments (Moscatelli et al., 2007; Idilli et al., 2013). In the presence of Noc, movement of newly tip-internalized vesicles is delayed in the acidic inverted cone region and vesicles that could be delivered to the degradation pathway are misallocated to the Golgi apparatus (Idilli et al., 2013). Even if mathematical models have shown that the movement of vesicles in the clear zone depends on diffusion and advection (Kroeger et al., 2009; Chebli et al., 2013), MTs could play a role as tracks for endocytic vesicles addressed to the degradation pathway or could be involved in recycling/redistribution of plasma membrane components to maintain functional membrane polarization in the apical PM. In addition, MTs play a role in PVC delivery to and/or fusion with tubular vacuoles (Onelli et al., 2018). The use of SYP21 as a marker of PVCs made it possible to identify for the first time the crucial role of PVCs and tubular vacuoles in the MT-dependent degradation pathway. The emerging idea is that MTs play a major role in different processes in pollen tube degradation pathways: MTs could primarily favor the delivery and/or fusion of PVCs with tubular vacuoles. As stated for trafficking of cellulose synthase complex (CSC), where cortical MTs play a role in positioning and targeting of Golgi-derived small CSC vesicles for their correct fusion

with the PM (Crowell et al., 2009; Gutierrez et al., 2009; Paredez et al., 2006), MTs could play a similar role in properly localizing PVCs near vacuoles to promote fusion events.

RATIONALE

Lipid analysis of detergent insoluble membrane domains (DIMs) purified from tobacco pollen tubes showed that they are characterized by high sterol content, increased content of hydroxylated very long chain fatty acids (VLCFA) sphingolipids and phospholipids enriched with saturated fatty acids (Moscatelli et al., 2015), in line with criteria for membrane raft microdomains isolated from animals (Simon and Sampaio, 2011) and plant somatic or cultured cells (Cacas et al., 2012). Moreover, the polarized distribution of sterols and L_o domains in apical-subapical regions of pollen tubes suggests that lipid rafts could be involved in maintaining the polarized distribution pattern of lipids and proteins in the plasma membrane and, consequently, in regulating Rac/Rho -dependent signaling pathway which, in turn, determines the dynamics of actin cytoskeleton in the apex and regulates polarized secretion (Kost et al., 1999; Gu et al., 2001; Pechlivanis and Kuhlmann, 2006; Zou et al., 2011;).

The goal of this study is to unravel the role of lipid rafts microdomains on tip growth in pollen tubes of *Nicotiana tabacum*, using an experimental approach which considers the effects of lipid raft disorganization.

EXPERIMENTAL APPROACH

Preliminary data using BCD in pollen tubes of *Nicotiana tabacum* showed that sterol depletion dramatically altered the polarized distribution of both L_o domains and purified DIMs (Moscatelli et al., 2015). Although it is recognized that sterol deprivation - using chelating agents as BCD or molecules inhibiting sterol biosynthesis like statins - alters the organization of lipid microdomains (Chamberlain et al., 2001; Lang et al., 2001; Taverna et al., 2004), both these approaches displayed limitations. Several studies showed that BCD might have pleiotropic effects on the distribution of membrane components as it removes sterols from both L_o and L_d domains (Zidovetzki and Levitan, 2007). In addition, the effect of statins could not be due to sterol deprivation only as the inhibition of mevalonate pathway also induces the reduction of farnesyl diphosphate which is required for protein isoprenylation, a modification regulating the function of proteins involved in signaling cascades, like Ras/Rho sGTPase family members (Pechlivanis and Kuhlmann, 2006).

Notably, Zaragozic acid/Squalestatin, inhibits the squalene synthase which catalyzes the first reaction of the metabolic pathway that is exclusively involved in sterol biosynthesis (Baxter et al., 1992). The use of Squalestatin was extremely useful for studying the role of sterols and lipid rafts in tip growing cells like neurons and pollen tubes (Linetti et al. 2009; Villette et al. 2015).

A further approach for studying the contribution of lipid raft microdomains to polarized growth will be to disorganize lipid raft microdomains by inhibiting sphingolipids biosynthesis. Myriocin, isolated from the fungus *Isaria sinclairii*, inhibits Serin palmitoyl-CoA transferase, which is the first and rate-determining enzyme in the sphingolipid biosynthetic pathway (Fujita et al., 1994). Myriocin was shown to induce depletion of sphingolipids in organisms as evolutionary distant as *Chlamydomonas reinhardtii* and mammalian cells (Kong et al., 2015; Lee et al., 2012)

Based on these reports, Squalestatin and Myriocin will be employed as drugs to inhibit sterols and sphingolipids biosynthesis in tobacco pollen tubes.

RESULTS AND DISCUSSION

Squalestatin and Myriocin alter the lipid profile and pollen tube length

A recent study by Villette et al. (2015) showed that incubation with 1 µM Squalestatin induced sterol depletion in tobacco pollen tubes. To find the lowest concentration of Squalestatin which inhibits sterol biosynthesis, pollen was germinated in control medium and in medium supplemented with 0.5 µM or 1 µM Squalestatin for 2 hours. Control and treated pollen tubes were processed to separate microsomal fractions (P2); the analysis of sterol content in P2 isolated from cells cultured in in the absence (control) or in the presence of the drug revealed that, whereas 0.5 µM Squalestatin does not inhibit sterol biosynthesis, a significant decrease of total sterols was detected in microsomes isolated from pollen tubes grown in the presence of 1 µM Squalestatin (Fig. 3 a). As total sterol content decreased after incubation with 1 µM Squalestatin for 2 hours, these conditions were used in later experiments.

The analysis of lipids biosynthesis during microsporogenesis showed that pollen grains contain a stock of sterols, at the anthesis (Villette et al, 2015; Rotsch et al., 2017). However, *de novo* synthesis of cycloeucalenol was described during pollen germination and pollen tube growth in tobacco (Villette et al., 2015; Rotsch et al., 2017). To investigate the effect of Squalestatin on synthesis of cycloeucalenol, microsomes purified from control and treated pollen tubes were analyzed by Gas Chromatography-Mass Spectrometry (*GC-MS*) technique; this analysis showed that the amount of cycloeucalenol also decreased in pollen tubes incubated with Squalestatin, with respect to control (Fig. 3 b).

In previous studies 5 µM Myriocin was shown to deplete ceramides in *Chlamydomonas reinhardtii* (Kong et al., 2015). Since the use of 10 µM Myriocin in tobacco pollen tubes induces a relevant alteration in protein expression in soluble fraction (unpublished results, Supplementary Fig. S1; courtesy of Monica Scali, Department of Life Science, University of Siena), we decided to employ a lower concentration of the drug. Thus, pollen was germinated in a control medium or in a medium containing 5 µM Myriocin for 2,5 hours and then microsomal fractions were prepared from control and drug treated pollen tubes. Lipid analysis showed that 5 µM Myriocin induced a decrease in the content of Glycosyl lnositol Phospho Ceramides (GIPC) and Glucosyl Ceramides (GluCer) (Fig. 3 c). Interestingly, a parallel increase of Steryl-glucoside (SG) and free sterols was also detected in Myriocin treated cells, suggesting that by inhibiting the synthesis of sphingolipids the treatment with Myriocin may have induced a shift in the utilization of glucose (less GluCer and more SG) and an increase in free sterol and SG content to compensate the decrease of sphingolipids in the membranes/membrane domains (Fig. 3 c).

All lipid analysis in control and treated pollen tubes were performed by Prof. Patrick Moreau and Prof. Lilly Maneta-Peyret at the Laboratoire de Biogenèse Membranaire, Université Bordeaux Segalen.

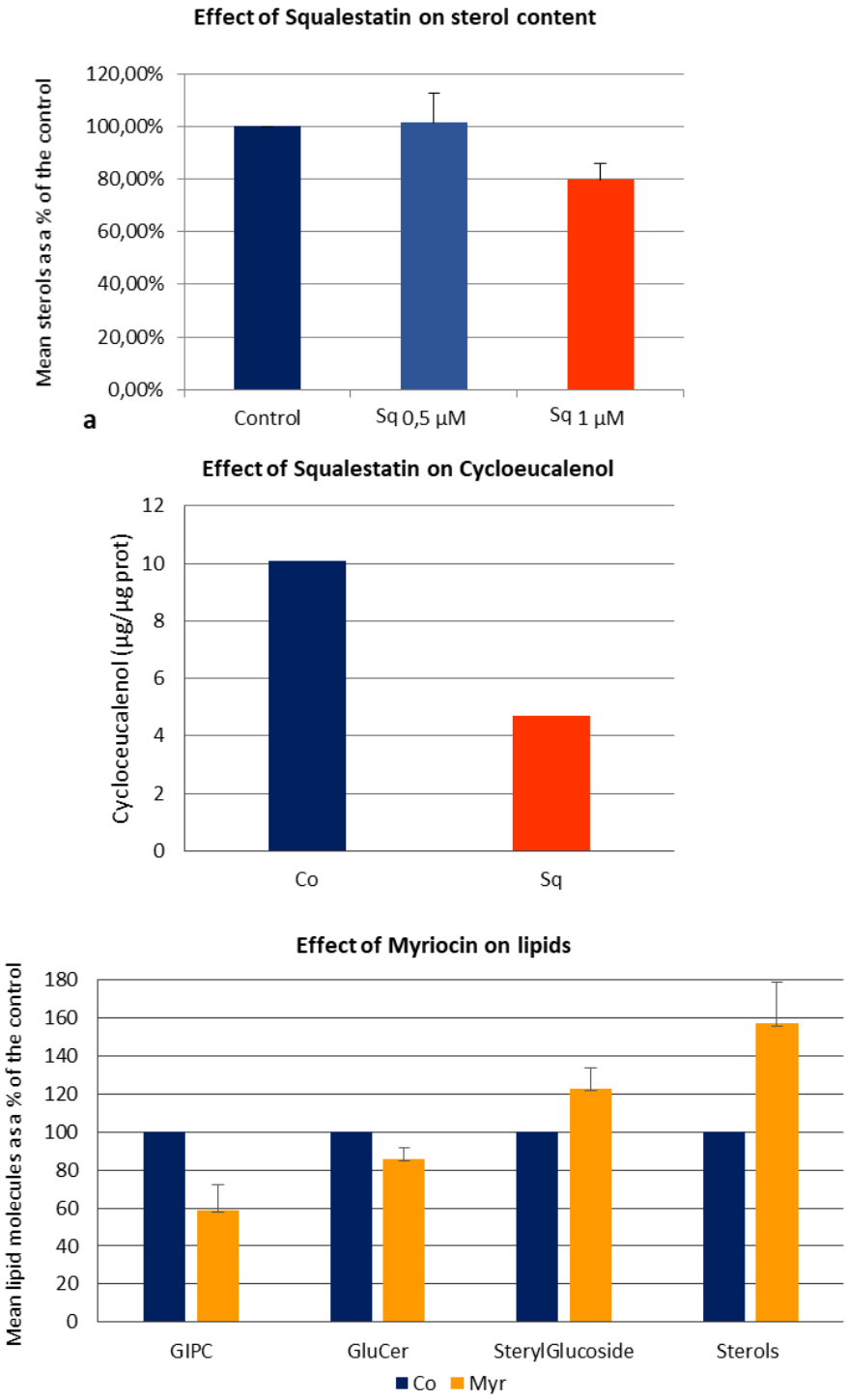

Fig. 3 Lipid analysis (a) Squalestatin (1µM) significantly reduces the content of sterols in P2 (mean values as a percentage of control, N= 8) . **(b)** *De novo* synthesis of cycloeucalenol was affected by 1µM Squalestatin (N=2). **(c)** Myriocin 5µM significantly affects the level of Glycosy lnositol Phospho Ceramides (GIPC) and Glucosyl Ceramide (GluCer). On the other hand, an increase of both Steryl Glucoside and total sterols is observed (mean values as a percentage of control, N>3). All lipid analysis were performed by Prof. Patrick Moreau and Prof. Lilly Maneta-Peyret; Laboratoire de Biogenèse Membranaire, Université Bordeaux Segalen.

The effect of sterol and sphingolipid depletion on protein profile of microsomes (P2) and soluble (S2) fractions was also investigated; one-dimensional gel electrophoresis did not reveal any difference in the polypeptide pattern between Squalestatin or Myriocin treated pollen tube, with respect to control (Fig. 4A, B, compare protein profile of Control with Sq or with Myr), suggesting that these drug concentrations affect the lipid profile without causing a dramatic alteration in protein expression.

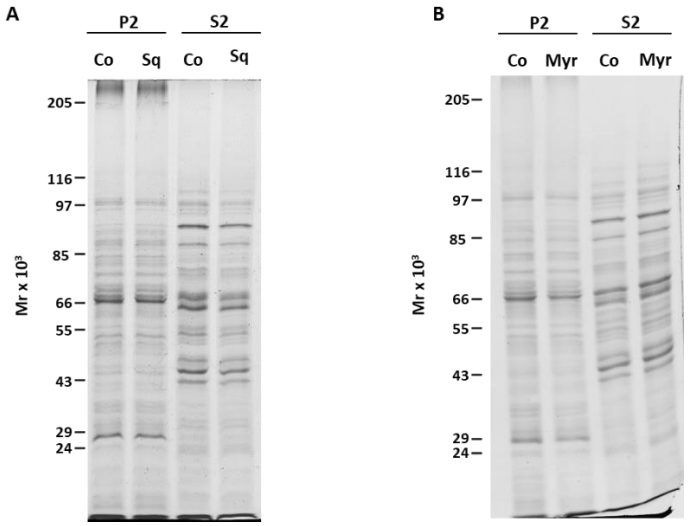

Fig. 4. Effect of Squalestatin and Myriocin on polipeptidic profile of membrane (P2) and soluble (S2) fractions. Pollen tubes treated with Squalestatin **(A)** and Myriocin **(B)** do not show modifications in polypeptidic pattern.

Previous data showed that sorting of sterol-sphingolipid enriched domains to the apical PM of polarized cells occurs in the TGN (Simons and van Meer, 1988; Simons and Ikonen, 1997; Surma et al., 2012). Additional evidence suggests a more complex scenario, in which oligomerization of GPI-anchored proteins on Golgi membranes leads small raft domains to coalesce into more stable platforms, that in turn contribute to membrane curvature and vesicle fission during apical sorting (Paladino et al., 2004; Paladino et al., 2007). In pollen tubes of angiosperms, post Golgi trafficking leads to the accumulation of SVs in the clear zone, a prerequisite for vesicle fusion to the apical plasma membrane (Hepler and Winship, 2015); thus, it is likely that changes in sterols or sphingolipids content could alter lipid rafts and modify tip secretion and pollen tube growth.

To investigate whether sterol or sphingolipids depletion affect pollen tube growth, the length of control and treated pollen tubes was measured after 2 and 2.5 hours, in the absence or in the presence of Squalestatin or Myriocin, respectively. Pollen tubes germinated and grown in the presence of 1 µM Squalestatin or 5 µM Myriocin were significantly shorter than the control tubes in three different experiments (Student's t-Test < 0.001) (Fig. 5A, a; 5B, a); on the other hand, in observing the pollen tube morphology we did not detect a loss of polarity in drugs treated pollen tubes, with respect to control tubes (Fig.5A, b, c; Fig. 5B, b, c).

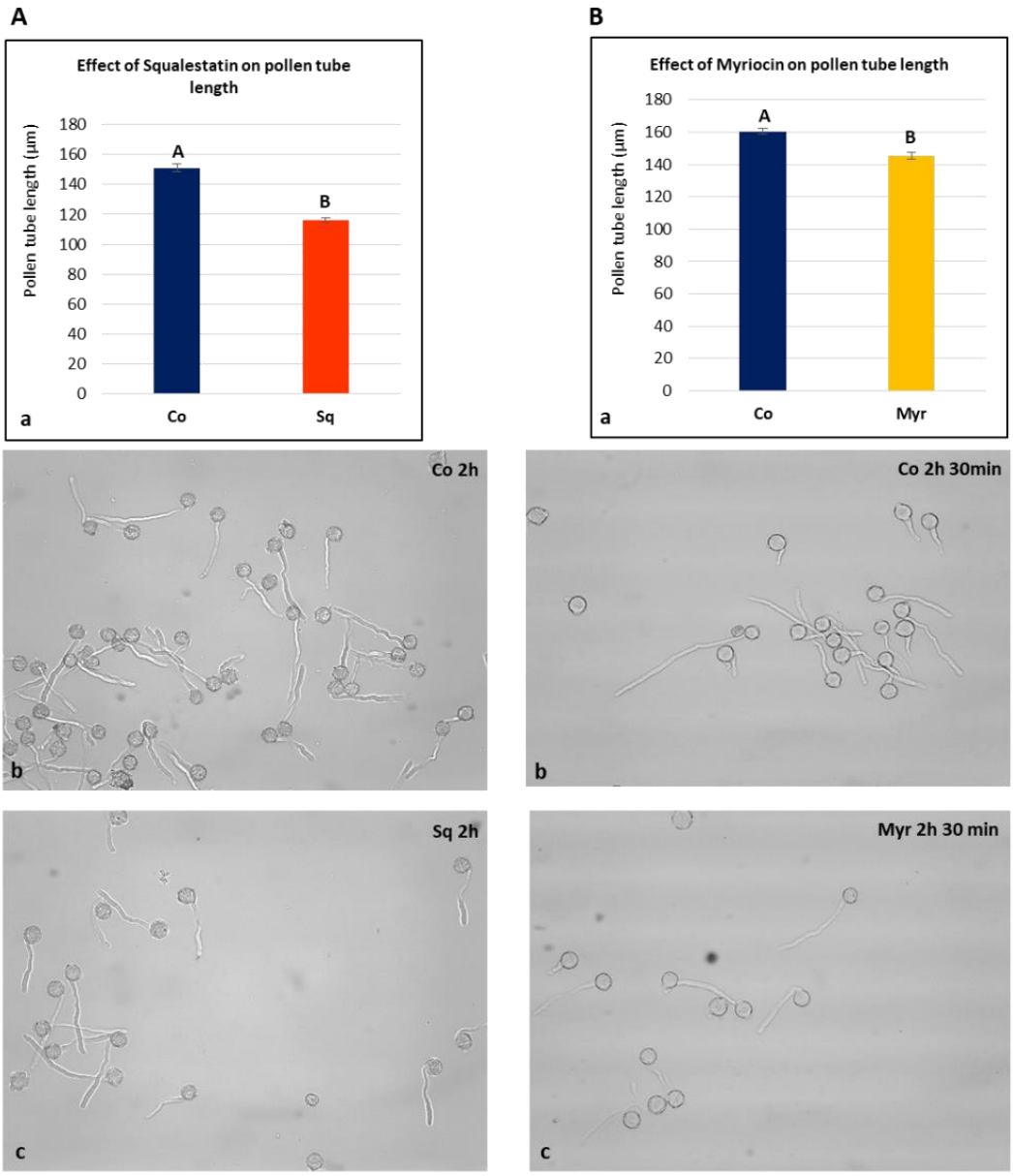

Fig. 5 Effect of sterols and sphingolipids depletion on pollen tube length. (A) pollen tubes grown in the presence of Squalestatin are significantly shorter than control pollen tubes (Student's t-Test <0.0001) (a); the morphology of pollen tubes does not reveal a loss of polarity at the tip (b, c). **(B)** pollen tubes grown in the presence of Myriocin are significantly shorter than control cells (Student's t-Test <0.0001) (a); the morphology of pollen tubes does not reveal a loss of polarity at the tip (b, c)

In addition, since *de novo* synthesis of cycloeucalenol was highly compromised in pollen tubes grown in the presence of 1 µM Squalestatin, germination assays were performed in order to highlight consequences on the germination rate. Data in progress suggest that sterol deprivation seems to affect the early stages of pollen tube emission and growth in tobacco pollen tubes.

Angiosperm pollen tubes show a distinctive pulsed growth occurring by alternating steps of vesicle fusion and tip expansion following a typical periodicity (Cardenas et a., 2008; McKenna et

al., 2009). Therefore, the extent of tip expansion depends on the concerted action of cytoplasm turgor pressure and cell wall stiffness (Hepler et al., 2013).

Data derived from sterol and sphingolipids inhibition could imply changes in the dynamics of the secretory pathway, leading to alterations of cell wall composition and stiffness and/or changes in turgor pressure, due to Ca^{2+} and proton fluxes (Hepler et al., 2013).

Squalestatin and Myriocin alter the morphology and dynamics of the actin fringe

Following the classical model of tube growth, Golgi-derived secretory vesicles are conveyed by cytoplasmic streaming to the apex where some of them fuse with the PM, reversing outside highly esterified pectins and new tracts of PM (Li et al. 1997; Helper and Bosch, 2005; Hepler et al. 2013). Distinct populations of AFs have been identified along pollen tubes and are involved in membrane trafficking: axial actin bundles in the shank and distal regions are responsible for the reverse fountain cytoplasmic streaming (Vidali et al., 2001; Cardenas et al., 2005), while in the apical flanks (2-5 µm from the apical PM), short, dynamic AFs are organized into the fringe, which has been shown to regulate targeting of SVs and pectin secretion (Lovy-Wheeler et al. 2005; Rounds et al. 2014).

The localization of L_o domains in the apical region, together with previous studies showing that 50% of P2 actin is localized in DIMs (Moscatelli et al., 2015, see FigS3), have led to a hypothesis that modification of lipid rafts could influence the actin state in the apex and consequently in the secretory pathway. In light of this evidence we decided to explore whether changes in pollen tube elongation involve the organization and dynamics of the actin fringe.

To investigate this point, pollen grains were transiently transformed using a plasmid which codifies for the fusion protein Lifeact-EGFP under the control of the pollen specific promoter LAT52 (Vidali et al., 2009). Control and treated pollen tubes display a cortical actin fringe in the apical flanks, characterized by short AFs (Fig. 6A, compare upper with medial and lower panels); however, the analysis of images obtained by time lapse experiments revealed that the mean area occupied by the actin fringe is significantly higher in Myriocin (N=14) and Squalestatin (N=11) treated pollen tubes, with respect to control tubes (N=17) (Fig. 6B, a; $P< 0.001$), suggesting that sphingolipid and sterol depletion modified the organization of the fringe, by increasing the number of AFs or by altering their distribution area in the apical dome. Whereas AFs of the fringe appeared more widely distributed with respect to control in Myriocin treated pollen tubes (Fig. 6A, compare upper and medium panel), in pollen tubes incubated with Squalestatin - despite the localization of the fringe being similar to that of control cells - it seems to be denser, suggesting an increase in the number of AFs (Fig. 6A, compare upper and lower panel).

Moreover, the comparison of the mean area occupied by the actin fringe over time showed that this difference is significant for each time point, also suggesting changes in fringe dynamics in pollen tubes incubated with drugs with respect to control tubes (Fig. 6B, b).

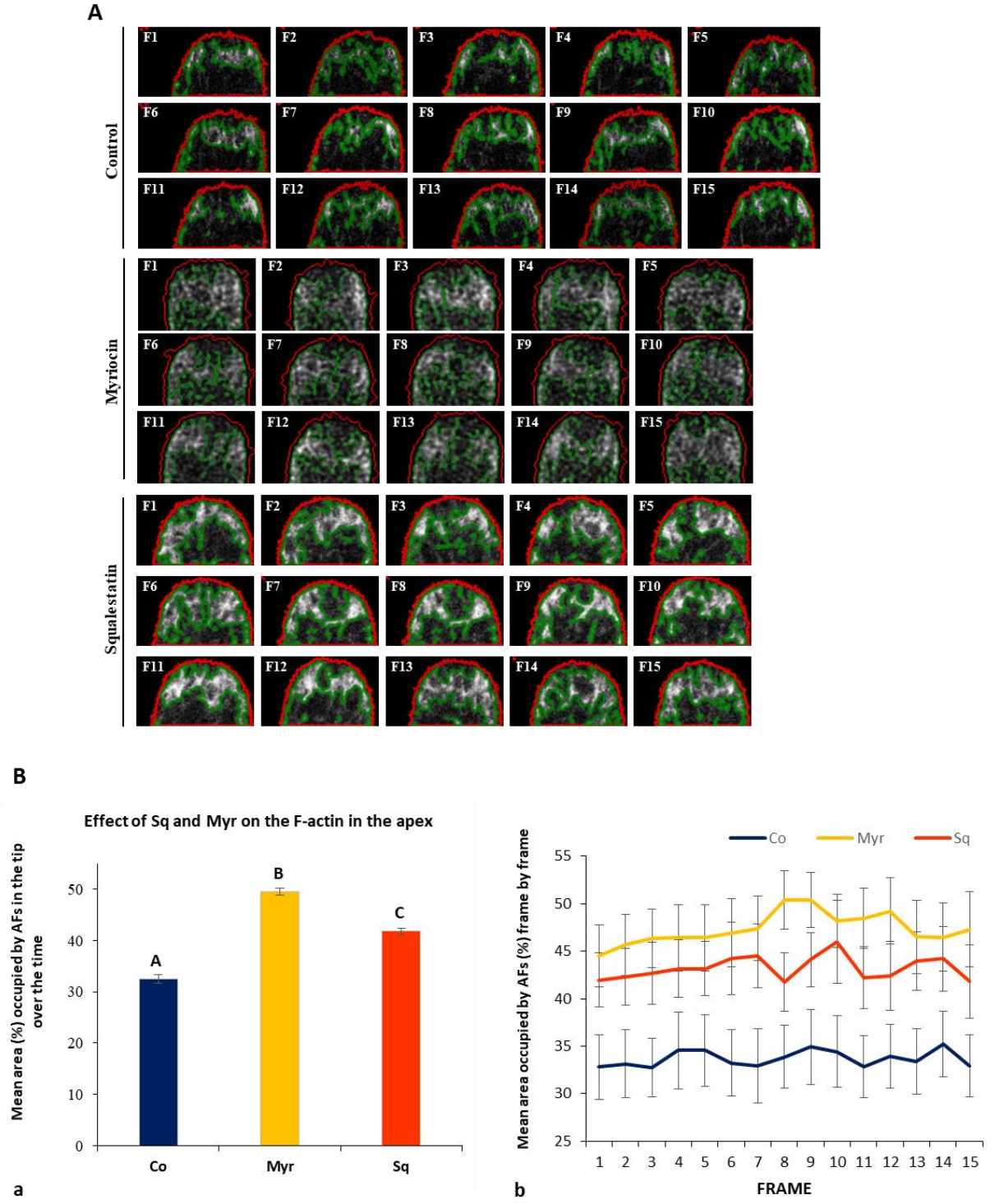

Fig. 6 (A) Analysis of cortical actin fringe in Control, Myriocin and Squalestatin treated pollen tubes (upper, medial and lower panel, respectively). Images was deconvolved with Huygens professional version 19.04 software and processed with CellProfiler software. ROI in red defines first 5 µm of pollen tube and area occupied by AFs is defined by the green line. **(B)** (a) The mean area (%) occupied by AFs is calculated for each treatment. The mean area occupied by the actin fringe is significantly higher in Myr and Sq treated cells, with respect to Control tubes ($P<0.001$). (b) Comparisons of the mean area occupied by AFs over the time show that this difference is significant for each frame.

Previous studies showed that about 50% of actin is associated with microsomes in control pollen tubes. To investigate whether Squalestatin or Myriocin modify the actin partitioning between membranes and soluble fraction, P2 and S2 from control and treated pollen tubes were assayed with an anti-actin monoclonal antibody. Western blotting analysis showed that, whereas Squalestatin significantly lowered the interaction of actin with microsomes (Fig. 7A, western blot and graph, $P<0.05$), in the presence of Myriocin, the interaction of actin with membranes was significantly enhanced (Fig. 7B, western blot and graph, $P<0.05$).

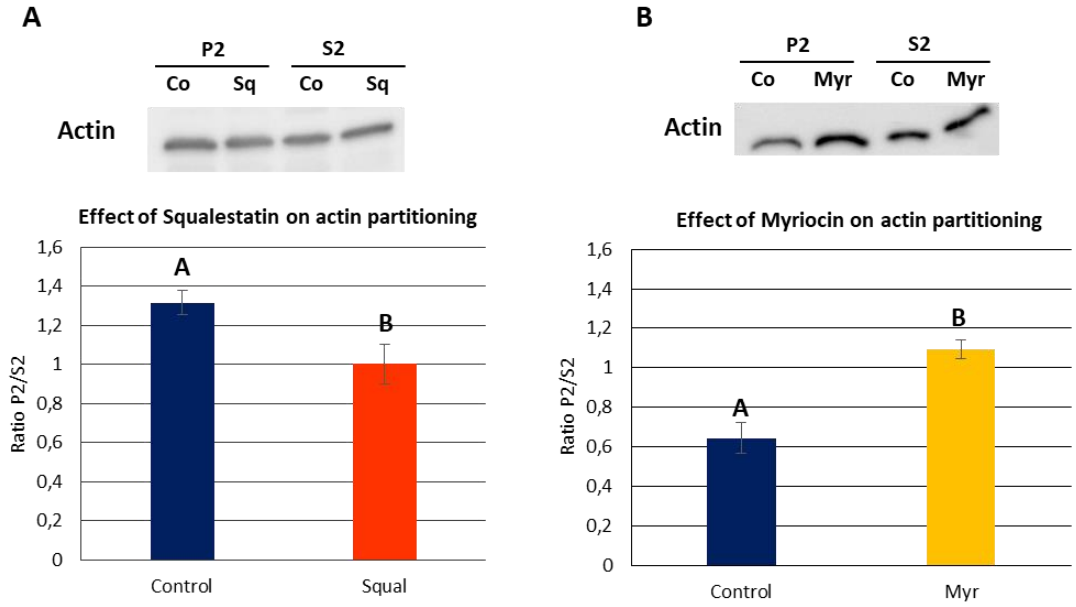

Fig. 7. Effect of Squalestatin and Myriocin on actin partitioning between membrane (P2) and soluble (S2) fractions. **(A)** Western blotting analysis, with an anti-actin monoclonal antibody, shows that Squalestatin significantly lowered the interaction of actine with microsome (western and graph; $P<0.005$). **(B)** In Myriocin treated cells, the interaction of actin with membranes is significantly enhanced (western and graph; $P<0.005$).

As it is well established that the acto-myosin system is mainly responsible for long range movements of organelle and vesicles, modification of actin interaction with microsomes in cells treated with Squalestatin or Myriocin suggests that changes in lipid profile could alter membrane trafficking (see below).

The morphology and dynamics of the actin fringe in the tip region is controlled by molecular mechanisms that couple RhoGTPase-mediated signaling pathways with oscillation patterns of Ca^{2+} at the very tip, thus contributing to maintaining pollen tube polarity (Kost et al. 1999; Fu et al. 2001; Gu et al. 2005; Hwang et al. 2005; Lee et al. 2008; Li et al., 2018). Phosphatidylinositol monophosphate kinases, which synthesize PtdIns(4,5)P_2, have been identified as one of Rho effectors (Chong et al., 1994; Hartwig et al., 1995). Stimulation of PtdIns(4,5)P_2 synthesis by the activity of the Rho family of sGTPases could represent a pathway to couple actin organization and post-Golgi membrane traffic. Particularly, PtIns4,5P_2 regulates actin organization via its interaction with key

actin binding proteins such as profilin, gelsolin, and vinculin (Janmey, 1994). We could speculate that changes in lipid composition, and presumably in the organization of L_o domains, induced by Squalestatin or Myriocin, could have altered the amount or the distribution of RhoGTPases or PtIns4,5P_2 and/or their interaction with actin binding proteins, thus affecting the organization and dynamics of the actin fringe. It has been shown that the expression of a mutated, dominant negative form of RhoGTPase inhibits pollen tube elongation, whereas the expression of a constitutively active form redistributes RhoGTPase in a wider area of the apex, thereby inducing depolarized growth. These experimental conditions induced AFs disorganization in the apex and polymerization of long actin bundles in the tip, respectively (Kost et al., 1999; Fu et al. 2001; Gu et al. 2005; Hwang et al. 2005; Lee et al. 2008; Li et al., 2018).

In our experiments, pollen tubes with an altered lipid profile did not show long actin bundles extending in the tip region or changes in cell polarity, suggesting that modifications in the content of sterols/sphingolipids did not induce a dramatic increase in the presence or in the activity of RhoGTPases. On the other hand, variations in the organization of the actin fringe do not exclude a modification in some steps of the RhoGTPase/PtdIns(4,5)P_2 signaling cascade. In this regard, transient transformation experiments with the fluorescence-tagged Pleckstrin homology (PH) domain of human phospholipase C (PLC)δ1 (Kost et al., 1999), which can serve as a PtdIns(4,5)P_2 specific reporter, could reveal changes in the distribution of this signaling lipid. In addition, more experiments are necessary to investigate how the distribution of PtdIns(4,5)P_2 influences the activity of actin-binding proteins and, accordingly, the organization of the actin fringe.

Studies of actin dynamics *in vivo* have shown that actin fringe remodeling during pulsed growth also occurs according to cyclic increases in cytosolic Ca^{2+} in the extreme tip (Gu et al. 2005; Hwang et al. 2005; Lee et al. 2008; Cardenas et al., 2008; McKenna et al. 2009; Cheung et al. 2010; Rounds et al., 2014).

The interplay between PtdIns(4,5)P_2 signaling pathway in the apical PM and Ca^{2+} gradient provides an additional mechanism for regulating the actin assembly state in the growing domain. The maintenance of a polarized distribution of PtdIns(4,5)P_2 involves the function of Phospholipase C, which hydrolyzes PtdIns(4,5)P_2 into DAG and IP3 in the apical flanks of growing pollen tubes (Helling et al., 2006); there is ample evidence showing that IP3 is involved in regulating Ca^{2+} homeostasis during pollen tube growth (Franklin-Tong et al., 1996; Camacho and Malho, 2003). In vivo experiments using dyes specific for free intracellular Ca^{2+} will be necessary to reveal possible changes in Ca^{2+} fluctuations in pollen tubes after treatments with Squalestatin or Myriocin.

Pulsed growth comprises steps of SV fusion with the apical PM alternating with phases of tip extension. The extent of the latter depends on cytoplasm hydrostatic pressure, which, in turn, is

regulated by Ca^{2+} and proton fluxes (Hepler et al., 2013). In addition, the activity of proton ATPases in PM regions behind the very tip induces the formation of an alkaline band, which contributes to the building of the actin fringe (Lovy-Wheeler et al., 2006; Certal et al., 2008).

All these considerations highlight that modification of actin organization and dynamics in the apex could result from different, interconnected molecular pathways. As outlined, our results open many perspectives for studying the role of lipid rafts microdomains in regulating polarized proteins distribution and activity and the organization of actin cytoskeleton.

The organization and dynamics of the actin fringe has been directly correlated to secretion. Low concentrations of LatB (1-2 nM) induce actin fringe depolymerization but maintain the integrity of actin bundles and the cytoplasmic streaming in the shank and distal regions; in these experimental conditions pulsed growth shifted into continuous basal growth in lily pollen tubes (Vidali et al., 2001; Cardenas et al., 2008; Vidali et al., 2009; Rounds et al. 2014). More studies, using Brefeldin A and Potassium Cyanide (KCN), further supported a direct correlation between polarized secretion and actin fringe integrity (Rounds et al., 2014). In particular, in the presence of KCN, which dissipates the actin fringe, the pattern of pectin secretion is more diffuse, involving a wide area of the apex (Rounds et al., 2014).

Thus, modifications in the cycle of actin fringe dynamics could alter pulsed growth and could be one condition affecting post-Golgi secretion during the pollen tube growth.

Levels of sterols and sphingolipids regulate cell wall deposition

Pectin deposition

Retarded pollen tube growth might involve modifications on cell wall deposition. The pollen tube wall consists of a primary pecto-cellulosic wall and a secondary callosic wall, which is deposited as an inner sheath behind the tip (Li et al., 1994; Taylor and Hepler, 1997; Hepler et al., 2001). Pectins appear to be major components of the cell wall at the tube tip; in particular, pectins are secreted at the tip, in their highly esterified form (Lord, 2000). De-esterification of pectins occurs behind the growing tip, thanks to the activity of the enzyme pectin methylesterases (PME); de-esterification exposes pectin carboxyl residues, which can be cross-linked by calcium, increasing the cell wall stiffness (Derksen et al., 1995; Li et al. 1997). Two isoforms of PME have been identified in tobacco pollen tubes and early studies by immunogold labeling suggested that esterified pectins and PME colocalized in Golgi-derived SVs, supporting the hypothesis that PMEs could be transferred to the cell wall in a precursor form and be activated at the tip during pollen tube growth (Li et al., 2002; Giovane et al., 2004; Bosch and Hepler 2005). More recently, data on post-Golgi membrane trafficking actually

suggests that different pathways are involved for the transport of highly esterified pectins and PME to the apical PM; whereas pectins could be delivered to PM through the sorting activity of TGN, secretion of PME could not involve the TGN (Wang et al., 2016), but, on the contrary, a sorting activity in the clear zone (see below, chapter on RaA4d).

Pectin methylesterases (PMEs) catalyze de-esterification of pectins in the apoplasm, thus regulating dynamic changes in cell wall rigidity/extensibility, during the pollen tube growth (Hepler and Bosch, 2005; Hepler et al., 2013).

To test the effect of sterols and sphingolipids modification on pectin secretion, immunofluorescence assays were performed on control and Squalestatin or Myriocin treated pollen tubes, using the monoclonal antibody JIM7, which recognizes highly esterified pectins. Whereas somatic cells of *Arabidopsis* mutants, with deficiencies in sterol biosynthesis, did not reveal alterations in pectin deposition (Schrick et al., 2004), in tobacco pollen tubes modifications of the lipid profile dramatically altered the deposition of highly esterified pectins.

According to previous observations (Bosch et al., 2005), esterified pectins were more concentrated in the tip regions compared to the shank, both in control cells and in cells incubated with drugs (Fig.8A, a-f). Quantification of fluorescence intensity in the tip and the shank (Fig.8A, a; white and yellow ROIs, respectively) showed that both Myriocin and Squalestatin induced an increase of esterified pectins in these regions (Fig.8B, a, c). Moreover, the ratio analysis of tip versus shank fluorescence intensity showed that the difference in esterified pectins between these regions is maintained in pollen tubes incubated with Myriocin and Squalestatin (Fig. 8B b, d), suggesting that the increase in secretion of esterified pectins was not accompanied by a concomitant increase in secretion of PME, thereby supporting the hypothesis of distinct secretory pathways for the two cargoes. Further *in vivo* experiments will be necessary to study the effect of a modification of lipid profiles on PME secretion.

The increased amount of esterified pectins in treated pollen tubes suggests that modification of the lipid profile could promote post-Golgi SVs targeting/fusion with the tip PM, with respect to control tubes. This alteration could derive from changes in the sRhoGTPase activity at the PM which, in turn, regulates the presence of PtdIns(4,5)P_2 in the apical PM, thus promoting the fusion of SVs. On the other hand, we have shown that the morphology and dynamics of the actin fringe is modified after lipid alterations. A more stable actin fringe could be responsible for maintaining a higher amount of post-Golgi SVs in the apical region, thus increasing their chance of interacting with the tip PM (Rounds et al., 2014).

In addition, increased secretion could also imply modifications in membrane trafficking at the Golgi apparatus and/or at the TGN level, which is directly involved in sorting pectin containing SVs

(Wang et al., 2016). Notably, both the morphology of TGN and of the clear zone are changed in treated pollen tube, with respect to control tubes (see below, chapters on membrane trafficking).

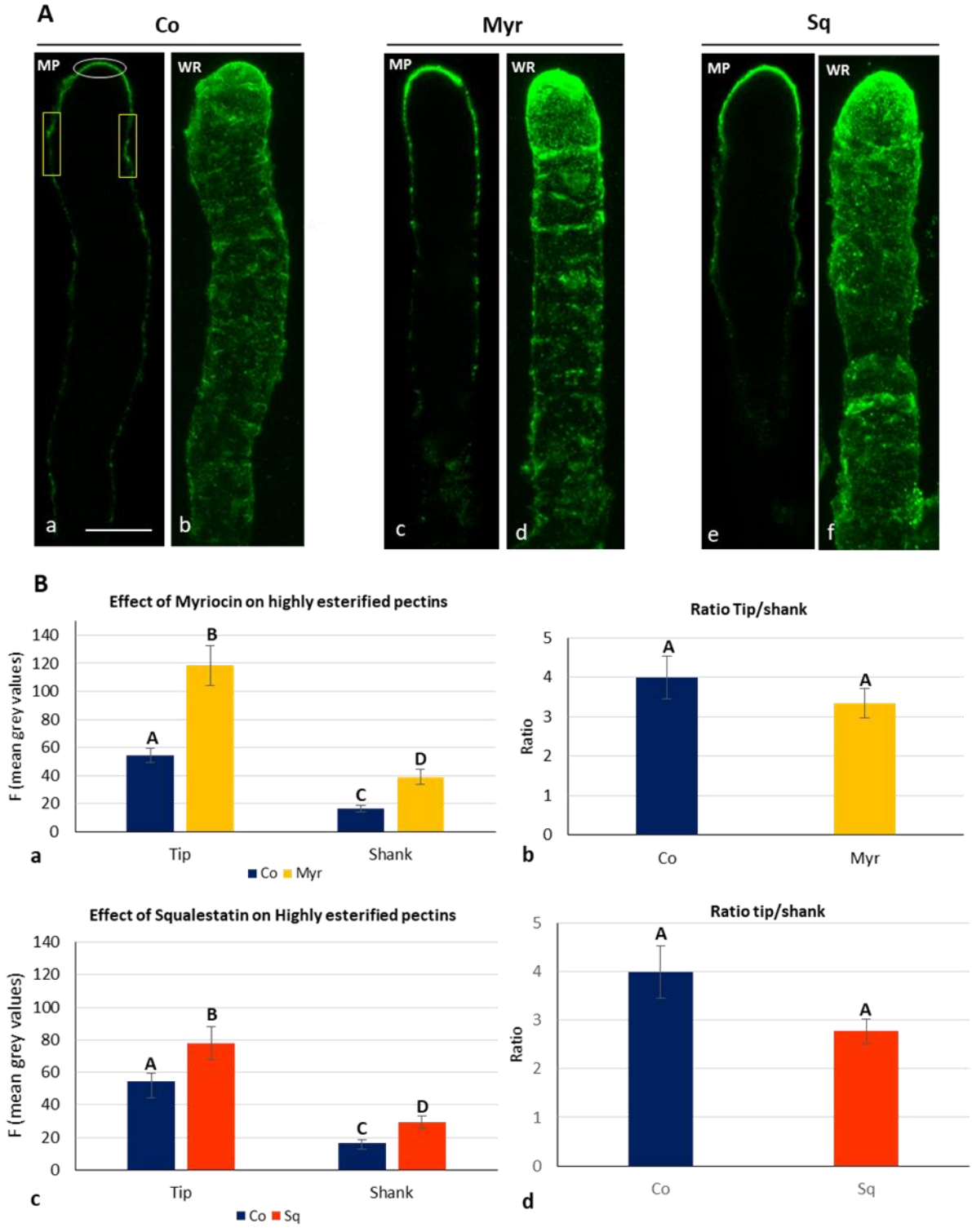

Fig. 8 Effect of Myriocin and Squalestatin on pectin secretion. (A) Distribution of methyl-esterified pectins determined by labelling with JIM7 antibody in Control (a, b), Myriocin (c, d) and Squalestatin (e, f) treated pollen tubes. Medial plane (MP). Whole reconstruction (WR). **(B)** Quantification of Fluorescence intensity in tip and shank (white and yellow ROIs, respectively, as shown in panel A, a) showed that both Myriocin and Squalestatin induced an increased in esterified pectins in these regions (a, c). The difference in esterified pectins between tip and shank is maintained in pollen tubes grown in presence of inhibitors (b, d). Bars = 10 µm.

Cellulose deposition

The primary cell wall of pollen tubes also comprises cellulose microfibrils, components that are highly resistant to tensile stress (Aouar, et al., 2010), and contribute to control the direction of cell expansion and the diameter of pollen tubes (Green, 1962; Chebli et al., 2012) during their travel toward the embryo sac for double fertilization (Geitmann, 2010; Chebli et al., 2012).

Formation of linear polymers of glucose β1-4 depends on the activity of the cellulose synthase complex (CSC), a transmembrane protein formed by multiple cellulose synthase catalytic subunits (CESA). CESA subunits become inserted in the apical PM upon the fusion of post-Golgi SVs (Cai et a., 2011; Chebli et al., 2012); in fact, rosettes of cellulose synthase have been observed by ultrastructural observations in the membranes of vesicles and Golgi cisternae, suggesting that CSCs are assembled before they reach the PM (Haigler and Brown, 1986) and are already active on SV membranes (Cai et al., 2011; Fayant et al., 2010; Chebli et al., 2012). However, the non-crystalline state of cellulose microfibrils secreted at the apex ensures that their secretion does not impair pollen tube extension (Aouar et al., 2010; Chebli et al., 2012).

In addition, several studies suggested that the lipid environment of CSCs regulates the organization and function of CESA within the PM lipid bilayer (Paradez et al., 2006; Gutierrez et al., 2009; Schrick et al., 2004; Schrick et al., 2012).

To analyze the effect of lipid modification on cellulose deposition, pollen tubes grown in control medium or in medium containing Myriocin or Squalestatin were stained using the fluorescent dye calcofluor white, specific for cellulose microfibrils. Fluorescence intensity was measured in the cell wall of the tip and the shank (Fig. 9A, a-c, see red and blue ROIs, respectively). In control pollen tubes a gradient of increasing fluorescence intensity was observed from the tip to the shank (Fig. 9A, a, b; Fig. 9B, a), confirming that cellulose deposition is more relevant in the latter rather than in the apex. Comparing control and treated cells, a significant increase in fluorescence intensity was observed in tip regions of pollen tubes germinated in the presence of both Myriocin and Squalestatin, with respect to control cells (Fig. 9A, d-g; Fig. 9B, a, b; $P< 0,05$). On the contrary, fluorescence intensity in the shank did not change in pollen tubes incubated with the drugs, with respect to control cells (Fig. 9A a-g; Fig. 9B, a, b). Interestingly, whereas the treatment with Myriocin does not alter the fluorescence ratio tip/shank, with respect to control cells (Fig. 9B, c), in pollen tubes grown in the presence of Squalestatin the tip/shank ratio is significantly higher than the control (Fig. 9B, d; $P<0,05$), suggesting a more pronounced effect of Squalestatin in cellulose deposition in the tip region, with respect to Myriocin.

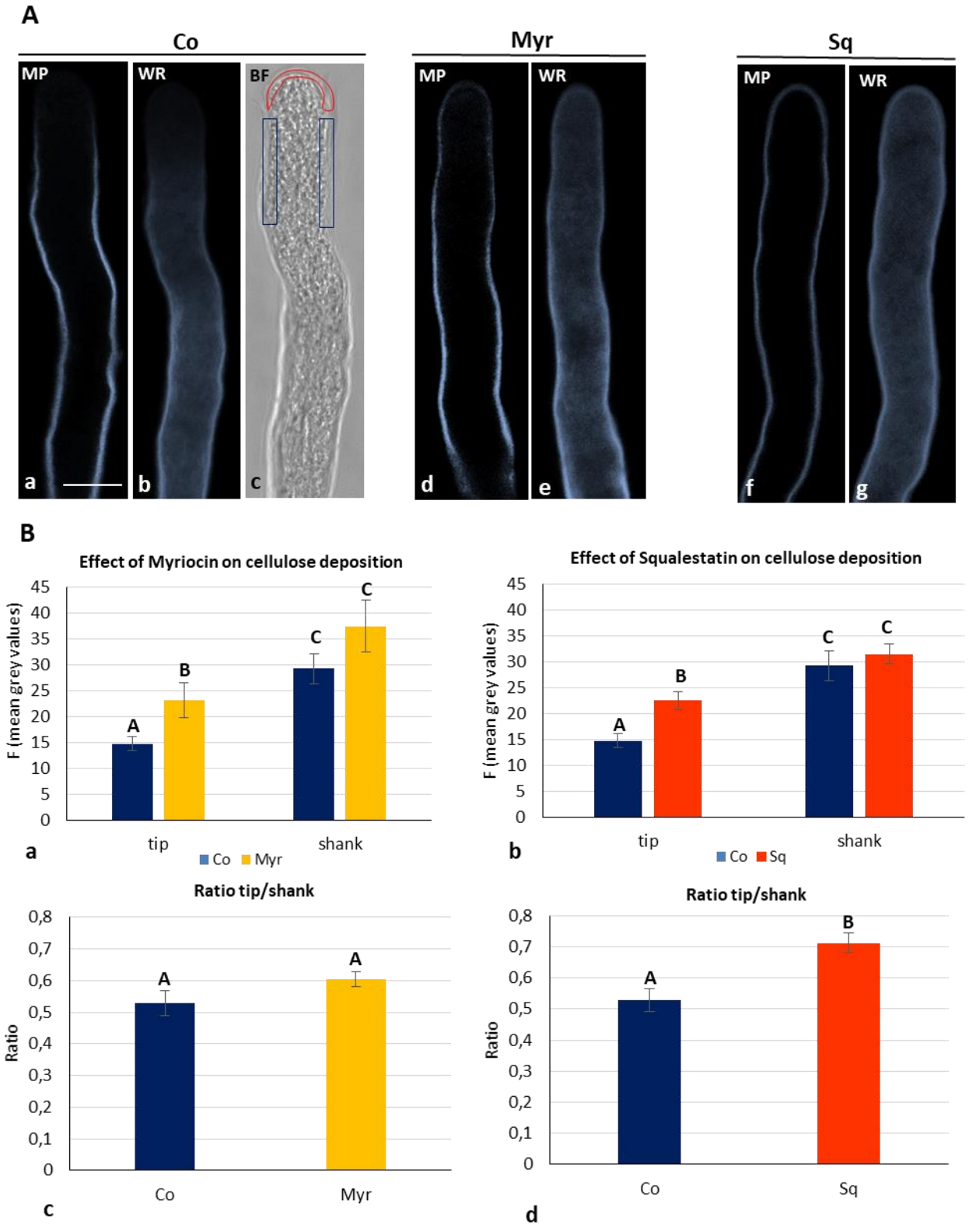

Fig. 9 Effect of Myriocin and Squalestatin on cellulose deposition. (A) Distribution of cellulose determined by staining with Calcofluor white in control and treated pollen tubes (a, b; d, e; f, g). While a gradient of increasing fluorescence was observed along the tube in control cells, in pollen tubes grown in the presence of inhibitors a more intense fluorescence also appears in the tip region. **(B)** Fluorescence intensity was measured in the tip and shank cell wall (ROIs red and blue, respectively as reported in A, c). A significant increase in fluorescence intensity was observed in Myriocin and Squalestatin treated pollen tubes (a, b); $P<0.05$. Myriocin does not modify the fluorescence tip/shank ratio with respect to control cells (c); in the presence of Squalestatin the tip/shank ratio is significantly higher than the control (d); $P<0.05$). Bars = 10 µm.

In DIMs isolated from tobacco pollen tubes, sterols and GluCer were enriched three and two times respectively, with respect to microsomes (Moscatelli et al., 2015). Myriocin and Squalestatin alter the lipid pattern in different ways (Fig. 3), suggesting, in any case, that a dramatic modification of lipid rafts activity leading to changes in cellulose deposition could depend on the alteration of sterol/sphingolipid ratio. Studies on *Arabidopsis* mutants, showed that defects in sterol biosynthesis affected cellulose deposition in somatic cells, as sterols represent the first acceptor of glucose (to produce steryl glucosides) in the nucleation phase of the formation of cellulose polymer by CSCs (Bessueille et al., 2009; Schrick et al., 2012).

The significant increase of cellulose in the apex of pollen tubes could be explained by considering the effect of Myriocin on the lipid profile. In fact, microsomes purified from pollen tubes grown in the presence of Myriocin had a decrease in GluCer/GIPC and a concomitant increase in total sterols, and particularly steryl glucosides, which could represent seeds for the increased nucleation of cellulose microfibrils in the tip region.

The use of the sterol biosynthesis inhibitor fenpropimorph showed that DIMs could still be present in the Golgi apparatus, but not in the PM in *Arabidopsis* somatic cells, suggesting a crucial role of DIMs in maintaining a proper post-Golgi secretory activity (Laloi et al., 2007). The increase of sterols, due to the effect of Myriocin, could also be responsible for increasing the secretion of CSCs in the apical flanks of growing pollen tubes (Bessueille et al., 2009; Schrick et al., 2012). CESA subunits are transported to the apex by the acto-myosin dependent cytoplasmic streaming as integral membrane polypeptides of SVs; here, it was postulated that they are captured by the actin fringe. The altered dynamics of the actin fringe in the tip region and the modification of the clear zone morphology could have a synergic effect in modifying the fusion of SVs at the apex.

In vivo transient transformation experiments, with constructs reporting CESA-fluorescent reporter proteins, should be carried out to study in detail the contribution of sterol increase on cellulose nucleation or in promoting SV formation/fusion. The increase of cellulose deposition in the apex, even if in a non-crystalline state, could impair the correct tip extension in pollen tubes incubated with Myriocin, and could be responsible for the reduced tube length observed with respect to control tubes (Fig. 5).

Callose deposition

During pollen tube elongation, a secondary cell wall, constituted by (1→3)-β-D-glucan (callose) is synthetized by callose synthase. The deposition of callose does not occur at the very tip of the pollen tube, but rather in the shank and the distal regions up to 2-3 μm behind the tip PM (Ferguson et al., 1998; Cai et al., 2011; Chebli et al., 2012).

Analyses of DIMs purified from poplar and tobacco revealed that, in addition to CSCs, callose synthase (CalS) is also highly enriched in PM lipid rafts microdomains (Bessueille et al., 2009). For this reason, we hypothesized that modification of sterol/sphingolipid content could also affect the presence or the activity of callose synthase. Callose deposition was studied in control pollen tubes and in pollen tubes grown with Myriocin or Squalestatin, using the callose specific fluorescent dye Aniline Blue. Analysis of fluorescence intensity, measured in the apex (up to 5 µm from the tip PM) and in the shank (from 5 µm to 30 µm from the tip PM) (Fig. 10A; red and blue ROIs for the tip and the shank, respectively), showed that in pollen tubes incubated with Myriocin the callose deposition at the tip was significantly lower with respect to control tubes (Fig. 10A, a-c, d-f; Fig. 10B, a) suggesting a modification in callose synthase secretion/activity at the pollen tube apex, with respect to the shank, where the amount of callose was similar in control and Myriocin-treated cells. The analysis of callose deposition along pollen tubes, from the very tip down to 30 µm from tip PM, was analyzed in more detail by ImageJ- Plot Profile analysis; values of mean fluorescence intensity (N>10) were plotted in the graph shown in Fig. 11, a. In pollen tubes grown in the presence of Myriocin, compared to control tubes, the slope of the curve is significantly lower over a distance of up to about 10 µm from the tip PM, suggesting that callose deposition occurs farther from the tip. On the other hand, no differences were observed in callose deposition between control and Squalestatin-treated pollen tubes (Fig. 10B b, d); moreover, the analysis of mean intensity fluorescence from the tip down to 30 µm from the apical PM also confirmed that sterol depletion by using 1 µM Squalesatin does not affect callose deposition (Fig. 11, a).

Previous data showed that sterols are present in the PM along the pollen tube, showing a higher concentration in the apex (up to about 10 µm from the tip PM); this distribution partly mirrors that of the L_o domains, which concentrate in the apical PM (until 20 µm from the tip PM) and then degrade toward distal regions in tobacco pollen tubes (Moscatelli et al., 2015). Besides a decrease in sphingolipid content, in pollen tubes grown in the presence of Myriocin, an increase of total sterols was observed, as a compensative mechanism (Fig. 3); thus, these alterations might have induced a disorganization of the lipid rafts microdomains and a wider distribution of sterols in pollen tube apex/shank. Changes in sphingolipid/sterol ratio in lipid rafts may have altered the activity of CalS along the pollen tube; alternatively, since lipid rafts are responsible for modulating actin fringe dynamics and membrane sorting in post-Golgi secretion, modifications in the lipid profile might alter the dynamics of secretory activity in the tip, leading to mislocalization of CalS secretion from the tip to the shank.

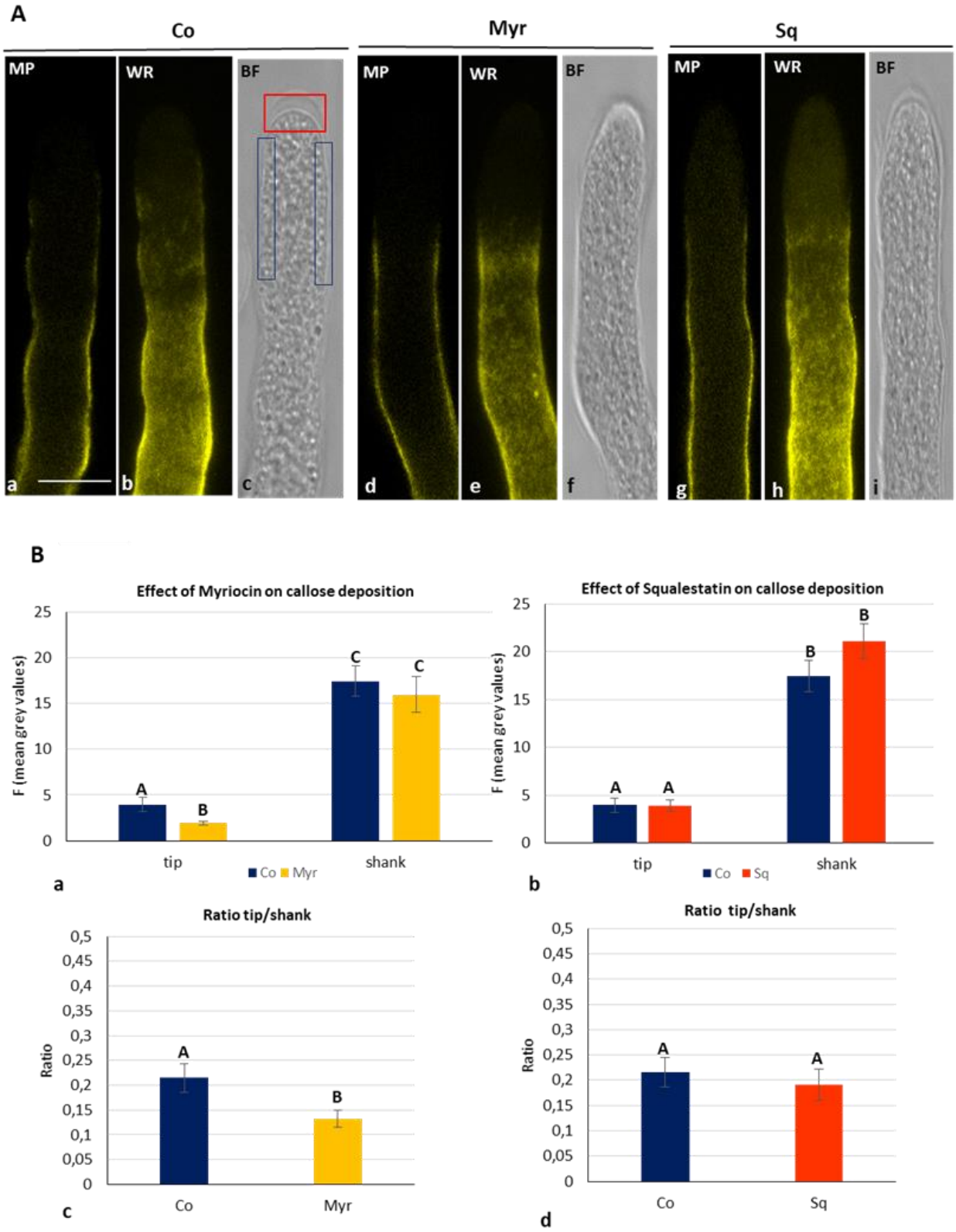

Fig. 10 Effect of Myriocin and Squalestatin on callose deposition. (A) Distribution of callose determined by staining with fluorescent dye Aniline Blue in control and treated pollen tubes (a, b; d, e; f, g). **(B)** Analysis of fluorescence intensity was measured in the apex (up to 5µm from the tip PM) and shank (from 5 to 30 µm from the tip PM), as shown in Fig.9A, c; red and blue ROIs respectively). In pollen tubes grown with Myr the callose deposition at the tip is significantly lower with respect to control tubes (a); $P<0.005$. No differences are observed in callose distribution between control and Squalestatin treated pollen tubes (b). In presence of Myr the ratio tip/shank is significantly lower (c), on the contrary, Sq does not modify the fluorescence ratio tip/shank with respect to control (d). Bars = 10 µm.

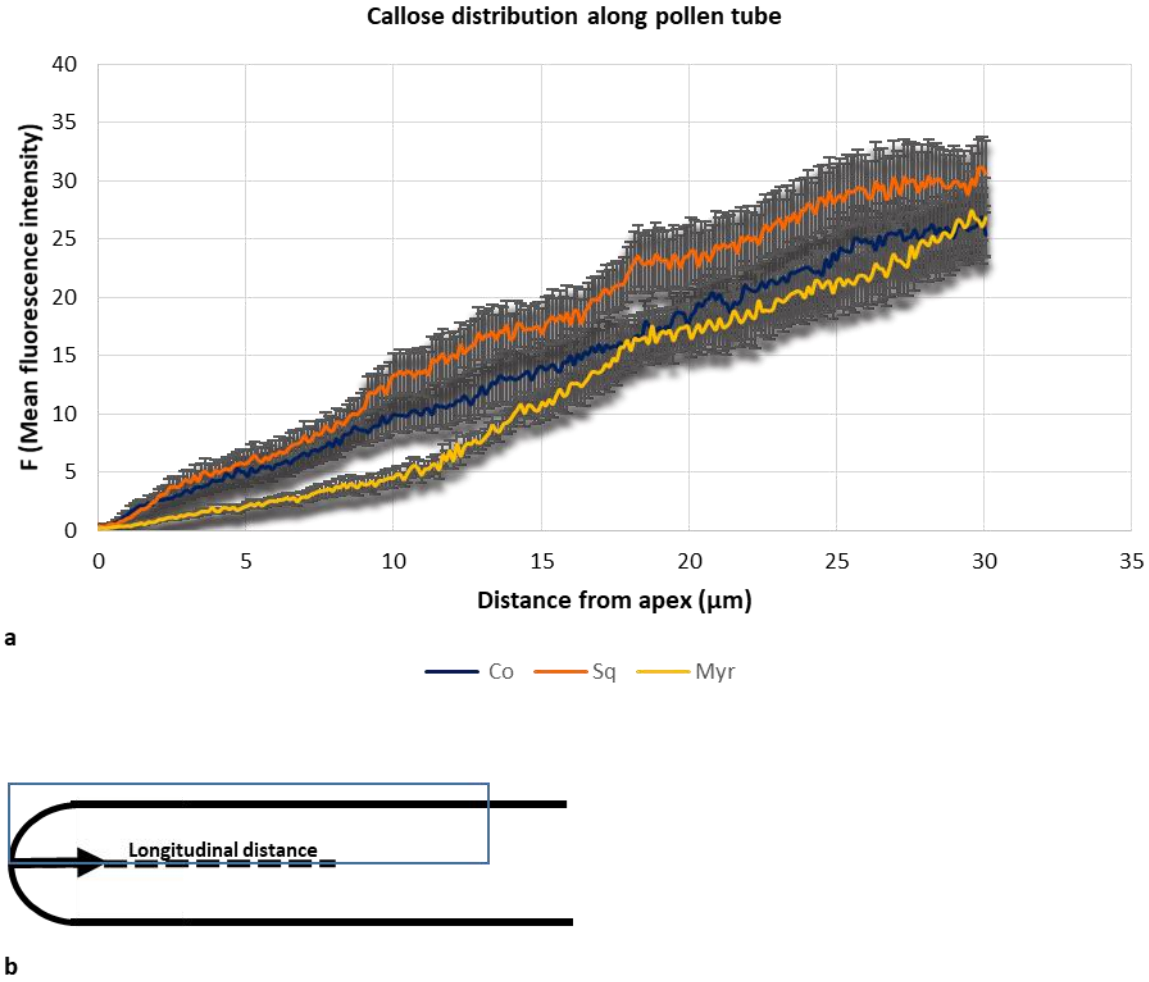

Fig. 11 Analysis of Aniline Blue fluorescence distribution as mesured by ImageJ, Plot Profile. (a) Each line represents the mean of grey values measured in all analysed pollen tubes (N>10). The y-axis represents the Mean Fluorescence Intensity, while the x-axis represents the distance from the pollen tube tip (0 point). Error bars represent SE. **(b)** To measure the Mean fluorescence intensity along the pollen tube edge (first 30 µm), a ROI was plotted as in fig. b and "Plot profile" analysis was used for measurment.

Investigating the morphology and dynamics of the clear zone

Growing pollen tubes exhibit an apical region, rich in vesicles and deprived of large organelles, called the clear zone (Hepler and Winship, 2015). The origin and maintenance of this region during the pollen tube growth, as well as its function, have been the object of study for a long time; early data allowed to hypothesize that the clear zone was filled with SVs, carried to the tip region by cytoplasmic streaming, occurring on long actin bundles which do not invade the tip; alternatively, short, fine actin filaments in the apex could be involved in trapping SVs, thus favoring their interaction with the apical PM (Heslop-Harrison et al., 1988). More recent studies have suggested a higher complexity, since it was shown that the clear zone also comprises tip-internalized endocytic vesicles and recycling vesicles (Helling et al., 2006; Moscatelli et al., 2007; Moscatelli et al., 2012). In particular, experiments of MT depolymerization by Nocodazole, allowed us to

hypothesize that the clear zone might be a further sorting compartment (Idilli et al., 2013) involved in the control of PM composition at the tip region, and in defining vesicles of the clear zone as transport vesicles, rather than simply SVs (Szumlanski and Nielsen, 2009).

As lipid rafts are believed to regulate membrane trafficking and given also that membrane trafficking within the clear zone could be directly involved in apical secretion, we decided to investigate the effect that sterol/sphingolipid modifications exert on the morphology of the clear zone *in vivo*.

To unravel the role played by lipid rafts in secretion, we transiently transformed pollen tubes with LAT52-GFPRabA4d. This protein belongs to the RabA4 subfamily of Rab sGTPases which are key regulators of membrane trafficking. RabA4d is specifically expressed in vesicles accumulating in the clear zone of growing cells, suggesting the involvement of RabA4d in regulating vesicles targeting/delivery and vesicles fusion at the pollen tube tip (Szumlanski and Nielsen, 2009). In addition, it has been shown that in tobacco pollen tubes, RabA4d colocalized with FM4-64, suggesting that it could be also involved in endocytic vesicles trafficking/recycling in the apical region (Szumlanski and Nielsen, 2009).

As expected, in transiently transformed LAT52-GFPRabA4d tobacco control pollen tubes, RabA4d is localized on vesicles accumulating in the clear zone (Fig. 12A, a-c), often with a "tail" extending in the shank, with the characteristic V-shape morphology. Perturbation of lipid rafts by 1 µM Squalestatin or 5 µM Myriocin induced an alteration of vesicles distribution in the tip (Fig. 12A, d-i; Fig. 12B, a-c). In fact, the sphingolipids depletion/sterol increase that is triggered by Myriocin seemed to reduce the area occupied by the clear zone, as vesicles appeared to be mostly concentrated in the tip dome with respect to control tubes (Fig. 12A, d-f; Fig. 12B, b). This morphological alteration was accompanied by a significant reduction in the mean fluorescence intensity respect to the control tubes ($p < 0.05$; Fig. 12B, d), while the mean area (%) occupied by RabA4d compartments appeared similar in control and pollen tubes treated with Myriocin (Fig. 12B, e). In addition, RabA4d-vesicle distribution in the shank of pollen tubes incubated with Myriocin appeared less defined with respect to control pollen tubes (Fig. 12A, d, e; Fig. 12A, a, b).

Treatment with Squalestatin induced a more severe modification of RabA4d-vesicle pattern distribution. Pollen tubes with a reduced quantity of sterols showed an expansion of the clear zone with the V-shape extending more deeply from the tip into shank/distal regions (Fig. 12A, g-i). An analysis of fluorescence intensity did not evidence differences in the apex between control and Squalestatin treated pollen tubes. On the contrary, a significant increase of the mean fluorescence intensity, along with an increase of the area occupied by RabA4d compartments in the shank, was detected in pollen tubes depleted of sterols, with respect to control ($p < 0.01$; Fig. 12B, d,e).

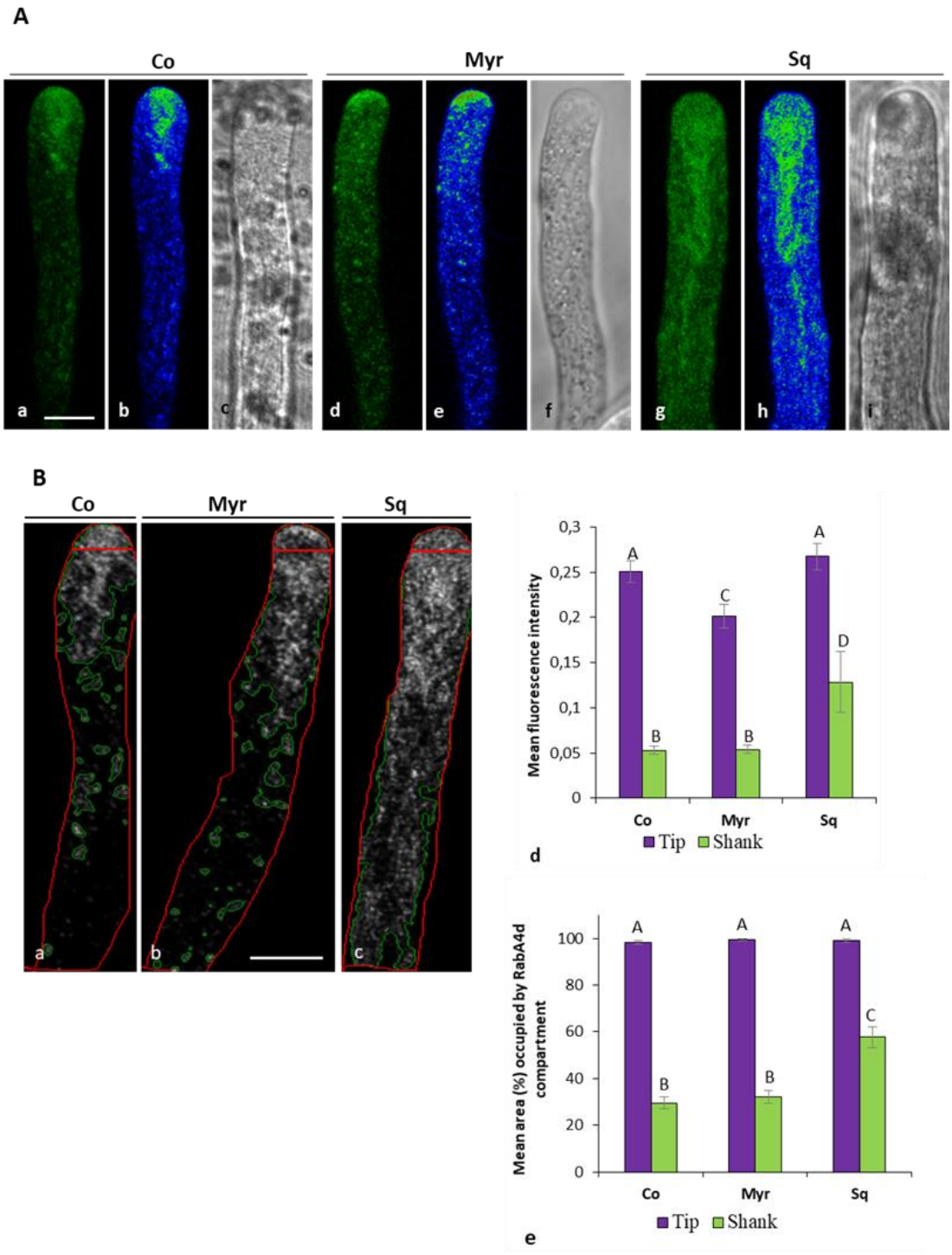

Fig.12 Analysis of morphology and dynamics of the clear zone. (A) Pollen tubes were transiently transformed with LAT52-GFPRabA4d. In control cells RabA4d localized on vesicles accumulating in the clear zone with the characteristic V-shaped morphology (a,b). In Myr treated pollen tubes vesicles appear mostly concentrated in the tip dome (d, e). With Sq an expansion of the clear zone with the V-shape extending more deeply from the tip to shank/distal regions is observed (g, h). Fluorescence intensity revealed by pseudo-coloured images in b, e, h. **(B)** Analysis of fluorescence intensity for each experimental condition on deconvolved images. ROIs in red define the first 5 µm of pollen tube tip, and the following 60 µm along shank and distal regions. Area occupied by fluorescence is defined by the green line (a, b, c). Myr induces a significant reduction in mean fluorescence intensity in the tip with respect to control tubes (d; $P<0.05$), while the mean area occupied by RabA4d compartments appeared similar in control and pollen tubes incubated with Myr (e). Sq induces, in shank and distal regions, a significant increase of mean fluorescence intensity and of the area occupied by RabA4d compartments (d, e; $P<0.01$). Bars 10 µm

As a whole, these data suggest that lipid raft perturbation results in a severe alteration of the morphology of RabA4d compartments and affects membrane trafficking in the clear zone. Specifically, although treatment with Myriocin did not induce a significant alteration in the area occupied by RabA4d, it modifies the distribution of RabA4d vesicles within this region, since an accumulation was observed in a restricted area at the vey tip, suggesting that changes in the sterol/sphingolipid ratio altered membrane trafficking within the clear zone.

On the other hand, the increase in RabA4d fluorescence intensity observed in both the tip and the shank after sterol depletion suggests that a delay/obstacle in fusion/recycling of transport vesicles occurred at the tip in treated cells. Consequently, a larger number of RabA4d vesicles were captured by the fountain reverse streaming to become widespread in shank and distal regions.

Interestingly, *raba4d* null mutants showed that this protein is also important for the proper trafficking/deposition of pectins into the cell wall (Szumlanski and Nielsen, 2009). In fact, in these mutants highly methyl esterified pectins were observed in both the tip and in regions distal from the tip, indicating that RabA4d plays a role in pectin delivery to PM. The pattern of pectin distribution observed after lipid raft perturbation (see above) mimicked that observed in the *raba4d* null mutant, suggesting that lipid rafts are involved in RabA4d vesicles trafficking and fusion to the PM. These data further support the hypothesis that the clear zone represents a sorting compartment for secretion/endocytosis/recycling events that occur at the very tip of the pollen tubes. Furthermore, it was observed that in the *raba4d* null mutant, callose distribution into the cell wall was not affected, suggesting different routes for pectin and callose synthase (CalS) secretion (Szumlanski and Nielsen, 2009) and, also, that exocytosis of CalS was RabA4d independent. The presence of different pathways for the deposition of distinct cell wall components was confirmed by the observation that in tobacco pollen tubes, PME is localized in compartments that are distinct from the conventional Golgi-TGN-PM trafficking. In fact, a different exocytic process mediated by a Golgi-derived transport compartments and independent by TGN for the polar secretion and targeting of PME has been recently identified (Wang H, et al., 2016). These differences in the secretory pathways could make it possible to maintain a pectin secretion pathway (Golgi-TGN-PM) separated from that of PME (Golgi –PM), to avoid early interaction between the enzyme and its substrate. (Micheli 2001; Wang et al., 2016).

Thus, the clear zone could represent a hub where different secretory pathways converge and, at the same time, it could also function as a sorting compartment to direct endocytic and SVs to diverse destinations.

It is possible to speculate that an altered ratio between sphingolipids and sterols could regulate the sorting function of the clear zone; in fact, besides the alteration of pectin distribution, treatment with Myriocin also induced a mislocalization of callose deposition (see above).

On the other hand, sterol depletion did not affect callose deposition, confirming that differentially modulated lipid profiles of rafts microdomains could regulate the secretory pathways of different cell wall components in different ways.

Moreover, detection of CalS activity in isolated DIMs and biochemical characterization of glucans synthesized in vitro by DIMs confirm the occurrence of CalS, as well as CESAs, in lipid rafts (Colombani et al., 2004; Bessueille et al., 2009; Morel et al., 2006). Alteration of lipid rafts could directly affect the delivery of CalS containing vesicles from TGN to PM.

Raft domains are involved in post-Golgi trafficking

The modifications induced in cell wall deposition by Squalestatin and Myriocin treatments suggested that secretion could be affected. In apical cells, this process was strictly associated to cytoskeleton and Golgi/TGN trafficking and functions.

Protein identification in pollen tube DIMs revealed that, besides actin, tubulin is also associated to rafts (Moscatelli et al., 2015). In pollen tubes microtubules play a role in endocytosis, exocytosis and in membrane trafficking (Idilli et al., 2013; Onelli et al., 2018). In fact, while actin filaments are responsible to drive the cytoplasmic reverse fountain streaming and to favor the fusion of SVs with the PM at the apex, microtubules contribute to the fine positioning of organelles and are involved in determining organelle morphology and shaping (Hepler et al., 2001; Brandizzi et al., 2013; Onelli et al., 2015). Specifically, MTs are involved in the control of endocytosis and secretion in the central domain of the tip (Idilli et al., 2013). In addition, MTs play a role in PVC delivery to and/or fusion with tubular vacuoles (Onelli et al., 2018). Proteins involved in membrane trafficking were also identified in pollen tube DIMs (Moscatelli et al., 2015). These proteins play a role both in ER-Golgi and in post-Golgi trafficking or in endocytosis.

Beside the roles of several protein machineries in the functional membrane organization and dynamics, in the last years several evidences from different eukaryotic models highlighted the relationships between lipid metabolism and membrane morphodynamics, showing lipids, enzyme of their metabolism and lipid-modified proteins as key regulators of membrane homeostasis on which the secretory pathway and the membrane trafficking depend (Moreau, 2007).

In model membrane it has been demonstrated that the sterol structure can affect membrane curvature and prepare membranes for budding or fusion events (Bacia et al., 2005); in animals cells, cholesterol has been shown to be involved in the biogenesis of secretory vesicles from the TGN

(Wang et al., 2000), and may be required to drive fusion events by virtue of its structure and physiochemical properties. (Churchward et al., 2005). In addition, cholesterol levels in mammalian Golgi membranes must be tightly regulated since an excess of this molecule can induce vesiculation of Golgi complex (Grimmer et al., 2005). In plant cells different evidences suggested a relationship between sterol metabolism and Golgi morphology; inhibition of sterol synthesis by Fenpropimorph blocks Cyclopropilsterol maturation in the ER, interferes with secretion and induces a fenestration effect of Golgi bodies (Hartman et al., 2002). In addition, disturbing Golgi morphology with BFA treatment reduces the synthesis of phytosterols (Mérigout et al., 2002).

In addition, sphingolipids may be critical for Golgi membrane morphodynamics in animal and plant cells (Fukunaga et al., 2000; Nakamura et al., 2001; Melser et al., 2010).

In tobacco leaf epidermal cells, inhibition of Glucosylceramide synthase induces a reduction in the intracellular transport of soluble and membrane proteins to the cell surface (Melser et al., 2010) and critical changes in the morphology of the Golgi bodies together with a retention of secretory proteins in the ER and Golgi membranes in *Arabidopsis thaliana* seedlings (Melser et al., 2010). In *Arabidopsis*, subdomains of TGN are characterized by differences in sphingolipids and sterols. TGN-associated secretory vesicles are enriched in sterols and sphingolipids with α-hydroxilated very-long-chain fatty acids (hVLCFAs) containing 24 or 26 atoms of carbon (Wattelet-Boyer et al., 2016). It has been shown that perturbation between hFAs that contain acyl-chain length ≥ 24 and fatty acids with a shorter acyl chain - without modifying the total amount of sphingolipids - leads to a loss of PIN2 polarity at apical membrane and to defects in the morphology and the interconnection of TGN-associated vesicles, which show an increased average diameter, appear more swollen and seem to remain in cluster (Wattelet-Boyer et al., 2016). Thus, these observations suggest that the secretory sorting of apical-localized proteins and sub-compartmentalization of TGN are influenced by the nature and the length of the acyl chains of sphingolipids.

All these evidences highlight the importance of sterols and sphingolipids enriched domains in the integrity of organelles involved in secretory pathway and in secretion itself.

To study the role of lipid rafts in secretion and post-Golgi trafficking in pollen tubes, transient transformation with the Golgi marker pLAT52–GFPRAB2 was performed with or without drugs affecting sterols and sphingolipids. Rab2 was shown to be expressed in the cis-face of Golgi apparatus (Cheung et al., 2002) and to be a major participant in ER-to-Golgi membrane trafficking. It has been observed that dominant-negative mutations of NtRab2 inhibited pollen tube growth and the normal localization patterns of different classes of marker proteins that entered the pollen tube secretory pathway, including Golgi resident proteins, cell membrane and secreted proteins. pLAT52–

GFPRAB2 transformation of control pollen tubes allowed to visualize round organelles with a mean area of 0.5 μm^2 (Fig. 13A, a; 13B, g), distributed in the shank and excluded from the clear zone (Fig. 13A, a, b). These organelles usually follow the reverse fountain streaming before returning to the distal area of the pollen tube (Cheung et al., 2002) and were observed up to 10 µm from the tip, in the shank area, and only rarely they reached the clear zone (Fig. 13B, h). Interestingly, Golgi bodies localized closer to the clear zone with respect to organelles marked with Rab2-GFP tagged protein, were observed by TEM (Idilli et al., 2013). It has been proposed that activities performed by Rab2 protein could be mostly required in cells with frequent secretory events, whereas they are not as critical in cells that do not exhibit a high secretion rate (Cheung et al., 2002). These evidences suggest that Golgi bodies close to the clear zone, revealed by electron microscopy observations, could not express high levels of Rab2 proteins. In this regard, since it was hypothesized that organelles distributed in different area of the pollen tube could play different functions (Onelli et al., 2018), the existence of Golgi bodies with different activities in the apex and in the shank/distal area is not unlikely. We could hypothesize that secretion could be mostly attributed to Golgi travelling along the actin filaments in the shank and distal area, while Golgi bodies immediately behind the tip could be involved in endocytosis/recycling of vesicles coming from the clear zone.

In tobacco pollen tubes, perturbation of membrane lipid composition did not affect Rab2-Golgi area and movement (Fig. 13A, c-f; 12B, g, h). In fact, the decrease of Golgi area induced by 5 µM Myriocin or its increase observed after 1 µM Squalestatin treatment, are not significant (Fig.13B, g).

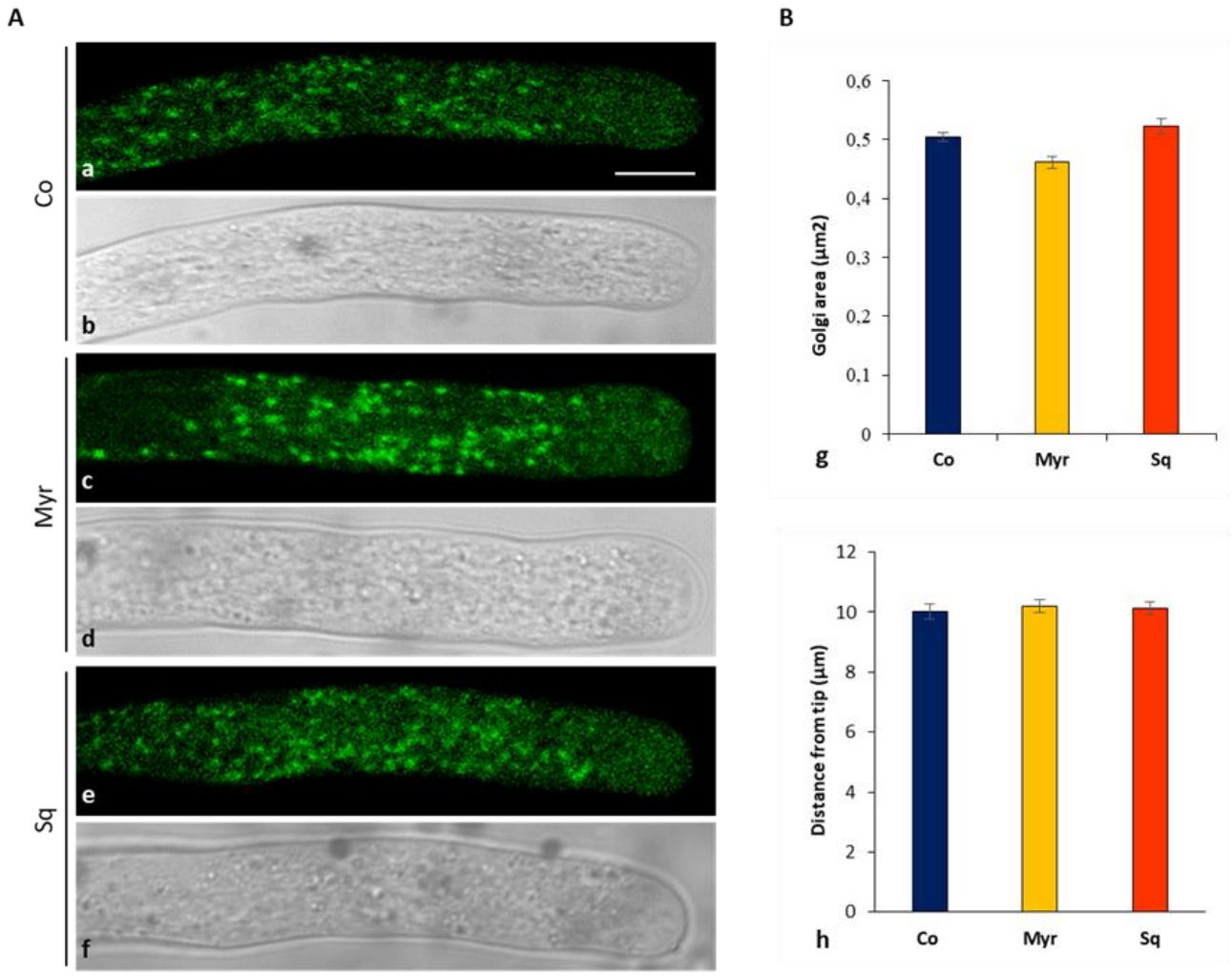

Fig. 13 Effect of Myriocin and Squalestatin on Golgi trafficking. (A) The fusion protein GFP–Rab2 allowed to visualize round organelles distributed in the shank and excluded from the clear zone, in control, Myr and Sq treated pollen tubes (a, c, e); bright field in b, d, f. **(B)** In control cells Rab2-compartments have a mean area of 0,5 µm^2 (g) and are observed about to 10 µm from tip (h). Depletion of sphingolipids and sterols do not influence Rab2-Golgi area and distance from the tip (g,h). Scale bar = 10 µm

In *Allium porrum* and *Arabidopsis thaliana* seedling cells, perturbation of both sterols and glucosylceramide synthesis induces alteration of Golgi morphology (Hartmann et al., 2002; Laloi et al., 2007; Melser et al., 2010). However, the sterols and sphingolipids inhibitors used in these studies are different from Squalestatin and Myriocin and operated at different steps of the lipid biosynthetic pathways. Furthermore, in tobacco pollen tubes, *de novo* synthesis of sterols involves only two different molecules: cycloeucalenol and an unidentified sterol with a mass of 412 Da, which was hypothesized to be methylenepollinastanol on the basis of its mass and the spectrum very similar to that of cycloeucalenol (Villette et al., 2015; Rotsch et al., 2017). It was observed that the amount of these sterols increases during pollen tube growth whereas the sterol species that are already present in the mature pollen are not synthesized *de novo* (Villette et al., 2015; Rotsch et al., 2017). The synthesis of cycloeucalenol and methylenepollinastanol requires less steps than the synthesis of

stigmasterol (observed at high level in plant somatic cells); it was hypothesized that the lower number of steps required to synthesize pollen tube specific sterols allows the fast pollen tube growth (Rotsch et al., 2017). Therefore, the induced perturbation of sterol synthesis might involve only these sterol species and may not be sufficient to affect Golgi morphology and function. In addition, sterols are synthetized in ER, assembled along with sphingolipids in rafts in the Golgi apparatus; then, rafts are clustered/segregated in the TGN and in vesicles budding from the TGN to be delivered towards the PM (Melser et al., 2010; Short 2009; Klemm et al., 2009). The increasing gradient of sterols observed from trans Golgi cisternae to the TGN vesicles (Melser et al., 2010; Short 2009; Klemm et al., 2009), suggests that Golgi bodies might not be the main organelle-target of sterol depletion.

In addition, we must consider that Rab2-GFP reporter protein allowed us to visualize only the cis face of the Golgi apparatus and in this regard, to investigate whether raft perturbation influences Golgi morphology, preliminary TEM observations of pollen tubes fixed by High-Pressure Freeze Fixation (HPFF) technique were performed. After Squalestatin treatment Golgi bodies showed a different morphology, with cisternae that appeared swollen and more distant from each other with respect to the control ones (Fig. 14 a, b). Morphometric analysis and observations on Myriocin-treated pollen tubes are also currently in progress.

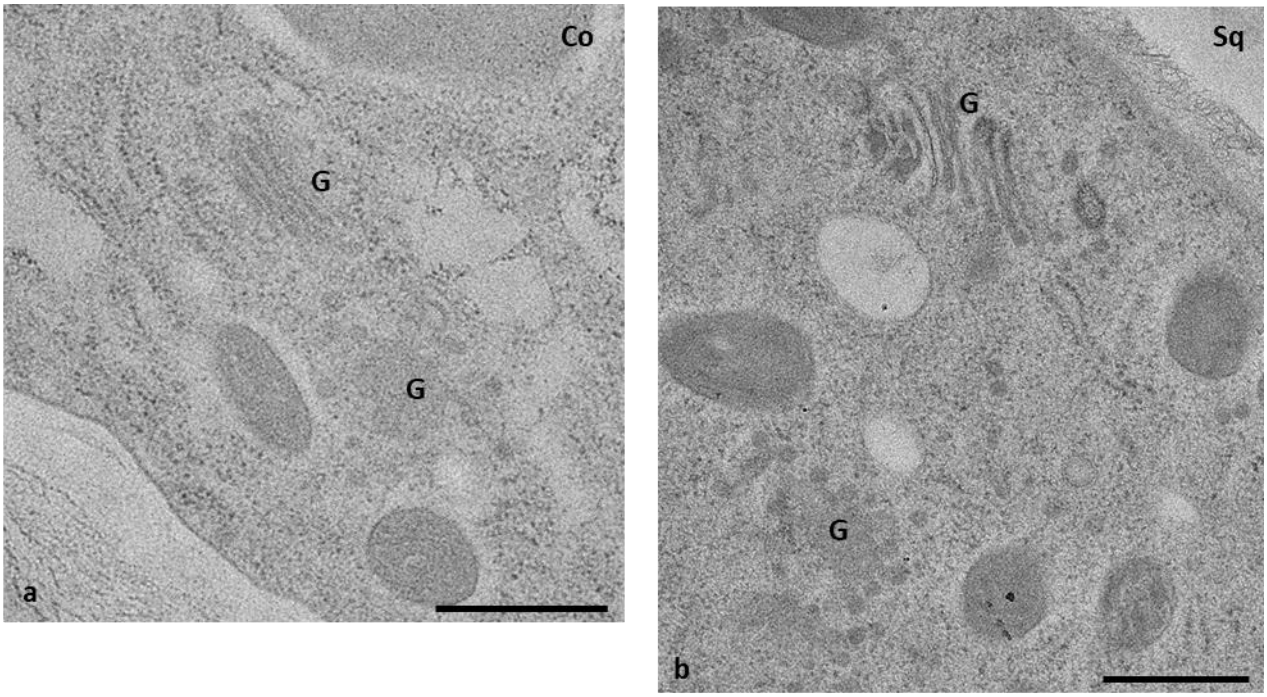

Fig. 14 Effect of Squalestatin on Golgi morphology. In pollen tubes grown in presence of Squalestatin Gogi bodies seems to show a different morphology. Cisternae appears swollen and more distant one from the other with respect to the control. Scale bars = 500 nm.

Finally, the distance of Rab2 positive Golgi from the tip was the same in control cells and in pollen tubes incubated with 5 µM Myriocin or 1 µM Squalestatin (Fig. 13B, h), suggesting that Golgi trafficking was not affected by sterols and sphingolipids alteration.

Therefore, it is possible to hypothesize that the association of actin with rafts domains did not occur in Golgi bodies, where rafts are not yet definitively assembled.

It is known that the lipid composition of organelles varies progressively throughout the secretory pathway; the ER displays a relatively low concentration of sterols and sphingolipids, which accumulate toward the PM (Simons and van Meer, 1988). In yeast it has been demonstrated that the TGN exhibits the ability to sort membrane lipids; this TGN sorting activity selectively enriches ergosterol and sphingolipids species in a population of secretory vesicles derived from TGN, carrying different cargos destined to PM (Klemm et al., 2009; Surma et al., 2011). These evidences, together with the observation that ergosterol and sphingolipids enriched vesicles show a higher membrane order than the late Golgi cisternae, suggest that lipid rafts do coalesce and concentrate into vesicles budding from the TGN (Klemm et al., 2009). Moreover, these data support a role of sphingolipids and sterols in polarity and polar delivery to PM.

To investigate if TGN is affected by sterols and sphingolipids depletion, pollen tubes were transiently transformed with the pLAT52–YFPSYP61 plasmid. Syp61 is a syntaxin, which defines a TGN compartment carrying cell wall cargoes (Drakakaki, 2015; Rosquete et al., 2018). Specifically, proteomic and cell biology analysis revealed that CESA travels towards PM in Syp61 positive vesicles (Drakakaki, 2015; Worden et al., 2015; Kang et al., 2011).

YFP-SYP61 revealed numerous organelles widely distributed in the pollen tubes, with the exclusion of the clear zone (Fig.15A, a-d). These organelles had a mean area of 200 nm^2 (Fig.15B, a) and *in vivo* observations revealed that they are distributed along the typical reverse fountain streaming. Compared to the Golgi bodies, Syp61-positive TGN travelled closer to the clear zone (Fig.15B, b), suggesting its involvement in the sorting of exocytic/endocytic vesicles. In order to study the effect of lipid raft perturbation on TGN, pollen tubes were treated with 5 µM Myriocin and 1 µM Squalestatin. The distribution of TGN in pollen tubes did not changed after drugs treatment (Fig.15A, e-l). Similarly, the decrease of sphingolipids, together with the increase of sterols, induced by Myriocin, did not affect the TGN area (Fig.15B, a). On the contrary, sterol depletion by Squalestatin induces a significant increase of Syp61 positive TGN area (Fig. 15A, a; $P<0.01$). Since Syp61 is localized in specific domains of the organelle (Klemm et al., 2009; Surma et al., 2011), the increase of TGN area suggests that sterol depletion could slow down the formation of vesicles addressed to the PM. This is in line with the evidence that lipid-lipid and lipid-protein interaction

could be also involved in budding of vesicles from the membrane surface (Itoh and Takenawa, 2009; Itoh and De Camilli, 2006) whereas it seems apparently in contrast with the increase of pectin secretion observed in tobacco pollen tube after lipid rafts perturbation (see above).

The higher secretion rate could not depend on TGN activity but rather on the stabilization of the actin fringe which could facilitate the secretory vesicles fusion events or on a different trafficking of vesicles at the tip as observed by RabA4d analyses. Vesicles marked by RabA4d in the clear zone belong to secretory and endocytic pathways. It is possible that endocytic vesicles also contained cell wall components. The accumulation of these vesicles in the raft-perturbed pollen tubes could make them available for immediate recycling in the flank, where a stable actin fringe could facilitate their fusion with the PM and thus the recycling of pectin to the cell wall.

In alternative, raft perturbation in Golgi bodies could induce an alteration of TGN maturation. The TGN/EE exists as Golgi-associated TGNs (GA-TGNs) at the trans-side of the Golgi stacks and as Golgi-independent TGNs (GI-TGNs), which are physically detached from the Golgi stacks (Viotti et al., 2010; Kang et al., 2011; Uemura et al., 2014). The proposed model assumes that the GA-TGN matures into the GI-TGN and then into secretory vesicles (Uemura et al. 2019; Renna and Brandizzi, 2020). Sterol depletion by Squalestatin in pollen tubes could affect GI-TGN budding from the GA-TGN allowing the formation of enlarged Syp61-TGN.

Trafficking of TGN in the apex of the pollen tube was also affected by lipids raft perturbation. Sterol depletion allowed TGN to arrive closer to the clear zone with respect to untreated pollen tubes (Fig.15B, b; $P<0.01$) while in Myriocin treated pollen tubes TGN stopped early in the shank (Fig.15B, b; $P<0.05$).

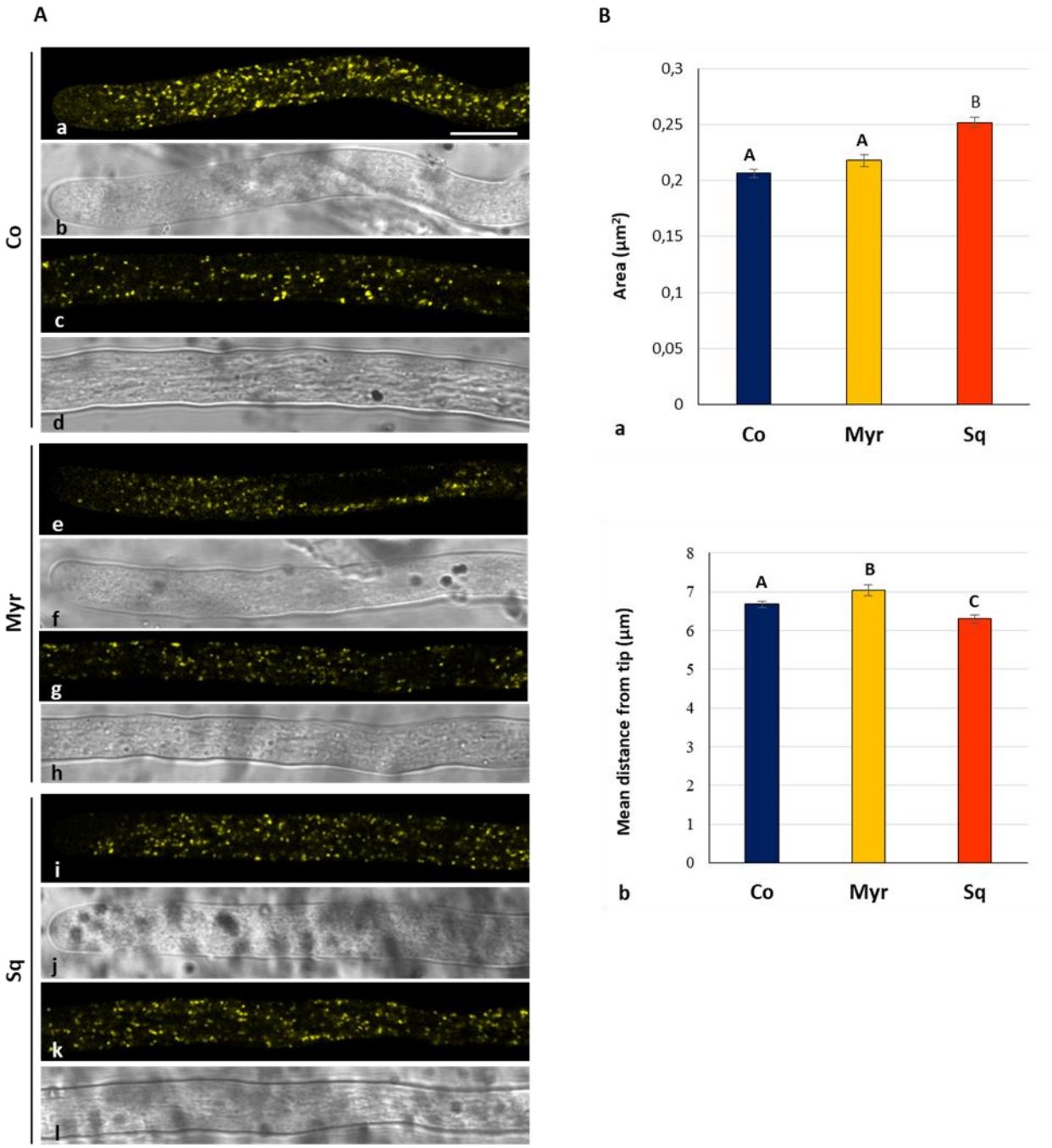

Fig. 15 Effect of sterols and sphingolipids inhibitors on TGN. (A) Transient transformation with pLAT52- YFPSYP61, shows numerous organelles distributed along distal and shank regions, but excluded from the clear zone (a-l). (B) Whereas Squalestatin induces a significant increase of Syp61-TGN areas ($P<0.01$), Myriocin does not affect TGN area (a). Trafficking of TGN in the apex is affected by lipid rafts perturbation(b). Myriocin and Squalestatin have opposite effect on the proximity to the clear zone: in Myr treated pollen tubes TGN stops early in the shank ($P<0.05$, n), while sterols inhibition allows TGN to travel closer to the clear zone with respect to the control cells ($P<0.05$, n). Scale bar = 10 µm

Alteration of TGN trafficking could be due to the modification of actin partitioning between microsomal and soluble fractions. In fact, biochemical analyses showed that Squalestatin and Myriocin treatments had opposite effect on actin interaction with membranes: after sterol depletion, the interaction of actin with membranes decreases, while in presence of Myriocin the association is

enhanced (see above Fig. 7). Raft perturbation could alter the association of TGN with microfilaments and so their trafficking in the pollen tube.

Modification of TGN trafficking in the pollen tube apex and the slowdown of vesicle formation after perturbation of sterol/sphingolipids ratio, suggest that lipid rafts in pollen tubes are involved in secretion and could be responsible for modification in the deposition of cell wall components which in turn affects pollen tube growth.

Sterols and sphingolipids depletion affects organelles involved in the degradation pathways

Biochemical and confocal observations evidenced that sterol-containing domains have been identified in membranes of isolated vacuoles in *Beta vulgaris* root (Nurminsky et al., 2017; Nesterkina et al., 2015; Ozolina et al., 2013) and in yeast (Hurst and Fratti, 2020). In addition, altered vacuole morphology has been observed in yeast mutants that are defective in sphingolipid synthesis (Faergeman al., 2004). Also in plants, an impaired sphingolipid biosynthesis might result in defects in vacuole biogenesis given that sphingolipids are enriched in the tonoplast in plant cells (Verhoek et al., 1983; Yoshida and Uemura, 1986).

It is therefore possible that if rafts are assembled in Golgi /TGN, in plant cells they are also involved in sorting toward the degradation pathways. This route goes through PVCs which maturation allows them to fuse with vacuoles (Onelli and Moscatelli 2013). Biochemical and confocal analyses revealed that in the pollen tube, delivery of PVCs to vacuoles and fusion with tubular vacuole is MTs dependent (Onelli et al., 2018).

Therefore, it could be hypothesized that raft perturbation affects degradation pathways altering organelle membrane composition and/or by modifying MT dynamics.

To investigate the involvement of rafts in the degradation pathways, pollen tubes transiently transformed with the pLAT52–YFPSYP21 plasmid were treated with 5 µM Myriocin and 1 µM Squalestatin.

In the pollen tube, SYP21 is a marker for round organelles, identified as PVCs, and for highly dynamic tubular vacuoles spanning pollen tube longitudinally (Onelli et al., 2018), (Fig.16A, a, b). It was hypothesized that SYP21-tubular vacuoles could function in the long-distance transport of molecules and/or as endosomal compartments in the pollen tube shank, while in the distal area they fuse to form large vacuoles (Onelli et al., 2018).

Lipid raft perturbation induced in pollen tubes a significant increase of the Syp21-PVC area (Fig. 16 B, a; $P>0.01$). The same effect was observed after MTs depolymerization suggesting that alteration of rafts could affect MTs dynamics and in turn induce an increase of the Syp21-PVC area. This increase could be probably due to the homotypic fusion of PVCs occurring before their fusion with

vacuoles. In fact, in *Arabidopsis* root hairs PVCs interact together, tethering transiently in a movement defined as dancing-endosome interaction, which allows PVCs to come close together, fuse and separate, or fuse together in a stable manner, becoming larger (von Wangenheim et al., 2016). As in animals and yeasts, also in pollen tube it is possible that the regulation of endosome dimension, preventing excessive late endosome enlargement, ensures correct fusion with vacuoles (Arlt et al., 2015; Liu et al., 2015; Onelli et al., 2018).

In *Nicotiana* pollen tubes it was hypothesized that MTs could mediate this homotypic fusion (Onelli et al., 2018). In addition to the increase of PVC area, MTs depolymerization altered the localization of Syp21, which was only observed on PVCs and disappeared or decreased on tubular vacuoles (Onelli et al., 2018).

While in Sq-treated pollen tube no modification was revealed in Syp21 localization in the tubular vacuoles, after Myr treatment, Syp21 did not disappeared from the tubular vacuole but, on the contrary, was enhanced in distal regions, as revealed by pseudo-colored images (Fig. 16A, j). Further analysis of fluorescence intensity are in progress, and could confirm these data.

The different behavior exerted by raft perturbation and MTs depolymerization on localization of Syp21 on tubular vacuoles, could suggest that alteration of ordered domains did not affect PVC delivery to vacuoles. Since PVCs originate from specific domain of TGN (Onelli and Moscatelli 2013), it is possible to hypothesize that, similarly to Syp61 domains, the formation of PVCs from TGN was delayed and larger PVCs were sorted. Afterwards, the delivery of PVCs occurred and Syp21 appeared in vacuoles as a result of PVC fusion.

Interestingly, the degradation pathway involves MVBs in which cargoes destined for degradation are trapped in the internal vesicle system (Ueda et al., 2001). The delivery of plasma membrane proteins/lipids to vacuoles requires previous ubiquitination, which is the signal for ESCRT-dependent sorting to the degradation pathway (Herberth et al., 2012). ESCRT-mediated sorting of cargoes destined for degradation occurs in TGN/EEs and it is hypothesized that MVBs originate from the maturation of specific TGN/EE domains (Scheuring et al., 2012). Studies on *Arabidopsis* vacuolar membrane microdomains identified in vacuole also proteins belonging to ESCRT-III complex which plays a role in EE membrane invagination, determining the inner morphology of MVBs (Raiborg et al., 2009). Rafts perturbation could affect the function of ESCRT-mediated sorting machinery allowing the formation of larger PVC.

Moreover, a recycling of Syp 21 was also hypothesized from tubular vacuoles to TGN (Onelli et al. 2018); thus, it is possible to assume that while recycling of Syp21, after Squalestatin treatment could occur normally, Myriocin could inhibit this process leading to Syp21 accumulation on tubular vacuoles.

To investigate whether raft alteration influences the movement of Syp21-PVCs in pollen tubes, the distance of these organelles from the very tip was measured. In control pollen tube, PVCs remain distant from the tip, as expected since these organelles are not involved in secretion and this behavior was similar after lipid raft perturbation (Fig. 16B, b), suggesting that AF modification in the apex due to the action of inhibitors did not affect cytoplasmic movements of PVCs.

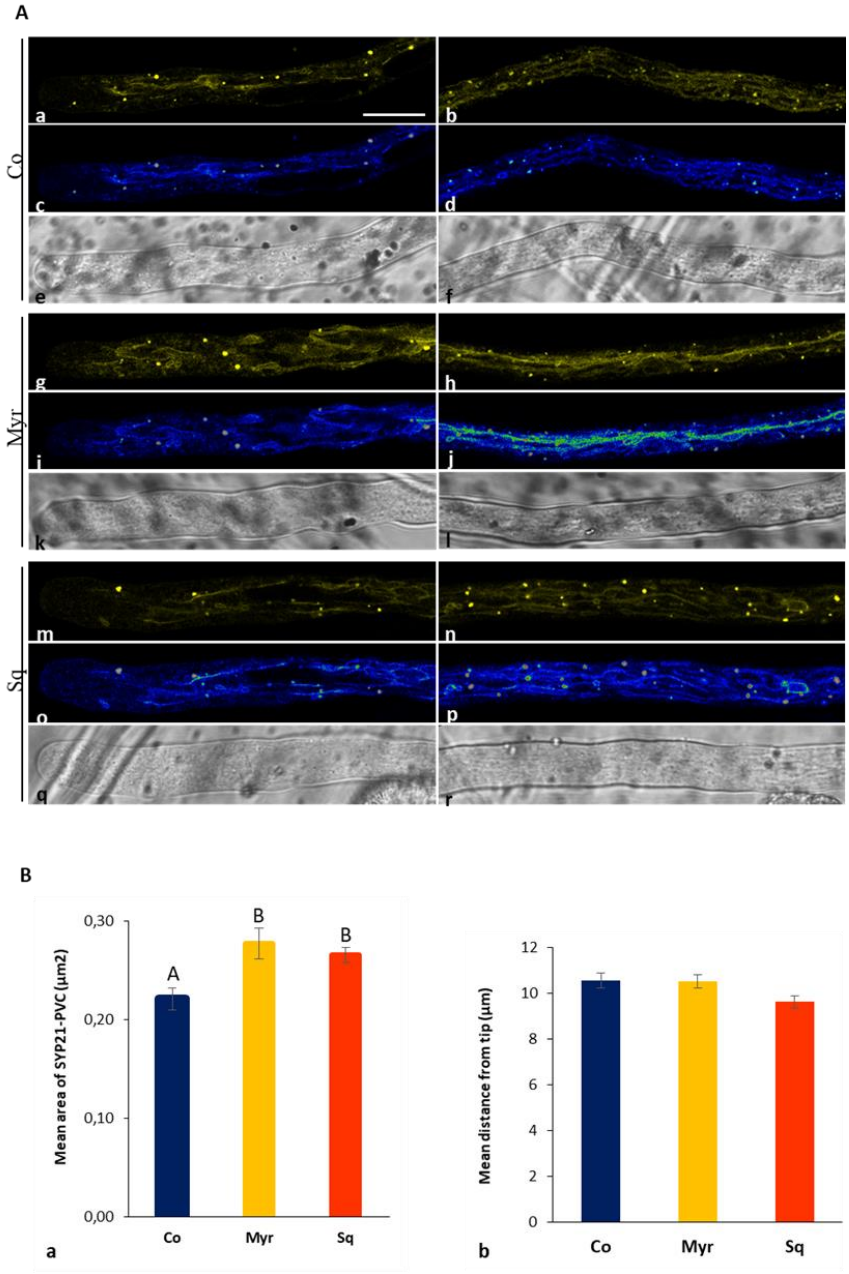

Fig. 16 Effect of Myriocin and Squalestatin on PVCs and tubular vacuoles. (A) YFP-SYP21 fusion protein detects round organelles (PVCs) widely distributed in pollen tubes except in the tip and highly dynamic tubular vacuoles, longitudinally distributed along the tubes in control and treated cells (a, b; g, h; m, n). Pseudo-coloured images in c, d; I, j; o, p. **(B)** Lipid raft perturbation, by Myr and Sq, induces in pollen tubes a significant increase of Syp21-PVC area (a; P>0.01). In addition, after Myr treatment Syp21 localization in tubular vacuoles is enhanced as shown in pseudo-coloured images (Fig. 15A, j), while in Sq treated pollen tubes no modification were revealed in Syp21 localization in tubular vacuoles. Measure of the distance of Syp21-PVC from tip reveals that in control pollen tube, PVC remains distant from tip, as expected since these organelles are not involved in secretion and this behavior was similar after lipid raft perturbation (b). Scale bar = 10 µm.

The effect of inhibitors on tubular vacuoles was investigated by using a fluorescent dye (CMAC). In tobacco pollen tubes, tubular vacuoles extended in the shank and distal area but they never reached the tip (Fig. 17A, a-f), (Onelli et al., 2018). The area occupied by vacuoles in control and in cells treated with drugs was analyzed up to 30 µm from the apical PM (Fig. 17B a-c). Pollen tubes treated with Myriocin displayed a significant increase in vacuole area with respect to the control and Squalestatin grown pollen tubes (Fig. 17B, d; $P < 0.01$), suggesting that alteration of lipid composition induced by Myriocin (decrease of sphingolipids and increase of sterols) modified tonoplast and vacuole morphology. Moreover, it is known that movement and dynamics of membranous compartments are largely dependent on actin filaments. Actin filaments, in tobacco BY-2 cells and root hair cells, play a role in maintaining vacuole morphology since when AFs were depolymerized the vacuoles were deformed, fragmented and lost their dynamics suggesting an actomyosin-dependent regulation of vacuolar shape and dynamics (Kutsuna et al. 2003 , Ovecka et al. 2005; Higaki et al. 2006).

In this regard, the modification of actin partitioning between microsomes and soluble fractions of pollen tubes treated with both drugs with respect to control, led to hypothesize that alteration of sphingolipid/sterol ratio of tonoplast, induced by Myriocin, altered the interaction of tonoplast with the acto-myosin system. Additional experiments of transient transformation using Lifeact-EGFP and labelling of vacuoles with CMAC and detailed colocalization analysis in shank and distal regions will allow to reveal if lipid alteration affects interaction with actin cytoskeleton.

Other experiments in *Physcomitrella patens* protonemata showed that also depolymerization of MTs dramatically affected shape and dynamics of tubular vacuoles (Oda et al., 2009). In addition, in tobacco pollen tubes Oryzalin affected the distribution pattern of vacuoles and induced their lateral association (Idilli et al., 2013) suggesting that the shape and dynamics of tubular vacuole could also be dependent on MTs.

Biochemical characterization of tobacco pollen tube DIMs revealed that 30% of tubulin recovered in microsomes is localized in lipid rafts; intriguingly, we could speculate that shape and dynamics of tubular vacuoles depends on the concerted action of AFs and MTs. Further investigations are necessary to clarify this point.

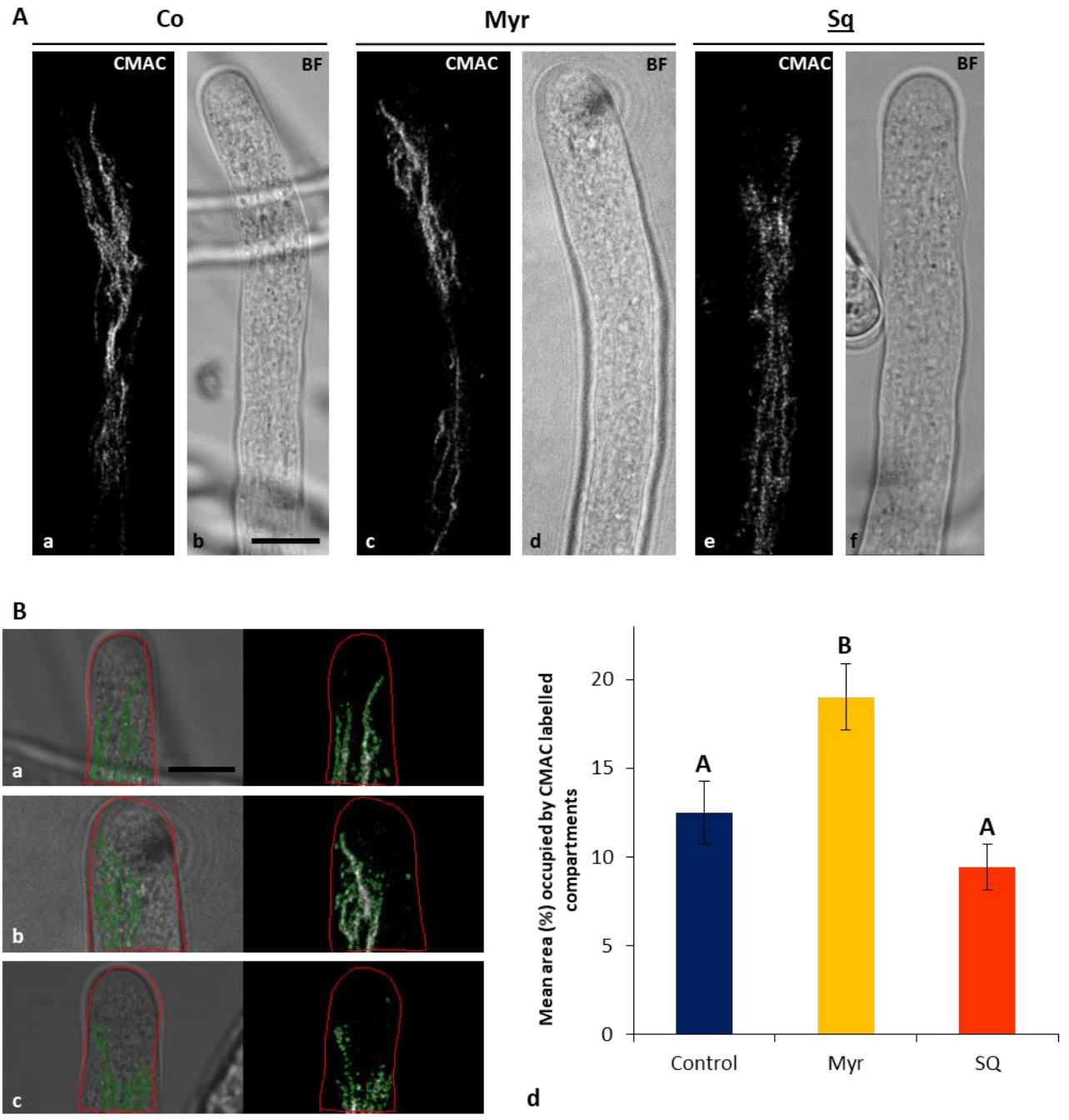

Fig. 17 Vacuole morphology. (A) Vacuoles have been visualized by using CMAC, in Control and in Myr or Sq treated pollen tubes (a, c, f) Bright Field images (BF) of pollen tube are shown in b, d, e. Bar = 10 µm. **(B)** The area occupied by vacuoles was analyzed in 30 µm from the tip PM (a-c); pollen tubes grown in the presence of Myr displayed a vacuole area significantly higher than Control and sq treated pollen tubes ($P < 0.01$) (d). Bar = 10µm

CONCLUSIONS

Cell polarity and tip growth are involved in a wide range of biological processes in different cell types and organisms.

The growing pollen tube is one of the most fascinating model system to study mechanisms underlying polarized growth. Beside the asymmetric localization of proteins along the PM and the unequal distribution of organelles, recently evidences of the requirement of polarized distribution of sterols and membrane lipid rafts in pollen tubes emerged.

In this work, using an experimental approach that involves the disorganization of lipid rafts by inhibiting the biosynthesis of sterols and sphingolipids, we have gained some understanding of the role of membrane microdomains in pollen tubes growth of *Nicotiana tabacum*.

Results presented in this work highlight that alteration of sterols/sphingolipids ratio in cell membranes has pleiotropic effects; we observed modifications on cytoskeletal organization and dynamics, secretion and membrane trafficking.

Biochemical and *in vivo* approaches show that changes in lipid profiles alter actin association with membranes and dynamics of the actin fringe in the tip region of pollen tubes, together with severe alterations of the clear zone morphology and dynamics. These results seem to have a synergic effect on secretory activity and evidence a role for lipid microdomains in regulating exocytosis of cell wall components in the apex, since composition and properties of the major components of pollen tubes cell wall is affected by the alteration of sterol/sphingolipid ratio.

Also, perturbation of lipid rafts seems to mostly affect TGN, its maturation and the development of compartments which originate from it and that are involved both in secretion and in degradation pathway. In detail, Squalestatin induces an increase of TGN area, and both inhibitors influence its trafficking along pollen tube. Concerning effects on degradation pathways, perturbation of lipid rafts induces an increase of PVCs area and alteration of tubular vacuoles dynamics suggesting a role for sterols and sphingolipids microdomains in regulating morphology and dynamics of organelles involved in the degradation pathways in pollen tubes.

Altogether these results support evidences of a role for sterols and sphingolipids, not only as fundamental structural components of membranes, but also in regulating intracellular membrane morphodynamics and polar secretion in plant cells.

Nevertheless, how lipid rafts integrity and their polarized distribution are maintained and how lipid rafts regulate or promote crosstalk between different cellular processes governing pollen tube

growth, is still to be unraveled. This data offers many suggestions, opening new, intriguing insights for future research.

MATERIALS AND METHODS

Probes and Drugs

Zaragozic acid/Squalestatin (Sigma Aldrich, USA) was dissolved in Ethanol to a concentration of 6.6 mM and then diluted to concentrations of 0.5 µM and 1 µM in the culture medium. A stock solution of Myriocin (Sigma Aldrich, USA) in methanol was prepared to a concentration of 4.98 mM and diluted to 5 µM concentration in the culture medium.

A stock solution 10 mM of Blue-CMAC in DMSO (Invitrogen) was prepared and used at 2 µM final dilution. Calcofluor white and aniline blue were used to a final concentration of 0.005% and 0.1% respectively.

Germination assay and pollen tube measurement

Pollen of *Nicotiana tabacum* (L.) was collected from plants grown in the Botanical Garden (Città Studi) of Milan University during summer and stored at –20°C. Pollen grains (3 mg/ml) were cultured in BK liquid medium (Brewbaker and Kwack, 1963) supplemented with 12% (w/v) sucrose at 23 ± 2°C with or without Squalestatin 0.5 µM/ 1 µM or Myriocin 5 µM for 2 hours and for 2.5 hours, respectively. Control and treated pollen tubes were fixed (fix solution: 12% sucrose, 100 mM PIPES pH 6.9, 5 mM $MgSO_4$, 0.5 mM $CaCl_2$, 3.7% formaldehyde; Squalestatin 0.5 µM/1 µM or Myriocin 5 µM were added in fix solution) and observed by the Leica optical microscope DM RB, using a Leica N PLAN 10X objective. Images were collected by the Leica video camera MC 170 HD. The length of control and treated pollen tubes after 2 and 2.5 hours of germination in BK medium with or without drugs were calculated by ImageJ software (National Institutes of Health) (Schneider et al., 2012) and analyzed by Student's t-test using the program Excel.

Lipid analysis

For the analysis of sphingolipids and glucosylceramides, 1 ml of hot isopropanol/hexane/water (55/20/25, v/v) was added in each P2 pellet fraction. The solution was vortexed and incubated at 60°C for 20 min. After centrifugation at 3000 g for 10 min, the supernatant was transferred to another tube and the pellet extracted twice more with the hot solvent. The supernatants were combined and evaporated to dryness at 40°C then were resuspended in Tetrahydrofuran/Methanol/H2O (40/20/40 v/v).

Their lipid content was analysed by High Performance Thin Layer chromatography (HPTLC). Before the analysis HPTLC plates (Silicagel 60 F254 Merck) were impregnated for 3 min with freshly prepared 0.2 M ammonium acetate in methanol, and further dried at 110°C for 15 min. The lipid extracts were chromatographed in Chloroform/Methanol/ 4 N NH4OH (9/7/2, v/v).

For the analysis of sterols, each P2 pellet fraction was resuspended in 0.5ml H2O, then 2 ml of Chloroform/Methalol (2/1, v/v) were added and vortexed. After 1 hour, the tubes were centrifuged at 3000 g for 10 min, the supernatant was transferred to another tube where it was evaporated to dryness.

The lipid extracts were analysed by HPTLC or further processed for GC-MS.

For HPTLC: lipids were resuspended in chloroform/methanol (2/1, v/v) and chromatography was performed using Hexane/Ethyl ether/Acetic acid (90/15/2, v/v).

For GC-MS: saponification was first carried out by addition of 1ml of ethanol and 0.1 ml of KOH 11 N to each lipid extract as well as 5 µg cholesterol as an internal standard; tubes were incubated at 80°C for 1 hour. Sterols were extracted with 1 ml of hexane and 2ml H2O; tubes were vortexed and centrifuged at 3000 g for 10min. The supernatant was transferred to another tube and was evaporated to dryness under nitrogen gas stream before silylation.

Sterols were derivatized with 200 µl of N,O-Bis(trimethylsilyl)trifluoroacetamide with 0.1% triméthylchlorosilane (BSTFA/TMCS) and incubation at 110°C for 15 min. BSTFA was evaporated under nitrogen gas stream, and the samples were dissolved in hexane. GC analysis was carried out with an Agilent 7890A Plus GC unit with flame ionization detector (Agilent). Silylated sterols were separated on a 30 m HP-5MS column (Agilent) using a temperature gradient of 150°C increased to 280°C at 10°C min−1, held for 10.5 min, and decreased to 150°C at 20°C min−1. Sterols were identified by GC-MS (Agilent) using the same column and temperature gradient.

Immunofluorescence microscopy

Pollen of *Nicotiana tabacum* was germinated with or without 1 µM Squalestatin or 5 µM Myriocin and fixed as reported above. Cells were rinsed 3 times for 5 min using TBS and then incubated with JIM 7 rat monoclonal antibody 1: 15 overnight at 4°C. Cells were rinsed in TBS and later incubated with anti-rat FITC antibody 1:200 for 2 hours. After three rinse in TBS, samples were observed using a Leica TCS SP8 microscope with a 63X oil immersion (NA 1.4) objective (Leica Microsystems, GmbH, Wetzlar, Germany). The 488 nm laser lines were used to excite GFP and fluorescence was collected in the 480–520 nm emission windows. Mean fluorescence intensity in tip and shank (see white and yellow ROIs in Fig. 8A, a) was measured by ImageJ software and statistical analyzed by Student's t-test using the program Excel.

Transient Gene Expression

For transient gene expression, pollen grains were collected from fresh flowers of *Nicotiana tabacum* (L.) and allowed to germinate at 23°C on solid medium as reported by Kost et al., (1998).

The expression vectors pLIFEACT-EGFP, pRABA4D-GFP, pRAB2-GFP, pSYP21-YFP and pSYP61-YFP were transferred to mature pollen grains on solid culture medium using a helium-driven particle accelerator (PDS-1000/He; Bio-Rad, Hercules, CA, USA). Pollen grains were placed under the stopping screen at a distance of 8 cm and bombarded in a vacuum of 28 inches of mercury using a helium pressure of 1100 psi, according to the manufacturer's recommendation (Bio-Rad) (Sanford et al., 1993). Gold particles (1 µm) were coated with plasmid DNA. pLIFEACT-EGFP (4 µg), pRABA4D-GFP (4 µg), pRAB2-GFP (4 µg), pSYP21-YFP (3 µg) and pSYP61-YFP (4 µg) were used to coat 1.5 mg of gold particles, which were used to bombard 2 samples of pollen grains (Kost et al., 1998). Bombarded cells were kept at 23 °C in the dark for 5 h before

observation. 2 hours and 2.5 hours before observation, samples were incubated with PTNT medium with or without 1 µM Squalestatin or 5 µM Myriocin.

Samples transformed with pSYP21-YFP and pSYP61-YFP were observed using a Leica TCS SP5 microscope with a 63x oil immersion (NA 1.4) objective (Leica Microsystems, GmbH, Wetzlar, Germany). The 458 nm laser lines were used to excite YFP and fluorescence was collected in the 520–550 nm emission windows.

To analyze the fluorescence signal deriving from pLIFEACT-EGFP, pRABA4D-GFP transient transformation in control and in pollen tubes incubated with Squalestatin or Myriocin, time-lapse experiments were performed in live, transiently transformed cells with SP2 CLSM (Leica) equipped with an argon ion laser (458, 476, 488, 496, 514 nm excitation). EGFP and GFP were excited using the 488 nm laser line and fluorescence was imaged between 480–520 nm. A 63X Leica oil immersion plan apo (NA 1.25) objective and a 2.0 zoom were used for all the experiments. To compare different experimental conditions, live data mode acquisitions were always performed with the same laser intensity and PMT settings. Time course analysis was carried out with the Leica TCS SP2 software time course option (15 frames - minimize) for 250 s. Observations were based on control, Squalestatin- and Myriocin-treated pollen tubes.

Images acquired by confocal microscopy were deconvolved with Huygens Professional version 19.04 (Scientific Volume Imaging, The Netherlands, http://svi.nl) and loaded into the open-source software program CellProfiler (Broad Institute, Cambridge, MA). Images were then segmented to identify objects. The process had four main steps: identification of the tube and rotation in order to align all of them vertically, creation of a ROIs of 5 µm from the tip (pLIFEACT-EGFP), a ROI of 5 µm from the tip and a ROI of 60 µm for shank and distal region (pRABA4D-GFP), identification of staining (green channel) and tabulation of measurements. Upon completion of the pipeline, a spreadsheet containing the percent of area covered by actin, clear zone vesicles, over total area of the tube in the ROI for each tube was generated and exported for further image analysis. Values were processed for statistical analysis using Excel software.

Calcofluor, Aniline blue and Blue-CMAC staining.

Blue-CMAC 2 µM (Molecular probes, Invitrogen) was added to pollen tubes grown with and without 1 µM Squalestatin or 5 µM Myriocin, on solid culture medium (Kost et al., 1998) for 15 min. The dye was then removed and the tubes were rinsed with liquid culture medium for 5 min. Confocal observation were performed with Leica TCS SP5 confocal microscope. The 405 laser lines were used to excite Blue-CMAC and the fluorescence was collected in the 440–480 nm emission windows. The percent of area covered by vacuoles, was measured as reported above, in paragraph “Transiente gene expression”, in a ROI of 30 µm from tip PM.

Calcofluor staining: pollen tubes grown in BK medium, 12% sucrose with and without 1 µM Squalestatin or 5 µM Myriocin, were fixed as reported above. Cells were rinsed 3 time for 5 min in TBS solution and then incubated with Calcofluor solution 0.005% final concentration for 1 min. After two rinses in TBS, samples were observed with Leica TCS SP5 confocal microscope. The 405 laser line were used to excite Calcofluor and the fluorescence was collected in the 420-480 nm emission windows. Mean fluorescence

intensity in tip and shank (see red and blue ROIs in Fig. 9A, c) was measured by ImageJ software and statistical analyzed by Student's t-test using the program Excel.

Aniline blue staining: pollen tubes grown in BK medium, 12% sucrose with and without 1 µM Squalestatin or 5 µM Myriocin, were fixed as reported above. Cells were rinsed 3 time for 5 min in TBS solution and callose was visualized using 0.1% aniline blue in K3PO4. The 405 laser line were used to excite Aniline blue and the fluorescence was collected in the 460-550 nm emission windows. Mean fluorescence intensity in tip and shank (see red and blue ROIs in Fig. 10A, c) was measured by ImageJ software and analyzed by Student's t-test using the program Excel. The analysis of callose deposition along first 30 µm from tip PM, was analyzed in more detail by ImageJ- Plot Profile analysis and values of mean fluorescence intensity were plotted in the graph. Statistical analysis were performed using the program Excel.

Pollen tube microsomes

Nicotiana tabacum (L.) pollen collected in the Botanical Garden Città Studi, as described above, was hydrated in a humid chamber overnight. Pollen (3 mg/ml) was germinated in BK medium as reported above, with or without Squalestatin 1 µM or Myriocin 5 µM. Pollen tubes were rinsed with 10 ml of incomplete TNE buffer (mM Tris, 150 mM NaCl, mM EGTA, 1 mM PMSF, 10 µg/ml TAME) containing 12% sucrose, with or without Squalestatin 1 µM or Myriocin 5 µM and centrifuged at 2000 r.p.m. for 10 min at 10°C in a Beckmann JS13.1 rotor. Pollen tubes were homogenized on ice in two volumes of complete TNE (mM Tris, 150 mM NaCl, mM EGTA, 1 mM PMSF, 10 µg/ml TAME, 10 µg/ml leupeptin, 10 µg/ml pepstatin A, 4 µM aprotinin, 8 µM antipain) using a 2 ml Potter (teflon/glass) homogenizer. The homogenate was centrifuged at 572 g for 4 minutes at 4°C and the post nuclear supernatant loaded onto a 20% sucrose cushion (3 ml) in incomplete TNE buffer and centrifuged at 64,200 g (23.000 r p m in the Beckman SW-60 rotor) for 30 minutes at 4°C. The P2 pellet was resuspended in cold complete PEM buffer. Aliquots of P2 and supernatant (S2) were protein assayed (Bradford) using BSA as standard protein.

SDS-PAGE and western blotting

SDS-PAGE analysis was performed using 10% linear acrylamide concentration according to the method of Laemmli (Laemmli, 1970). Gels were stained with Coomassie Brilliant Blue R250. Western blot was performed according to Towbin et al. (1979). The anti-actin monoclonal antibody (clone purchased from Sigma, USA) was used at final dilution of 1:25.000 and detected as outlined in the Amersham ECL kit booklet. The signal was acquired by using Chemidoc system. Quantification of protein levels was carried out with the ImageJ Software. Values were processed for statistical analysis using Excel.

TEM analyses

Pollen tubes were grown on BK culture medium with and without 1 µM Squalestatin and then embedded in low melting agarose 5%. Samples were fixed by High pressure freezing and postfixed with 1%

Osmium tetroxide-acetone in a freeze substitution system (Leica) from -80 to room temperature for 5 days. Embedding in Spurr resin were performed at room temperature according to the protocols supplied (Polyscience). 80 nm ultra-thin sections, obtained using a Reichert Jung Ultracut E microtome, were collected on Cu grids and observed with an EFTEM LEO 912AB transmission electron microscope (Zeiss, Jena, Germany) operating at 80 kV.

REFERENCES

Adhikari, P.B., Liu, X., Wu, X. et al. (2020). Fertilization in flowering plants: an odyssey of sperm cell delivery. Plant Mol Biol 103, 9–32

Ahmed, S. N., Brown, D. A. and London, E. (1997). On the origin of sphingolipid/cholesterol-rich detergent-insoluble cell membranes: physiological concentrations of cholesterol and sphingolipid induce formation of a detergent-insoluble, liquid-ordered lipid phase in model membranes. Biochemistry 36, 10944-10953.

Alexandersson, E., Saalbach, G., Larsson C., Kjellbom, P. (2004). *Arabidopsis* Plasma Membrane Proteomics Identifies Components of Transport, Signal Transduction and Membrane Trafficking. Plant Cell Physiol. 45(11): 1543–1556

Aouar, L., Chebli, Y. and Geitmann, A. (2010). Morphogenesis of complex plant cell shapes: the mechanical role of crystalline cellulose in growing pollen tubes. Sex. Plant Reprod. 23, 15–27. doi: 10.1007/s00497-009-0110-7.

Arlt H, Auffarth K, Kurre R, Lisse D, Piehler J, Ungermann C. (2015). Spatiotemporal dynamics of membrane remodeling and fusion proteins during endocytic transport. Mol. Biol. Cell 26, 1357–1370. (doi:10.1091/mbc.E14-08-1318)

Bacia, K., Schwille, P., Kurzchalia, T. (2005). Sterol structure determines the separation of phases and the curvature of the liquid-ordered phase in model membranes. Proc Natl Acad Sci 102:3272-7

Baluska, F.; Samaj, J.; Hlavacka, A.; Kendrik-Jones, J.; Volkmann, D. (2004). Actin-dependent fluid phase endocytosis in inner cortex cells of maize root apices. J. Exp. Bot., 55, 463–473.

Bandmann, V.; Homann, U. (2012). Clathrin-independent endocytosis contributes to uptake of glucose into BY-2 protoplasts. Plant J., 70, 578–584.

Bashline L, Li S, Anderson CT, Lei L, Gu Y. (2013). The endocytosis of cellulose synthase in *Arabidopsis* is dependent on μ2, a clathrin-mediated endocytosis adaptin. Plant Physiol., 163:150-60.

Bashline L, Li S, Zhu X, Gu Y. (2015). The TWD40-2 protein and the AP2 complex cooperate in the clathrin-mediated endocytosis of cellulose synthase to regulate cellulose biosynthesis. Proc Natl Acad Sci U S A. 112:12870-5.

Bateman, A., et al. (2004). The Pfam protein families database. Nucleic Acids Res.32,D138–D141.

Berken, A., Thomas, C., Wittinghofer, A., (2005). A new family of RhoGEFs activates the Rop molecular switch in plants. Nature 436, 1176-1180

Bessueille, L., Sindt, N., Guichardent, M., Uichardant, M., Djerbis, S., Teeri, T. T., and Bulone V. (2009). Plasma membrane microdomains from hybrid aspen cells are involved in cell wall polysaccharide biosynthesis. Biochem. J. 420, 93–103.

Bloch, D., Pleskot, R., Pejchar, P., Potocký, M., Trpkošová, P., Cwiklik, L., Vukašinović, N., Sternberg, H., Yalovsky, S., Žárský, V. (2016). Exocyst SEC3 and Phosphoinositides Define Sites of Exocytosis in Pollen Tube Initiation and Growth. Plant Physiol 172, 980-1002

Bordenave, M., and Goldberg, R. (1994). Immobilized and free apoplastic pectinmethylesterases in mung bean hypocotyl. Plant Physiol. 106, 1151–1156.

Borner, G.H.; Sherrier, D.J.; Weimar, T.; Michaelson, L.V.; Hawkins, N.D.; Macaskill, A.; Napier, J.A.;Beale, M.H.; Lilley, K.S.; Dupree, P. (2005). Analysis of detergent-resistant membranes in arabidopsis. Evidence for plasma membrane lipid rafts. Plant Physiol.137, 104–116.

Bosch, M. and Hepler, P.K. (2005b). Pectin Methylesterases and Pectin Dynamics in Pollen Tubes. The Plant Cell, Vol. 17, 3219–3226

Bosch, M., and Hepler, P.K. (2005). Silencing of the tobacco pollen pectin methylesterase NtPPME1results in retarded in vivo pollen tube growth. Planta (2006) 223: 736–745

Bosch, M., Cheung, A.Y. and Hepler, P.K. (2005). Pectin Methylesterase, a Regulator of Pollen Tube Growth. Plant Physiol. 138, 1334-1346

Bove, J.; Vaillancourt, B.; Kroeger, J.; Hepler, P.K.; Wiseman, P.W.; Geitmann, A. (2008). Magnitude and direction of vesicle dynamics in growing pollen tubes using spatiotemporal image correlation spectroscopy and fluorescence recovery after photobleaching. Plant Physiol. 147, 1646–1658.

Brandizzi, F., Wasteneys, G.O. (2013). Cytoskeleton-dependent endomembrane organization in plant cells: an emerging role for microtubules. Plant J. 75, 339-349

Brewbaker, J. L. and Kwack, B. H. (1963). The essential role of calcium ions in pollen germination and pollen tube growth. Am. J. Bot. 50, 859– 865.

Brown, D. A. and London, E. (1997). Structure of detergent-resistant membrane domains: does phase separation occur in biological membranes? Biochem. Biophys. Res. Commun. 240, 1-7

Brown, D. A. and London, E. (2000). Structure and function of sphingolipid- and cholesterol-rich membrane rafts. J. Biol. Chem. 275, 17221-17224.

Brown, D.A.; Rose, J.K. (1992). Sorting of GPI-anchored proteins to glycolipid-enriched membrane subdomains during transport to the apical cell surface. Cell 1992,68, 533–544.

Brownfield, L.; Ford, K.; Doblin, M. S.; Newbigin, E.; Read, S.; Bacic, A. (2007). Proteomic and biochemical evidence links the callose synthase in *Nicotiana alata* pollen tubes to the product of the NaGSL1 gene. Plant J. 52:147-156

Bulinski, J.C. and Gundersen, G.G. (1991). Stabilization of post-translational modification of microtubules during cellular morphogenesis. Bioessays. 13(6):285-93. doi: 10.1002/bies.950130605.

Cacas, J. L., Furt, F., Le Gue'dard, M., Schmitter, J. M., Bure', C., Gerbeau-Pissot, P., Moreau, P., Bessoule, J. J., Simon-Plas, F. and Mongrand, S. (2012). Lipids of plant membrane rafts. Prog. Lipid Res. 51, 272-299.

Cai, G., Faleri, C., Del Casino, C., Emons, A. M. C. and Cresti, M. (2011) Distribution of callose synthase, cellulose synthase, and sucrose synthase in tobacco pollen tube is controlled in dissimilar ways by actin filaments and microtubules. Plant Physiol. 155, 1169–1190.

Cai, G.; Bartalesi, A.; del Casino, C.; Moscatelli, A.; Tiezzi, A.; Cresti, M. (1993). The kinesin-immunoreactive homologue from *Nicotiana tabacum* pollen tubes: Biochemical properties and subcellular localization. Planta, 191, 496–506.

Cai, G.; Cresti, M. (2012). Are kinesins required for organelle trafficking in plant cells? Front. Plant Sci., 3, 170–179.

Cai, G.; Parrotta, L.; Cresti, M. (2015). Organelle trafficking, the cytoskeleton, and pollen tube growth. J Integr Plant Biol 57:63-78.

Camacho L. and Malhò R (2003). Endo/exocytosis in the pollen tube apex is differentially regulated by Ca^{2+} and GTPases. J. Exp. Bot. 54,83–92.

Cardenas L, Lovy-Wheeler A, Kunkel JG, Hepler PK (2008). Pollen tube growth oscillation and intracellular calcium levels are reversibly modulated by actin polymerization. Plant Physiol. 146, 1611–1621

Cardenas, L., Lovy-Wheeler, A., Wilsen, K. L. and Hepler, P. K. (2005). Actin polymerization promotes the reversal of streaming in the apex of pollen tubes. Cell Motil. Cytoskel. 61, 112–127.

Catoire, L., Pierron, M., Morvan, C., duPenhoat, C.H., and Goldberg, R.(1998). Investigation of the action patterns of pectin-methylesterase isoforms through kinetic analyses and NMR spectroscopy. Implications in cell wall expansion. J. Biol. Chem.273,33150–3315

Certal, A. C., Almeida, R. B., Carvalho, L. M., Wong, E., Moreno, N., Michard, E., Carneiro, J., Rodrigue'z-Le'on, J., Wu, H. M., Cheung, A. Y. et al. (2008). Exclusion of a proton ATPase from the apical membrane is associated with cell polarity and tip growth in *Nicotiana tabacum* pollen tubes. Plant Cell 20, 614-634

Chamberlain, L. H., Burgoyne, R. D. and Gould, G. W. (2001). SNARE proteins are highly enriched in lipid rafts in PC12 cells: implications for the spatial control of exocytosis. Proc. Natl. Acad. Sci. USA 98, 5619-5624.

Chebli and Geitmann (2007). Mechanical principles governing pollen tube growth. Floricul. Ornam. Biotech. 1: 232-245

Chebli, Y., Kaneda, M., Zerzour, R. and Geitmann, A. (2012). The cell wall of the *Arabidopsis* pollen tube-spatial distribution, recycling and network formation of polysaccharides. Plant Physiol. 160, 1940–1955.

Chebli, Y.; Kroegerb, J.; Geitmann, A. (2013). Transport Logistics in Pollen Tubes. Molecular Plant 6(4):1037-1052

Chen, C. Y-H.; Cheung, A.Y.; Wu, H-m. (2003). Actin-Depolymerizing Factor Mediates Rac/Rop GTPase–Regulated Pollen Tube Growth plant cell 15, 237-249

Chen S, Ehrhardt DW, Somerville CR (2010). Mutations of cellulose synthase (CESA1) phosphorylation sites modulate anisotropic cell expansion and bidirectional mobility of cellulose synthase. Proc Natl Acad Sci U S A, 107:17188-17193.

Chen S, Jia H, Zhao H, Liu D, Liu Y, Liu B, Bauer S, Somerville C. (2016). Regulation of anisotropic cell expansion and bidirectional mobility of cellulose synthase by phosphorylation of S211 andT212 of CESA3. Plant Physiol. 171(1):242-50.

Chen, C.Y.; Wong, E.I.; Vidali, L.; Estavillo, A.; Hepler, P.K.; Wu, H.M.; Cheung, A.Y. (2002). The regulation of actin by actin depolymerizing factor in elongating pollen tubes. Plant Cell 14, 2175-2190.

Chen, H.; Bernstein, B.W.; Bamburg, J.R. (2000). Regulating actin-filament dynamics in vivo. Trends Biochem Sci. 25(1):19-23.

Chen, M., Han, G., Dietrich, C. R., Dunn, T. M. and Cahoon, E. B. (2006). The essential nature of sphingolipids in plants as revealed by the functional identification and characterization of the *Arabidopsis* LCB1 subunit of serine palmitoyltransferase. Plant Cell 18, 3576-3593.

Cheung AY, Duan QH, Costa SS, de Graaf BH, Di Stilio VS, Feijo J, Wu HM. (2008). The dynamic pollen tube cytoskeleton: live cell studies using actin-binding and microtubule-binding reporter proteins. Mol Plant, 1:686-702.

Cheung, A.Y. and Wu, H.M. (2004). Overexpression of an *Arabidopsis* formin stimulates supernumerary actin cable formation from pollen tube cell membrane. Plant Cell. 16(1):257-69

Cheung, A.Y.; and Wu, H.M. (2008). Structural and signaling networks for the polar cell growth machinery in pollen tubes. Annu. Rev. Plant Biol. 59: 547-572

Cheung, A.Y.; Niroomand, S.; Zou, Y.; Wu, H.M. (2010). A transmembrane formin nucleates subapical actin assembly and controls tip focused growth in pollen tubes. Proc Natl Acad Sci U S A 107:16390-16395.

Chong, L. D., Traynor-Kaplan, A., Bokoch, G. M. and Schwartz. M. A. (1994). The small GTP-binding protein Rho regulates a phosphatidylinositol 4-phosphate 5-kinase in mammalian cells. Cell 79, 507–513.

Churchward, M.A., Rogasevkaia, T., Höfgen, J., Bau, J., Coorssen, J.R. (2005). Cholesterol facilitates the native mechanism of Ca^{2+}-triggered membrane fusion. J Cell Sci 118:4833-48

Clausen, M.H., Willats, W.G.T., and Knox, J.P. (2003). Synthetic methyl hexagalacturonate hapten inhibitors of anti-homogalacturonan monoclonal antibodies LM7, JIM5 and JIM7. Carbohydr. Res. 338,1797–1800.

Colombani, A.,Djerbi, S., Bessueille, L., Blomqvist, K., Ohlsson, A., Berglund, T. (2004). In vitro synthesis of (1-3)-b-D-glucan (callose) and cellulose by detergent extracts of membranes from cell suspension cultures of hybrid aspen. Cellulose 11, 313–327.

Court, H. and Sudbery, P. (2007). Regulation of Cdc42 GTPase activity in the formation of hyphae in *Candida albicans*. Mol. Biol. Cell 18, 265-281

Cremona, O. and De Camilli, P. (2001). Phosphoinositides in membrane traffic at the synapse.J. Cell Sci.114, 1041–1052

Crowell, E.F.; Bischoff, V.; Desprez, T.; Rolland, A.; Stierhof, Y.D.; Schumacher, K.; Gonneau, M.; Höfte, H.; Vernhettes, S. (2009). Pausing of Golgi bodies on microtubules regulates secretion of cellulose synthase complexes in Arabidopsis. Plant Cell. 21:1141-1154.

D'Avino, R., Camardella, L., Christensen, T.,Giovane, A., and Servillo, L. (2003). Tomato pectin methylesterase: Modeling, fluorescence, and inhibitor interaction studies-comparison with the bacterial (*Erwinia chrysanthemi*) enzyme. Proteins 53,830–839.

Dardelle, F.; Lehner, A.; Ramdani, Y.; Bardor, M.; Lerouge, P.; Driouich, A.; Mollet J-C. (2010). Biochemical and Immunocytological Characterizations of *Arabidopsis* Pollen Tube Cell Wall. Plant Physiology 153, 1563–1576

de Win, A.H.; Pierson, E.S. and Derksen, J. (1999). Rational analyses of organelle trajectories in tobacco pollen tubes reveal characteristics of the actomyosin cytoskeleton. Biophysical J. 76, 1648–1658.

de Curtis, I. (2008). Functions of Rac GTPases during neuronal development. Dev. Neurosci. 30, 47-45.

DeBrabander, M.J., Van de Veire, R.M.L., Aerts, F.E.M., Borgers, M., and Jannsen, P.A. (1976). The effects of methyl [5-(2-thienylcarbonyl)-1H-benzimidazol-2-yl] carbamate (R17 943: NSC 238159), a new synthetic antitumoral drug interfering with microtubules, on mammalian cells cultured *in vitro*. Cancer Res. 36, 905–916.

Del Casino, C.; Li, Y-Q.; Moscatelli, A.; Scali, M.; Tiezzi, A.; Cresti, M. (1993). Distribution of microtubules during growth of tobacco pollen tubes. Biology of the Cell 79, 125-132

Derksen J, Janssen GJ, Wolters-Arts M, Lichtscheidl I, Adlassnig W, Ovecka M, Doris F, Steer M (2011). Wall architecture with high porosity is established at the tip and maintained in growing pollen tubes of *Nicotiana tabacum*. Plant J. 68:495-506.

Derksen, J.; Knuiman, B.; Hoedemaekers, K.; Anouchka, G.; Bonhomme, S.; Pierson, E.S. (2002). Growth and cellular organization of *Arabidopsis* pollen tubes in vitro. Sex Plant Reprod 15, 133-139

Derksen, J.; Rutten, T.L.M.; van Amstel, T.; de Win, A.; Doris, F.; Steer, M. (1995). Regulation of pollen tube growth. Acta Bot. Neerl. 44,93–119.

DerMardirossian, C. and Bokoch, G.M. (2005). GDIs: central regulatory molecules in Rho GTPase activation.Trends Cell Biol.15, 356–363

Dietrich, C., Bagatolli, L. A., Volovyk, Z. N., Thompson, N. L., Levi, M., Jacobson, K. and Gratton, E. (2001). Lipid rafts reconstituted in model membranes. Biophys. J. 80, 1417-1428.

Dietrich, C., Han, G., Chen, M., Berg, R. H., Dunn, T. M., Cahoon, E. B. (2008). Loss-of-function mutations and inducible RNAi suppression of Arabidopsis *LCB2* genes reveal the critical role of sphingolipids in gametophytic and sporophytic cell viability. Plant J 54:284-298

Dowd, P.E.; Coursol, S.; Skirpan, A.L.; Kao, T.H.; Gilroy, S. (2006). Petunia phospholipase C1 is involved in pollen tube growth. Plant Cell, 18, 1438–1453.

Drakakaki, G. (2015). Polysaccharide deposition during cytokinesis: Challenges and future perspectives. Plant Sci 236: 177–184

Dutta, R.; Robinson, K.R. (2004). Identification and characterization of stretch-activated ion channels in pollen protoplasts, Plant Physiol. 135 (2004) 1398–1406.

Edidin, M. (2003). The state of lipid rafts: from model membranes to cells. Annu. Rev. Biophys. Biomol. Struct. 32, 257-283.

Erhardt, D.W.; Shaw S.L. (2006). Microtubule dynamics and organization in plant cortical array. Annu Rev Plant Biol. 41, 57-64

Etienne-Manneville, S. and Hall, A. (2002). Rho GTPases in cell biology. Nature 420, 629-635

Ewers, H. and Helenius, A. (2011). Lipid mediated endocytosis. Cold Spring Harb. Perspect. Biol., doi:10.1101/cshperspect.a004721.

Faergeman, N. J., Feddersen, S., Christiansen, J. K., Larsen, M. K., Schneiter, R., Ungermann, C., et al. (2004). Acyl-CoA-binding protein, Acb1p, is required fornormal vacuole function and ceramide synthesis in *Saccharomyces cerevisiae*. Biochem. J.380, 907–918.

Fan, L.M.; Wang, Y. F.; Wang, H.; Wu W. H. (2001). In vitro *Arabidopsis* pollen germination and characterization of the inward potassium currents in *Arabidopsis* pollen grain protoplasts. J. Exp. Bot. 52, 1604-1614

Faurè, J., Vignais, P. V., Dagher MC. (1999). Phosphoinositide-dependent activation of Rho A involves partial opening of the RhoA/Rho-GDI complex. Eur.J. Biochem.262, 879–889

Fayant, P.; Girlanda, O.; Chebli, Y.; Aubin, C-E.; Villemure, I. and Geitmann, A. (2010). Finite Element Model of Polar Growth in Pollen Tubes. The Plant Cell, Vol. 22: 2579–259

Feijo JA, Sainhas J, Hackett GR, Kunkel JG, Hepler PK. 1999. Growing pollen tubes possess a constitutive alkaline band in the clear zone and a growth-dependent acidic tip. J. Cell Biol. 144:483–96

Feijó, J.A.; Moreno, N. (2004). Imaging plant cells by two-photon excitation, Protoplasma 223 (2004) 1–32.

Ferguson, C.; Teeri, T.T.; Siika-aho, M., Read, S.M.; Bacic, A. (1998). Localization of cellulose and callose in pollen tubes and grains of *Nicotiana tabacum*. Planta 206:452-460

Firon N., Nepi M. and Pacini E. (2012). Water status and associated processes mark critical stages in pollen development and functioning. Ann. bot. 109(7):1201-14.

Fisher, D.D.; Gilroy, S.; Cyr, J.R. (1996). Evidence for opposing effects of calmodulin on cortical microtubules. Plant Physiol. 112: 1079-1087

Franchi G.G., Nepi M., Dafni A., and Pacini E. (2002). Partially hydrated pollen: taxonomic distribution, ecological and evolutionary significance. Plant Syst. Evol. 234: 211–227.

Franchi G.G., Nepi M., Dafni A., and Pacini E. (2014). Is flower/corolla closure linked to decrease in viability of desiccation-sensitive pollen? Facts and hypotheses: a review of current literature with the support of some new experimental data. Plant Syst Evol 300:577–584.

Franchi G.G., Piotto B., Nepi M., Baskin C.C., Baskin J.M. and Pacini E. (2011). Pollen and seed desiccation tolerance in relation to degree of developmental arrest, dispersal, and survival. J.Exp.Bot. 62(15) 5267–5281.

Franklin-Tong, V. E., Drobak, B. K., Allan, A. C., Watkins, P. A. C., and Trewavas. A. J. (1996). Growth of pollen tubes of *Papaver rhoeas* is regulated by a slow-moving calcium wave propagated by inositol 1,4,5-trisphosphate. Plant Cell 8, 1305–1321.

Frick, M.; Bright, N.A.; Riento, K.; Bray, A.; Merrified, C.; Nichols, B.J. (2007). Coassembly of flotillins induces formation of membrane microdomains, membrane curvature, and vesicle budding. Curr. Biol. 17, 1151–1156.

Fu Y, Wu G, Yang Z (2001). Rop GTPase-dependent dynamics of tiplocalized F-actin controls tip growth in pollen tubes. J. Cell Biol. 152, 1019–1032.

Fukunaga, T., Nagahama, M., Hatsuzawa, K., Tani, K., Yamamoto A., Tagaya, M. (2000). Implication of sphingolipid metabolism in the stability of the Golgi apparatus. J. Cell. Sci 113:3299-3307

Furt, F., König, S., Bessoule, J. J., Sargueil, F., Zallot, R., Stanislas, T., Noirot, E., Lherminier, J., Simon-Plas, F., Heilmann, I. et al. (2010). Polyphosphoinositides are enriched in plant membrane rafts and form microdomains in the plasma membrane. Plant Physiol. 152, 2173-2187.

Gadeyne A, Sánchez-Rodríguez C, Vanneste S, Di Rubbo S, Zauber H, Vanneste K, Van Leene J, De Winne N, Eeckhout D, Persiau G, Van De Slijke E, Cannoot B, Vercruysse L, Mayers JR, Adamowski M, Kania U, Ehrlich M, Schweighofer A, Ketelaar T, Maere S, Bednarek SY, Friml J, Gevaert K, Witters E, Russinova E, Persson S, De Jaeger G, Van Damme D. (2014). The TPLATE adaptor complex drives clathrin-mediated endocytosis in plants. Cell. 156:691-704.

Gaffe, J.; Tieman D. M., Handa A. K. (1994). Pectin Methylesterase Isoforms in Tomato (*Lycopersicon esculentum*) Tissues (Effects of Expression of a Pectin Methylesterase Antisense Gene) Plant Physiol 105: 199-203

Geitman, A. and Cresti, M. (1998). Ca^{2+} Channels control the rapid expansion in pulsating growth of *Petunia Hybrida* pollen tubes. J. Plant Physiol. 152, 439-447

Geitmann, A. (2010). How to shape a cylinder: pollen tube as a model system for the generation of complex cellular geometry? Sex. Plant Reprod. 23, 63–71.

Geitmann, A. and Parre, E. (2004). The local cytomechanical properties of growing pollen tubes correspond to the axial distribution of structural cellular elements. Sex. Plant Reprod. 17, 9-16

Gelfand, V.I. and Bershadsky, A.D. (1991). Microtubule dynamics: mechanism, regulation, and function. Annu. Rev. Cell Biol. 7:93-116.

Gibson, R.M. and Wilson-Delfosse, A.L. (2001). RhoGDI-binding-defective mutant of Cdc42Hs targets to membranes and activates filopodia formation but does not cycle with the cytosol of mammalian cells. Biochem. J.359, 285–294

Giovane, A., Servillo, L., Balestrieri, C., Raiola,A., D'Avino, R., Tamburrini, M., Clardiello,M.A., and Camardella, L. (2004). Pectin methylesterase inhibitor. Biochim. Biophys. Acta1696,245–252.

Goode, B.L.; Eck, M.J. (2007). Mechanism and function of formins in the control of actin assembly. Annu. Rev. Biochem., 76, 593–627.

Gossot, O. and Geitmann ,A. (2007). Pollen tube growth: coping with mechanical obstacles involves the cytoskeleton. Planta 226:405-416.

Grebnev, G.; Ntefidou, M. and Kost, B. (2017). Secretion and Endocytosis in Pollen Tubes: Models of Tip Growth in the Spot Light. Front. Plant Sci. 8:154. doi: 10.3389/fpls.2017.00154

Green, P. B. (1962). Mechanism for plant cellular morphogenesis. Science 138, 1404–1405.

Grimmer, S., Ying, M., Wälchi, S., van Deurs, B., Sandvig, K. (2005). Golgi vesiculation induced by cholesterol occurs by a dynamin- and cPLA2-dependent mechanism. Traffic 6:144-56

Gu, Y., Li, S., Lord, E.M. and Yang Z. (2006). Members of a novel class of *Arabidopsis* Rho guanine nucleotide exchange factors control Rho GTPase-dependent polar growth. Plant Cell18, 366–381

Gu, Y.; Fu, Y.; Dowd, P.; Li, S.; Vernoud, V.; Gilroy, S.; Yang, Z. (2005). A Rho family GTPase controls actin dynamics and tip growth via two counteracting downstream pathways in pollen tubes j cell biol 2005, 169, 127-138

Gu, Y.; Vernoud,V.; Fu,Y.; Yang Z. (2003). ROP GTPase regulation of pollen tube growth through the dynamics of tip-localized F-actin. J. Exp. Bot. 54, 93-101

Gu, Y.; Wang, Z.; Yang, Z. (2004). ROP/RAC GTPase: an old new master regulator for plant signaling. Curr. Opin. Plant. Biol. 7(5):527-36.

Guo J, Yang Z. (2020). Exocytosis and endocytosis: coordinating and fine-tuning the polar tip growth domain in pollen tubes. J Exp Bot. 71(8):2428-2438.

Guo, F.; McCubbin, A.G. (2012). The pollen-specific R-SNARE/longin PiVAMP726 mediates fusion of endo- and exocytic compartments in pollen tube tip growth. J. Exp. Bot. 63, 3083–3095.

Gutierrez, R.; Lindeboom, J.J.; Paredez, A.R.; Emons, A.M.; Ehrhardt, D.W. (2009). *Arabidopsis* cortical microtubules position cellulose synthase delivery to the plasma membrane and interact with cellulose synthase trafficking compartments. Nat Cell Biol. 11:797-806.

Haigler, C. H. and Brown, R. M. (1986). Transport of rosettes from the golgi apparatus to the plasma membrane in isolated mesophyll cells of *Zinnia elegans* during differentiation to tracheary elements in suspension culture. Protoplasma 134, 111–120.

Hammond, J.W.; Cai, D.; Verhey, K.J. (2008). Tubulin modifications and their cellular functions. Curr. Opin. Cell Biol. 20 (1), 71-76.

Hartmann MA, Perret AM, Carde JP, Cassagne C, Moreau P. (2002). Inhibition of the sterol pathway in leek seedlings impairs phosphatidylserine and glucosylceramide synthesis but triggers an accumulation of triacylglycerols. Biochim Biophys Acta. 1583(3):285-96. doi: 10.1016/s1388-1981(02)00249-4.

Hartwig, J.H.; Bokoch, G.M.; Carpenter, C.L.; Janmey, P.A.; Taylor L.A.; Toker A. et al. (1995). Thrombin receptor ligation and activated Rac uncap actin filament barbed end though phosphoinositide synthesis in permeabilized human platelets. Cell 82, 643-653.

Hay, J.C.; Fisette, P.L.; Jenkins, G.H.; Fukami, K.; Takenawa, T.; Anderson, R.A. and Martin, T.F.J. (1995). ATP-dependent inositide phosphorylationrequired for Ca^{2+}-activated secretion. Nature 374, 173–177

Hazan, I.; and Liu, H., (2002). Hyphal Tip-Associated Localization of Cdc42 Is F-Actin Dependent in *Candida albicans*. Eukaryot Cell. 1(6): 856–864.

Heilmann I, Ischebeck T. (2016). Male functions and malfunctions: the impact of phosphoinositides on pollen development and pollen tube growth. Plant Reprod. 29(1-2):3-20.

Helling, D., Possart, A., Cottier, S., Klahre, U. and Kost, B. (2006). Pollen tube tip growth depends on plasma membrane polarization mediated by tobacco PLC3 activity and endocytic membrane recycling. Plant Cell 18, 3519-3534

Hennessey, E.S.; Drummond, D.R.; Sparrow, J.C. (1993). Molecular genetics of actin function. Biochem. J. 1;291

Hepler, P. K., Rounds, C. M. and Winship. L. J. (2013). Control of cell wall extensibility during pollen tube growth. Mol. Plant 6, 998–1017.

Hepler, P.K. and Bosch, M. (2005). Pectin methylesterases and pectin dynamics in pollen tubes. Plant Cell 17, 3219–3226.

Hepler, P.K. and Winship, L.J. (2015). The pollen tube clear zone: clues to the mechanism of polarized growth. J. Integr. Plant Biol. 57, 79-92.

Hepler, P.K.; Vidali, L.; Cheung, A.Y. (2001). Polarized cell growth in higher plants. Annu. Rev. Cell Dev. Biol. 17: 159-187

Herberth, S.; Shahriari, M.; Bruderek, M.; Hessner, F.; Müller, B.; Hülskamp, M.; Schellmann, S. (2012). Artificial ubiquitylation is sufficient for sorting of a plasma membrane ATPase to the vacuolar lumen of Arabidopsis cells. Planta, 236, 63–77.

Heslop-Harrison, J. (1987). Pollen germination and pollen tube growth. International Review of Cytology 107: 1-78

Heslop-Harrison, J., Heslop-Harrison, Y., Cresti, M., Tiezzi, A. and Moscatelli, A. (1988). Cytoskeletal elements, cell shaping and movement in the angiosperm pollen tube. J. Cell Sci. 91, 49-60,

Heslop-Harrison,J.(1975). "The adaptive significance of the exine,"in The Evolutionary Significance of the Exine, Linnean Society Symposium Series, eds J.K.Fergusonand J.Muller (London:Linnean Society of London), 27–37.

Hoebeke, J., Van Nijen, G., and DeBrabander, M. (1976). Interactions of oncodazole (R 17934), a new anti-tumoral drug, with rat brain tubulin. Biochem. Biophys. Res. Commun. 69, 319–324.

Hoessli, D.C.; Ilangumaran, S.; Soltermann, A.; Robinson, P.J.; Borisch, B.; Din, N. (2000). Signaling through sphingolipid microdomains of the plasma membrane: The concept of signaling platform. Glycoconjugate J. 17:191–197

Holdaway-Clarke TL, Hepler PK. 2003. Control of pollen tube growth: role of ion gradients and fluxes. New Phytol. 159:539–563.

Holdaway-Clarke, T.L.; Feijó, J.A.; Hackett, G.R.; Kunkel, J.G.; Hepler, P.K. (1997). Pollen tube growth and the intracellular cytosolic calcium gradient oscillate in phase while extracellular calcium influx is delayed, Plant Cell 9, 1999–2010.

Hurst LR, Fratti RA. (2020). Lipid Rafts, Sphingolipids, and Ergosterol in Yeast Vacuole Fusion and Maturation. Front Cell Dev Biol. 3;8:539.

Idilli, A.I.; Morandini, P.; Onelli, E.; Rodighiero, S.; Caccianiga, M.; Moscatelli, A. (2013). Microtubule depolymerization affects endocytosis and exocytosis in the tip and influences endosome movement in tobacco pollen tubes. Mol Plant 6:1109-1130.

Idilli, A.I.; Onelli, E.; Moscatelli, A. (2012). Low concentration of LatB dramatically changes the microtubule organization and the timing of vegetative nucleus/generative cell entrance in tobacco pollen tubes. Plant Signal. Behav., 7, 947–950.

Ilangumaran, S. and Hoessli, D. C. (1998). Effects of cholesterol depletion by cyclodextrin on the sphingolipid microdomains of the plasma membrane. Biochem. J. 335, 433-440.

Ischebeck, T., Stenzel, I., Hempel, F., Jin, X., Mosblech, A. and Heilmann, I. (2011). Phosphatidylinositol-4,5-bisphosphate influences Nt-Rac5-mediated cell expansion in pollen tubes of *Nicotiana tabacum*. Plant J. 65, 453-468.

Ischebeck, T.; Seiler, S.; Heilmann, I. (2010). At the poles across kingdoms: phosphoinositides and polar tip growth. Protoplasma 240, 13-31;

Ishizaki, T.; Morishima, Y.; Okamoto, M.; Furuyashiki, T.; Kato, T.; Narumiya, S. (2001). Coordination of microtubules and actin cytoskeleton by the Rho effector mDia1. Nat. Cell Biol. 3, 8–14.

Islas-Flores, T., Rahman, A., Ullah, H., Villanueva, M. A. (2015). The Receptor for Activated C Kinase in Plant Signaling: Tale of a Promiscuous Little Molecule. Front. PlantSci. 6:1090.doi: 10.3389/fpls.2015.01090

Itoh T, Takenawa T. (2009). Mechanisms of membrane deformation by lipid-binding domains. Prog. Lipid Res. 48:298–305.

Itoh, T., and P. De Camilli. (2006). BAR, F-BAR (EFC) and ENTH/ANTH domains in the regulation of membrane-cytosol interfaces and membrane curvature. Biochim. Biophys. Acta. 1761:897–912.

Janmey, P. A. (1994). Phosphoinositides and calcium as regulators of cellular actin assembly and disassembly. Annu. Rev. Physiol. 56, 169–191.

Janmey, P.A.; Xian, W; Flanagan L.A. (1999). Controlling cytoskeleton structure by phosphoinositide-protein interactions: phosphoinositide binding protein domains and effects of lipid packing. Chem Phys Lipids. 101(1):93-107

Jiang, L.X., Yang, S.L., Xie, L.F., Puah, C.S.,Zhang, X.Q., Yang, W.C., Sundaresan, V., and Ye, D. (2005). VANGUARD1 encodes a pectin methylesterase that enhances pollen tube growth in the *Arabidopsis* style and transmitting tract. Plant Cell 17,584–596.

Joshi, H.C. (1998). Microtubule dynamics in living cells. Curr. Opin. Cell Biol. 10, 35-44.

Kai Liu, K.; Jian, Y.; Sun, X.; Yang, C.; Gao, Z.; Zhang, Z.; Liu, X.; Li, Y.; Xu, J.; Jing, Y.; Mitani, S.; He, S.; Yang, C. (2016). Negative regulation of phosphatidylinositol 3-phosphate levels in early-to-late endosome conversion. J. Cell Biol. 212, 181–198. (doi:10.1083/jcb. 201506081)

Kang B, Nielsen E, Lai M, Mastronarde D, Andrew L (2011). Electron Tomography of RabA4b- and PI-4K β 1-Labeled Trans Golgi Network Compartments in Arabidopsis. Traffic 12: 313–329

Klahre, U. and Kost, B. (2006). Tobacco RhoGTPase ACTIVATING PROTEIN1 restricts signaling of RAC/Rop to the apex of pollen tubes. Plant Cell 18, 3033–3046

Klahre, U., Becker, C., Schmitt, A. C., Kost, B. (2006). Nt-RhoGDI2 regulates Rac/Rop signaling and polar cell growth in tobacco pollen tubes. Plant J. 46(6):1018-31.

Klemm RW, Ejsing CS, Surma MA, Kaiser HJ, Gerl MJ, Sampaio JL, de Robillard Q, Ferguson C, Proszynski TJ, Shevchenko A, Simons K. (2009). Segregation of sphingolipids and sterols during formation of secretory vesicles at the trans-Golgi network. J Cell Biol. 185:601-12. doi: 10.1083/jcb.200901145.

Knox, J.P., Linstead, P.J., King, J., Cooper, C., and Roberts, K.(1990). Pectin esterification is spatially regulated both within cell walls and between developing tissues of root apices. Planta 181,512–521.

Kong, J. N., Hardina, K., Dinkinsa, M., Wanga, G., Hea, Q., Mujadzica, T., Zhua, G., Bielawski, J., Spassieva, S. and Bieberich, E. (2015). Regulation of *Chlamydomonas* flagella and ependymal cell motile cilia by ceramide-mediated translocation of GSK3. Mol. Biol. Cell 26, 4451-4465.

König, S.; Ischebeck, T.; Lerche, J.; Stenzel, I.; Heilmann, I. (2008). Salt-stress-induced association of phosphatidylinositol 4,5-bisphosphate with clathrin-coated vesicles in plants. Biochem. J. 415, 387–399.

Kost B, Lemichez E, Spielhofer P, Hong Y, Tolias K, Carpenter C (1999). Rac homologues and compartmentalized phosphatidylinositol 4, 5-bisphosphate act in a common pathway to regulate polar pollen tube growth. *J. Cell Biol.* 145:317–330.

Kost, B. (2008). Spatial control of Rho (Rac-Rop) signaling in tip-growing plant cells. Trends Cell Biol. 18, 119-127.

Kost, B.; Mathur, J.;Chua, N-H. (1999). Cytoskeleton in plant development. Curr. opin. Plant Biol 2, 462-470

Kost, B.; Spielhofer, P.; Chua, N. H. (1998). A GFP-mouse talin fusion protein labels plant actin filaments in vivo and visualizes the actin cytoskeleton in growing pollen tubes. Plant J. 16, 393-401

Krichevsky A, Kozlovsky SV, Tian GW, Chen MH, Zaltsman A, Citovsky V. 2007 How pollen tubes grow. *Dev. Biol.* 303:405–420.

Kroeger, J.H. and Geitmann, A. (2012). Pollen tube growth: Getting a grip on cell biology through modelling. Mech. Res. Commun. 2012, 42, 32–39.

Kroeger, J.H.; Bou Daher, F.; Grant, M.; Geitmann, A. (2009). Microfilament orientation constrains vesicle flow and spatial distribution in growing pollen tubes. Biophys. J. 97, 1822–1831.

Laemmli, U. K. (1970). Cleavage of structural proteins during the assembly of the head of bacteriophage T4. Nature 227, 680-685

Laitiainen, E.; Nieminen, K.M.; Vihinen, H.; Raudaskoski, M. (2002). Movement of generative cell and vegetative nucleus in tobacco pollen tubes is dependent on microtubule cytoskeleton but independent of the synthesis of callose plugs. Sex Plant Reprod 15:195-204.

Laloi, M., Perret, A. M., Chatre, L., Melser, S., Cantrel, C., Vaultier, M. N., Zachowski, A., Bathany, K., Schmitter, J. M., Vallet, M. et al. (2007). Insights into the role of specific lipids in the formation and delivery of lipid microdomains to the plasma membrane of plant cells. Plant Physiol. 143, 461-472.

Lam, S.K.; Siu, C.L.; Hillmer, S.; Jang, S.; An, G.; Robinson, D.G.; Jiang, L. (2007). Rice SCAMP1 defines clathrin coated, trans Golgi-located tubular-vesicular structures as an early endosome in tobacco BY-2 cells. Plant Cell 19, 296–319.

Lancelle, S.A.; Cresti, M.; Hepler, P.K. (1987). Ultrastructure of the cytoskeleton in freeze-substituted pollen tubes of *Nicotiana alata*. Protoplasma 140, 141–150.

Lancelle, S.A.; Hepler, P.K. (1992). Ultrastructure of freeze-substituted pollen tubes of *Lilium longiflorum*. Protoplasma 167, 215–230.

Lang, T., Bruns, D., Wenzel, D., Riedel, D., Holroyd, P., Thiele, C. and Jahn, R. (2001). SNAREs are concentrated in cholesterol-dependent clusters that define docking and fusion sites for exocytosis. EMBO J. 20, 2202-2213.

Le Grimellec C, Friedlander G, Giocondi MC. (1988). Asymmetry of plasma membrane lipid order in Madin-Darby Canine Kidney cells. Am J Physiol. 255:F22-32.

Lee Y.J., Szumlanski A., Nielsen E., Yang Z. (2008). Rho-GTPase-dependent filamentous actin dynamics coordinate vesicle targeting and exocytosis during tip growth. Journal of Cell Biology, 181,1155–1168.

Lee, Y-S., Choi, K-M., Lee, S. Sin, D-M. Yoo, K-Si, Lim, Y., Lee, Y-M., Hong, J.-T., Yun, Y-P. and Yoo. H-S. (2012). Myriocin, a serine palmitoyltransferase inhibitor, suppresses tumor growth in a murine melanoma model by inhibiting de novo sphingolipid synthesis. Cancer Biology & Therapy 13, 92–100.

Lefebvre, B., Furt, F., Hartmann, M. A., Michaelson, L. V., Carde, J. P., Sargueil-Boiron, F., Rossignol, M., Napier, J. A., Cullimore, J., Bessoule, J. J. et al. (2007). Characterization of lipid rafts from *Medicago truncatula* root plasma membranes: a proteomic study reveals the presence of a raft-associated redox system. Plant Physiol. 144, 402-418.

Lei L, Li S, Bashline L, Gu Y (2014). Dissecting the molecular mechanism underlying the intimate relationship between cellulose microfibrils and cortical microtubules. Front. Plant Sci. 5:90.

Lerouxel O, Cavalier DM, Liepman AH, Keegstra K. (2006). Biosynthesis ofplant cell wall polysaccharides - a complex process. Current Opinion in Plant Biology 9, 621–630.

Li YQ, Moscatelli A, Cai G, Cresti M. 1997 Functional interactions among cytoskeleton, membranes, and cell wall in the pollen tube of flowering plants. Int. Rev. Cytol. 176:133–199.

Li, H., Luo, N., Wang, W., Liu, Z., Chen, J., Zhao, L., Tan, L., Wang, C., Qin, Y., Li, C., Xu, T. and Yang, Z. (2018). The REN4 rheostat dynamically coordinates the apical and lateral domains of *Arabidopsis* pollen tubes. Nature Communication DOI: 10.1038/s41467-018-04838-w.

Li, H.; Lin, Y.; Heath, R.M.; Zhu, M.X.; Yang, Z. (1999). Control of pollen tube tip growth by a Rop GTPase-dependent pathway that leads to tip-localized calcium influx. Plant Cell 11, 1731-1742.

Li, R.; Liu, P.; Wan, Y.; Chen, T.; Wang, Q.; Mettbach, U.; Baluska, F.; Samaj, J.; Fang, X.; Lucas, W.J. (2012). A membrane microdomain-associated protein, Arabidopsis Flot1, is involved in a clathrin-independent endocytic pathway and is required for seedling development. Plant Cell 24, 2105–2122.

Li, Y. Q., Chen, F., Linskens, H.F., Cresti, M. (1994) Distribution of unesterified and esterified pectins in cell wall of pollen tubes. Sex. Plant Reprod. 7, 145–152.

Li, Y.Q.; Mareck, A.; Faleri, C.; Moscatelli, A.; Liu, Q.; Cresti, M. (2002). Detection and localization of pectin methylesterase isoforms in pollen tubes of *Nicotiana tabacum* L. Planta 214, 734-740

Li, Y-Q., Moscatelli, A., Cai, G. and Cresti, M. (1997). Functional interaction among cytoskeleton, membranes and cell wall in the pollen tube of flowering plants. Int. Rev. Cytol. 176, 133-199.

Li, YQ; Mareck, A; Faleri, C; Moscatelli A; Liu, Q; Cresti, M. (2002). Detection and localization of pectin methylesterase isoforms in pollen tubes of *Nicotiana tabacum* (L.). Planta 214, 734-740.

Lin, O., Fuji, R. N., Yang, W., Cerione, R. A. (2003). RhoGDI is required for Cdc42-mediated cellular transformation.Curr. Biol.13, 1469–1479

Linetti, A., Fratangeli, A., Taverna, E., Valnegri, P., Maura Francolini, M., Cappello, V., Matteoli, M., Passafaro, M. and Rosa, P. (2010). Cholesterol reduction impairs exocytosis of synaptic vesicles. J. Cell Sci. 123, 595-605.

Lingwood, D. and Simons, K. (2010). Lipid rafts as a membrane-organizing principle. Science 327, 46-50.

Lipowsky, R. (1993). Domain-induced budding of fluid membranes. Biophys. J. 64:1133–1138.

Liu J, Hussey PJ. (2014). Dissecting the regulation of pollen tube growth by modeling the interplay of hydrodynamics, cell wall and ion dynamics. Front Plant Sci. 5:392. doi: 10.3389/fpls.2014.00392.

London, E. (2002). Insights into lipid raft structure and formation from experiments in model membranes. Curr. Opin. Struct. Biol. 12, 480-486.

Lord, E, (2000). Adhesion and cell movement during pollination: cherchez la femme. Trends Plant Sci. 5, 368–373.

Lovy-Wheeler, A., Kunkel, J. G., Allwood, E. G., Hussey, P. J. and Hepler P. K. (2006) Oscillatory increases in alkalinity anticipates growth and may regulate actin dynamics in pollen tubes of lily. Plant Cell, 18, 2182–2183.

Lovy-Wheeler, A., Wilsen, K. L., Baskin, T. I., Hepler, P. K. (2005) Enhanced fixation reveals the apical cortical fringe of actin filaments as a consistent feature of the pollen tube. Planta, 221, 95–104.

Lovy-Wheeler, A.; Cárdenas, L.; Kunkel, J.G.; Hepler, P.K. (2007). Differential organelle movement on the actin cytoskeleton in lily pollen tubes. Cell Motil. Cytoskel., 64, 217–232.

Malho, R.; Camacho, L.; Moutinho, A. (2000). Signaling pathways in pollen tube growth and reorientation. Ann. Bot. 85, 59-68.

Manes, S., R. Ana Lacalle, C. Gomez-Mouton, and A.C. Martinez. (2003). From rafts to crafts: membrane asymmetry in moving cells. Trends Immunol. 24:320-326

Margolis, R.L. and Wilson, L. (1998). Microtubule treadmilling: what goes around comes around. Bioessays 20, 830-836.

Markham, J. E., Molino, D., Gissot, L., Bellec, Y., He'maty, K., Marion, J., Belcram, K., Palauqui, J. C., Satiat-Jeunemaıˆtre, B. and Faure, J. D. (2011). Sphingolipids containing very-long-chain fatty acids define a secretory pathway for specific polar plasma membrane protein targeting in *Arabidopsis*. Plant Cell 23, 2362-2378.

Martin, S. W. and Konopka, J. B. (2004). Lipid raft polarization contributes to hyphal growth in *Candida albicans*. Eukaryot. Cell 3, 675-684.

Martin, T. F.J. (2001). PI(4,5)P2 regulation of surface membrane traffic. Curr. Opin. Cell Biol. 13(4):493-9.

McFarlane, H. E., Döring, A., Persson, S., (2014). The cell biology of cellulose synthesis. Annual review of plant biology 65, 69-94

McKenna, S. T., Kunkel, J. G., Bosch, M., Rounds C. M., Vidali, L. Winship, L. J. and Hepler, P. K. (2009). Exocytosis Precedes and Predicts the Increase in Growth in Oscillating Pollen Tubes. Plant Cell 21, 3026–3040.

Meijer, H. J. G. and Munnik, T. (2003). Phospholipid-based signaling in plants. Annu. Rev. Plant. Biol. 54, 265-306

Melser, S., Batailler, B., Peypelut, M., Poujol, C., Bellec, Y., Wattelet-Boyer, V., Maneta-Peyret, L., Faure, J. D. and Moreau, P. (2010). Glucosylceramide biosynthesis is involved in Golgi morphology and protein secretion in plant cells. Traffic 11, 479-490.

Melser, S.; Molino, D.; Batailler, B.; Peypelut, M.; Laloi, M.; Wettelet-Boyer, V.; Bellec, Y.; Faure, J. D.; Moreau, P. (2011). Links between lipid homeostasis, organelle morphodynamics and protein trafficking in eukaryotic and plant secretory pathways. Plant Cell Rep 30:177-193

Men, S.; Boutté, Y.; Ikeda, Y.; Li, X.; Palme, K.; Stierhof, Y.D.; Hartmann, M.A.; Moritz, T.; Grebe, M. (2008). Sterol-dependent endocytosis mediates post-cytokinetic acquisition of PIN2 auxin efflux carrier polarity. Nat. Cell Biol. 10, 237–244.

Meng D, Gu Z, Yuan H, Wang A, Li W, Yang Q, Zhu Y, Li T(2014). The microtubule cytoskeleton and pollen tube Golgi vesicle system are required for in vitro S-RNase internalization and gametic self-incompatibility in apple. Plant Cell Physiol 2014,55:977-989

Mérigout, P., Képès, F., Perret, A.M., Satiat-Jeunemaitre, B, Moreau, P. (2002). Effects of brefeldin A and nordihydroguaiaretic acid on endomembrane dynamics and lipid synthesis in plant cells. FEBS let 518:88-92.

Messerli, M.A.; Creton, R.; Jaffe, L.F.; Robinson, K.R. (2000). Periodic increases in elongation rate precede increases in cytosolic Ca2+ during pollen tube growth, Dev. Biol. 222 84–98.

Michard, E.; Simon, A.A.; Tavares, B.; Wudick, M.M.; Feijó, J.A. (2017). Signaling with Ions: The Keystone for Apical Cell Growth and Morphogenesis in Pollen Tubes. Plant. Physiol. 173, 91-111;

Micheli, F. (2001). Pectin methylesterases: Cell wall enzymes with important roles in plant physiology. Trends Plant Sci 6, 414–419.

Miguel Angel Del Pozo, M. A.; Kiosses, W.B.; Alderson, N.B.; Meller, N.; Hahn, K.M.; Schwartz, M.A. (2002). Integrins regulate GTP-Rac localized effector interactions through dissociation of Rho-GDI. Nat. Cell Biol. 4, 232-239

Molendijk, A.J; Ruperti, B.; Palme, K. (2004). Small GTPases in vesicle trafficking. Curr. Opin. Plant Biol. 7(6):694-700

Mongrand, S., Morel, J., Laroche, J., Claverol, S., Carde, J. P., Hartman, M. A., Bonneu, M., Simon Plas, F., Lessire, R. and Bessoule, J. J. (2004). Lipid rafts in higher plant cells: purification and characterization of Triton X-100-insoluble microdomains from tobacco plasma membrane. J. Biol. Chem. 279, 36277-36286.

Moreau, P. (2007). Lipids – Architects and regulators of membrane dynamics and trafficking. Plant Signal Behav 2(3):157-9.

Morel, J.S.; Claverol, S.; Mongrand, F.; Furt, J.; Fromentin, J.J.; Bessoule, J.P.; Blein, F.; Simon-Plas, F. (2006). Proteomics of plant detergent-resistant membranes. Mol. Cell Proteomics, *5*, 1396–1411.

Moscatelli A., Gagliardi., A., Maneta-Peyret, L., Bini, L., Stroppa, N., Onelli, E., Scali, M., Idilli, A. I. and Moreau, P. (2015). Characterization of detergent-insoluble membranes in pollen tubes of *Nicotiana tabacum* (L.). Biol. Open, doi:10.1242/bio.201410249.

Moscatelli, A. and Idilli, A. I. (2009). Pollen tube growth: a delicate equilibrium between secretory and endocytic pathways. J. Integr. Plant Biol. 51, 727-739

Moscatelli, A.; Ciampolini, F.; Rodighiero, S.; Onelli, E.; Cresti, M.; Santo, N.; Idilli, A.I. (2007). Distinct endocytic pathways identified in tobacco pollen tubes using charged nanogold. J. Cell Sci. 120, 3804–3819.

Moscatelli, A.; Idilli, A.I.; Rodighiero, S.; Caccianiga, M. (2012). Inhibition of actin polymerisation by low concentration Latrunculin B affects endocytosis and alters exocytosis in shank and tip of tobacco pollen tubes. Plant Biol., doi:10.1111/j.1438-8677.2011.00547.x.

Moustacas, A.M., Nari, J., Borel, M., Noat, G., and Ricard, J. (1991). Pectin methylesterase, metal ions and plant cell-wall extension. The role of metal ions in plant cell-wall extension. Biochem. J. 279, 351-354

Nakamura, M.; Kuroiwa, N.; Kono, Y.; Takatsuki, A. (2001). Glucosylceramide synthesis inhibitors block pharmacologically induced dispersal of the Golgi anterograde membrane flow from the endoplasmic reticulum: implication of sphingolipid metabolism in maintenance of the Golgi architecture and anterograde membrane flow. Biosci Biotech Biochem 65:1369-1378

Nebenführ, A., Ritzenthaler, C., and Robinson, D. G. (2002). Brefeldin a: deciphering an enigmatic inhibitor of secretion. Plant Physiol. 130, 1102–1108. doi: 10.1104/pp.011569

Nesterkina, I.S.; Ozolina, N.V.; Nurminsky, V.N. (2015). Characteristics of lipids in microdomains extracted by different methods from vacuolar membranes. Biochem. Moscow Suppl. Ser. A 9, 252–258

Nishizuka Y. (1988). The molecular heterogeneity of protein kinase C and its implications for cellular regulation. Nature. 334(6184):661-5.

Nurminsky, V.N., Nesterkina, I.S., Spiridonova, E.V. (2017). Identification of sterol-containing domains in vacuolar membranes by confocal microscopy. Biochem. Moscow Suppl. Ser. A 11, 296–300

O'Luanaigh N, Pardo R, Fensome A, Allen-Baume V, Jones D,Holt MR et al. (2002). Continual production of phosphatidic acidby phospholipase D is essential for antigen-stimulated membraneruffling in cultured mast cells. *Mol. Biol. Cell* **13**, 3730–3746

Oda. Y.; Hirata, A.; Sano, T.; Fujita, T.; Hiwatashi, Y.; Sato, Y.; Kadota, A.; Hasebe, M.; Hasezawa, S. (2009). Microtubules regulate dynamic organization of vacuoles in *Physcomitrella patens*. Plant Cell Physiol. 50(4):855-68.

Ohtani, Y., Irie, T., Uekama, K., Fukunaga, K. and Pitha, J. (1989). Differential effects of alpha-, beta- and gamma-cyclodextrins on human erythrocytes. Eur. J.Biochem. 186, 17-22.

Okamoto, T.; Schlegel, A.; Scherer, P.E., Lisanti, M.P. (1998). Caveolins, a family of scaffolding proteins for organizing ‘‘preassembled signaling complexes’’ at the plasma membrane’’. J. Biol. Chem. 273:5419–5422

Onelli, E., Beretta, M., Moscatelli, A., Caccianiga , M., Pozzi, M., Stroppa, N. and Adamec, L. (2020). The aquatic carnivorous plant *Aldrovanda vesiculosa* (Droseraceae) exhibits altered developmental stages in male gametophyte. Protoplasma.

Onelli, E.; Idilli, A.I.; Moscatelli, A. (2015). Emerging roles for microtubules in angiosperm pollen tube growth highlight new research cues. Front Plant Sci 6:51.

Onelli, E.; Prescianotto-Baschong, C.; Caccianiga, M.; Moscatelli, A. (2008). Clathrin-dependent and independent endocytic pathways in tobacco protoplasts revealed by labelling with charged nanogold. J. Exp. Bot. 59, 3051–3068

Opekarova M, Tanner W (2003). Specific lipid requirements of membrane proteins—a putative bottleneck in heterologous expression. Biochim Biophys Acta Biomembranes 1610:11–22

Ovecka, M., Berson, T., Beck, M., Derksen, J., Samaj, J., Baluska, F. and Lichtscheidl, I. K. (2010). Structural sterols are involved in both the initiation and tip growth of root hairs in *Arabidopsis thaliana*. Plant Cell 22, 2999-3019.

Ozolina N.V., Nesterkina I.S., Kolesnikova E.V., Salyaev R.K., Nurminsky V.N., Rakevich A.L., Martynovich E.F., Chernyshov M.Yu. (2013). Tonoplast of *Beta vulgaris* L. contains detergent-resistant membrane microdomains. Planta. 237 (3), 859–871.

Paladino, S., Sarnataro, D., Pillich, R., Tivodar, S., Nitsch, L. and Zurzolo, C. (2004). Protein oligomerization modulates raft partitioning and apical sorting of GPI-anchored proteins. J. Cell Biol. 167, 699-709.

Paladino, S., Sarnataro, D., Tivodar, S. and Zurzolo, C. (2007). Oligomerization is a specific requirement for apical sorting of glycosyl-phosphatidylinositol anchored proteins but not for non-raft-associated apical proteins. Traffic 8, 251-258

Paradez, A., Wright, A., and Ehrhardt, D. W. (2006). Microtubule cortical array organization and plant cell morphogenesis. Curr. Opin. Plant Biol. 9, 571–578.

Paredez, A.R., Somerville, C.R., and Ehrhardt, D.W.(2006). Visualization of cellulose synthase demonstrates functional association with microtubules. Science 312, 1491–1495.

Parre, E., and Geitmann, A. (2005). Pectin and the role of the physical properties of the cell wall in pollen tube growth of *Solanum chacoense*. Planta 220,582–592

Parton, R.M.; Fischer-Parton, S.; Watahiki, M.K.; Trewavas, A.J. (2001). Dynamics of the apical vesicle accumulation and the rate of growth are related in individual pollen tubes. J. Cell Sci. 114, 2685–2695.

Pechlivanis, M. and Kuhlmann, J. (2006). Hydrophobic modifications of Ras proteins by isoprenoid groups and fatty acids – more than just membrane anchoring. Biochim. Biophys. Acta 1764, 1914-1931.

Peskan, T.; Westermann, M.; Oelmuller, R. (2000). Identification of low-density Triton X-100-insoluble plasmamembrane microdomains in higher plants. FEBS J. 267, 6989–6995.

Picton, J. M. and Steer, M.W. (1983). Membrane recycling and the control of secretory activity in pollen tubes. J. Cell Sci. 63, 303–320

Picton, J.M.; Steer M.W. (1982). A model for the mechanism of tip extension in pollen tubes. J. Theor. Biol. 98, 15–20.

Pierson, E.S.; Derksen, J.; Traas, J.A. (1986). Organization of microfilaments and microtubules in pollen tubes grown in vitro or in vivo in various angiosperms. European Journal of Cell Biology 41, 14-18.

Pierson, E.S.; Miller, D.D.; Callaham, D.A.; Shipley, A.M.; Rivers, B.A.; Cresti, M. (1994). Pollen tube growth is coupled to the extracellular calcium ion flux and the intracellular calcium gradient: effect of BAPTA-type buffers and hypertonic media. Plant Cell 6, 1815–1828

Pierson, E.S.; Miller, D.D.; Callaham, D.A.; van Aken, J.; Hackett, G.; Hepler, P.K. (1996). Tip-localized calcium entry fluctuates during pollen tube growth, Dev. Biol. 174 (1996) 160–173.

Pike L.J. 2006 Rafts defined: a report on the Keystone symposium on lipid rafts and cell function. J. Lipid Res. 47: 1597-1598

Pina, C., Pinto, F., Feijo´, J.A., and Becker, J.D. (2005). Gene family analysis of the Arabidopsis pollen transcriptome reveals biological implications for cell growth, division control and gene expression regulation. Plant Physiol. 138,744–756.

Piperno, G.; LeDizet, M.; Chang, X.J. (1987). Microtubules containing acetylated alpha tubulin in mammalian cells in culture. J. Cell Biol. 104, 289-302.

Pollard, T.D. (2007). Regulation of actin filament assembly by Arp2/3 complex and formins. Annu. Rev. Biophys. Biomol. Struct. 36, 451–477.

Potocký, M., Elias, M., Profotova B., Novotna Z., Valentova O., Zarsky V., (2003). Phosphatididc acid produced by phospholipase D is required for tobacco pollen tube growth. Planta 217, 122–130.

Poulter, N.S.; Vatovec, S.; Franklin-Tong, V.E. (2008). Microtubules are a target for self-incompatibility signaling in Papaver pollen. Plant Physiol, 146:1358-1367.

Qin, T.; Lui, X. M.; Li, J. J.; Sun, J. B.; Song, L. N. and Mao, T. L. (2014). Arabidopsis microtubule-destabilizing protein 25 functions in pollen tube growth by severing actin filaments. Plant Cell 26, 325-339.

Qiu, J.L.; Jilk, R.; Marks, M.D.; Szymanski, D.B. (2002). The arabidopsis SPIKE1 gene is required for normal cell shape control and tissue development. Plant cell 14, 101-118

Qu, X.; Zhang, H.; Xie, Y.; Wang, J.; Chen, N.; Huang, S. (2013). Arabidopsis villins promote actin turnover at pollen tube tips and facilitate the construction of actin collars. Plant Cell 25:1803-1817.

Raiborg, C. and Stenmark, H. (2009). The ESCRT machinery in endosomal sorting of ubiquitylated membrane proteins. Nature 458, 445–452.

Rajendran, L., and Simons, K. (2005). Lipid rafts and membrane dynamic. Journal of Cell Science 2005 118: 1099-1102

Ren, C. and Kermode, A.R. (2000). An Increase in Pectin Methyl Esterase Activity Accompanies Dormancy Breakage and Germination of Yellow Cedar Seeds. Plant Physiol 124: 231-242

Robinson, K.R. and Messerli, M.M. (2002). Pulsating ion fluxes and growth at the pollen tube tip. Science 162, 51-53.

Roche, Y., Gerbeau-Pissot, P., Buhot, B., Thomas, D., Bonneau, L., Gresti, J., Mongrand, S., Perrier-Cornet, J. M. and Simon-Plas, F. (2008). Depletion of phytosterols from the plant plasma membrane provides evidence for disruption of lipid rafts. FASEB J. 22, 3980-3991.

Rockel N, Wolf S, Kost B, Rausch T, Greiner S. (2008). Elaborate spatial patterning of cell-wall PME and PMEI at the pollen tube tip involves PMEI endocytosis, and reflects the distributionof esterified and de-esterified pectins. Plant J 53:133-143.

Romagnoli, S.; Cai, G.; Cresti, M. (2003). In vitro assays demonstrate that pollen tube organelles use kinesin-related motor proteins to move along microtubules. Plant Cell 2003, 15, 251–269.

Romer, W., L. Berland, V. Chambon, K. Gaus, B. Windschiegl, D. Tenza, M.R. Aly, V. Fraisier, J.C. Florent, D. Perrais, et al. (2007). Shiga toxin induces tubular membrane invaginations for its uptake into cells. Nature. 450:670–675.

Rosenberger, C.M.; Brumell, J.H.; Finlay, B.B. (2000). Microbial patho-genesis: lipid rafts as pathogen portals. Curr Biol 10:R823–R825

Rosquete, M.R.; Davis, D.J.; Drakakaki, G. (2018). The Plant Trans-Golgi Network: Not Just a Matter of Distinction. Plant Physiol. 176(1):187-198.

Rotsch, A.H.; Kopka, J.; Feussner, I.; Ischebeck, T. (2017). Central metabolite and sterol profiling divides tobacco male gametophyte development and pollen tube growth into eight metabolic phases. Plant J. 92(1):129-146.

Rounds, C. M., Hepler, P. K. and Winship L. J. (2014). The apical actin fringe contributes to localized cell wall deposition and polarized growth in the Lily pollen tube. Plant Physiol. 166, 139–151.

Rounds, C.M., and Bezanilla M., (2013). Growth mechanisms in tip-growing plant cells. Annu Rev Plant Biol. 2013;

Saheki, Y. and de Camilli, P. (2012). Synaptic vesicle endocytosis. Cold Spring Harb. Perspect. Biol. 2012, doi:10.1101/cshperspect.a005645.

Salun, C.; James, D.J.; Chamberlain, L.H. (2004). Lipid rafts and the regulation of exocytosis. Traffic 5:255–264

Sampathkumar A, Gutierrez R, McFarlane HE, Bringmann M,Lindeboom J, Emons AM, Samuels L, Ketelaar T, Ehrhardt DW, Persson S. (2013). Patterning and lifetime of plasma membrane-localized cellulose synthase is dependent on actin organization in *Arabidopsis* interphase cells. Plant Physiology 162, 675–688.

Samson et al., 1979 Samson, F., Donoso, A.J., Heller-Bettingher, I., Watson, D., and Himes, R.H. (1979). Nocodazole action on tubulin assembly, axonal ultrastructure and fast axoplasmic transport. J. Pharm. Exp. Ther. 20, 411–417.

Sanford, J.C.; Klein, T.M.; Wolf, E.D.; Allen, N. (1993). Delivery of substances into cells and tissues using a particle bombardment process. J. Particle Scie. Technol. 5:27-37

Scheible N, McCubbin A. (2019). Signaling in Pollen Tube Growth: Beyond the Tip of the Polarity Iceberg. Plants (Basel) 8(6):156.

Scheuring, D.; Künzl, F.; Viotti, C.; San Wan Yan, M.; Jiang, L.; Schellmann, S.; Robinson, D.G.; Pimpl, P. (2012). Ubiquitin initiates sorting of Golgi and plasma membrane proteins into the vacuolar degradation pathway. BMC Plant Biol. doi:10.1186/1471-2229-12-164

Schneider C. A.; Rasband W. S.; Eliceiri K. W. (2012). NIH Image to ImageJ: 25 years of Image Analysis. Nat Methods. 9(7): 671–675.

Schrick, K., DeBolt, S. and Bulone, V. (2012). Deciphering the molecular functions of sterols in cellulose biosynthesis. Front. Plant Sci. 3:84. doi:10.3389/fpls.2012.00084

Schrick, K., Fujioka, S., Takatsuto, S., Stierhof, Y. D., Stransky, H., Yoshida, S., et al. (2004). A link between sterol biosynthesis, the cell wall, and cellulose in *Arabidopsis*. Plant J. 38, 227–243.

Schroeder, R., London, E. and Brown, D. (1994). Interactions between saturated acyl chains confer detergent resistance on lipids and glycosylphosphatidylinositol (GPI)-anchored proteins: GPI-anchored proteins in liposomes and cells show similar behavior. Proc. Natl. Acad. USA 91, 12130-12134.

Short B. (2009). Lipid rafts inflate at the trans-Golgi. J Cell Biol. 185: 567. doi: 10.1083/jcb.1854if

Silvius, J.R. (2003). Role of cholesterol in lipid raft formation: Lessons from lipid model systems. Biochim. Biophys. Acta 1610, 174–183.

Simons, K. and Ikonen, E. (1997). Functional rafts in cell membranes. Nature 387, 569-572.

Simons, K. and Sampaio, J. L. (2011). Membrane organization and lipid rafts. Cold Spring Harb. Perspect. Biol. 3(10):a004697.

Simons, K. and Toomre, D. (2000). Lipid rafts and signal transduction. Nat. Rev. Mol. Cell Biol. 1, 31-39.

Simons, K. and van Meer, G. (1988). Lipid sorting in epithelial cells. Biochemistry 27, 6197-6202.

Simons, K.; Gerl, M.-J. (2010). Revitalizing membrane rafts: New tools and insights. Nat. Rev. Mol. Cell Biol. 11, 688–699.

Singer, S. J. and Nicolson, G. L. (1972). The fluid mosaic model of the structure of cell membranes. Science 175, 720-731.

Steer MW, Steer JM. 1989 Pollen tube tip growth. *New Phytol.* 111:323–358.

Steinhorst and Kudla (2013). Calcium - a central regulator of pollen germination and tube growth. Biochimica et Biophysica Acta 1833: 1573-1581

Steinhorst, L. and Kudla, J. (2013). Calcium - a central regulator of pollen germination and tube growth. Mol. Cell Res 1833, 1573-1581

Stenzel, I.; Ischebeck, T.; Vu-Becker, L.H.; Riechmann, M.; Krishnamoorthy, P.; Fratini, M.; Heilmann, I. (2020). Coordinated Localization and Antagonistic Function of NtPLC3 and PI4P 5-Kinases in the Subapical Plasma Membrane of Tobacco Pollen Tubes. Plants 2020, 9, 452

Stępka, M., Ciampolini, F., Charzynska, M., and Cresti, M.(2000). Localization of pectins in the pollen tube wall of *Ornithogalum virens* L. Does the pattern of pectin distribution depend on the growth rate of the pollen tube? Planta 210,630–635.

Stevenson, J.M.; Perera, I.Y.; Heilmann, I.I.; Persson, S.; Boss, W.F. (2000). Inositol signaling and plant growth. Trends Plant Sci. 5, 252–258.

Surma MA, Klose C, Klemm RW, Ejsing CS, Simons K (2011). Generic Sorting of Raft Lipids into Secretory Vesicles in Yeast. Traffic 12: 1139–1147

Sweeney, D:A.; Siddahanta, A.; Shields, D. (2002). Fragmentation and reassembly of the Golgi apparatus in vitro: a requirement for phosphatidic acid and phosphatidylinositol 4,5 bisphosphate synthesis. J. Biol. Chem. 77, 3030-3039.

Szumlanski AL, Nielsen E. (2009). The Rab GTPase RabA4d regulates pollen tube tip growth in *Arabidopsis thaliana*. Plant Cell. 21(2):526-544. doi:10.1105/tpc.108.060277

Takai, Y.; Sasaki, T.; Matozaki, T. (2001). Small GTP-binding proteins. Physiol. Rev. 81,153–208

Taverna, E., Saba, E., Rowe, J., Francolini, M., Clementi, F. and Rosa, P. (2004). Role of lipid microdomains in P/Q-type calcium channel (Cav2.1) clustering and function in presynaptic membranes. J. Biol. Chem. 279, 5127-5134.

Taylor, L.P. and Hepler, P.K. (1997). Pollen germination and tube growth. Annu Rev Plant Physiol Plant Mol Biol 48, 461–491.

Tiezzi, A.; Moscatelli, A.; Cai, G.; Bartalesi, A.; Cresti, M. (1992). An immunoreactive homolog of mammalian kinesin in *Nicotiana tabacum* pollen tubes. Cell Motil. Cytoskel. 21, 132–137.

Towbin, H.; Staehelin, T. and Gordon, J. (1979). Electrophoretic transfer of proteins from polyacrylamide gels to nitrocellulose sheets. Procedure and some application. Proc. Natl. Acad. Sci. USA 76, 4350-4354

Turner, T.; Bacic, A.; Harris, P.J.; Read, S.M. (1998). Membrane fractionation and enrichment of callose synthase from pollen tubes of *Nicotiana alata* Planta 205:380-388

Uemura, T., Nakano, R.T., Takagi, J. et al. (2019). A Golgi-released subpopulation of the trans-Golgi network mediates protein secretion in *Arabidopsis*. Plant Physiol. 179, 519–532.

Uemura, T., Suda, Y., Ueda, T. & Nakano, A. (2014). Dynamic behavior of the trans-Golgi network in root tissues of *Arabidopsis* revealed by super-resolution live imaging. Plant Cell Physiol. 55, 694–703.

van Meer G., Simons K. (1988). Lipid polarity and sorting in epithelial cells. J Cell Biochem. 36(1):51-8. doi: 10.1002/jcb.240360106. PMID: 3277985.

Valverde, A.M.; Sinnett-Smith, J.; Van Lint, J.; Rozengurt, E. (1994). Molecular cloning and characterization of protein kinase D: a target for diacylglycerol and phorbol esters with a distinctive catalytic domain Proc. Natl. Acad. Sci. USA 1994 91, 8572-8576

Van Aelst, L. and D'Souza-Schorey, C. (1997). Rho GTPases and signalling network. *Gene Dev.* **11**, 2295–2322.

Verhoek, B., Haas, R., Wrage, K., Linscheid, M., and Heinz, E. (1983). Lipids and enzymatic activities in vacuolar membranes isolated via protoplasts from oat primary leaves. Z Naturforsch38c:770–777.

Vernoud, V.; Horton, A.C.; Yang, Z.; Nielsen, E. (2003). Analysis of the small GTPase gene superfamily of *Arabidopsis*. Plant Physiol.131, 1191–1208

Vidali, L., McKenna, S. T. and Hepler, P. K. (2001). Actin polymerization is essential for pollen tube growth. Mol. Biol. Cell 12, 2534–2545.

Vidali, L., Rounds, C. M., Hepler, P. K., and Bezanilla, M. (2009). Lifeact-mEGFP Reveals a Dynamic Apical F-Actin Network in Tip Growing Plant Cells. PLoS ONE 4(5): e5744. doi:10.1371/journal.pone.0005744.

Vidali, L.; Yokota, E.; Cheung, A.Y.; Shimmen, T.; Hepler, P.K. (1999). The 135 KDa actinbundling protein from *Lilium longiflorum* pollen is the plant homologue of villin. Protoplasma 209, 283-91

Villette, C., Berna, A., Compagnon, V. and Schaller, H. (2015). Plant Sterol Diversity in Pollen from Angiosperms. Lipids. DOI 10.1007/s11745-015-4008-x.

Viotti C, Bubeck J, Stierhof YD, Krebs M, Langhans M, van den Berg W, van Dongen W, Richter S, Geldner N, Takano J, et al (2010) Endocytic and secretory traffic in *Arabidopsis* merge in the trans-Golgi network/ early endosome, an independent and highly dynamic organelle. Plant Cell 22: 1344–1357

Vogler, H.; Santos-Fernandez, G.; Mecchia, M.A.; Grossniklaus, U. (2019). To preserve or to destroy, that is the question: the role of the cell wall integrity pathway in pollen tube growth. Curr. Opin. Plant. Biol 52, 131-139;

von Wangenheim D, Rosero A, Komis G, Samajova O, Ovecka M, Voigt B, Samaj J. (2016). Endosomal interactions during root hair growth. Front. Plant Sci. 6, 1262.

Wang, Y., Yhiele, C., Huttner, W.B. (2000). Cholesterol is required for the formation of regulated and constitutive secretory vesicles from the trans-Golgi network. Traffic 1:952-62

Wang, H., Zhuang, X., Cai, Y., Cheung, A. Y., and Jiang, L. (2013). Apical F-actin regulated exocytic targeting of NtPPME1 is essential for construction and rigidity of the pollen tube cell wall. Plant J. 76, 367–379.

Wang, H.; Tse, Y.C.; Law, A.H.; Sun, S.S.; Sun, Y.B.; Xu, Z.F.; Hillmer, S.; Robinson, D.G.; Jiang, L. (2010). Vacuolar sorting receptors (VSRs) and secretory carrier membrane proteins (SCAMPs) are essential for pollen tube growth. Plant J. 61, 826–838.

Wang, H.; Zhuang, X.; Wang, X.; Law, A.H.Y.; Zhao, T.; Du, S.; Loy, M.M.T.; Jiang, L. (2016). A distinct pathway for polar exocytosis in plant cell wall formation. Plant Physiol 172:1003–1018.

Wang, Q.; Kong, L.; Hao, H.; Wang, X., Lin, J.; Samaj, J. (2005). Effects of Brefeldin A on pollen germination and tube growth. Antagonistic effects on endocytosis and secretion. Plant Physiol. 139, 1692–1703

Wang, W.; Wang, L.; Chen, C.; Xiong, G.; Tan, X-Y.; Yang, K-Z.; Wang, Z-C.; Zhou, Y.; Ye, D.; Chen, L-Q. (2011). Arabidopsis CSLD1 and CSLD4 are required for cellulose deposition and normal growth of pollen tubes. J Exp Bot 62:5161-5177

Wattelet-Boyer, V., Brocard, L., Jonsson, K., Esnay, N., Joubès, J., Domergue, F., Mongrand, S., Raikhel, N., Bhalerao, R.P., Moreau, P. and Boutté, Y. (2016). Enrichment of hydroxylated C24- and C26-acyl-chain sphingolipids mediates PIN2 apical sorting at *trans*-Golgi network subdomains. Nat Commun 7:12788

Wen, F.; Zhu, Y.; Hawes, M.C. (1999). Effect of Pectin Methylesterase Gene Expression on Pea Root Development. The Plant Cell 11, 1129–1140.

Winge, P.; Brembu, T. and Bones, A.M. (1997). Cloning and characterization of rac-like cDNAs from *Arabidopsis thaliana*. Plant Mol. Biol.35, 483–495

Worden, N.; Park, E.; Drakakaki, G. (2012). Trans-Golgi network: an intersection of trafficking cell wall components. J Integr Plant Biol 54: 875–86

Yang, C. and Kazanietz, M.G. (2003). Divergence and complexities in DAG signaling: looking beyond PKC. Trends Pharmacol. Sci. 24, 602-608

Ye, J.; Zheng, Y.; Yan, A.; Chen, N.; Wang, Z.; Huang, S.; Yang, Z. (2009). *Arabidopsis* formin3 directs the formation of actin cables and polarized growth in pollen tubes. Plant Cell, 21, 3868–3884.

Yoshida, S., Uemura, M. (1986). Lipid Composition of Plasma Membranes and Tonoplasts Isolated from Etiolated Seedlings of Mung Bean (*Vigna radiata* L.). Plant Physiol. 82(3):807-12

Zhang, M.J.; Zhang, X.S.; Gao, X-Q. (2020). ROS in the Male–Female Interactions During Pollination: Function and Regulation. Front. Plant. Sci, 11, 177

Zhang, Y. and McCormick, S. (2007). A distinct mechanism regulating apollen-specific guanine nucleotide exchange factor for the smallGTPase Rop in *Arabidopsis thaliana*.Proc. Natl. Acad. Sci. U. S. A.104, 18830–18835

Zhao, Y.; Yan, A.; Feijó, J.A.; Furutani, M.; Takenawa, T.; Hwang, I.; Fu, Y.; Yang, Z. (2010). Phosphoinositides regulate clathrin-dependent endocytosis at the tip of pollen tubes in *Arabidopsis* and tobacco. Plant Cell 2010, 22, 4031–4044.

Zhu, L.; Zhang, Y.; Kang, E.; Xu, Q.; Wang, M.; Rui, Y.; Liu, B.; Yuan, M.; Fu, Y. (2013). MAP18 regulates the direction of pollen tube growth in *Arabidopsis* by modulating F-actin organization. Plant Cell 25:851-867.

Zhu, L.; Zhang, Y.; Kang, E.; Xu, Q.; Wang, M.; Rui, Y.; Liu, B.; Yuan, M.; Fu, Y. (2013). MAP18 regulates the direction of pollen tube growth in *Arabidopsis* by modulating F-actin organization. Plant Cell 25:851-867.

Zidovetzki, R. and Levitan, I. (2007). Use of cyclodextrins to manipulate plasma membrane cholesterol content: evidence, misconceptions and control strategies. Biochim. Biophys. Acta 1768, 1311-1324.

Zonia L, Munnik T. (2011). Understanding pollen tube growth: the hydrodynamic model versus the cell wall model. Trends Plant Sci. 16(7):347-52.

Zonia, L. and Munnik, T. (2008). Vesicle trafficking dynamics and visualization of zones of exocytosis and endocytosis in tobacco pollen tubes. Journal of Experimental Botany, 59, 861–873.

Zonia, L. Muller M. Munnik, T (2006). Hydrodynamics and cell volume oscillations in the pollen tube apical region are integral components of the biomechanics of *Nicotiana tabacum* pollen tube growth. Cell Biochem. Biophys. 46, 209–232

Zonia, L. Munnik, T. (2007). Life under pressure: hydrostatic pressure in cell growth and function. Trends Plant Sci. 12, 90–97

Zonia, L.; Cordeiro, S.; Tupy, J.; Feijó J.A. (2002). Oscillatory chloride efflux at the pollen tube apex has a role in growth and cell volume regulation and is targeted by inositol 3,4,5,6-tetrakisphosphate. Plant Cell 14 2233–2249.

Zou,Y., Aggarwal, M., Zheng, W-G., Wu, H-M. and Cheung, AY. (2011). Receptor-like kinases as surface regulators for RAC/ROP-mediated pollen tube growth and interaction with the pistil. AoB PLANTS 2011 plr017.

SUPPLEMENTARY FIGURE S1

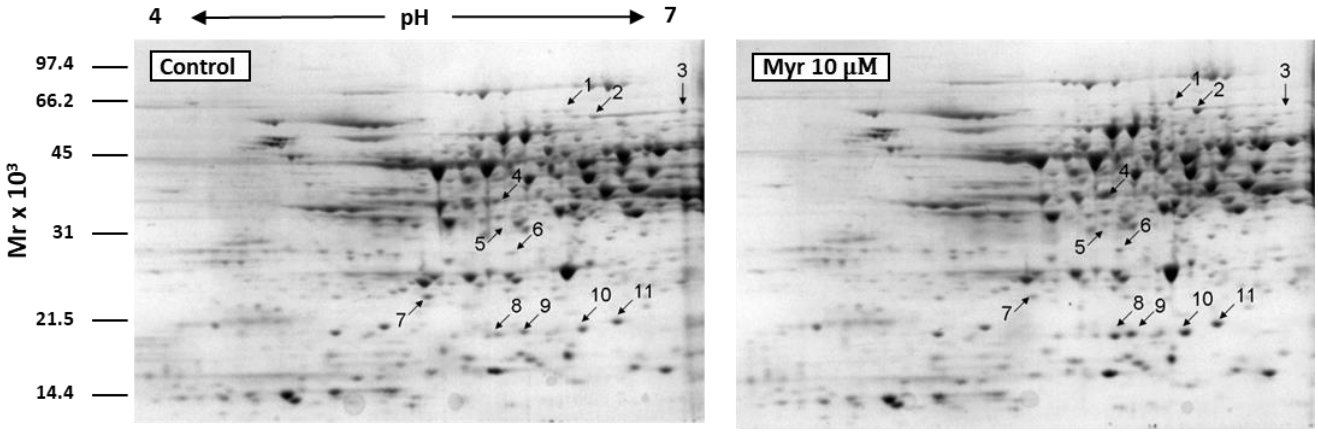

Fig. S1 Effect of 10µm Myr on pollen tube soluble proteome. 2-DE of pollen tube soluble proteome in Control cells, and after Myr treatment. Differentially abundant protein species (DAPs) are indicated by arrows. (Courtesy of Monica Scali, Department of Life Science, University of Siena).

PART II

The following chapters refer to other collaborations during my PhD

Chapter 2

Onelli E, Scali M, Caccianiga M, Stroppa N, Morandini P, Pavesi G, Moscatelli A. (2018). Microtubules play a role in trafficking prevacuolar compartments to vacuoles in tobacco pollen tubes. Open Biol. 8(10):180078.

At the beginning of my PhD, in my laboratory, studies on degradative pathways in pollen tubes, was in progress. In particular on the role of microtubules in trafficking of PVCs to tubular vacuoles. I took part in the project performing different experiments. The use of SYP21 made it possible to identify, for the first time, PVCs and tubular vacuoles as crucial steps in the MT-dependent degradation pathways. Probs and techinques used in this work became useful for study membrane trafficking in my PhD project.

Chapters 3, 4 and 5 refers to the LOW METAL project, supported by the Ministry of Agriculture Food and Forestry Policies (MIPAF). I worked on this project two years before PhD, but later, collaboration with colleagues continued in order to publish our results on phytoremediation solution for the refinement of livestock wastewaters.

Chapter 3

Stroppa N, Onelli E, Hejna M, Rossi L, Gagliardi A, Bini L, Baldi A, Moscatelli A. (2020). *Typha latifolia* and *Thelypteris palustris* behavior in a pilot system for the refinement of livestock wastewaters: A case of study. Chemosphere. 240:124915. doi:10.1016/j.chemosphere.2019.124915. Epub 2019 Sep 20.

Chapter 4

Hejna M, Moscatelli A, Stroppa N, Onelli E, Pilu S, Baldi A, Rossi L. (2020). Bioaccumulation of heavy metals from wastewater through a *Typha latifolia* and *Thelypteris palustris* phytoremediation system. Chemosphere. 241:125018. doi: 10.1016/j.chemosphere.2019.125018. Epub 2019 Oct 11. PMID: 31683415.

Chapter 5

Hejna, M.; Onelli, E.; Moscatelli, A.; Bellotto, M.; Cristiani, C.; Stroppa, N.; Rossi, L. (2021). Heavy-Metal Phytoremediation from Livestock Wastewater and Exploitation of Exhausted Biomass. Int. J. Environ. Res. Public Health 18, 2239. ttps://doi.org/10.3390/ijerph18052239

Chapter 6

Onelli E, Beretta M, Moscatelli A, Caccianiga M, Pozzi M, Stroppa N, Adamec L. (2021). The aquatic carnivorous plant *Aldrovanda vesiculosa* (Droseraceae) exhibits altered developmental stages in male gametophyte Protoplasma. 258(1):71-85. doi: 10.1007/s00709-020-01553-6. Epub 2020 Sep 11. PMID: 32918205.

In collaboration with Institute of Botany of the Czech Academy of Sciences, in this work we studied reproductive biology of *Aldrovanda vesiculosa* L, a rare and endangered aquatic carnivorous plant. The plants mainly propagate vegetatively; our aim was to study Aldrovanda pollen structure in pollen collected from flowers of different ages and development stages (opened and non-opened anthers) in plants of several world populations, to elucidate the conserved pollination traits of Aldrovanda and the reason for its poor seed set.

OPEN BIOLOGY

rsob.royalsocietypublishing.org

Research

Cite this article: Onelli E, Scali M, Caccianiga M, Stroppa N, Morandini P, Pavesi G, Moscatelli A. 2018 Microtubules play a role in trafficking prevacuolar compartments to vacuoles in tobacco pollen tubes. *Open Biol.* **8**: 180078. http://dx.doi.org/10.1098/rsob.180078

Received: 3 May 2018
Accepted: 4 October 2018

Subject Area:
cellular biology/biochemistry

Keywords:
microtubules, prevacuolar compartment, pollen tube, *Nicotiana tabacum*, vacuole

Authors for correspondence:
Elisabetta Onelli
e-mail: elisabetta.onelli@unimi.it
Alessandra Moscatelli
e-mail: alessandra.moscatelli@unimi.it

Electronic supplementary material is available online at https://dx.doi.org/10.6084/m9.figshare.c.4265108.

THE ROYAL SOCIETY PUBLISHING

Microtubules play a role in trafficking prevacuolar compartments to vacuoles in tobacco pollen tubes

Elisabetta Onelli[1], Monica Scali[2], Marco Caccianiga[1], Nadia Stroppa[1], Piero Morandini[1], Giulio Pavesi[1] and Alessandra Moscatelli[1]

[1]Department of Biosciences, Milan University, Via Celoria 26, 20133 Milan, Italy
[2]Department of Life Science, Siena University, Via A. Moro 2, 53100 Siena, Italy

AM, 0000-0003-0912-5697

Fine regulation of exocytosis and endocytosis plays a basic role in pollen tube growth. Excess plasma membrane secreted during pollen tube elongation is known to be retrieved by endocytosis and partially reused in secretory pathways through the Golgi apparatus. Dissection of endocytosis has enabled distinct degradation pathways to be identified in tobacco pollen tubes and has shown that microtubules influence the transport of plasma membrane internalized in the tip region to vacuoles. Here, we used different drugs affecting the polymerization state of microtubules together with SYP21, a marker of prevacuolar compartments, to characterize trafficking of prevacuolar compartments in *Nicotiana tabacum* pollen tubes. Ultrastructural and biochemical analysis showed that microtubules bind SYP21-positive microsomes. Transient transformation of pollen tubes with LAT52-YFP-SYP21 revealed that microtubules play a key role in the delivery of prevacuolar compartments to tubular vacuoles.

1. Introduction

Pollen tubes are tip-growing cells that convey sperm to the embryo sac for double fertilization in angiosperms [1,2]. However, they are also intriguing cell models for studying membrane trafficking during polarized cell growth. Continuous plasma membrane (PM) recycling maintains distinct functional domains in the apex (5 µm from the tip PM) with respect to the shank (5–25 µm from the tip PM) and distal region (behind the male germ unit), and is due to a fine balance between exocytosis and endocytosis [3,4].

Time-lapse analysis and ultrastructural observations using charged nanogold has partially characterized two endocytic pathways. Plasma membrane internalized in the shank is mostly sent to the Golgi apparatus to be reused in the secretion pathway and partly conveyed to vacuoles through the trans-Golgi network (TGN) [5]. On the other hand, PM internalized in the apex mostly goes to the degradation pathway bypassing the Golgi/TGN apparatus [5]. Specific drugs affecting actin filament (AF) and microtubule (MT) integrity have further defined these degradation pathways: PM internalized in the shank is delivered to multivesicular bodies (MVBs)/prevacuolar compartments (PVCs) and then to vacuoles in an AF-dependent way [6], while PM endocytosed in the tip is conveyed to vacuoles, bypassing the Golgi/TGN, in a MT-dependent manner [7].

The routes of vacuole delivery, which require dynamic interaction between membrane compartments and the cytoskeletal apparatus, have not been fully characterized in pollen tubes. In lily, PVCs were identified by the presence of LIVSR and BP80 and found to be distributed throughout the pollen tube, except in the apical inverted-cone region [8]. In addition, in *Arabidopsis thaliana* it was observed that vacuolar protein sorting 41 (AtVPS41) is involved in late events of degradation pathways in pollen tubes [9]. The importance of

degradation pathways for proper pollen–pistil interaction was recently highlighted and the integrity of degradation pathways plays a crucial role in the proper transport of female cues to vacuoles, in vacuole biogenesis and in pollen tube penetration of style transmitting tissue [9].

It is largely accepted that AFs are responsible for the cytoplasmic streaming that transports organelles and vesicles in the plant cell cytoplasm [10]. In pollen tubes, long AF bundles convey secretory vesicles to the inverted cone region [10] where fine AFs organize into a cortical fringe that undergoes rapid turnover during pulsed growth [11]. The actin fringe plays a role in control of clear zone formation [12] and in exo/endocytosis in the apex and shank, being a prerequisite for pollen tube growth [6,13]. Given their key role in cytoplasmic streaming and pollen tube growth, the structure and function of AFs have been widely studied.

By contrast, the role of MTs in membrane trafficking needs to be characterized. In somatic cells, MTs take part in cell plate formation during cytokinesis and contribute to cell morphogenesis, regulating localized secretion of cellulose synthase complexes to the PM [14,15]. They also contribute to the fine positioning of organelles and are involved in determining organelle morphology and shaping [16–20]. In pollen tubes, MTs control movement of the male germ unit [21] and positioning of large vacuoles in the distal regions of the tube [22]. More recently, it was reported that MTs also play a role in exocytosis in the central region of the tip and in endosome trafficking [7,19]. Specifically, MT perturbation by nocodazole delayed transport of endocytic vesicles to the vacuoles [7] and redirected the endocytosed material to the Golgi apparatus, suggesting that MTs are involved in transport of endosomes towards vacuoles [7].

As the putative function of MTs in degradation pathways has not yet been thoroughly investigated in pollen tubes, the goal of this study is to characterize membrane trafficking to vacuoles and the role of MTs in these pathways.

For this purpose, different drugs affecting MT polymerization were employed together with SYP21 as a marker of PVCs [23–25]. Binding experiments using taxol-purified MTs and biochemical analysis revealed that MTs interact with SYP21-positive compartments *in vitro*. Transient transformation of pollen grains with pLAT52:YFP-SYP21 plasmid showed that SYP21 localized in round organelles identified as PVCs and on tubular vacuoles in growing tobacco pollen tubes. Perturbation of MTs by different drugs revealed that they are involved in endosome trafficking and in mediating PVC delivery to, and/or fusion with, tubular vacuoles.

2. Results

2.1. Microtubules preferentially bind organelles involved in degradation pathways

In a previous study, internalization assays using charged nanogold showed that MTs play a role in the movement of endocytic vesicles, internalized in the clear zone, towards vacuoles [7].

To confirm that MTs interact with specific organelles, taxol-stabilized MTs were incubated with microsomes purified from tobacco pollen tubes in the presence of AMP-PNP, which allows ATP-dependent permanent binding between MTs and organelles. Transmission electron microscope (TEM) observations showed that about 40% of organelles observed on the grids interact with MTs (figure 1). Most of these compartments showed diameters from 50 to 500 nm (figure 1) and organelles larger than 600 nm were also observed (about 10%; figure 1*d*,*e*). The membrane delimiting most of these compartments appeared smooth and, as observed in MVBs, inner vesicles were evident (figure 1*e*). In other cases, the outer membrane was decorated with small particles that seem to mediate the interaction with MTs (figure 1*f* arrow, *g*). Binding of organelles to MTs occurred preferentially along the MT wall and only occasionally at their end (about 5%; figure 1*c*). The unbound organelles in the grids were isolated (electronic supplementary material, figure S1A,B), suggesting that binding with MTs was not due to high organelle concentration. In the absence of AMP-PNP very few organelles (about 5%) appeared associated with MTs, confirming that AMP-PNP stabilized organelles/MTs binding.

The binding experiments therefore showed that MTs interact with different membrane compartments in tobacco pollen tubes.

To further confirm the interaction between MTs and organelles and in order to investigate the identity of these compartments, western blot analysis was performed (figure 2). Microsomes, incubated with or without MTs (+ or −MT, respectively), were collected by centrifuging through 1.2 M sucrose cushions. The cushion made it possible to separate MT-bound organelles, recovered in the pellet (P fraction), from free organelles, which mostly remained on the surface of the cushion (I fraction). Electrophoretic analysis showed that most proteins were recovered in the I fraction, while the solubilized proteins (S) and P fractions had a lower protein content (figure 2*a*), suggesting that most unbound organelles remained on the cushion. Tubulin was detected in the P fraction, as expected (compare +MT and −MT in figure 2*a*; asterisk). The P fractions with and without MTs (P +/−MT, respectively) were probed using antibodies against organelle-specific markers (figure 2*b*). Western blot and quantitative analysis performed in four independent experiments showed significant enrichment of SYP21 in P +MT compared to P −MT samples (figure 2*b*,*c*), suggesting that MTs interact preferentially with organelles involved in the late degradation pathway. Although enrichment of V-H^+ATPase was observed in P +MT, it was not statistically significant (figure 2*c*).

Antibodies against H^+ATPase, GRP78/Bip and Arf1, which recognize protein markers of PM, endoplasmic reticulum (ER) and Golgi apparatus, respectively [26–28], did not reveal any difference in P +MT and P −MT samples (figure 2*b*,*c*), suggesting that these organelles partly pelleted through the sucrose cushion independently of MTs.

The antibody against SYP21 was also used in immunogold studies in MT-bound organelles (figure 3). About 40% of organelles observed in the grids were labelled by SYP21 antibody in four different experiments (50 images for each experiment were considered). The diameter of labelled compartments ranged from 50 nm to 600 nm (figure 3) in line with the size reported for PVCs in somatic cells [24]. Control experiments performed with normal rabbit serum and with secondary antibody did not show any staining (electronic supplementary material, figure S1C,D, respectively).

These results further sustain the hypothesis that MTs preferentially bind compartments involved in degradation pathways in the tobacco pollen tube.

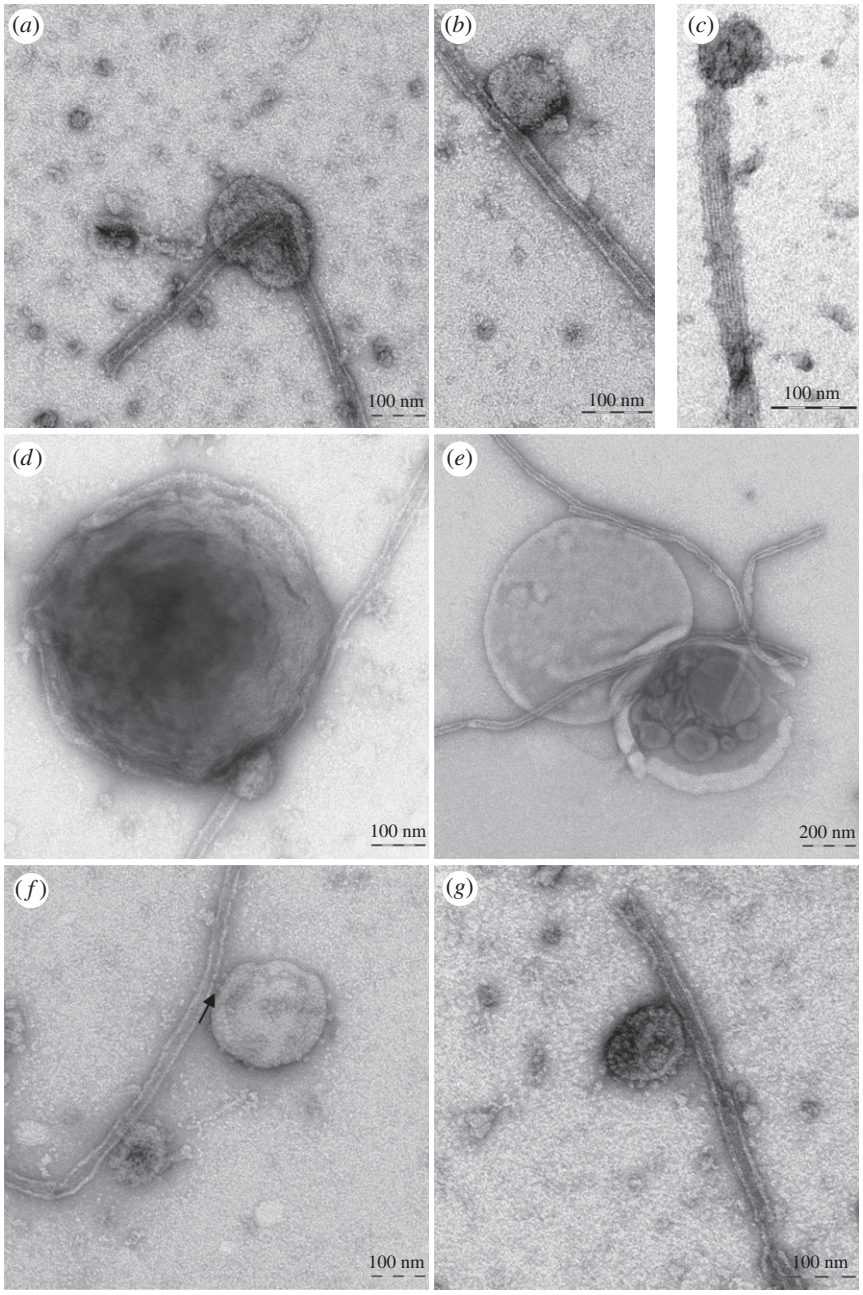

Figure 1. Taxol-purified MTs bind pollen tube microsomes *in vitro*. (*a–c*) Organelles bound to MTs show sizes ranging from 50 to 200 nm in diameter. These organelles, delimited by smooth membranes, preferentially bind to the MT wall and are only occasionally observed at MT ends (*c*). (*d,e*) MTs also bind compartments larger than 600 nm delimited by smooth membranes. Like MVBs, some of these compartments show inner vesicles (*e*). (*f,g*) In some cases, outer membranes of MT-bound compartments are decorated with small particles that appear to mediate their interaction with MTs (arrow). Scale bars, *a–d,f,g* = 100 nm; *e* = 200 nm.

2.2. The binding between MTs and SYP21-positive organelles was specific and ATP-dependent

Enrichment of SYP21 in the P +MT fraction in the presence of AMP-PNP suggested a specific interaction. To confirm the specificity of the MT/SYP21 organelle binding, proteins on the surface of microsomes were stripped with a high concentration of KCl before incubation with MTs (figure 4). The efficiency of stripping was confirmed by a decrease in microsome protein content after KCl treatment (50% with respect to untreated organelles), in three different experiments (figure 4*c*). Western blot analysis using antibodies against protein markers of Golgi apparatus, ER and vacuoles showed that Arf1, GRP78/Bip and the epsilon subunit of V-H^+ATPase were stripped from the organelle surface and recovered in the soluble fraction after salt treatment (figure 4*a*, SDS-PAGE; figure 4*b*, western blot, S-KCl lane). Conversely, SYP21 co-pelleted with MTs as expected, since it has a transmembrane domain in the C-terminus (figure 4*b*, P-KCl −/+MT lane) [26].

Enrichment of SYP21 in the P +MT fraction could suggest that binding of SYP21-positive organelles may not be mediated by surface proteins. However, TEM analysis of MT-bound organelles after KCl stripping showed that the number of compartments bound to MTs increased considerably with respect to untreated microsomes in three different experiments (figure 4*d*) and the organelle delimiting membranes appeared smoother than those of untreated microsomes (figure 4*e,f*; comparison of figure 1).

These findings suggested that specific organelle surface proteins could regulate the interaction with MTs, since in their absence random interactions between MTs and organelles were observed.

The use of AMP-PNP suggested that proteins having ATPase activity could be responsible for the binding between

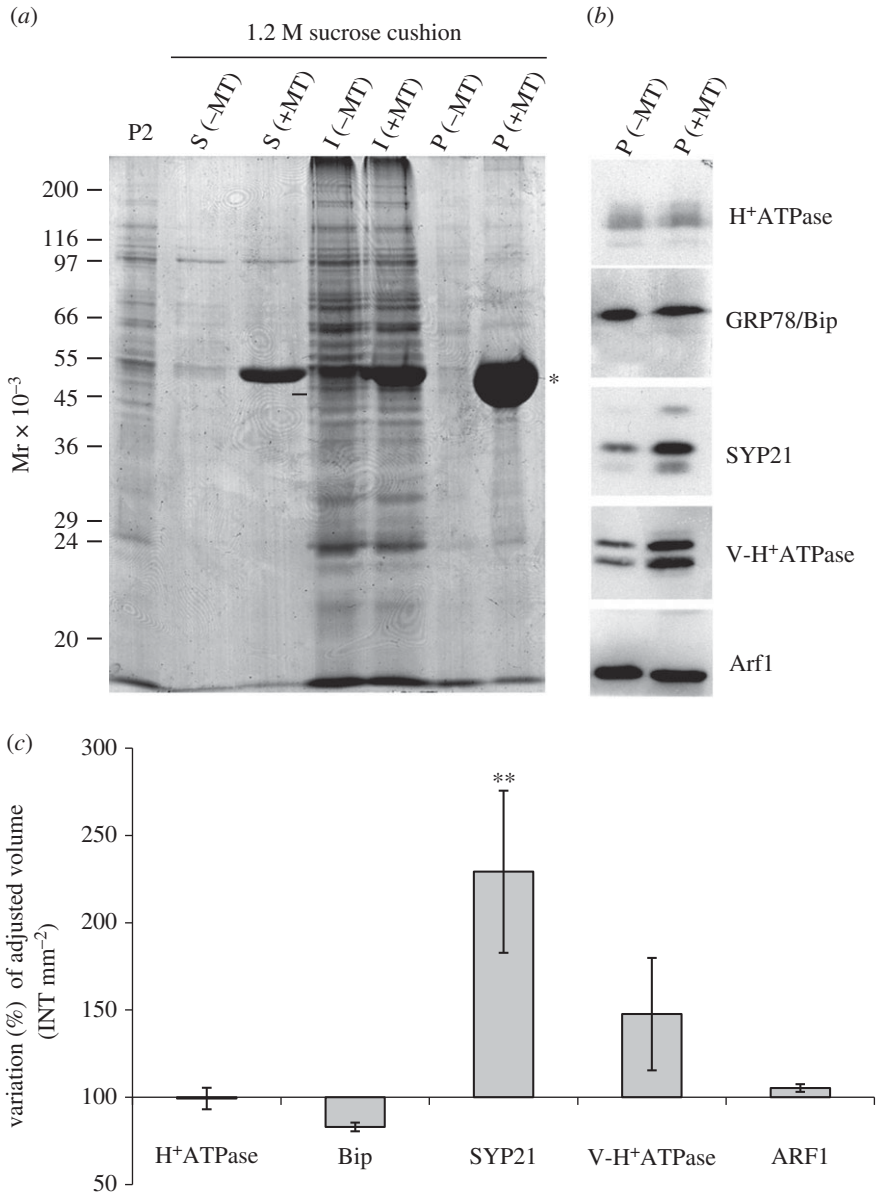

Figure 2. Biochemical characterization of MT-binding experiments. (*a*) Electrophoretic profile of pollen tube microsomal pellet (P) sedimented through a sucrose cushion in the presence or absence of taxol-stabilized MTs (+/−MT, respectively). S lanes show the electrophoretic pattern of soluble polypeptides that do not enter the sucrose cushion irrespective of the presence (+MT) or absence of MTs (−MT). Most organelles remain at the cushion interface in control experiments (I −MT) and MT assays (I +MT). Tubulin was detected particularly in the P +MT fraction (asterisk). (*b*) Antibodies against H^+ATPase, GRP78/Bip, Arf1, V-H^+ATPase and SYP21, probed by western blot on P +/−MT samples, recognize protein markers for PM, ER, Golgi apparatus, vacuoles and PVCs. (*c*) Quantitative analysis using Quantity One software shows significant (Student's *t*-test, $^{**}p < 0.01$) enrichment of SYP21 in P +MT compared to P −MT samples. The graph shows adjusted volume (intensity (INT) mm^{-2}) and percentage variation in P +MT with respect to P −MT samples after normalization to the latter. Enrichment of V-H^+ATPase was not significant (Student's *t*-test, $p > 0.05$). Error bar indicates standard error ($n = 4$).

SYP21 organelles and MTs. To investigate the nature of this interaction in more detail, binding experiments were performed in the presence of ATP instead of AMP-PNP (figure 5). Western blot analysis showed that in the presence of ATP, SYP21 was still enriched in the P +MT with respect to the P −MT fraction (figure 5*b*, comparison of −/+ MT), providing further support for binding specificity of SYP21 organelles to MTs. However, the amount of SYP21 in the +MT pellet in the presence of ATP, calculated in four different experiments, was considerably lower than in P +MT in the presence of AMP-PNP (figure 5*b*; graph), suggesting that the SYP21 compartments interact cyclically with MTs in an ATP-dependent manner. The cycling binding of SYP21 organelles with MTs was also confirmed by evidence that the amount of proteins in the MT pellet in the presence of ATP was considerably lower than in MT pellets in the presence of AMP-PNP (figure 5*c*). On the other hand, the amount of GRP78/Bip-, V-H^+ ATPase- and Arf1-positive organelles did not change in P +MT in the presence of ATP (figure 5*a*, comparison of P −/+MT).

Moreover, TEM analysis of MT pellets obtained in the presence of ATP showed that the morphology of organelles bound to MTs was similar to that observed in the presence of AMP-PNP (figure 5*e–g*; comparison of figure 1) and confirmed that the number of organelles bound to MTs decreased with respect to experiments using AMP-PNP (figure 5*d*).

All these experiments further support the idea that the interaction of SYP21 organelles with MTs may be mediated by ATP-dependent proteins. However, additional experiments are necessary to identify and characterize the proteins

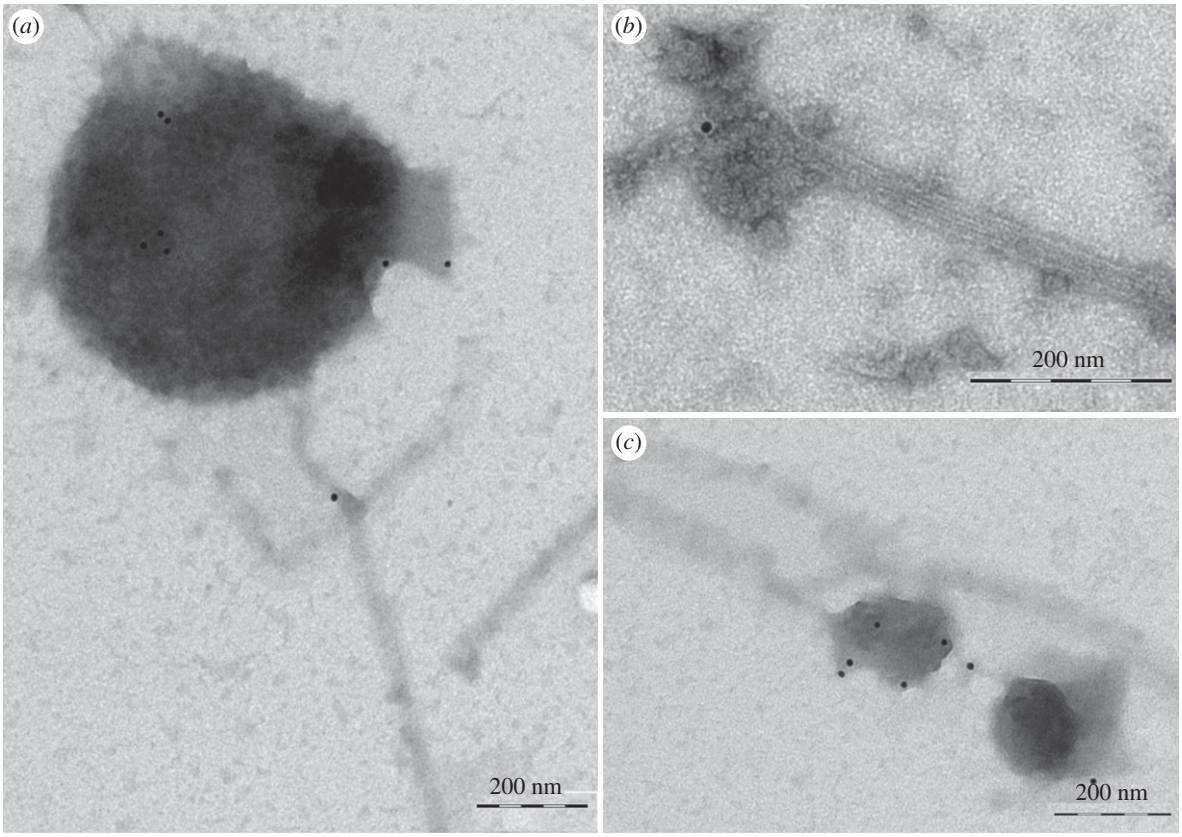

Figure 3. Immunogold labelling of MT-bound compartments. (*a–c*) Anti-SYP21 antibody labels organelles bound to taxol-stabilized MTs. The diameter of labelled compartments ranges from 100 to 700 nm. Scale bar, *a–c* = 200 nm.

mediating the binding between SYP21-positive compartments and MTs.

2.3. Sub-fractionation experiments showed a relationship between MTs and organelles involved in the degradation pathway

To better define the role of MTs in trafficking towards vacuoles, we analysed the effect of low concentration of oryzalin (a drug which dramatically depolymerizes MTs in pollen tubes) [7,22] on the distribution of membrane compartments after centrifuging through a continuous sucrose density gradient, using antibodies against SYP21 and V-H$^+$ATPase (figure 6). To minimize the side effects of oryzalin on pollen tube growth, we used a concentration of the drug (0.1 µM) that did not induce loss of cytoplasmic polarity or descent of big vacuoles into the apex (see §2.5).

Electrophoretic analysis of sucrose density fractions, derived from pollen tubes grown with or without oryzalin, showed greater modifications of polypeptide pattern in fractions 3–7 and 16–21 (figure 6*a*). Specifically, polypeptides with molecular mass in the range 97–150 kDa showed a wider distribution in oryzalin-treated samples (fractions 2–6, see box in figure 6*a*) than in controls (fractions 4–6). On the other hand, polypeptides that were widely distributed in the control experiments (fractions 16–23) were present in fractions 16–20 and peaked in fractions 19–20 in oryzalin-treated samples (see box in figure 6*a*).

These experiments showed that oryzalin altered the mobility of membrane compartments through the sucrose density gradient, suggesting that MT depolymerization could affect membrane trafficking, leading to changes in membrane compartment composition.

To evaluate the effect of oryzalin on the distribution of compartments involved in late degradation pathways, the fractions obtained after centrifuging microsomes through sucrose density gradients were probed using anti-SYP21 and anti-V-H$^+$ATPase antibodies as markers of PVCs and vacuoles, respectively (figure 6*b*,*c*). In immunoblot assays of control pollen tubes, SYP21 was detected continuously in fractions 3–14 with three distinct peaks in fractions 6, 10 and 13. It was also present in fractions 16–19, 21 (figure 6*b*). Otherwise, in sub-fractionation experiments, SYP21 was only present in two distinct peaks in fractions 2–6 and 11–15 of oryzalin-treated pollen tubes. SYP21 was also observed in the higher sucrose density fractions 19–23.

In western blot experiments, anti-V-H$^+$ATPase labelled compartments in high-density fractions 20–23 of control pollen tubes (figure 6*c*), whereas after oryzalin treatment the membrane compartments recognized by V-H$^+$ATPase antibody were also recorded in fractions 4–6 (figure 6*c*). Notably, V-H$^+$ATPase- and SYP21-labelled organelles partially overlapped in the same fraction (19, 21) in control pollen tubes, while after oryzalin treatment this overlap was enhanced both in high- (20–23) and low-density fractions (4–6), suggesting that the membrane composition and content of these organelles were altered by MT depolymerization.

These observations suggest that MT depolymerization affected trafficking involving both the SYP21 and V-H$^+$ATPase compartments.

MT depolymerization also affected Bip1 and Arf1 distribution throughout the sucrose density gradient in different ways (electronic supplementary material, figure S2). In control pollen-tube-derived microsomes, Bip1 was detected in

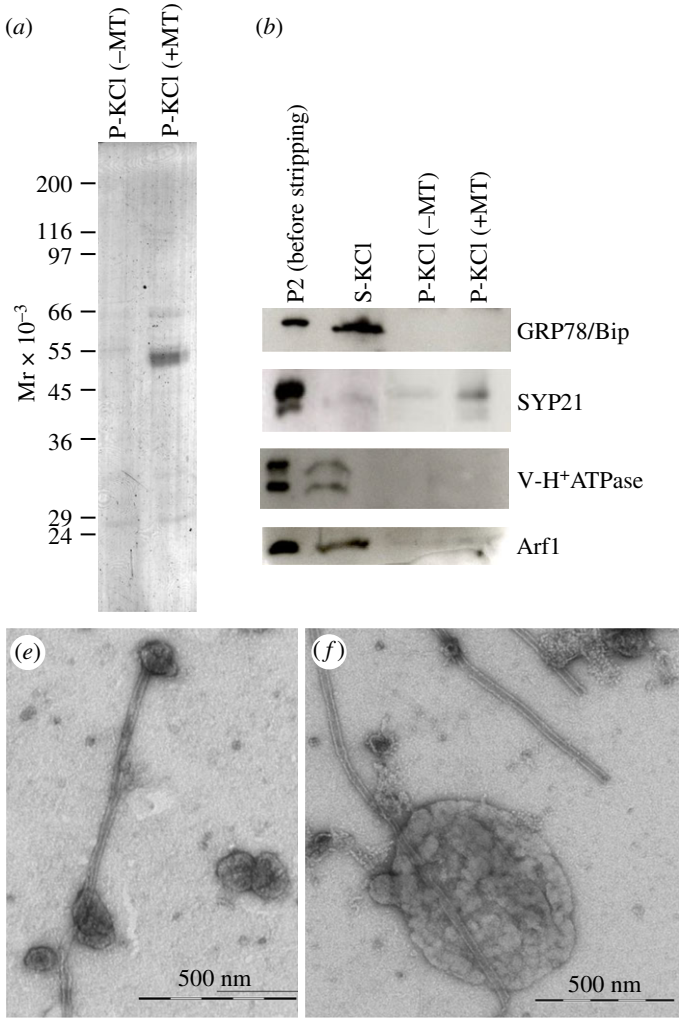

Figure 4. Binding specificity of pollen tube organelles to MTs. (*a*) Electrophoretic profiles of P fractions (+/−MT) after organelle stripping with KCl. (*b*) Western blot analysis of P samples +/−MT shows that GRP78/Bip, Arf1 and V-H$^+$ATPase are recovered in the soluble fraction after KCl treatment, while SYP21 organelles are pelleted preferentially in +MT samples. (*c*) The graph shows the variation in percentage protein content after normalization to the unstripped P2 in three different experiments. The protein content of microsomes decreases after incubation with KCl. (*d*) The graph shows the percentage variation in organelle number per micrometre of MT in KCl-treated samples with respect to untreated microsomes, normalized to unstripped P2 in three independent experiments. Quantitative analysis of MT-bound KCl-stripped organelles shows that the number of compartments bound to MTs increased considerably with respect to untreated microsomes. (*e*,*f*) Ultrastructural observations show that the membrane delimiting KCl-treated organelles is smooth. Scale bars, *e*,*f* = 500 nm.

low (3–7; electronic supplementary material, figure S2A) and high sucrose density fractions (20–23; electronic supplementary material, figure S2A). Oryzalin treatment maintained this distribution, also spreading Bip1 in fractions 1 and 2. Arf1 was widely distributed through the sucrose density gradient in control experiments (electronic supplementary material, figure S2B), while MT depolymerization restricted its distribution (3, 10–11, 15, 18; electronic supplementary material, figure S2B) and decreased its presence particularly in the higher sucrose density fractions.

2.4. SYP21 is localized on PVCs and tubular vacuoles in tobacco pollen tubes

To study the localization of SYP21 in growing pollen tubes, pollen grains were transiently transformed with YFP-SYP21 construct under the control of pollen-specific promoter LAT52. We tested growing plasmid concentrations and the lowest concentration that allows to observe SYP21 staining was chosen. Since we elicited ectopic expression of *Arabidopsis* SYP21 in *Nicotiana tabacum* pollen tubes, the average growth rate of untransformed cells was compared with that of pLAT52/YFP-SYP21-transformed pollen tubes in order to avoid undesired side-effects on pollen tube physiology: the transformation did not significantly affect pollen tube growth rate (Student's *t*-test, $p > 0.05$; electronic supplementary material, figure S2C). YFP-SYP21 revealed round organelles (figure 7*a*,*b*) having a mean area of 0.2 µm^2 in transformed pollen tubes (figure 7*c*). The area of most of SYP21-labelled compartments (98%) was in the range 0.05–0.70 µm^2 with a peak at 0.1–0.2 µm^2 (figure 7*c*). Only 2% of SYP21-positive compartments exceeded 1 µm^2, suggesting that these large bodies could be caused by exogenous expression of SYP21 which induced aggregation of organelles. Notably, a discontinuity in the frequency distribution was observed, since no compartments with areas between 0.7 and 1.0 µm^2 were detected (figure 7*c*, arrow). These areas were coherent with SYP21 organelle size observed in immunogold analysis of binding experiments using SYP21 antibody (figure 3). In addition, TEM observation showed SYP21-positive organelles with a diameter of 50 nm, which were not revealed by laser confocal microscopy. SYP-21-positive organelles exhibited long-range movements along the pollen tube, excluding the

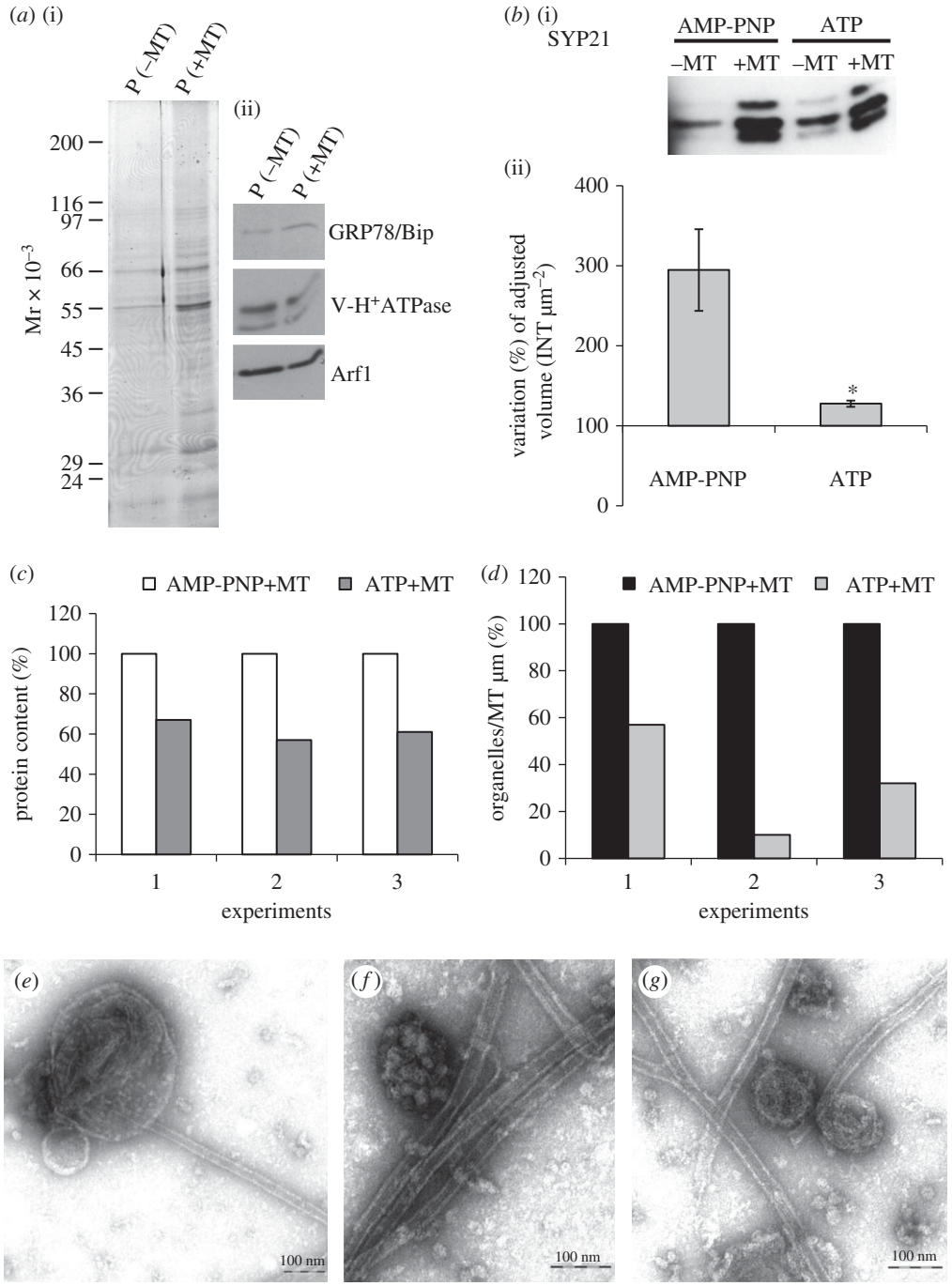

Figure 5. Microsomes bind MTs in an ATP-dependent manner. (*a*) Electrophoretic profiles of P +/−MT fractions in the presence of ATP (i) and western blot analysis using GRP78/Bip, V-H$^+$ ATPase, SYP 21 and Arf1 antibodies on P +/−MT fractions in the presence of ATP (ii). In the presence of ATP, the same content of ER, vacuole and Golgi markers is detected in −MT and +MT samples. (*b*) Western blot experiments using anti-SYP21 antibody show that SYP21-positive compartments are more frequent in P +MT than in P −MT samples in the presence of AMP-PNP and ATP (i). Quantitative analysis using Quantity One software (ii) shows percentage variation in adjusted volume of +MT with respect to −MT (assumed 100%) after incubation with ATP or AMP-PNP (mean values; Student's *t*-test, $*p < 0.05$; error bar indicates standard error; $n = 4$). Fewer SYP21-positive organelles bound to MTs in the presence of ATP than in the presence of AMP-PNP. (*c*) The graph shows the variation in percentage protein content after normalization to AMP-PNP-treated P2 in three different experiments. In the presence of ATP, less protein is recovered in the P fractions. (*d*) The graph shows the percentage variation in organelle number per micrometre of MT in ATP-treated samples with respect to AMP-PNP treated microsomes, normalized to AMP-PNP samples in three independent experiments Quantitative analysis shows fewer organelles per micrometre of MT in P +MT pellets of ATP-treated samples than in samples incubated with AMP-PNP. (*e–g*) Ultrastructural observations do not show differences in the morphology of MT-bound organelles between ATP- and AMP-PNP-treated samples. Scale bar, $e–g = 100$ nm.

clear zone, a transportation pattern typical of AF-dependent cytoplasmic streaming (electronic supplementary material, movie S1).

Overexpression of YFP-SYP21 in pollen tubes induced aggregation of positive organelles to form larger structures (figure 7*d*,*e*), which were clusters of smaller bodies (figure 7*f*). These clusters took several shapes and moved in an irregular way along the pollen tube, showing quick movements alternating with pauses (data not shown). SYP21-positive clusters never reached the apex of the pollen tube. Pollen tube growth was not affected by SYP21 overexpression (from 3.7 µm min^{-1} in the control to 3.4 µm min^{-1} in SYP21-overexpressed pollen tubes; Student's *t*-test, $p > 0.05$). Thus, overexpression induced clusters as observed in somatic cells

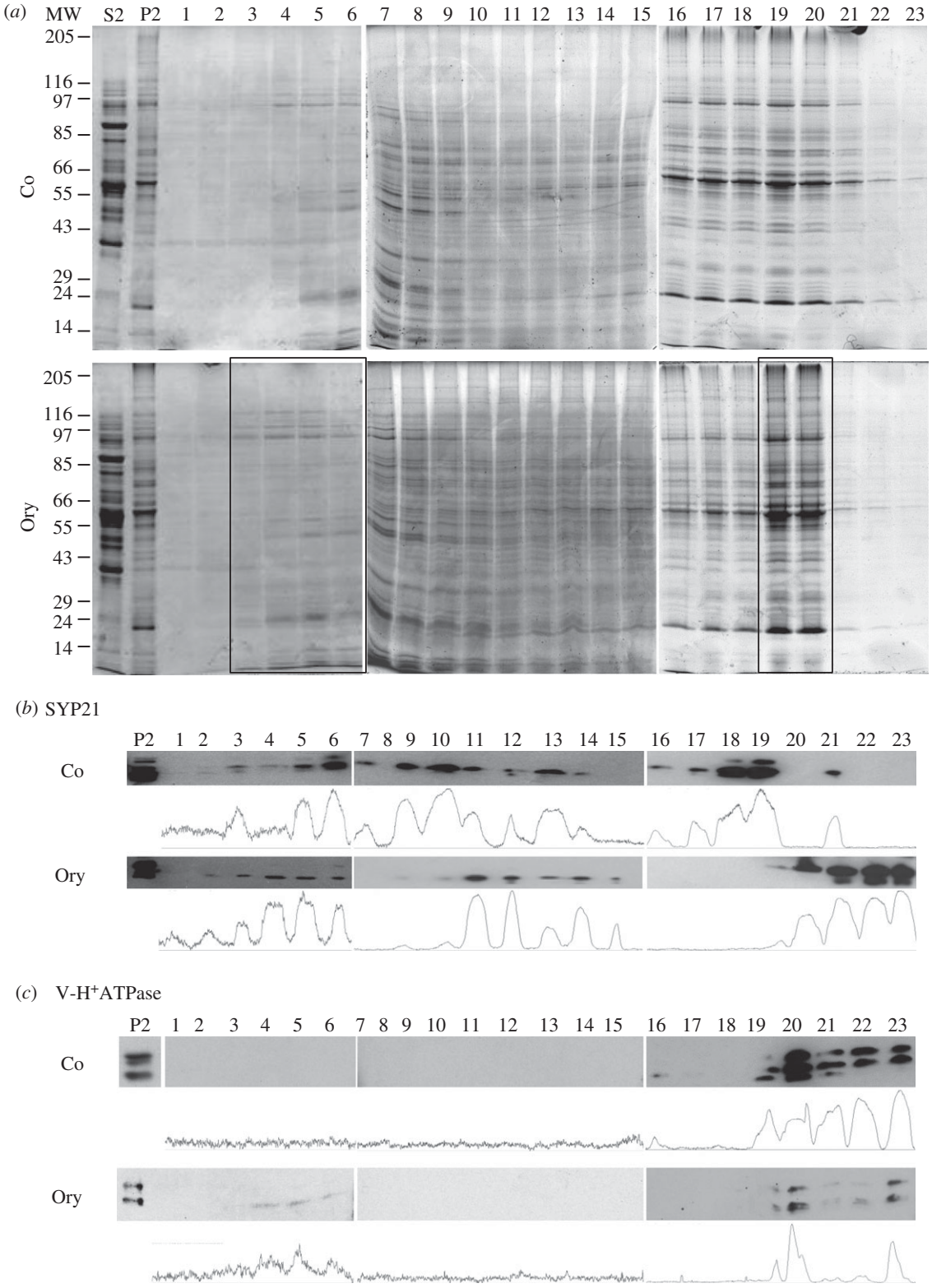

Figure 6. MT depolymerization by oryzalin affects migration of SYP21-positive compartments in sub-fractionation experiments. (*a*) Electrophoretic profiles of microsomes separated through continuous sucrose gradients. Microsome fractions of control pollen tubes (Co; upper panel) compared to those of pollen tubes grown in the presence of oryzalin (Ory; lower panel). A wider distribution of polypeptides having molecular mass between 150 and 97 kDa is evident in the oryzalin sample (fractions 2–6, box) than in control (fractions 4–6). In contrast, polypeptides in control fractions 16–23 are widely distributed with respect to oryzalin-treated samples which peaked in fractions 19–20 (box). (*b*) Western blot analysis using anti-SYP21 antibody in control pollen tubes continuously detected SYP21 in fractions 3–19 with peaks in fractions 6, 10, 13, 18–19 and 21 (see also ImageJ quantification analysis). Oryzalin treatment alters the distribution of SYP21-positive compartments, since SYP21 is present in two peaks (fractions 2–6 and 11–15) and in fractions 19–23. (*c*) Anti V-H^+ATPase antibodies mark compartments in fractions 19–23 in control and oryzalin-treated pollen tubes. After oryzalin treatment, the compartments recognized by the V-H^+ATPase antibody are also recorded in the lower density fractions 4–6.

[24], suggesting that SYP21-positive organelles in tobacco pollen tubes can also be identified as PVCs.

To obtain further evidence that SYP21-positive compartments are actually PVCs, the pollen tubes were treated with 0.5 µM wortmannin (Wm) (figure 8), which has been shown to affect PVC size in somatic cells [8,29,30]. This concentration of Wm did not significantly decrease pollen tube growth rate (Student's *t*-test, $p > 0.05$ with respect SYP21-transformed

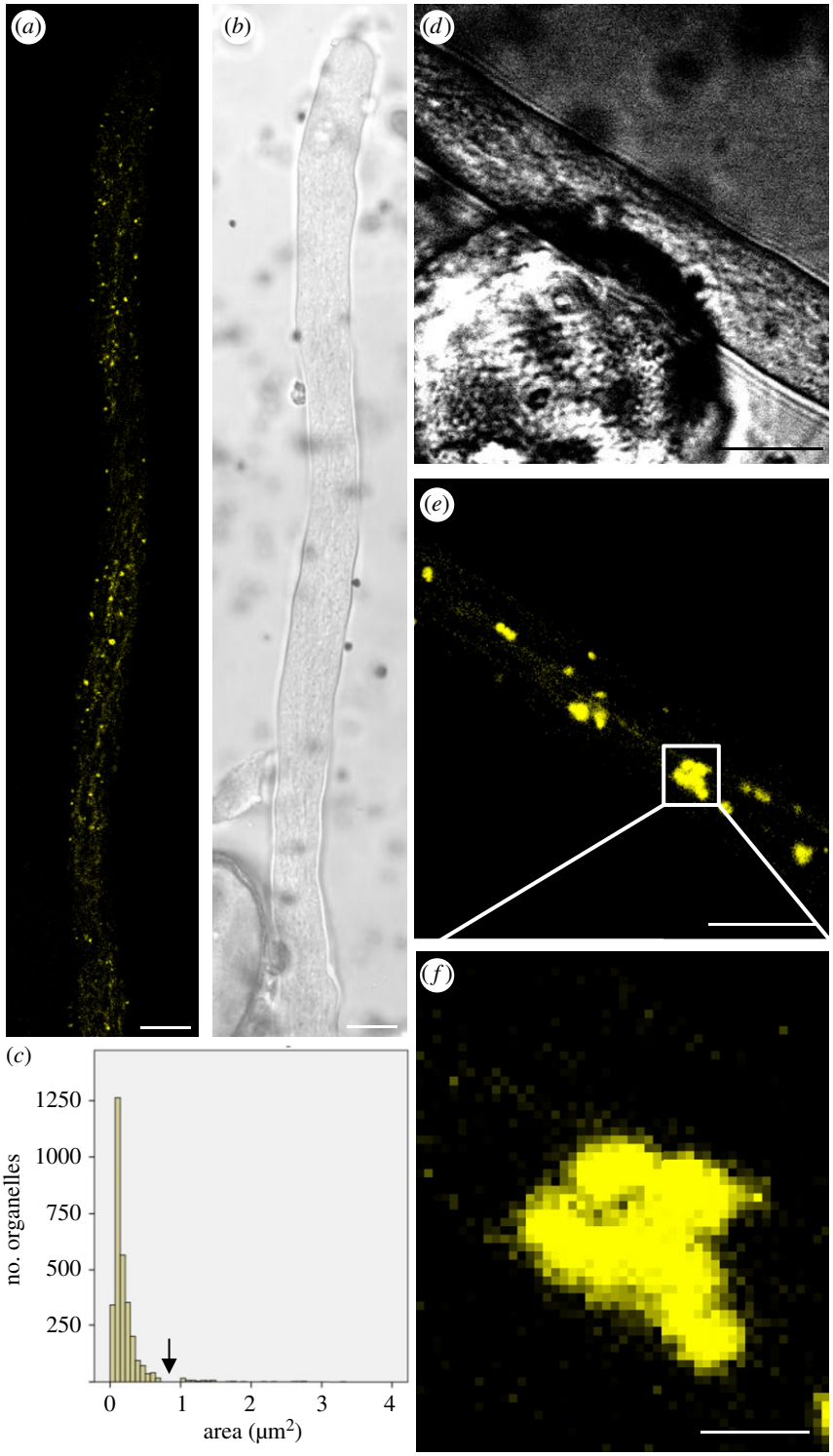

Figure 7. Identification of PVCs by transient transformation of pollen tubes with pLAT52:YFP-SYP21. (*a,b*) YFP-SYP21 detects round organelles widely distributed in pollen tubes except in the tip and more distal regions where there are large vacuoles. YFP-SYP21 also localizes in dynamic tubular compartments spanning the pollen tube longitudinally (*b*, bright field). (*c*) Round organelles have a mean area of about 0.2 μm^2. Most SYP21-positive compartments (98%) measure between 0.05 and 0.7 μm^2 with a peak at 0.1–0.2 μm^2. A discontinuity is evident in the frequency distribution of SYP21-positive organelle area between 0.7 and 1.0 μm^2 (arrow). (*d–f*) Overexpression of YFP-SYP21 induces aggregation of round organelles into large clusters (*d*, bright field). Scale bar, $a–e = 10$ μm; $f = 2.5$ μm.

and 0.05% DMSO treated pollen tubes; electronic supplementary material, figure S2C) although about 40% of tubes did not grow. Wortmannin induced significant enlargement of SYP21-positive compartments (ANOVA test: $F_{6.11498} = 140{,}439$, $p < 0.0001$) with respect to controls (Tukey's test between control and Wm samples, $p < 0.01$) and 0.05% DMSO-treated pollen tubes (Tukey's test between DMSO and Wm samples, $p < 0.01$; figure 8*a–p*). The SYP21 labelling, clearly visible in the delimiting membrane, shows that Wm induced the fusion of SYP21-positive compartments, as expected (figure 8*m–o*), further sustaining that SYP21 identified PVCs in pollen tubes. Moreover, control and DMSO-treated pollen tubes were also significantly different (Tukey's test between control and DMSO samples, $p < 0.01$). In addition, areas reached 6 μm^2 in the presence of Wm but did not exceed 4 μm^2 in DMSO-control samples (figure 8*q*), and in controls and DMSO-treated pollen tubes the percentage of SYP21-positive organelles having an area greater than 1 μm^2

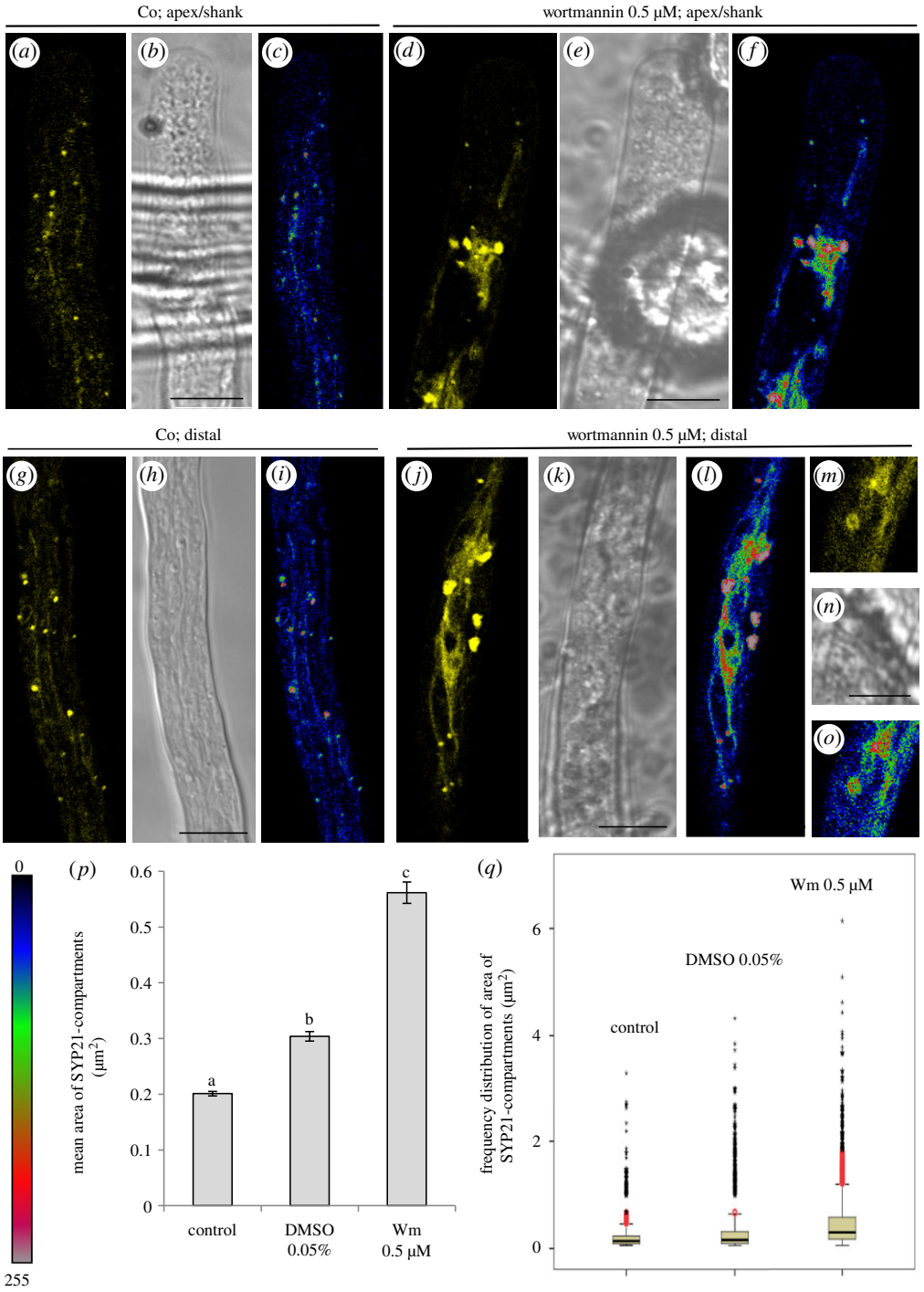

Figure 8. Wortmannin (Wm) treatment induces homotypic fusion of SYP21-positive compartments. (*a,b*) Distribution of YFP-SYP21 in the apex/shank of control pollen tubes (*b*, bright field). (*c*) Fluorescence intensity of YFP-SYP21 revealed by pseudo-coloured images (black/blue and red/grey indicated lower and higher fluorescence, respectively). (*d,e*) Distribution of YFP-SYP21 in the apex/shank of Wm-treated pollen tubes (*e*, bright field). (*f*) Fluorescence intensity of YFP-SYP21 revealed by pseudo-coloured images. (*g,h*) Distribution of YFP-SYP21 in the distal region of control pollen tubes. (*i*) Fluorescence intensity of YFP-SYP21 revealed by pseudo-coloured images. (*j,k*) Distribution of YFP-SYP21 in the distal region of Wm-treated pollen tubes. (*l*) Fluorescence intensity of YFP-SYP21 revealed by pseudo-coloured images. (*m,n*) Detail of YFP-SYP21 labelling on the surface of PVCs, induced by Wm treatment. (*o*) Fluorescence intensity of YFP-SYP21 revealed by pseudo-coloured images. All the pictures show growing pollen tubes. *a–l* Scale bar, 10 µm. (*p*) Graph shows mean area of SYP21-positive compartments in control, DMSO- and Wm-treated pollen tubes. A significant increase ($p < 0.0001$) in mean area of SYP21-positive round bodies was observed in Wm-treated with respect to control and DMSO-treated pollen tubes. Error bar indicates standard error. (*q*) Box plots of frequency distribution of areas of SYP21-positive bodies. Boxes show the interquartile range (Hspread) and median (horizontal line). The lines extend from the lowest to the highest value in 1.5 Hspread from the end of the box. Red circles represent values between 1.5 and 3 Hspread and black asterisks represent extreme values above 3 Hspread. The increase in mean area (see *m*) of round organelles after Wm treatment was due to an increase in the number of organelles having an area >1 µm^2 and to an increase in PVC size (up to 6 µm^2).

was only 2% and 7%, respectively, while in Wm-treated pollen tubes it reached 20% (figure 8*q*).

To further confirm that SYP21-positive compartments were actually PVCs, tobacco pollen grains were transiently transformed with pLAT52/GFP-BP80-CT [8] (electronic supplementary material, figure S3). BP80 transformation did not affect pollen tube growth rate (from 4.3 µm min^{-1} in control to 4.1 µm min^{-1} in BP80 pollen tubes; Student's

t-test, $p > 0.05$). Like with SYP21, BP80-positive compartments appeared as rounded organelles distributed in the pollen tube cytoplasm, excluding the apex (electronic supplementary material, figure S3A–D). To ensure that SYP21 and BP80 stained the same particles, cotransformation experiments using pLAT52/YFP-SYP21 and pLAT52/GFP-BP80 were performed (electronic supplementary material, figure S3F–M). To avoid the interference of YFP and GFP signals, transformed pollen tubes were observed as reported by Foresti *et al*. [24]. Crosstalk experiments showed that the emission spectrum of YFP and GFP does not overlap (electronic supplementary material, figure S4A–F). Both in the apex/shank and in the distal region, round organelles appeared simultaneously stained with YFP-SYP21 and GFP-BP80 (electronic supplementary material, figure S3F–M). The cotransformation induced a lower signal in both channels with respect to single transformation. Moreover, to further sustain the presence of YFP-SYP21 and GFP-BP80 on the same organelles, the frequency distribution of BP80-positive organelle areas were analysed and compared with that of SYP21-positive compartments: the area distribution of two kind of organelles perfectly overlapped in the 0.05–0.7 μm^2 range (electronic supplementary material, figure S3E). The Pearson correlation of the two distributions of the frequencies with which each value was detected by SYP21 and B80 was high ($r = 0.95$). Likewise, the Mann–Whitney paired test did not detect any significant difference between the two distributions (p-value > 0.05). In the graph (electronic supplementary material, figure S3E) only organelles with an area less than 0.7 μm^2 were considered, since the largest BP80-PVCs measured 0.63 μm^2. Together this data revealed that BP80 and SYP21 both identify PVCs.

Besides localizing in round organelles, surprisingly SYP21 also seemed to localize along tubular structures spanning the pollen tube longitudinally (figure 7*a*). These structures looked like the dynamic tubular compartments already observed in pollen tubes [7,31]. The compartments were distributed in the shank and distal regions of the tube but did not reach the tip (figure 8*a*,*b*,*g*,*h*). On the contrary, BP80 did not show this longitudinal distribution (electronic supplementary material, figure S3A,C).

Control transformation experiments using pLAT52/YFP did not significantly affect pollen tube growth (from 4.4 $\mu m\ min^{-1}$ in the untransformed to 5.4 $\mu m\ min^{-1}$ in YFP pollen tubes; Student's *t*-test, $p > 0.05$) and showed a diffuse cytoplasmic staining suggesting that YFP, differently from pLAT52/YFP-SYP21, does not have a specific localization (electronic supplementary material, figure S5A–F).

Interestingly, these SYP21-positive tubular compartments were affected by Wm, which induced tubule aggregation (figure 8*d–f*, *j–o*), suggesting that Wm could have an effect similar to that observed in round organelles. In addition, Wm treatment increased the localization of SYP21 on the tubular compartments in the shank and distal regions, with respect to controls (figure 8, compare *a–c* with *d–f* and *g–i* with *j–o*). Notably, since low concentrations of Wm that promote homotypic fusion of PVCs did not cause aggregation between round and tubular compartments, we may suppose that they are functionally distinct compartments.

In pollen tubes, Wm (0.8 μM) has been reported to affect AFs [30], whereas its influence on MTs has not been investigated. To ascertain that the homotypic fusion of PVCs and tubular vacuole coalescence described above were not side-effects of cytoskeletal alterations, the distribution pattern of AFs in pollen tubes incubated with 0.5 μM Wm was studied by transient transformation with pLAT52/Lifeact-mEGFP (electronic supplementary material, figure S6). In growing pollen tubes, no differences were observed in the organization of the actin fringe or of AFs in the shank and distal regions, among controls, Wm- and 0.05% DMSO-treated cells (electronic supplementary material, figure S6A–C).

When the effect of a low concentration of Wm on MTs was investigated by immunofluorescence microscopy, it seemed to have a stabilizing effect in tobacco pollen tubes, since long MT bundles were observed in the shank (electronic supplementary material, figure S7G), whereas only short randomly oriented MT strands were observed in controls and 0.05% DMSO-treated pollen tubes (electronic supplementary material, figure S7A,B).

The tubular compartments stained by YFP-SYP21 resembled tubular vacuoles previously identified in pollen tubes by CDFDA [7,31]. To unambiguously identify the SYP21-positive tubular compartments, pollen tubes were stained with yeast vacuole marker Blue-CMAC, henceforth CMAC (electronic supplementary material, figure S5G–L) [32,33]. This dye is a membrane-permeable chloromethyl coumarin derivative that is largely sequestered into vacuoles. The network of interconnected tubules stained by CMAC extended longitudinally in the cell from the shank (about 5 μm from the apical PM) to the distal area (electronic supplementary material, figure S5G–L). These tubules were highly dynamic and sometimes seemed to outline the V-shaped apical domain (electronic supplementary material, figure S5G,H; see box). Large vacuoles in the oldest parts of the tubes were also stained by CMAC and appeared to arise by coalescence of tubular vacuoles (electronic supplementary material, figure S5 K–L; see box).

In order to exclude that transient transformation experiments induced changes in morphology and behaviour of membrane compartments involved in the degradative pathways, the simultaneous staining with CMAC of pLAT52/YFP transient transformed pollen tubes showed that morphology and distribution of tubular vacuoles were not affected (electronic supplementary material, figure S5E,F). Further attempts to visualized PVCs by using acridine orange in pLAT52/YFP transformed pollen tubes failed because the pollen tubes died or burst (data not shown).

In order to confirm the presence of SYP21 on tubular vacuoles, colocalization experiments were carried out, showing that YFP-SYP21 colocalized with CMAC on both PVCs and tubular compartments (figure 9*a–j*). The use of CMAC ensures that the emission spectrum does not overlap with that of YFP, as confirmed by crosstalk experiments (electronic supplementary material, figure S4G–L). No significant differences (Student's *t*-test, $p > 0.05$) in colocalization Pearson's coefficient were detected between the apical and distal regions in control pollen tubes (figure 10*a*). Interestingly, not all YFP-SYP21-positive PVCs colocalized with CMAC (figure 9*a–h*, arrows indicate PVCs not stained by CMAC; figure 10*b*). These data suggested the presence of free PVCs in the cytoplasm (not colocalizing with CMAC) and PVCs close to/fusing with tubular vacuoles (colocalizing with CMAC). Colocalization points were observed at the periphery of SYP21-positive vesicles, suggesting fusion events between PVCs and tubular vacuoles. Large vacuoles stained with CMAC were not labelled with YFP-SYP21 (electronic supplementary material, figure S8A,C,E,G).

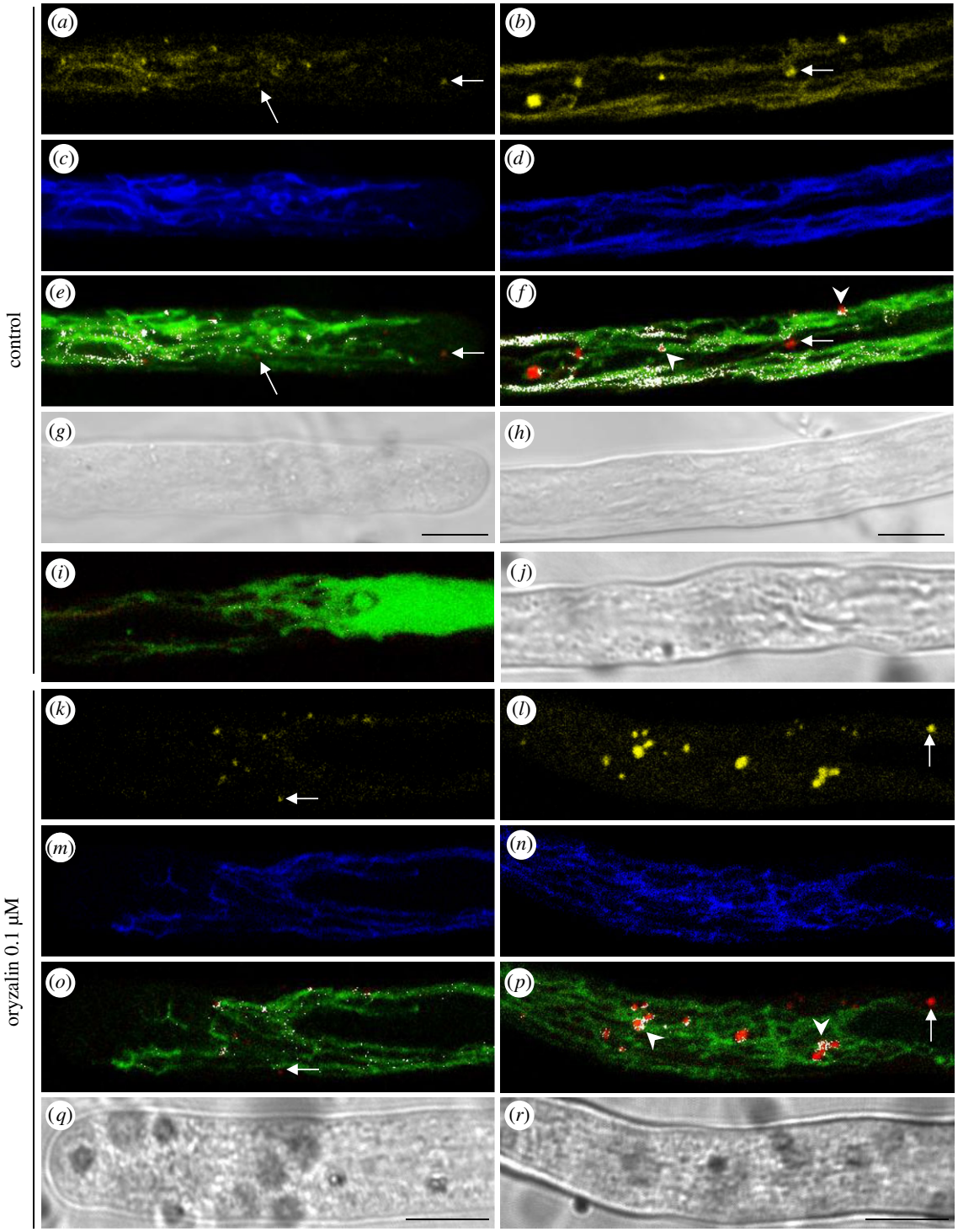

Figure 9. MT depolymerization by oryzalin affects PVC maturation and delivery to and/or fusion with tubular vacuoles. (*a–j*) YFP-SYP21/CMAC colocalization experiments in the apex/shank and distal areas of control pollen tubes. Yellow staining indicates SYP21 localized on round bodies and tubular compartments in the apex/shank and distal area (*a* and *b*, respectively). Blue staining of tubular compartments by CMAC reveals that they are indeed tubular vacuoles (*c* apex/shank, *d* distal area). White spots represent SYP21/CMAC colocalization points (*e* apex/shank, *f* distal area). In control pollen tubes, YFP-SYP21 colocalizes with CMAC on the delimiting membrane of PVCs (*f*; see arrowheads) and on tubular compartments. Distal vacuoles did show colocalization points (*i* and *j*). Bright field images of apical and distal regions of pollen tubes (*g* and *h*, respectively). (*k–r*) YFP-SYP21/CMAC colocalization experiments in the apex and distal area of oryzalin-treated pollen tubes. Yellow staining represents YFP-SYP21 distribution in the apical and distal regions (*k* and *l*, respectively). Blue staining shows tubular vacuoles stained with CMAC (*m* apex/shank, *n* distal area). SYP21/CMAC colocalization is shown as white points (*m* apex/shank, *n* distal area). After oryzalin treatment, colocalization points concentrate on PVCs and disappear almost completely from tubular vacuoles (*m* and *n*). Loss of SYP21 in tubular vacuoles is greater in the distal area than in the apex (*k–r*). The colocalization experiments show an absence of colocalization (*o* and *p*) of CMAC and SYP21 in several PVCs in control and treated pollen tubes (see arrows). Bright field images of apical and distal regions of pollen tubes (*q* and *r*, respectively). All the pictures are of growing pollen tubes. Scale bar, 10 µm.

To further characterize SYP21-positive organelles at the ultrastructural level, immunogold analysis was performed on pollen tubes (electronic supplementary material, figure S9; arrows). The anti-SYP21 antibody recognized compartments that were not uniform in morphology, appearing as vacuoles or small vesicles (electronic

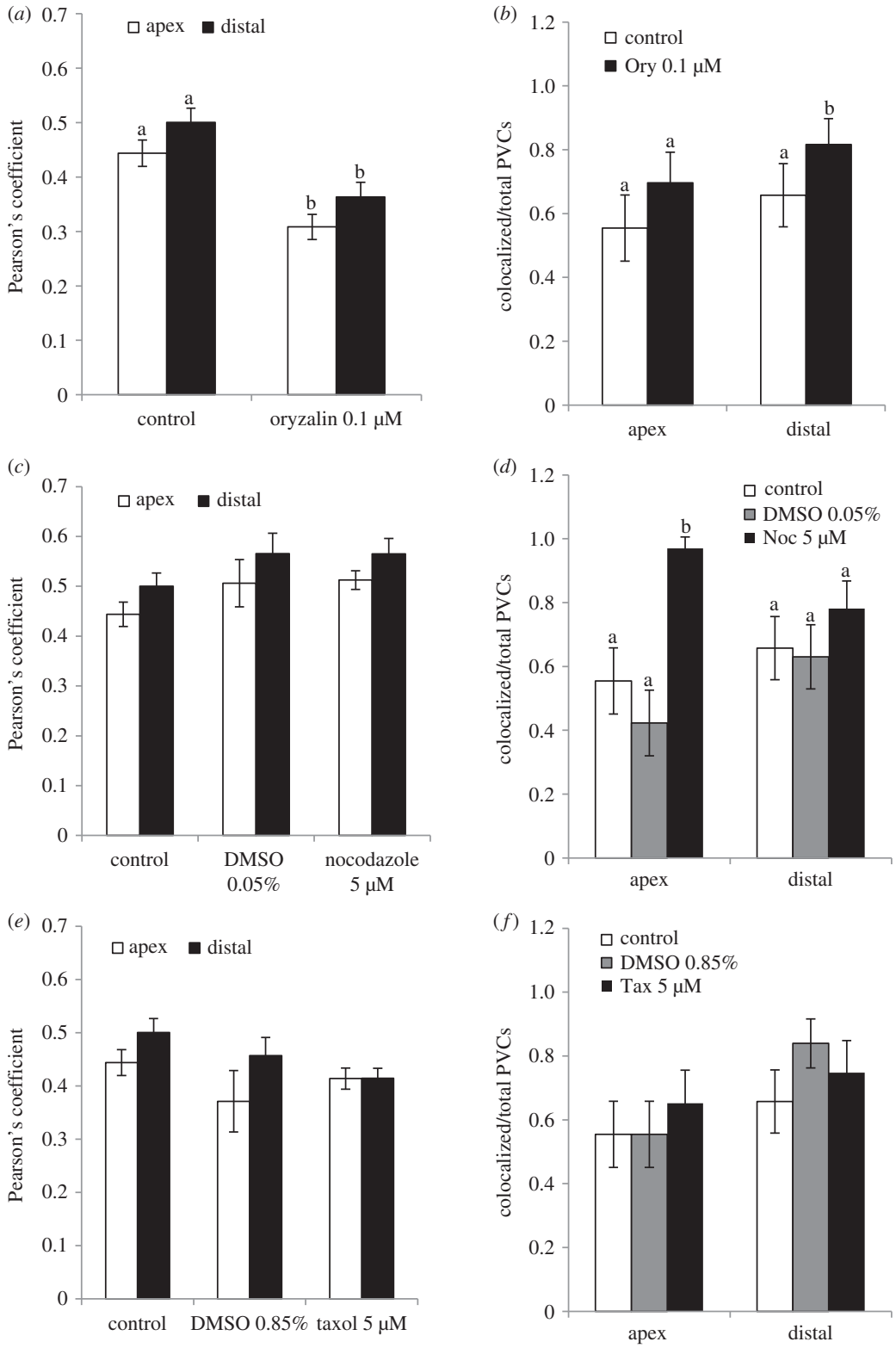

Figure 10. Colocalization experiments in the presence of MT drugs. (*a*) Pearson's coefficient shows a significant decrease in YFP-SYP21/CMAC colocalization in oryzalin-treated pollen tubes with respect to control ($p < 0.01$). (*b*) Number of PVCs colocalizing with CMAC with respect to the total number of PVCs observed in control and oryzalin (Ory)-treated pollen tubes. With oryzalin treatment, the number of PVCs showing YFP-SYP21/CMAC colocalization increases significantly in the distal area ($p < 0.05$). (*c*) Pearson's coefficient shows that nocodazole induces an increase in colocalization compared to control and 0.05% DMSO-treated pollen tubes. (*d*) Number of PVCs showing YFP-SYP21/CMAC colocalization in control, 0.05% DMSO- and 5 µM nocodazole (Noc)-treated pollen tubes. After nocodazole treatment an increase in colocalized PVCs with respect to total PVCs was observed in the apex/shank of pollen tubes ($p < 0.01$). (*e*) Pearson's coefficient shows that colocalization of YFP-SYP21 and CMAC in taxol-treated cells is not significantly different from colocalization in control and 0.85% DMSO-treated samples ($p > 0.05$). (*f*) Microtubule-stabilizing agents (taxol (Tax) and 0.85% DMSO) do not induce a significant increase in colocalized PVCs with respect to total PVCs ($p > 0.05$). The letters a and b indicate significantly different values. Error bar indicates standard error ($n = 12$).

supplementary material, figure S9C), vesicle clusters (electronic supplementary material, figure S9D) or compartments comprising both vesicles and tubules (electronic supplementary material, figure S9B,E,F) and sometimes showing inner membranes (electronic supplementary material, figure S9E,F).

2.5. MT perturbation affected localization of SYP21 between PVCs and tubular vacuoles

To highlight the role of MTs in the degradation pathway involving SYP21-positive compartments, pollen tubes were treated with the MT depolymerizing agent oryzalin. Oryzalin treatment did not stop pollen tube growth, however it induced a significant decrease in growth rate compared to controls (Student's *t*-test, $p < 0.01$; electronic supplementary material, figure S2C).

In control tobacco pollen tubes, MTs are organized in longitudinal bundles in distal areas and in short, randomly oriented strands in the shank and apex (electronic supplementary material, figure S7A). Treatment with oryzalin depolymerized both the short MT strands and most distal bundled MTs (electronic supplementary material, figure S7D). To confirm a previous report showing that oryzalin did not affect AFs [7], tobacco pollen tubes transiently transformed with LAT52-lifeact and treated with oryzalin were observed (electronic supplementary material, figure S6D). No differences were revealed in the organization of the actin fringe or of AFs in the shank and distal regions, between oryzalin-treated pollen tubes and controls (electronic supplementary material, figure S6A,D). On the contrary, as already observed [34], pollen tube treatment with low concentration of LatB, which depolymerized AFs, induced a rearrangement of MTs in the apex/shank: the short MT fragments changed into long strands, often arranged in a helix structure along the long axis of the tube in the shank (electronic supplementary material, figure S7H) or organized in long filaments encapsulating the apex (electronic supplementary material, figure S7I).

Microtubule depolymerization altered the localization of YFP-SYP21, which was only observed on round organelles (PVCs) and disappeared or decreased considerably on tubular compartments, in the apical and distal areas (compare figure 8*a–c*, *g–i* and figure 11*a–f*, *j–m*). In parallel with the decrease in YFP-SYP21 on tubular vacuoles, the mean area of PVCs increased significantly (0.4 μm^2) compared with control (ANOVA test: $F_{6,11498} = 140.439$, $p < 0.0001$; Tukey's test between control and oryzalin samples, $p < 0.01$; figure 11*n*). Moreover, the number of PVCs larger in area than 1 μm^2 also increased considerably (up to 12%) with respect to control (2%) (figure 11*o*) and PVCs reached 5 μm^2 in the presence of oryzalin (figure 11*o*). These larger PVCs showed the surface labelling observed also after Wm treatment (figure 11*j–m*), suggesting that they originate by homotypic fusion. After oryzalin treatment, YFP-SYP21 was occasionally mislocalized (about 10% of cells) to the apical PM, to vesicles clustered in the V-shaped inverted cone region (figure 11*g–i*, circle) and to the tubular compartments (figure 11*g–i*, arrows), suggesting substantial changes in membrane trafficking in the apex.

This increase in PVC dimensions and the concomitant decrease in YFP-SYP21 on tubular compartments after oryzalin treatment suggested that MTs could play a role in membrane trafficking between PVCs and tubular vacuoles and in promoting the fusion of PVCs with vacuoles.

In contrast, a low concentration of nocodazole, which affects short apical MT strands (electronic supplementary material, figure S7E), did not induce changes in pollen tube growth rate (electronic supplementary material, figure S2C) and in YFP-SYP21 distribution or PVC mean dimension (0.2 μm^2) with respect to untreated pollen tubes (compare figure 8*a–c*,*g–i* with electronic supplementary material, figure S10A–H). In parallel, a significant increase in PVC mean area was observed in 0.05% DMSO-treated control cells with respect to untreated pollen tubes (ANOVA test: $F_{6.11498} = 140.439$, $p < 0.0001$, Tukey's test, $p < 0.01$; electronic supplementary material, figure S10G,H). Nocodazole treatment therefore reversed the effect of 0.05% DMSO on PVC dimensions in the apical and distal regions of the tubes (Tukey's test between control and nocodazole samples, $p > 0.05$), suggesting that this drug affects membrane trafficking in a different way from oryzalin.

In order to assess the effect of MT stabilization on PVC-vacuole trafficking as well, pollen tubes were incubated with 5 µM taxol. This treatment induced a weak decrease in pollen tube growth rate (Tukey's test, $p > 0.05$ with respect to SYP21-transformed and 0.85% DMSO-treated pollen tubes; electronic supplementary material, figure S2C). Microtubules in taxol-treated cells appeared as long bundles extending as far as the apex (electronic supplementary material, figure S7F). YFP-SYP21 labelling of tubular vacuoles decreased (electronic supplementary material, figure S10I–N) and PVC size increased with respect to untreated pollen tubes (electronic supplementary material, figure S10O–P; ANOVA test: $F_{6.11498} = 140.439$, $p < 0.0001$, Tukey's test between control and taxol samples, $p < 0.01$). A similar effect was observed in 0.85% DMSO-control cells (electronic supplementary material, figure S10O,P; Tukey's test between control and DMSO samples, $p < 0.01$), which showed more MTs in the cortical regions of the shank (electronic supplementary material, figure S7C). Taken together these results are strong evidence of a role of MTs in trafficking PVCs to tubular vacuoles.

To better define the role of MTs in trafficking towards vacuoles, colocalization experiments using YFP-SYP21 and CMAC were performed in control cells and in the presence of MT-active drugs (figure 10). After oryzalin treatment, the colocalization coefficient decreased significantly with respect to control (figure 10*a*; Student's *t*-test, $p < 0.001$ for apex/shank and for distal area). Moreover, colocalization points concentrated in PVCs, where they decorated the organelle-delimiting membrane (figure 9*f*,*p*; see arrowheads), and almost disappeared on tubular vacuoles, mainly in the distal region (figure 9*k–r*). Similarly, after oryzalin treatment the number of PVCs showing colocalization of SYP21 and CMAC increased significantly in the distal area (figure 10*b*; Student's *t*-test, $p < 0.05$; figure 9; arrows). Colocalization assays performed in the areas of pollen tubes with large vacuoles did not show any overlapping between CMAC and SYP21 in oryzalin treated pollen tubes (figure 9*i*,*f*, figure S8).

These findings suggest that MT depolymerization affects the delivery/fusion of PVCs to/with tubular vacuoles. Differences in PVC trafficking to vacuoles observed between the apex and distal area of the pollen tube could be due to different mechanisms regulating PVC/vacuole trafficking in these areas.

In pollen tubes treated with nocodazole, taxol or DMSO, the Pearson's coefficient did not vary significantly compared with control (Student's *t*-test, $p > 0.05$; figure 10*c*,*e*). However, in pollen tubes treated with MT-stabilizing agents (5 µM taxol or 0.05% and 0.85% DMSO), the colocalization points concentrated on PVCs and were missing on tubular vacuoles, especially in the distal area (figure 12*a–d*; *i–p*),

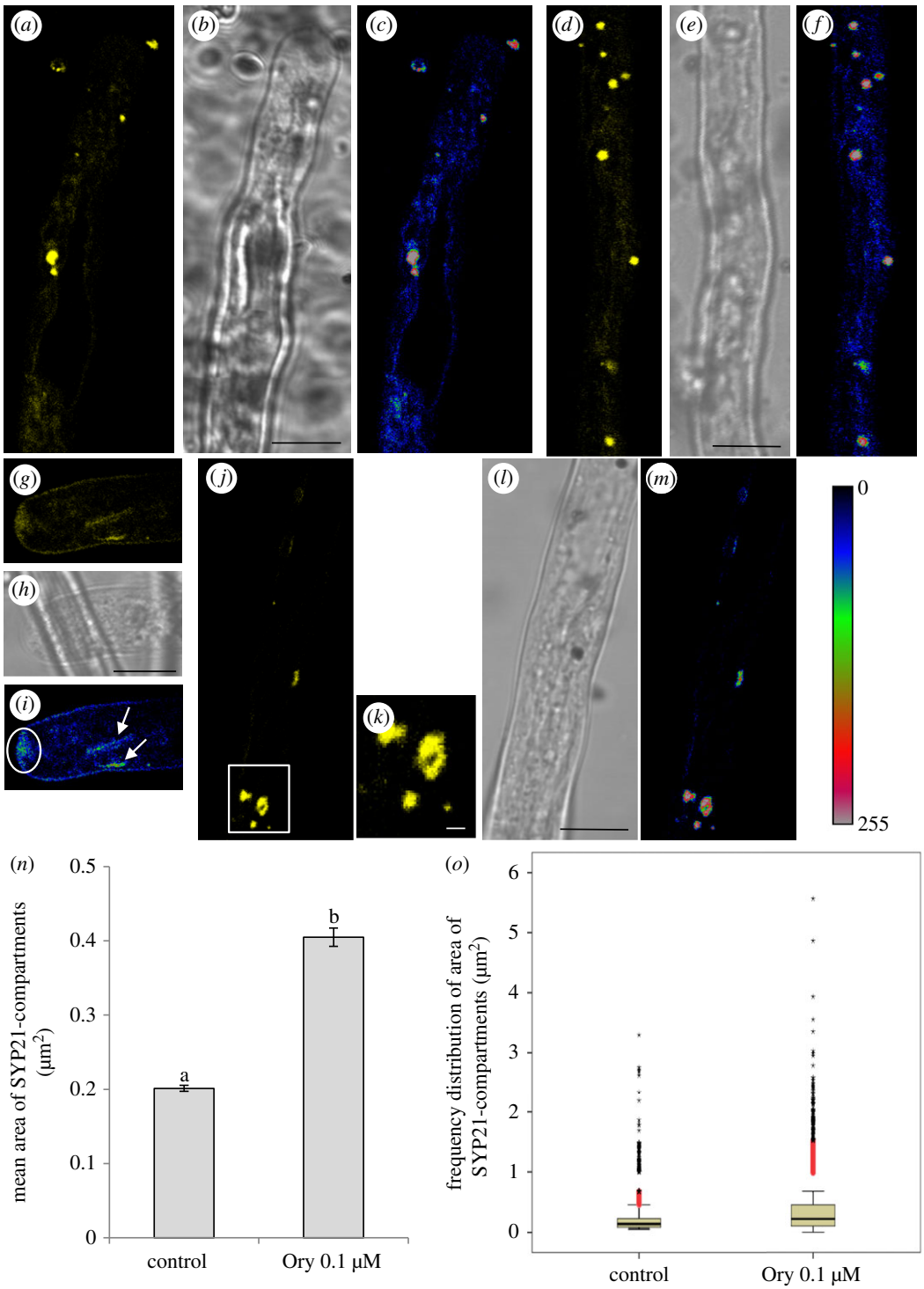

Figure 11. MT depolymerization by oryzalin affects trafficking of SYP21-positive compartments. (*a*,*b*) Oryzalin treatment enhances SYP21 staining on PVCs and considerably decreases the localization of SYP21 on tubular compartments in the apex/shank (*b*, bright field). (*c*) Pseudo-coloured images show YFP-SYP21 fluorescence intensity, which appears to be concentrated in PVCs. (*d*,*e*) The distribution of SYP21 in the distal area of oryzalin-treated pollen tubes is similar to that observed in the apex/shank (*e*, bright field). (*f*) Pseudo-coloured images show YFP-SYP21 fluorescence intensity which appears concentrated in PVCs. (*g*–*i*) SYP21 is occasionally found on the apical PM, on vesicles accumulating in the V-shape inverted cone region (*i*; circle; pseudo-coloured image) and on tubular compartments (*i*; arrows; pseudo-coloured image). (*j*–*l*) Labelling of YFP-SYP21 on the surface of large round PVCs (*l*, bright field). Magnification of PVC included in the box in (*j*) was shown in (*k*). (*m*) Pseudo-coloured images show YFP-SYP21 fluorescence intensity, which appears concentrated in PVCs and nearly lost in tubular vacuoles. All the pictures show growing pollen tubes. *a*–*j*,*l*,*m* scale bar, 10 μm; *k* scale bar, 1 μm. (*n*) The graph shows the mean area of SYP21 compartments in control and oryzalin-treated pollen tubes. The mean area of PVCs increased significantly compared with control (letters a and b indicate significantly different values, $p < 0.0001$). Error bar indicates standard error. (*o*) The box-plot shows that the number of PVCs having an area >1 μm^2 increased considerably in oryzalin-treated cells with respect to control. Some PVCs reached 5 μm^2 in area in the presence of oryzalin.

suggesting a delay in fusion of PVCs with vacuoles. In addition, unlike with oryzalin, MT stabilization did not induce a significant increment in the number of SYP21-positive PVCs colocalized with CMAC (Student's *t*-test, $p > 0.05$; figure 10*f*), supporting the idea that the dynamics of MTs affects fusion of PVCs with tubular vacuoles.

Otherwise, nocodazole treatment reversed the effect of 0.05% DMSO and the distribution of colocalization

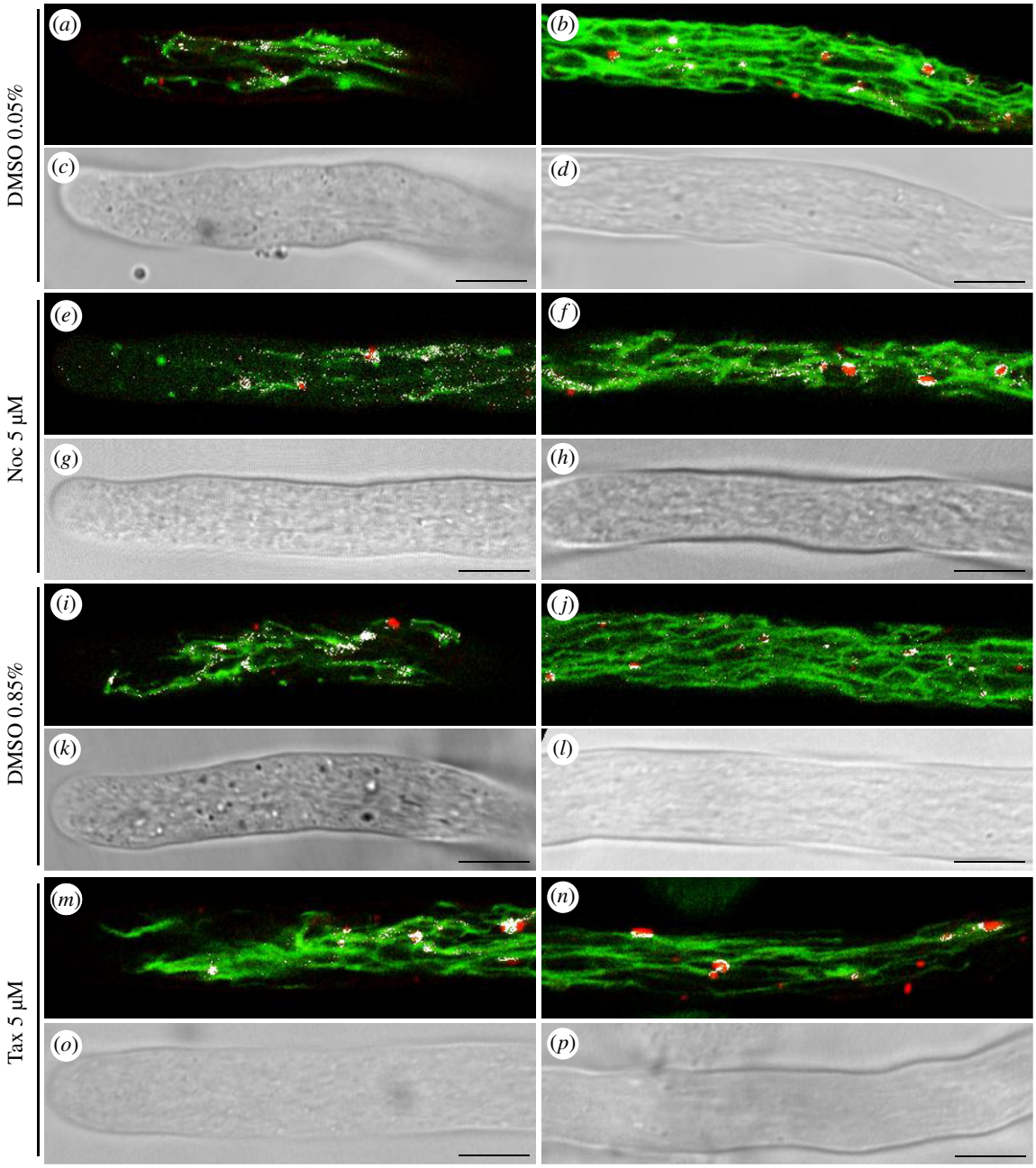

Figure 12. Colocalization of YFP-SYP21 and CMAC in pollen tubes treated with DMSO, nocodazole and taxol. (*a–d*) Colocalization of YFP-SYP21 and CMAC in the apex/shank (*a,c*) and distal area (*b,d*) of 0.05% DMSO-treated pollen tubes. Colocalized points are shown as white spots. (*e–h*) Colocalization of YFP-SYP21 and CMAC in the apex/shank (*e,g*) and distal area (*f,h*) of nocodazole-treated pollen tubes. (*i–l*) Colocalization of YFP-SYP21 and CMAC in the apex/shank (*i,k*) and distal area (*j,l*) of 0.85% DMSO-treated pollen tubes. (*m–p*) Colocalization of YFP-SYP21 and CMAC in the apex/shank (*m,o*) and distal area (*n,p*) of taxol-treated pollen tubes. All pictures show growing pollen tubes. Scale bar: 10 µm.

points was similar to that on PVCs and tubular vacuoles of untreated pollen tubes (figure 12*a–d*; *e–h*). Interestingly, the number of SYP21-positive PVCs colocalizing with CMAC increased significantly in the apex of nocodazole-treated pollen tubes with respect to controls (figure 10*d*; Student's *t*-test, $p < 0.001$ versus control and 0.05% DMSO), while in the distal area this difference was not significant (figure 10*d*; Student's *t*-test, $p > 0.05$ versus control and 0.05% DMSO).

These findings confirmed that trafficking of PVCs to vacuoles was regulated differently in the distal and apical areas and that vacuole function could vary in different pollen tube regions. In addition, MTs could play different roles in the interaction of these organelles in the apical and distal areas of tobacco pollen tubes.

3. Discussion

This is the first report of a relationship between PVCs and tubular vacuoles in growing pollen tubes of *Nicotiana tabacum*, determined by means of the marker SYP21. Our results also highlight differences in the nature and function of tubular and large vacuoles during pollen tube growth. The use of drugs affecting the polymerization and dynamics of MTs also showed that PVC delivery to/fusion with tubular vacuoles are regulated differently by MTs in the apex/shank and distal areas. Besides these new insights into membrane trafficking and SYP21 function, the present findings also sustain, in addition to the prevalence of AFs for long-range movements, the emerging role of MTs in fine membrane positioning and organelle interactions in pollen tubes.

3.1. SYP21 localizes on PVCs and tubular vacuoles in tobacco pollen tubes

Two degradation pathways identified in tobacco pollen tubes appeared to be differentially regulated by AFs and MTs [6]. In particular, perturbation of MTs delayed the delivery of tip-internalized endocytic vesicles to vacuoles and mislocalized internalized cargoes to the Golgi apparatus [7].

To better clarify the relationship between MTs and the compartments involved in the degradation pathways, SYP21 was used as marker for PVCs [25,35]. SYP21 is a t-SNARE that has been localized on the PVC delimiting membrane in tobacco leaf protoplasts [24]. This is the first time that localization of SYP21 in tobacco pollen tubes has been reported. In transiently transformed cells, SYP21 localized on round organelles widely distributed in the cytoplasm but excluded from the clear zone. Control Wm, SYP21 overexpression and BP80 transformation experiments showed that SYP21-positive round compartments observed in tobacco pollen tubes are actually PVCs [24,36,37]. In line with observations in plant somatic cells [24,38], analysis of size frequencies showed that PVCs measured 0.05 to 0.7 μm^2 in area. In addition, TEM observations and experiments of subcellular fractionation of pollen tubes revealed that membrane compartments recognized by SYP21 antibodies peaked in several fractions, confirming the presence of different populations of PVCs. Several populations of PVCs have also been reported in somatic cells [27,39].

Detailed analysis of the SYP21-positive PVC areas failed to detect any SYP21-PVCs in the 0.7–1.0 μm^2 range in tobacco pollen tubes, suggesting that SYP21-positive PVCs increase in size by homotypic fusion, or by fusion of endocytic vesicles up to a maximum area of 0.7 μm^2. The same size was observed in BP80-positive PVCs. Although PVCs with different dimensions could originate directly from the TGN, time-lapse imaging and multitracking analysis in *Arabidopsis* root hairs showed that PVCs interact together, tethering transiently in a movement defined as dancing-endosome interaction, which allows PVCs to come close together, fuse and separate, or fuse together in a stable manner, becoming larger [39]. The localization and dynamics of these PVCs were different in the apex and distal area of root hairs and were correlated with apical growth and endosome maturation. Late endosome fusion has also been observed in animals and yeasts [40–42], where spatio-temporal control of the process is postulated to prevent excessive enlargement of these compartments before fusion with lysosomes/vacuoles [41,42]. The regulation of endosome dimension, preventing excessive late endosome enlargement, ensures correct fusion with lysosomes [42]. In the pollen tube, analysis of the areas of SYP21 and BP80-positive PVCs suggested that a similar control mechanism could be present in tobacco pollen tubes.

Intriguingly, unlike GFP-BP80, SYP21 also localized on a network of highly dynamic tubules that extended longitudinally along the pollen tube as far as the apical area, without entering the clear zone. The morphology of this SYP21-tubular compartment resembled a tubular vacuole detected in *Arabidopsis* somatic cells by δ-TIP:GFP [43] and in tobacco and lily pollen tubes by the vacuolar marker CDFDA [7,31]. Double staining CMAC/YFP-SYP21 showed that SYP21 colocalized with CMAC in tubular vacuoles but never in large distal vacuoles, thus confirming the presence of SYP21 on tubular vacuoles and suggesting, for the first time, that tubular and large vacuoles are functionally different compartments.

The presence of SYP21 in vacuolar compartments was also supported by SYP21- and V-H^+ATPase-positive organelles found in the high-density sucrose fractions of microsome sub-fractionation experiments. The localization of SYP21 on vacuoles is controversial since SYP21 was reported to be specific for PVCs in somatic cells [26,27], whereas more recently this protein was detected on PVCs and vacuoles [25,38,44]. Intriguingly, in the tobacco pollen tubes, 0.5 µM Wm induced homotypic fusion of tubular vacuoles and increased SYP21 fluorescence in these compartments. On the other hand, Wm did not induce heterotypic fusion between round PVCs and tubular vacuoles. This data supports the idea that tubular vacuoles could retain some of the functions of PVCs, although these compartments appeared as different organelles.

In plants, vacuole fusion induced by Wm has only been observed in the *vti11* mutant (impaired tonoplast trafficking mutant - itt3/vti11) [45]. VTI11 is a SNARE complex polypeptide involved in homotypic vacuole fusion during vacuole biogenesis [37,45], which in plant somatic cells requires the fusion of tubular provacuoles derived from ER [46–48]. Analogously, the fusion of tubular vacuoles induced by Wm in tobacco pollen tubes suggests that this compartment could have provacuole-like identity. As a matter of fact, CMAC staining showed that in the more distal region of pollen tubes, tubules fused together and participated in large vacuole biogenesis. SYP21 did not colocalize with CMAC in these large vacuoles, suggesting that the delimiting membrane protein composition of tubular vacuoles changes before they coalesce into the large vacuole. It is also possible to imagine that SYP21 and other proteins could be recycled from the tonoplast back to PVCs or to the TGN to be reused in post-Golgi secretion.

Similar tubular vacuoles have also been observed in filamentous fungi having polarized growth [49]. In basidiomycetes and mycorrhizal fungi, tubular vacuoles play a role in bidirectional solute transport along hyphae, on a scale in the millimetre to centimetre range [50–52]. It cannot be excluded that this organelle functions in the long-distance transport of molecules in fungi and pollen tubes alike. In addition, the tubular vacuole in fungi is proposed to function as an endosomal compartment. In fact, t-SNARE AoVam3p localizes on the delimiting membrane of these tubular vacuoles as well as in late endosomes/PVCs. AoVam3p is the homologue of PEP12 from *Aspergillus oryzae* [53] and PEP12/SYP21 in plants [26]. The similar localization of AoVam3p and SYP21 suggests that tubular vacuoles could also function as endosomal compartments in pollen tubes.

Previous data on SYP21 function was controversial: although it was reported that *syp21* mutant cannot be rescued by expression of SYP22 in *Arabidopsis* somatic cells [35,54], other studies showed that SYP21 has interchangeable functions with SYP22 and SYP23 in PVC-vacuole fusion [25,38]. The presence of SYP21 on tubular vacuoles suggests that this SNARE could have a specific role in heterotypic fusion of PVCs with vacuoles or in mediating trafficking from the ER/TGN during vacuole biogenesis. Different pathways for protein delivery to vacuoles were recently identified in somatic cells, and involved direct trafficking from the ER or AP3-dependent/PVC-independent pathway [55–57]. However, these alternative pathways are still uncharacterized in pollen tubes.

3.2. MTs interact with organelles involved in degradation pathways

It is known that AFs mediate long transportation movements in somatic plant cells, while MTs are involved in the fine positioning of membrane compartments [14,15]. In pollen tubes, AFs and MTs both contribute to the transport of endosomes. Previous studies on endocytosis revealed that AFs are involved in shank-internalized PM trafficking, while MTs play a role in endocytosis, membrane sorting in the tip and transport of tip-internalized endocytic vesicles towards the vacuole [7].

To better characterize the role of MTs in the degradation pathways of tobacco pollen tubes, we used different *in vitro* and *in vivo* approaches that revealed direct interaction of organelles with purified MTs and differences in PVC behaviour under MT-perturbing drugs. The direct interaction between MTs and PVC *in vitro* was specific and ATP-dependent.

In pollen tubes, it has been shown that interaction of MTs with organelles could be mediated by motor proteins such as kinesins [58–61]. Kinesins stably bind to MTs in the presence of the ATP non-hydrolysable analogue AMP-PNP, and are released by ATP [62]. In fact, AMP-PNP has been widely used to purify MT motor proteins from a wide range of organisms [62,63]. The binding of SYP21-positive organelles to MTs was also AMP-PNP-enhanced and ATP-inhibited, suggesting that binding of SYP21-positive organelles was probably mediated by an ATP-dependent motor protein. In addition, TEM observations of MT-bound organelles suggested that this interaction could be mediated by particles decorating the membrane surface. These particles could be protein complexes that allow organelle–MT interaction. In somatic cells, CLASP has also been shown to be a plus-end-tracking MT-associated protein connecting sorting endosomes to MTs, probably by interacting with SNX1 [64]. This mechanism may also participate in the interaction of membrane compartments with MT extremities. Further experiments to characterize SYP21-positive endosome proteins, responsible for the interaction with MTs, are therefore needed to clarify this point.

Membrane fractionation experiments in the presence of oryzalin showed different migration of PVC compartments in the sucrose density gradient, supporting the idea that disturbance of MTs modifies PVC trafficking. In addition, weak modification in the distribution of Bip1 and Arf1, markers for ER and Golgi apparatus, respectively, also suggests a possible interaction between these compartments and MTs. In fact, MTs are reported to play a role in the maintenance of Golgi and ER morphology [14,16,18,65].

3.3. MTs play a role in PVC delivery to and/or fusion with tubular vacuoles

In transiently transformed pollen tubes, MT depolymerization by oryzalin caused SYP21 to accumulate on PVCs and almost disappear on tubular vacuoles. This effect was accompanied by PVC enlargement. It could be hypothesized that MTs affect the dynamic of dancing-endosome interactions [39] causing PVCs to fuse together in a stable manner so inducing the PVC enlargement. This could be an important cue to clarify the dynamic of these PVC interactions.

The PVC enlargement and the disappearance of SYP21 on tubular vacuoles together with colocalization analysis suggested that MT depolymerization affects PVC delivery to and/or fusion with tubular vacuoles. To be sure that PVC modification was due to MT depolymerization, preliminary experiments to check the integrity of AFs were performed following oryzalin treatment. Transient transformation using pLAT52/Lifeact-mEGFP did not show any detectable modification of AF pattern in the presence of oryzalin with respect to the control. On the other hand, since it is known that AFs play a major role in membrane movements in pollen tubes, it could also be worthwhile to do trafficking experiments in the presence of latrunculin B (LatB). However, in *Nicotiana tabacum* pollen tubes, 5 nM LatB dramatically altered MT pattern in the shank and tip. The AF-perturbing drug would therefore not provide unambiguous results on the actual role of AFs in PVC trafficking. As AFs and MTs are known to be intimately linked [66], we obviously cannot exclude cooperation between AFs and MTs in this process. Further experiments using different approaches could help to clarify this point.

Like MT depolymerization, MT stabilization by taxol induced similar changes in the localization of SYP21 on PVCs and tubular vacuoles. However, unlike after oryzalin treatment, Pearson's coefficients were similar in controls (untreated and 0.85% DMSO-treated) and taxol-treated cells, suggesting that MT stabilization may affect trafficking of SYP21 to PVCs, as well as PVC delivery to and/or fusion with vacuoles. In contrast, the number of PVCs that colocalized with CMAC was not enhanced in taxol-treated pollen tubes, even if their fusion with vacuoles was impaired. This supports the idea that MT depolymerization, but not MT stabilization, plays a role in the proper positioning of PVCs near the tubular vacuole to induce PVC/vacuole fusion.

Area frequencies and the results of fractionation experiments suggested that PVCs undergo modification before fusing with vacuoles and that MTs could be involved in this event. In *Arabidopsis* stem cells, PVC maturation was impaired by oryzalin and by FAB1/PIKfyve inhibitor, suggesting that endosome maturation requires recruitment of effector molecules, such as Ara7 and SNX1, by PI(3,5)P_2, as well as interaction of endosomes with cortical MTs [67,68]. Also in tobacco pollen tubes, perturbation of MTs may possibly affect the control of PVC size and PVC membrane/content composition.

The emerging idea is that MTs play a major role in different processes in pollen tube degradation pathways: MTs could primarily favour the delivery and/or fusion of PVCs with tubular vacuoles. As stated for trafficking of cellulose synthase complex (CSC), where cortical MTs play a role in positioning and targeting Golgi-derived small CSC vesicles for correct fusion with the PM [14,15,69], MTs could play a similar role in properly localizing PVCs near vacuoles to promote fusion events. The presence of colocalized points between YFP-SYP21 and CMAC on the surface of PVCs leads to the hypothesis that these compartments are transported near tubular vacuoles to promote fusion. The increase of colocalized PVCs after oryzalin and nocodazole, with respect to taxol, strongly supports that the MT dynamics is responsible for the proper positioning of PVCs with respect to tubular vacuoles and for the appropriate timing to allow fusion events.

In the emerging model, SYP21-PVCs move in the cytoplasm thanks to the AF dependent cytoplasmic streaming and are captured by MTs whose plus end dynamic instability could be responsible for positioning PVCs near tubular vacuoles to promote their fusion. MT perturbing agents prevent the proper positioning of PVCs and thus the fusion events

between PVCs and tubular vacuoles. The use of a MT-plus-end marker could better clarify this process.

In addition, MTs could also be involved in PVC modification by recruitment of effectors leading to PVC membrane and content changes. However, this hypothesis should be further investigated.

Experimental evidence also suggests that MTs influence PVC trafficking differentially in the apex/shank and distal regions. The different colocalization of SYP21-CMAC in tubular vacuoles of the tip/shank and distal area after MT drug treatments suggests that tubular vacuoles may have different functional domains along the pollen tube. In the pollen tube apex/shank, the delivery of PVCs to vacuoles may possibly not be inhibited completely by depolymerization of MTs. Alternatively, SYP21 could also reach the tubular vacuoles by MT-independent pathways. In fact, the journey of post-Golgi-secreted proteins involved in vacuole biogenesis and that of endocytic vesicles towards the vacuole may not involve PVCs or the TGN [5,55,56].

Differences between distal and apical PVC–tubular vacuole interaction were also highlighted by nocodazole treatment. Unlike oryzalin, which completely depolymerizes MTs along the tube, nocodazole increases the rate of GTP hydrolysis in the E-site of the β-tubulin subunit [70], thus increasing the time that MTs spend in pause and catastrophe phases in the apex/shank, leaving MTs in the distal areas unaltered [71].

While oryzalin increased the number of CMAC-stained SYP21-positive PVCs in the distal area, nocodazole was associated with a significant increase in the number of PVCs colocalizing with CMAC in the apex/shank, without any difference with respect to control in the distal area. These findings suggest that different MT populations affect PVC trafficking differently. Moreover, while DMSO appeared to improve homotypic PVC fusion and impair PVC delivery to and/or fusion with vacuoles in the apex/shank and distal regions, nocodazole reversed this effect, apparently inducing an increase in PVC–vacuole fusion events compared with DMSO, and preventing PVC enlargement. The increasing trend of the SYP21-CMAC colocalization coefficient in nocodazole-treated pollen tubes, though not significant, also suggests the existence of different pathways for SYP21 trafficking/recycling which were enhanced by nocodazole. Altogether, these observations suggest that dynamic MTs play a role in controlling PVC trafficking and delivery to proper position near the tubular vacuoles in the apex/shank. In the distal area, where long MT bundles were apparently not disturbed by nocodazole, PVC delivery to vacuoles was less affected. It could be interesting to investigate whether the behaviours of MTs in PVC trafficking in the apex/shank and distal area are influenced by different relationships between MTs and AFs.

The different trafficking observed for SYP21 and PVCs in the apex/shank and distal area of pollen tubes could reflect different functional significances of the degradation pathways in these regions. Prevacuolar compartments and tubular vacuoles in the apex/shank could possibly be involved mostly in endocytosis, and PVCs could play a major role in fast delivery of material destined for degradation to tubular vacuoles. Otherwise, PVCs and tubular vacuoles in the distal area could both participate in endocytosis and in biogenesis of large vacuoles. SYP21 could be retrieved from tubular vacuoles to PVCs/TGN before they coalesce into large vacuoles in the distal regions of the tubes.

4. Conclusion

The model emerging from these results predicts the involvement of MTs in trafficking to tubular vacuoles in tobacco pollen tubes. The use of SYP21 allowed us to identify, for the first time, PVCs and tubular vacuoles as crucial steps in the MT-dependent degradation pathway. Studies using different drugs affecting the polymerization status of MTs showed that different MT populations play specific roles in PVC trafficking and in PVC delivery to and/or fusion with tubular vacuoles in the apex/shank with respect to the distal regions. Furthermore, tubular vacuoles emerge as a multifunctional compartment, being involved in endosomal trafficking and in the biogenesis of large vacuoles.

5. Material and methods

5.1. Fluorescent probes and drugs

Wortmannin (Sigma) was dissolved in DMSO to a concentration of 10 mM and then diluted to 0.5 µM final concentration in the culture medium. Nocodazole (methyl 5-(2-thienylcarbonyl)-1 h benzimidazol-2-yl) (Fluka, USA) stock solution in DMSO had a concentration of 10 mM and was used in culture medium at a final dilution of 5 µM. Taxol (Paclitaxel; Sigma) was dissolved in DMSO to a concentration of 585 µM and then diluted to 5 µM final concentration in the culture medium. Oryzalin (methyl 5-(2-thienylcarbonyl)-1 h benzimidazol-2-yl) stock solution in water had a concentration of 1.38 M and was used in culture medium at a final dilution of 0.1 µM. Blue-CMAC (7-amino-4-chloromethylcoumarin) was resuspended in DMSO to a concentration of 10 mM and then diluted to 2 µM final concentration in culture medium.

5.2. Pollen tube growth

Nicotiana tabacum (L.) pollen was collected from plants in the Botanical Garden (Città Studi) of Milan University in summer and stored at −20°C. For biochemical, TEM and immunolabelling investigations, pollen grains were cultured in BK medium [72] supplemented with 12% (w/v) sucrose at 23 ± 2°C as reported by Moscatelli *et al*. [6]. For transient gene expression, pollen grains were collected from fresh flowers of *N. tabacum* (L.) and allowed to germinate at 23°C on solid medium as reported by Kost *et al*. [73].

5.3. Tubulin purification and preparation of taxol-stabilized microtubules

Microtubules from bovine brain were obtained by three cycles of temperature-dependent polymerization and depolymerization as reported by Williams and Lee [74]. Tubulin was purified by HiTrap Q XL anion exchange column (GE Healthcare, Uppsala, Sweden). Proteins were eluted with a KCl gradient from 0 to 1 M and tubulin was eluted at 0.55 M KCl. The fractions from 0.3 M KCl and 1 M KCl were analysed by SDS-PAGE and those with higher tubulin concentration were pooled. After addition of 1 mM GTP, the tubulin pool was assayed (Bradford method) for protein concentration using BSA as standard and frozen in liquid nitrogen before storage at −80°C. For binding experiments, MTs were polymerized from monomeric tubulin (10 mg ml^{-1}) in the presence of 1 mM GTP, 10% glycerol and

30 µM taxol at room temperature for 30 min. The microtubule sample was centrifuged at 12 000*g* for 50 min at 20°C and resuspended in Tx-PEM buffer (80 mM Pipes, pH 6.8, 1 mM $MgCl_2$, 1 mM EGTA and 5 µM taxol).

5.4. Microsome purification with and without peripheral protein stripping

Tobacco pollen tubes were grown in liquid BK medium for 2 h and then rinsed with 10 ml HEM buffer pH 7.4 (25 mM HEPES, 2 mM EGTA, 2 mM $MgCl_2$, 0.5 mM EDTA, 1 mM dithiothreitol (DTT), 1 mM phenylmethylsulfonyl fluoride (PMSF), 10 µg ml^{-1} TAME, 10 µg ml^{-1} leupeptin, 10 µg ml^{-1} pepstatin A, 4 µM aprotinin, 8 µM antipain) containing 12% sucrose. After centrifuging at 2000 r.p.m. for 10 min at 10°C in a Beckmann JS13.1 rotor, pollen tubes were homogenized on ice in two volumes of HEM buffer containing 10% mannitol. The homogenate was centrifuged at 572*g* for 4 min at 4°C and the supernatant loaded onto a 0.5 M sucrose cushion (3 ml) in HEM buffer and centrifuged at 64 200*g* for 23 min at 4°C. The pellet containing microsomes (P2) was resuspended in PEM buffer. Aliquots of P2 and supernatant (S2) were protein assayed (Bradford method) using BSA as standard protein. For peripheral protein stripping, P2 was incubated with 0.8 M KCl in HEM buffer, loaded onto a 0.5 M sucrose cushion in HEM buffer and centrifuged at 64 200*g* for 23 min at 4°C. These organelles, resuspended in HEM buffer, were used for binding experiments.

5.5. Binding assay with AMP-PNP or ATP

MTs polymerized as described above (100 µg protein) were incubated with microsomes (40 µg protein) for 30 min at room temperature (+MT). The microsomes had previously been incubated for 15 min with buffer, 5 mM AMP-PNP or 1 mM ATP and 5 µM taxol. Stripped microsomes (see above) were incubated with AMP-PNP. +/−MT-microsome samples were then centrifuged for 1 h at 33 300 r.p.m. in a Beckman SW60 rotor, at 20°C through a 1.2 M sucrose cushion to separate MTs bound to organelles from those not bound to organelles. Three different fractions were collected: soluble fraction (S), organelles lying on the cushion (I) and pelleted MTs and organelles (P). In parallel, a control sample without MTs (−MT) was treated as described for MT/microsome incubation. The P fractions with and without MTs (P +MT and P −MT, respectively) were used for TEM analysis or denatured for electrophoresis. Binding experiments carried out using AMP-PNP were repeated 25 times. Seven and 10 independent experiments were performed by using ATP and stripped microsomes, respectively. About 100 TEM images were taken for each experiment.

5.6. Sucrose density gradients

Pollen tubes grown on liquid BK medium were incubated with 0.1 µM oryzalin for 15 min. Microsome fractions obtained by growing pollen tubes in the absence (control) or presence of oryzalin were centrifuged through a continuous 15% to 65% sucrose gradient at 50 000*g* for 16 h. The sucrose gradient was obtained by three freezing/defrosting cycles of 40% sucrose solution in 50 mM imidazole, pH 7.5, 2 mM EDTA, 1 mM PMSF and 1 mM DTT. After centrifugation, fractions of 0.5 ml were recovered from the top of the gradient and then stored at −80°C or denatured for electrophoresis. Protein concentrations were assayed (Bradford method) using BSA as standard protein. Fractionation experiments were repeated three times.

5.7. SDS-PAGE and western blot analysis

SDS-PAGE analysis was performed using 10% linear acrylamide concentration according to the method of Laemmli [75]. Gels were stained with Coomassie Brilliant Blue R250. Western blot was performed according to Towbin *et al*. [76]. Arf1, V-H^+ATPase, H^+ATPase (Agrisera, Sweden), GRP78/Bip (Sigma) and SYP21 antibodies (kindly provided by N. Raikhel, University of California Riverside, USA) were used at final dilution of 1 : 2000 and detected as outlined in the Amersham ECL kit booklet. All gels and western blot images were scanned using Epson Perfection V750 PRO and Adobe Photoshop software. Quantification of protein levels was carried out with Quantity One Software, using the Volume tools to quantify bands, and the results were calculated as Adjusted Volume (volume minus background) of immunoreactive bands normalized to values obtained for tubulin in the same immunoblots.

5.8. pLAT52:YFP-SYP21, pLAT52:YFP:NOS and pLAT52-GFP:BP80 plasmid construction

The *LAT52* promoter-driven *YFP:SYP21* construct was generated by directional cloning. *YFP:SYP21* was removed from the *pC130035S:YFP:SYP21* construct [77] by *XbaI*/*SacI* digestion that was also used to remove *mGFP4:RabA4d:NOS* from the *pUC19LAT52:mGFP4:RabA4d:NOS* construct [78]. The *YFP:SYP21* region from *pC130035S:YFP:SYP21* was inserted into the cohesive *XbaI* and *Sac*I ends of the *pUC19LAT52* plasmid to create the translational fusion *LAT52*:*YFP:SYP21*. For the generation of the *pLAT52-GFP:BP80* construct, the Lat52 promoter (0.6 Kb) was moved as an XhoI-Bam HI fragment from pLat52-GFP-TUB6 [7] to pESC-LEU (Genbank accession #AF063849) for the sole purpose of providing a Hind III site next to XhoI. Next, the promoter was moved as a Hind III-BamHI fragment from pESC-LEU to pSGFP491 [8] using the same restriction sites to open the recipient plasmid, thereby substituting the 35S promoter with the Lat52 promoter. *NotI*/*SacI* digestion was used to remove the *SYP21* gene from the *LAT52* promoter-driven *YFP:SYP21:NOS* construct in order to create the *pUC19 LAT52*:*YFP:NOS* plasmid. Non-compatible sticky ends, produced by the double digestion *NotI*/*SacI*, were blunted using Klenow fragment. To separate the vector away from the *SYP21* gene cut out of it, we loaded the plasmid DNA on 0.8% agarose gel and purified the plasmid backbone bands using the QIAquick Gel Extraction Kit. The recovered plasmid backbone was used for self-ligation and transformation. The finished *pUC19 LAT52*:*YFP:NOS* construct was verified by sequencing and used for control experiments.

5.9. Transient gene expression and MT drug treatment

Expression vectors (1.2 µg pLAT52:YFP-SYP21, 1.5 µg pLAT52:YFP-SYP21 for overexpression, 1.5 µg pLAT52:GFP-BP80 and 0.78 µg pLAT52:Lifeact-mEGFP) were transferred to mature pollen grains on solid culture medium (see pollen tube growth) using a helium-driven particle accelerator (PDS-1000/He; Bio-Rad, Hercules, CA, USA). Pollen

grains were placed under the stopping screen at a distance of 8 cm and bombarded in a 28″Hg vacuum using a helium pressure of 1100 psi, according to the manufacturer's recommendation (Bio-Rad) [79]. Gold particles (1 µm) were coated with plasmid DNA as described by Kost *et al*. [73]. Bombarded cells were kept at 23°C in the dark for 5 h before observation. Microtubule-active drugs were added to solid culture medium and the pollen tubes were incubated for 5 min with 0.1 µM oryzalin and for 15 min with 5 µM nocodazole, 5 µM taxol, 0.5 µM Wm and 0.05% or 0.85% DMSO. Twenty transformation experiments were performed using pLAT52:YFP-SYP21 without drug treatments, while for each treatment three to five different experiments were done. Three different experiments were performed for pLAT52 : GFP-BP80 transformation. For each transformation experiment at least 20 pollen tubes were analysed.

5.10. Colocalization experiments

Pollen tubes were transiently transformed with pLAT52:YFP-SYP21 and grew as described above approximately 6 h after bombardment. Blue-CMAC 2 µM (Molecular probes, Invitrogen) was added to transiently transform pollen tubes on solid culture medium for 15 min. The dye was then removed and the tubes were rinsed by adding liquid culture medium to the solid culture medium for 5 min. Microtubule-active drugs were added to solid culture medium as described for transient gene expression. The fluorescence observations were carried out using a Leica TCS SP2 microscope with a 63× oil immersion (NA 1.4) objective (Leica Microsystems, GmbH, Wetzlar, Germany). The UV and 488-nm laser lines were used to excite Blue-CMAC and YFP, respectively, and the fluorescence was collected in the 440–480 and 520–550 nm emission windows to acquire Blue-CMAC and YFP, respectively. Images were recorded in sequential scan mode of the LCS software (Leica Microsystems, GmbH, Wetzlar, Germany) and aligned by Leica LASx software. Colocalization analysis was carried out using the JACoP plug-in of ImageJ software [80]. The degree of colocalization was evaluated by calculating Pearson's coefficient [80]. For visualization purposes, pixels with intensities exceeding user-defined thresholds for both channels were represented as white spots in overlapped images (colocalized points). Pearson's coefficients were calculated for each experiment using the same ROI in all images. For colocalization experiments between YFP-SYP21 and GFP-BP80 we used 514 nm and 458 nm laser lines to excite YFP and GFP, respectively; the fluorescence was detected in the 560–610 nm and 480–520 nm emission windows respectively, following the procedure reported above. For YFP-SYP21/CMAC colocalization, three to five different experiments were performed for each drug treatment. For YFP-SYP21/GFP-BP80 cotransformation, three different experiments were done. For each transformation experiment at least 20 pollen tubes were analysed.

5.11. Microtubule labelling

Microtubules were detected in pollen tubes grown in BK medium as control or in BK medium spiked with nocodazole (5 µM), DMSO (0.05%, 0.85%), oryzalin (0.1 µM), taxol (5 µM), Wm (0.5 µM) and latrunculin B (5 nM). Samples were then incubated in fixing solution (3.7% formaldehyde, 10% sucrose, 100 mM PIPES, 5 mM $MgSO_4$, 0.5 mM $CaCl_2$, 0.01% MBS pH 7.0) with drugs to prevent MT recovery during the early stages of fixation. Indirect immunofluorescence was performed as described in Idilli *et al*. [7] using the anti-α tubulin monoclonal antibody TUB 2.1 (purchased from Sigma, USA) at a concentration of 1 : 200. An FITC-conjugated anti-mouse secondary antibody was used at 1 : 200 final concentration (Invitrogen, USA). Optical sections (0.5 µm) and three-dimensional projections of specimens were obtained with a Leica TCS NT confocal microscope with a 40× objective for imaging. All images were recorded using a stepper motor to make Z-series.

5.12. Transmission electron microscopy and immunogold labelling

TEM analysis was performed on P fractions obtained in binding experiments with or without microtubules (P +MT and P −MT, respectively). Control samples (with AMP-PNP) and KCl- or ATP-treated samples were fixed to formvar carbon-coated nickel grids for 30 min and then quickly rinsed once with TX-PEM. After 10 min fixation in 2% glutaraldehyde, the grids were rinsed three times with 5 mM EGTA and negative stained with 1% uranyl acetate for 10 s. Immunogold labelling was performed on pollen tubes grown for 60 min in BK medium and processed for fixation by the protocol reported in Moscatelli *et al*. [5]. Seventy-nanometre ultra-thin sections, obtained using a Reichert Jung Ultracut E microtome, were collected on formvar carbon-coated nickel grids. Sections were blocked by incubation with 1% BSA for 1 h and, after three rinses of 5 min each in TSB, SYP21 antibody was used at a final concentration of 1 : 1500 for 2 h at room temperature. Grids were rinsed once in TBS with 0.1% Tween20 and twice in TBS and then incubated with 10 nm gold-conjugated goat anti-rabbit IgG (BB International, USA) diluted 1 : 100 in TBS. After three rinses with TBS, grids were incubated with 1% glutaraldehyde for 10 min, rinsed with distilled water and stained with 3% (w/v) uranyl acetate for 30 min. Observations were performed with an EFTEM LEO 912AB transmission electron microscope (Zeiss, Jena, Germany) operating at 80 kV.

5.13. Statistical analysis

Differences in Syp 21-compartment areas between treatments were analysed by Student's *t*-test and analysis of variance (ANOVA). Tukey's *post hoc* test of honestly significant difference (HSD) was used to sort all differences between treatments. Frequency distributions of SYP21-compartment areas were calculated and represented by box plots and histograms. All analyses were performed with IBM-SPSS Statistics 22 (IBM SPSS Inc., Chicago, IL, USA). The letters a and b in the graphs indicate significantly different values.

Data accessibility. This article has no additional data.

Authors' contributions. A.M. conceived the project; E.O. and A.M. planned the research, performed most of the experiments, analysed the data and wrote the paper; M.S. constructed the YFP-SYP21 plasmid under control of the pLAT52 pollen-specific promotor and did the quantitative analysis of western blot experiments; M.P. constructed the GFP-BP80 plasmid under control of the pLAT52 pollen-specific promotor; M.C. conducted the statistical analysis and appraised the manuscript; G.P. conducted the statistical analysis, N.S. performed SDS-PAGE and western blot analysis of fractionation experiments. All the authors gave their final approval for publication.

Competing interests. We declare we have no competing interests.

Funding. This research was funded by a Transition Grant from Milan University.

Acknowledgements. We are very grateful to Prof. NV. Raikhel (University of California, Riverside, USA) for providing pC130035S:YFP:SYP21 plasmid and the anti-SYP21 antibody used in many of the experiments. We thank Prof. PK. Hepler (Massachusetts University, Amherst, USA) for providing pLAT52:Lifeact-mEGFP plasmid and Prof. L. Jiang (The Chinese University of Hong Kong, China) for providing 35S:GFP:BP80 plasmid. Many thanks also to Dr Enrico Sala, Dr Mario Beretta and Valerio Parravicini for taking care of the tobacco plants. No conflict of interest is declared.

References

1. Navashin SG. 1898 Resultate einer Revision der Befruchtungsvorgange bei *Lilium martagon* und *Fritillaria tenella*. *Bull. Acad. Sci. St. Petersburg* **9**, 377–382.
2. Guignard ML. 1899 Sur les antherozoides et la double copulation sexuelle chez les vegetaux angiosperms. *Rev. Gén. Bot.* **11**, 129–135.
3. Moscatelli A, Idilli AI. 2009 Pollen tube growth: a delicate equilibrium between secretory and endocytic pathways. *J. Integr. Plant Biol.* **51**, 727–739. (doi:10.1111/j.1744-7909.2009.00842.x)
4. Onelli E, Moscatelli A. 2013 Endocytic pathways and recycling in growing pollen tubes. *Plants* **2**, 211–229. (doi:10.3390/plants202021)
5. Moscatelli A, Ciampolini F, Rodighiero S, Onelli E, Cresti M, Santo N, Idilli A. 2007 Distinct endocytic pathways identified in tobacco pollen tubes using charged nanogold. *J. Cell Sci.* **120**, 3804–3819. (doi:10.1242/jcs.012138)
6. Moscatelli A, Idilli AI, Rodighiero S, Caccianiga M. 2012 Inhibition of actin polymerization by low concentration Latrunculin B affects endocytosis and alters exocytosis in shank and tip of tobacco pollen tubes. *Plant Biol.* **14**, 770–782. (doi:10.1111/j.1438-8677.2011.00547.x)
7. Idilli AI, Morandini P, Onelli E, Rodighiero S, Caccianiga M, Moscatelli A. 2013 Microtubule depolymerization affects endocytosis and exocytosis in the tip and influences endosome movement in tobacco pollen tubes. *Mol. Plant* **6**, 1109–1130. (doi:10.1093/mp/sst099)
8. Wang H, Tse YC, Law AH, Sun SS, Sun YB, Xu ZF, Hillmer S, Robinson DG, Jiang L. 2010 Vacuolar sorting receptors (VSRs) and secretory carrier membrane proteins (SCAMPs) are essential for pollen tube growth. *Plant J.* **61**, 826–838. (doi:10.1111/j.1365-313X.2009.04111.x)
9. Hao L, Liu J, Zhong S, Gu H, Qu LJ. 2016 AtVPS41-mediated endocytic pathway is essential for pollen tube-stigma interaction in *Arabidopsis*. *Proc. Natl Acad. Sci. USA* **113**, 6307–6312. (doi:10.1073/pnas.1602757113)
10. Lovy-Wheeler A, Wilsen KL, Baskin TI, Hepler PK. 2005 Enhanced fixation reveals the apical cortical fringe of actin filaments as a consistent feature if the pollen tube. *Planta* **221**, 95–104. (doi:10.1007/s00425-004-1423-2)
11. Cárdenas L, Lovy-Wheeler A, Kunkel JG, Hepler PK. 2008 Pollen tube growth oscillations and intracellular calcium levels are reversibly modulated by actin polymerization. *Plant Physiol.* **146**, 1611–1621. (doi:10.1104/pp.107.113035)
12. Hepler PK, Winship LJ. 2015 The pollen tube clear zone: clues to the mechanism of polarized growth. *J. Integr. Plant Biol.* **57**, 79–92. (doi:10.1111/jipb.12315)
13. Vidali L, McKenna ST, Hepler PK. 2001 Actin polymerization is essential for pollen tube growth. *Mol. Biol. Cell* **12**, 2534–2545. (doi:10.1091/mbc.12.8.2534)
14. Crowell EF, Bischoff V, Desprez T, Rolland A, Stierhof YD, Schumacher K, Gonneau M, Höfte H, Vernhettes S. 2009 Pausing of Golgi bodies on microtubules regulates secretion of cellulose synthase complexes in *Arabidopsis*. *Plant Cell* **21**, 1141–1154. (doi:10.1105/tpc.108.065334)
15. Gutierrez R, Lindeboom JJ, Paredez AR, Emons AM, Ehrhardt DW. 2009 *Arabidopsis* cortical microtubules position cellulose synthase delivery to the plasma membrane and interact with cellulose synthase trafficking compartments. *Nat. Cell Biol.* **11**, 797–806. (doi:10.1038/ncb1886)
16. Wang W, Lazareva E, Kyreev I, Smirnova E. 2012 The role of microtubules in the maintenance of regular localization and arrangement of Golgi apparatus in root cells of *Triticum aestivum* L. *Proc. Biochem.* **47**, 1545–1551. (doi:10.1016/j.procbio.2012.01.001)
17. Brandizzi F, Wasteneys GO. 2013 Cytoskeleton-dependent endomembrane organization in plant cells: an emerging role for microtubules. *Plant J.* **75**, 339–349. (doi:10.1111/tpj.12227)
18. Hamada T, Ueda H, Kawase T, Hara-Nishimura I. 2014 Microtubules contribute to tubule elongation and anchoring of endoplasmic reticulum, resulting in high network complexity in *Arabidopsis*. *Plant Physiol.* **166**, 1869–1876. (doi:10.1104/pp.114.25232)
19. Onelli E, Idilli AI, Moscatelli A. 2015 Emerging roles for microtubules in angiosperm pollen tube growth highlight new research cues. *Front. Plant Sci.* **6**, 51. (doi:10.3389/fpls.2015.00051)
20. Griffing LR, Lin C, Perico C, White RR, Sparkes I. 2017 Plant ER geometry and dynamics: biophysical and cytoskeletal control during growth and biotic response. *Protoplasma* **254**, 43–56. (doi:10.1007/s00709-016-0945-3)
21. Sorri O, Åström H, Raudaskoski M. 1996 Actin and tubulin expression and isotype pattern during tobacco pollen tube growth. *Sex. Plant Reprod.* **9**, 255–263. (doi:10.1007/BF02152699)
22. Joos U, van Aken J, Kristen U. 1994 Microtubules are involved in maintaining the cellular polarity in pollen tubes of *Nicotiana sylvestris*. *Protoplasma* **179**, 5–15. (doi:10.1083/jcb.143.5.1183)
23. Sanderfoot AA, Kovaleva V, Zheng H, Raikhel NV. 1999 The t-SNARE AtVAM3p resides on the prevacuolar compartment in *Arabidopsis* root cells. *Plant Physiol.* **121**, 929–938. (doi:10.1104/pp.121.3.929)
24. Foresti O, daSilva LL, Denecke J. 2006 Overexpression of the *Arabidopsis* syntaxin PEP12/SYP21 inhibits transport from the prevacuolar compartment to the lytic vacuole in vivo. *Plant Cell* **18**, 2275–2293. (doi:10.1105/tpc.105.040279)
25. Shirakawa M *et al.* 2010 *Arabidopsis* Qa-SNARE SYP2 proteins localized to different subcellular regions function redundantly in vacuolar protein sorting and plant development. *Plant J.* **64**, 924–935. (doi:10.1111/j.1365-313X.2010.04394.x)
26. da Silva Conceição A, Marty-Mazars D, Bassham DC, Sanderfoot AA, Marty F, Raikhel NV. 1997 The syntaxin homolog AtPEP12p resides on a late post-Golgi compartment in plants. *Plant Cell* **9**, 571–582. (doi:10.1105/tpc.9.4.571)
27. Sanderfoot AA, Ahmed SU, Marty-Mazars D, Rapoport I, Kirchhausen T, Marty F, Raikhel NV. 1998 A putative vacuolar cargo receptor partially colocalizes with atPEP12p on a prevacuolar compartment in *Arabidopsis* roots. *Proc. Natl Acad. Sci. USA* **95**, 9920–9925. (doi:10.1073/pnas.95.17.9920)
28. Ranocha P *et al.* 2013 *Arabidopsis* WAT1 is a vacuolar auxin transport facilitator required for auxin homoeostasis. *Nat. Commun.* **4**, 2625. (doi:10.1038/ncomms3625)
29. Emans N, Zimmermann S, Fischer R. 2002 Uptake of a fluorescent marker in plant cells is sensitive to brefeldin A and wortmannin. *Plant Cell* **14**, 71–86. (doi:10.1105/tpc.010339)
30. Zhang Y, He J, Lee D, McCormick S. 2010 Interdependence of endomembrane trafficking and actin dynamics during polarized growth of *Arabidopsis* pollen tubes. *Plant Physiol.* **152**, 2200–2210. (doi:10.1104/pp.109.142349)
31. Lovy-Wheeler A, Cárdenas L, Kunkel JG, Hepler PK. 2007 Differential organelle movement on the actin cytoskeleton in lily pollen tubes. *Cell Motil. Cytoskeleton* **64**, 217–232. (doi:10.1002/cm.20181)
32. Cole L, Hyde GJ, Ashford AE. 1997 Uptake and compartmentalization of fluorescent probes by *Pisolithus tinctorius* hyphae: evidence for an anion transport mechanism at the tonoplast but not for fluid phase endocytosis. *Protoplasma* **199**, 18–29. (doi:10.1007/BF02539802)

33. Cole L, Orlovich DA, Ashford AE. 1998 Structure, function, and motility of vacuoles in filamentous fungi. *Fungal Genet. Biol.* **24**, 86–100. (doi:10.1006/fgbi.1998.1051)
34. Idilli AI, Onelli E, Moscatelli A. 2012 Low concentration of LatB dramatically changes the microtubule organization and the timing of vegetative nucleus/generative cell entrance in tobacco pollen tubes. *Plant Signal. Behav.* **7**, 947–950. (doi:10.4161/psb.20907)
35. Sanderfoot AA, Pilgrim M, Adam L, Raikhel NV. 2001 Disruption of individual members of *Arabidopsis* syntaxin gene families indicates each has essential functions. *Plant Cell* **13**, 659–666. (doi:10.1105/tpc.13.3.659)
36. Wang J, Cai Y, Miao Y, Lam SK, Jiang L. 2009 Wortmannin induces homotypic fusion of plant prevacuolar compartments. *J. Exp. Bot.* **60**, 3075–3083. (doi:10.1093/jxb/erp136)
37. Han ZJ, Rodriguez-Welsh SW, Rojas-Pierce M. 2014 Homotypic vacuole fusion requires VTI11 and is regulated by phosphoinositides. *Mol. Plant* **7**, 1026–1040. (doi:10.1093/mp/ssu019)
38. Uemura T, Morita MT, Ebine K, Okatani Y, Yano D, Saito C, Ueda T, Nakano A. 2010 Vacuolar/pre-vacuolar compartment Qa-SNAREs VAM3/SYP22 and PEP12/SYP21 have interchangeable functions in *Arabidopsis*. *Plant J.* **64**, 864–873. (doi:10.1111/j.1365-313X.2010.04372.x)
39. von Wangenheim D, Rosero A, Komis G, Šamajová O, Ovečka M, Voigt B, Šamaj J. 2016 Endosomal interactions during root hair growth. *Front. Plant Sci.* **6**, 1262. (doi:10.3389/fpls.2015.01262)
40. Puchner EM, Walter JM, Kasper R, Huang B, Lim W. 2013 Counting molecules in single organelles with superresolution microscopy allows tracking of the endosome maturation trajectory. *Proc. Natl Acad. Sci. USA* **110**, 16 015–16 020. (doi:10.1073/pnas.1309676110)
41. Arlt H, Auffarth K, Kurre R, Lisse D, Piehler J, Ungermann C. 2015 Spatiotemporal dynamics of membrane remodeling and fusion proteins during endocytic transport. *Mol. Biol. Cell* **26**, 1357–1370. (doi:10.1091/mbc.E14-08-1318)
42. Liu K *et al.* 2016 Negative regulation of phosphatidylinositol 3-phosphate levels in early-to-late endosome conversion. *J. Cell Biol.* **212**, 181–198. (doi:10.1083/jcb.201506081)
43. Hicks GR, Rojo E, Hong S, Carter DG, Raikhel NV. 2004 Geminating pollen has tubular vacuoles, displays highly dynamic vacuole biogenesis, and requires VACUOLESS1 for proper function. *Plant Physiol.* **134**, 1227–1239. (doi:10.1104/pp.103.037382)
44. Uemura T, Ueda T, Ohniwa RL, Nakano A, Takeyasu K, Sato MH. 2004 Systematic analysis of SNARE molecules in *Arabidopsis*: dissection of the post-Golgi network in plant cells. *Cell Struct. Funct.* **29**, 49–65. (doi:10.1247/csf.29.49)
45. Zheng J, Han SW, Munnik T, Rojas-Pierce M. 2014 Multiple vacuoles in *impaired tonoplast trafficking3* mutants are independent organelles. *Plant Signal Behav.* **9**, e972113. (doi:10.4161/psb.29783)
46. Marty F. 1999 Plant vacuoles. *Plant Cell* **11**, 587–600. (doi:10.1105/tpc.11.4.587)
47. Viotti C *et al.* 2013 The endoplasmic reticulum is the main membrane source for biogenesis of the lytic vacuole in *Arabidopsis*. *Plant Cell* **25**, 3434–3449. (doi:10.1105/tpc.113.114827)
48. Viotti C. 2014 ER and vacuoles: never been closer. *Front. Plant Sci.* **4**, 20. (doi:10.3389/fpls.2014.00020)
49. Richards A, Veses V, Gow NAR. 2010 Vacuole dynamics in fungi. *Fungal Biol. Rev.* **24**, 93–105. (doi:10.1016/j.fbr.2010.04.002)
50. Ashford AE. 1998 Dynamic pleiomorphic vacuole systems: are they endosomes and transport compartments in fungal hyphae? *Adv. Bot. Res.* **28**, 119–159. (doi:10.1128/EC.5.2.411-421.2006)
51. Ashford, AE, Allaway WG. 2002 The role of the motile tubular vacuole system in mycorrhizal fungi. *Plant Soil* **244**, 177–187. (doi:10.1023/A:1020271121683)
52. Darrah PR, Tlalka M, Ashford A, Watkinson SC, Fricker MD. 2006 The vacuole system is a significant intracellular pathway for longitudinal solute transport in basidiomycete fungi. *Eukaryot Cell* **5**, 1111–1125. (doi:10.1128/EC.00026-06)
53. Shoji JY, Arioka M, Kitamoto K. 2006 Vacuolar membrane dynamics in the filamentous fungus *Aspergillus oryzae*. *Eukaryot Cell* **5**, 411–421.
54. Sanderfoot AA, Kovaleva V, Bassham DC, Raikhel NV. 2001 Interactions between syntaxins identify at least five SNARE complexes within the Golgi/prevacuolar system of the *Arabidopsis* cell. *Mol. Biol. Cell* **12**, 3733–3743. (doi:10.1091/mbc.12.12.373)
55. Pedrazzini E, Komarova NY, Rentsch D, Vitale A. 2013 Traffic routes and signals for the tonoplast. *Traffic* **14**, 622–628. (doi:10.1111/tra.12051)
56. Rojas-Pierce M. 2013 Targeting of tonoplast proteins to the vacuole. *Plant Sci.* **211**, 132–136. (doi:10.1016/j.plantsci.2013.07.005)
57. Ebine K *et al.* 2014 Plant vacuolar trafficking occurs through distinctly regulated pathways. *Curr. Biol.* **24**, 1375–1382. (doi:10.1016/j.cub.2014.05.004)
58. Liu GQ, Cai G, Del Casino C, Tiezzi A, Cresti M. 1994 Kinesin-related polypeptide is associated with vesicles from *Corylus avellana* pollen. *Cell Motil. Cytoskeleton* **29**, 155–166. (doi:10.1002/cm.970290207)
59. Cai G, Romagnoli S, Moscatelli A, Ovidi E, Gambellini G, Tiezzi A, Cresti M. 2000 Identification and characterization of a novel microtubule-based motor associated with membranous organelles in tobacco pollen tubes. *Plant Cell* **12**, 1719–1736. (doi:10.1105/tpc.12.9.1719)
60. Li J, Xu Y, Chong K. 2012 The novel functions of kinesin motor proteins in plants. *Protoplasma* **249**, S95–S100. (doi:10.1007/s00709-011-0357-3)
61. Zhu C, Dixit R. 2012 Functions of the *Arabidopsis* kinesin superfamily of microtubule-based motor proteins. *Protoplasma* **249**, 887–899. (doi:10.1007/s00709-011-0343-9)
62. Vale RD, Reese TS, Sheetz MP. 1985 Identification of a novel force-generating protein, kinesin, involved in microtubule-based motility. *Cell* **42**, 39–50. (doi:10.1016/S0092-8674(85)80099-4)
63. Vallee RB, Sheetz MP. 1996 Targeting for motor proteins. *Science* **271**, 1539–1544. (doi:10.1126/science.271.5255.1539)
64. Ambrose C, Ruan Y, Gardiner J, Tamblyn LM, Catching A, Kirik V, Marc J, Overall R, Wasteneys GO. 2013 CLASP interacts with sorting nexin 1 to link microtubules and auxin transport via PIN2 recycling in *Arabidopsis thaliana*. *Dev. Cell* **24**, 649–659. (doi:10.1016/j.devcel.2013.02.007)
65. Mathur J, Mathur N, Kernebeck B, Srinivas BP, Hülskamp M. 2003 A novel localization pattern for an EB1-like protein links microtubule dynamics to endomembrane organization. *Curr. Biol.* **13**, 1991–1997. (doi:10.1016/j.cub.2003.10.033)
66. Lancelle SA, Hepler PK. 1991 Association of actin with cortical microtubules revealed by immunogold localization in *Nicotiana* pollen tubes. *Protoplasma* **165**, 167–172. (doi:10.1007/BF01322287)
67. Hirano T, Munnik T, Sato MH. 2015 Phosphatidylinositol 3-phosphate 5-kinase, FAB1/PIKfyve kinase mediates endosome maturation to establish endosome-cortical microtubule interaction in *Arabidopsis*. *Plant Physiol.* **169**, 1961–1974. (doi:10.1104/pp.15.01368)
68. Hirano T, Munnik T, Sato MH. 2017 Inhibition of phosphatidylinositol 3,5-bisphosphate production has pleiotropic effects on various membrane trafficking routes in *Arabidopsis*. *Plant Cell Physiol.* **58**, 120–129. (doi:10.1093/pcp/pcw164)
69. Paredez AR, Somerville CR, Ehrhardt DW. 2006 Visualization of cellulose synthase demonstrates functional association with microtubules. *Science* **312**, 1491–1495. (doi:10.1126/science.1126551)
70. Mejillano MR, Shivanna BD, Himes R. 1996 Studies on the nocodazole-induced GTPase activity of tubulin. *Arch. Biochem. Biophys.* **336**, 130–138. (doi:10.1006/abbi.1996.0540)
71. Vasquez RJ, Howell B, Yvon A-MC, Wadsworth P, Cassimeris L. 1997 Nanomolar concentrations of nocodazole alter microtubule dynamic instability *in vivo* and *in vitro*. *Mol. Biol. Cell* **8**, 973–985. (doi:10.1091/mbc.8.6.973)
72. Brewbaker JL, Kwack BH. 1963 The essential role of calcium ions in pollen germination and pollen tube growth. *Am. J. Bot.* **50**, 859–865. (doi:10.1002/j.1537-2197.1963.tb06564.x)
73. Kost B, Spielhofer P, Chua N-H. 1998 A GFP–mouse talin fusion protein labels plant actin filaments *in vivo* and visualizes the actin cytoskeleton in growing pollen tubes. *Plant J.* **16**, 393–401. (doi:10.1046/j.1365-313x.1998.00304.x)
74. Williams RC, Lee JC. 1982 Preparation of tubulin from brain. *Methods Enzymol.* **85B**, 376–385. (doi:10.1016/S0091-679X(10)95001-2)
75. Laemmli UK. 1970 Cleavage of structural proteins during the assembly of the head of bacteriophage T4. *Nature* **227**, 680–685. (doi:10.1038/227680a0)

76. Towbin H, Staehelin T, Gordon J. 1979 Electrophoretic transfer of proteins from polyacrylamide gels to nitrocellulose sheets: procedure and some applications. *Proc. Natl Acad. Sci. USA* **76**, 4350–4354. (doi:10.1073/pnas.76.9.4350)
77. Robert S, Chary SN, Drakakaki G, Li S, Yang Z, Raikhel NV, Hicks GR. 2008 Endosidin1 defines a compartment involved in endocytosis of the brassinosteroid receptor BRI1 and the auxin transporters PIN2 and AUX1. *Proc. Natl Acad. Sci. USA* **105**, 8464–8469. (doi:10.1073/pnas.0711650105)
78. Szumlanski AL, Nielsen E. 2009 The Rab GTPase RabA4d regulates pollen tube tip growth in *Arabidopsis thaliana*. *Plant Cell* **21**, 526–544. (doi:10.1105/tpc.108.060277)
79. Sanford JC, Smith FD, Russell JA. 1993 Optimizing the biolistic process for different biological applications. *Methods Enzymol.* **217**, 483–509. (doi:10.1016/B978-0-12-765561-1.50038-2)
80. Bolte S, Cordelières FP. 2006 A guided tour into subcellular colocalization analysis in light microscopy. *J. Microsc.* **224**, 213–232. (doi:10.1111/j.1365-2818.2006.01706.x)

Chemosphere 240 (2020) 124915

Contents lists available at ScienceDirect

Chemosphere

journal homepage: www.elsevier.com/locate/chemosphere

Typha latifolia and *Thelypteris palustris* behavior in a pilot system for the refinement of livestock wastewaters: A case of study

Nadia Stroppa [a], Elisabetta Onelli [a], Monika Hejna [b], Luciana Rossi [b], Assunta Gagliardi [c], Luca Bini [d], Antonella Baldi [b], Alessandra Moscatelli [a, *]

[a] Department of Biosciences, University of Milano, Via Celoria 26, 20133, Milan, Italy
[b] Department of Health, Animal Science and Food Safety, University of Milano, Via Celoria 10, 20133, Milan, Italy
[c] Dipartimento di Biologia Cellulare, Computazionale e Integrata - CIBIO, University of Trento, Via Sommarive 9, Povo, 38123, Trento, Italy
[d] Department of Life Science, University of Siena, Via Aldo Moro 2, 53100, Siena, Italy

HIGHLIGHTS

- *Thelypteris palustris* was more affected by metals than *Typha latifolia*.
- Salts of Zn and Cu induced cell wall remodeling and carbohydrate metabolism changes in both plants.
- Similar morphological alterations were induced by different mechanisms in both plants.

ARTICLE INFO

Article history:
Received 19 July 2019
Received in revised form
18 September 2019
Accepted 18 September 2019
Available online 20 September 2019

Handling Editor: T Cutright

Keywords:
Typha latifolia
Thelypteris palustris
Phytodepuration
Livestock wastewaters
Heavy metals

ABSTRACT

In animal livestock heavy metals are widely used as feed additives to control enteric bacterial infections as well as to enhance the integrity of the immune system. As these metals are only partially adsorbed by animals, the content of heavy metals in manure and wastewaters causes soil and ground water contamination, with Zn^{2+} and Cu^{2+} being the most critical output from pig livestock.

Phytoremediation is considered a valid strategy to improve the purity of wastewaters. This work studied the effect of Zn^{2+} and Cu^{2+} on the morphology and protein expression in *Thelypteris palustris* and *Typha latifolia* plants, cultured in a wetland pilot system.

Despite the absence of macroscopic alterations, remodeling of cell walls and changes in carbohydrate metabolism were observed in the rhizomes of both plants and in leaves of *Thelypteris palustris*. However, similar modifications seemed to be determined by the alterations of different mechanisms in these plants. These data also suggested that marsh ferns are more sensitive to metals than monocots. Whereas toleration mechanisms seemed to be activated in *Typha latifolia*, in *Thelypteris palustris* the observed modifications appeared as slight toxic effects due to metal exposure.

This study clearly indicates that both plants could be successfully employed in *in situ* phytoremediation systems, to remove Cu^{2+} and Zn^{2+} at concentrations that are ten times higher than the legal limits, without affecting plant growth.

1. Introduction

Livestock wastewaters are usually reused in agriculture after traditional depuration treatment (Nicholson et al., 2003). However, these wastewaters often contain metals that should be removed to prevent field contamination. The presence of metals is related to the animals' diet, which is enriched with this type of essential compounds to enhance the integrity of the immune system (Liu et al., 2018, Reg. UE1831/2003). Phytodepuration is a low cost and ecologically friendly technology for civil and industrial wastewater refinement (Peterson, 1998). It also improves livestock wastewaters in terms of organic substances through the construction of wetlands (Anning et al., 2013; Yang and Ye, 2009). However, its application in terms of metal removal from livestock wastewaters is still

* Corresponding author.
E-mail addresses: nadia.stroppa@unimi.it (N. Stroppa), elisabetta.onelli@unimi.it (E. Onelli), monika.hejna@unimi.it (M. Hejna), Luciana.rossi@unimi.it (L. Rossi), assunta.gagliardi@unitn.it (A. Gagliardi), luca.bini@unisi.it (L. Bini), antonella.baldi@unimi.it (A. Baldi), alessandra.moscatelli@unimi.it (A. Moscatelli).

https://doi.org/10.1016/j.chemosphere.2019.124915
0045-6535/

scarcely documented (Almeida et al., 2016).

In order to improve the knowledge regarding the efficiency and applicability of phytodepuration for metal removal from animal wastewaters, we set up two types of mesocosms, with *Typha latifolia* or *Thelypteris palustris* (marsh fern) to treat water spiked and not spiked with Zn^{2+} (44.02 mg/L) and Cu^{2+} (8.63 mg/L), the main metals present in livestock wastewaters. Chemical analyses showed that both plants were tolerant (they did not show any macroscopic alteration) and accumulated substantial amounts of metals in their tissues, particularly in the aboveground organs (see accompanying paper, Hejna et al., 2019). In particular, treated *T. latifolia* began to accumulate Zn^{2+} and Cu^{2+} after 15 days of metal exposure, since there was only a significant increase in metal concentration in T2 (Zn: $p < 0.001$; TLT = 271.64 ± 17.71 vs. TLC = 55.79 ± 17.71 mg/kg; Cu: $p < 0.001$; TLT = 47.54 ± 3.56 vs. TLC = 15.20 ± 3.56 mg/kg), suggesting that *T. latifolia* can accumulate Zn^{2+} and Cu^{2+} in its organs 45 days after the treatment. Moreover, *T. palustris* were also able to accumulate Zn^{2+} and Cu^{2+} in their organs. In fact, higher concentrations of metals were detected in TPT than in the control already 15 days (T1) after metal addition (Zn: $p < 0.001$; TPT = 414.67 ± 17.71 vs. TPC = 85.62 ± 17.71 mg/kg; Cu: $p < 0.001$; TPT = 136.12 ± 3.56 vs. TPC = 18.25 ± 3.56 mg/kg). Furthermore, we observed the decreasing trend of Zn and Cu in water and soil in treated mesocosms (TLT, TPT) in the end of the experiment (T2) compared with T0 for *T. latifolia* and *T. plaustris* plants (see accompayning paper Hejna et al., 2019).

However, the marsh fern was more efficient than *T. latifolia*, accumulating higher concentrations of all the metals in its organs more quickly. However, the mechanisms behind the tolerance and metal uptake in *T. latifolia* and *T. palustris* are not well known, despite their importance in understanding how systems work and thus how to maintain/increase their efficiency.

Plants growing in heavy metal polluted environments employ several mechanisms to increase stress tolerance or to prevent the entry of metals into the cells. Stress tolerance involves biochemical processes through the action of chaperone proteins, glutathione, metallothioneins, and phytochelatins (Doğanlar, 2013; Hasan et al., 2017; Petraglia et al., 2014; Yadav, 2010). In various plants, several genes induced under metal stress have been identified (Dubey et al., 2014; Kumar and Trivedi, 2016; Singh et al., 2016; Tiwari and Lata, 2018). Transcription factors or other proteins involved in metal detoxification, signal transduction, stress signal, ROS signaling have been identified as having an important role in heavy metal tolerance (Collin et al., 2008; Lingua et al., 2012; Rao et al., 2011; Viehweger, 2014).

On the other hand, mechanisms of stress avoidance act by limiting the metal assimilation by the root through the modification of the rhizosphere (Małachowska-Jutsz and Gnida, 2015; Meier et al., 2012), binding metals in the cell wall (Colzi et al., 2012; Krzesłwska, 2011; Le Gall et al., 2015; Oves et al., 2016), removing metals by glands and hydathodes or accumulating metals in vacuoles of ageing leaves (Małachowska-Jutsz and Gnida, 2015).

These tolerance mechanisms have also been reported in wetland plants which were shown to synthesize phytochelatins, peptides and exudates to chelate-free metal ions, to increase antioxidant enzyme activities and sequester heavy metals in organs or subcellular compartments (Fediuc and Erdei, 2002; Higuchi et al., 2015; Yang and Ye, 2009; Yang et al., 2000).

The aim of this work was to investigate the mechanisms behind the capacity of *T. latifolia* and *T. palustris* to accumulate Zn^{2+} and Cu^{2+} by analyzing the proteome and the morphology of cells and tissues in plants grown in a pilot wetland system.

Microscopy and proteomic analyses were performed on the leaves and rhizomes of plants after 45 days of metal exposure. For microscopical observations, sections were obtained from three different plants grown with or without the mineral feed additive premix, containing Zn^{2+} and Cu^{2+} at a concentration 14 times higher than the legal limit. Treatment was performed at single concentration of metals in order to observe phytoremediation in realistic farm condition. Morphological changes were observed in the rhizomes of both plants and in leaves of *T. palustris*, suggesting cell wall remodeling and changes in the carbohydrate metabolism. Interestingly, modifications were similar in the two plant species, however they seemed to be determined by different mechanisms. The morphological changes in treated plants were more pronounced in *T. palustris* than *T. latifolia,* thus revealing their higher sensitivity to heavy metals. Regarding proteomes, no modification was observed in *T. palustris*, while few changes were observed in the 1D-gel electrophoresis protein profile of *T. latifolia*, partially explaining the morphological modifications observed by light and TEM microscopy.

2. Materials and methods

2.1. Plant culture and sampling

A pilot wetland system comprising 4 tanks (2 m × 2 m x 1.2 m) was prepared in the Botanical Gardens of Milan University. Tanks were first lined with waterproof cloths, and two layers of stone chippings (diameter 1–3 cm and 1 cm) and sand were put in each tank. This substratum became sediment upon the addition of water. Finally, 210 kg of loam for plant culture (Flox Containerpflanzen, Blumenerde VitaFlor) was layered on the substratum. The same quantity of tap water (650 L) was added to each tank before placing the plants (purchased from Centro Flora Autoctona, Galbiate, LC, Italy).

Three-month-old plants of *T. latifolia* (30/tank) were placed in two tanks together with plants of *T. palustris* (60/tank). After 15 days (T0), in two tanks (metals: Met), one containing *T. latifolia* and the second containing *T. palustris,* the water was contaminated with Cu^{2+} and Zn^{2+} at 8.63 mg/L and 44.02 mg/L final concentrations, by dissolving 1.5 Kg of the mineral feed additive premix (feed Maxi CRC 0.5% supplied by Alpha). The water in the other two tanks (controls: Co) was not modified.

Three plants were sampled in each of the four tanks after the premix addition (T0) and 45 days (T2) after the plants had been placed. Before sampling each tank was divided into three regions and one plant was sampled from each region.

2.2. Light and transmission electron microscopy

Aerial (leaves) and subaerial (rhizomes/roots) organs of *T. latifolia* (Co/Met) and *T. palustris* (Co/Met) taken at different times were incubated in fixing solution (0.04 M Cacodylate pH 6.9, 2% Formaldehyde, 2% Glutaraldehyde) overnight at room temperature. Samples were repeatedly rinsed in 0.04 M Cacodylate pH 6.9, dehydrated with increasing concentrations of ethanol and embedded in LR white resin (Sigma). Semi-fine sections (2 μm) and ultra-thin sections (80 nm), were obtained using a Reichert Jung Ultracut E microtome.

The semi-fine sections were stained by 1% toluidine blue or Lugol and observed with a Leica DMRB light microscope. Ultra-thin sections were stained with 3% uranyl-acetate and observed with an EFTEM LEO 912AB transmission electron microscope (Zeiss) working at 80 kV.

Plants were collected from different corners of the wetland system and, in order to observe rhizomes at the same developmental stage, rhizomes with a comparable diameter were collected, located at the same distance from the shoots.

2.3. Indirect immunofluorescence and confocal microscopy

Rhizome sections of *T. latifolia* and *T. palustris* were put on slides and allowed to rehydrate by incubating them with 1% BSA (bovine serum albumin) in TBS (Tris/HCl 0.05 M pH 7.5, NaCl 0.15 M), in a moist chamber at room temperature for 45 min. Sections were rinsed once with TBS, and then incubated with LM19 and JIM7, the antibodies against low esterified (LEPs) and high esterified pectins (HEPs), respectively (PlantProbes). Both primary antibodies were diluted 1:10 and the incubation was performed overnight at 4 °C. Sections were rinsed twice in TBS and then incubated with the secondary antibody FITC conjugated (Rabbit Anti-Rat IgG + IgM + IgA H&L; Abcam) for 2 h at room temperature in the dark. Control experiments were also performed, in which the primary antibody was omitted.

Samples were observed using a Leica TCS NT SP2 confocal microscope; a 20X lens (zoom 2) was used for imaging. The 488-nm laser line was used to excite FITC and the fluorescence was collected in the emission window 494–550 nm. The organs of at least three plants for each tank were analyzed.

2.4. Protein extraction

Leaves and rhizomes of *T. latifolia* and *T. palustris* were frozen in liquid nitrogen immediately after collection and stored at −80 °C. Leaves and rhizomes were homogenized in liquid nitrogen and nitrogen ground powder was resuspended in five volumes of pre-cooled precipitation solution (10% TCA and 20 mM DTT in acetone). Proteins were precipitated overnight at −20 °C, then washed twice for 1 h at −20 °C with 20 mM DTT in acetone and pelleted by centrifugation for 30 min at 26000×*g* at 4 °C. Pellets were dried for 10 min under vacuum and resuspended in LSB1X for 1D-gel electrophoresis. Samples were sonicated for 30 min in a water-bath sonicator at 20 °C. The extracts were centrifuged for 30 min at 26000×*g*, at 15 °C and the supernatants were collected and stored at −80 °C.

Protein concentration was determined by the Bradford protein assay (Bradford, 1976).

2.5. One-dimensional electrophoresis

Proteins were resolved in denaturing 10% acrylamide 1D-gels in a discontinuous buffer system (Laemmli, 1970). MiniVe Vertical Electrophoresis System (GE Healthcare, USA) was used for analytical one-dimensional electrophoresis. For the preparatory 1D-gel electrophoresis of *T. latifolia* rhizomes, polypeptides were separated using 17 cm × 20 cm, 1.5 mm thick gels (Elettrofor, Rovigo, Italy). Proteins were visualized with Coomassie brilliant blue R250 and silver staining (Sinha et al., 2001). Three replicas were analyzed for at least three plants per tank.

2.6. Mass spectrometry and protein identification

Protein identification was performed as previously described (Hellman et al., 1995; Soskic et al., 1999). Bands of interest were manually excised, destained in ammonium bicarbonate 2.5 mM and acetonitrile 50% (v/v), and acetonitrile dehydrated. Before protein digestion, 1D gel-resolved proteins were reduced with 10 mM DTE in 25 mM ammonium bicarbonate (1 h at 56 °C) and then alkylated with 55 mM iodoacetamide in 25 mM ammonium bicarbonate at room temperature (45 min, in darkness). After incubation with 50 mM ammonium bicarbonate (10 min), protein bands were acetonitrile dehydrated. 1D gel-resolved proteins were rehydrated in trypsin solution (Sigma Aldrich, Italy) and in-gel protein digestion was performed by an overnight incubation at 37 °C. For MALDI-TOF MS, 0.75 ml of each protein digest was directly spotted onto the MALDI target and air-dried. A total of 0.75 ml of an alpha-cyano-4-hydroxycynnamic acid matrix solution was added to the dried samples and allowed to dry again. Mass spectra were acquired using an Ultraflex III MALDI-TOF/TOF mass spectrometer (Bruker Daltonics, Billerica, MA, United States). Spectra were analyzed by Flex Analysis v. 3.0. Peptide mass fingerprinting (PMF) database searches was carried out in NCBInr or Swiss-Prot/TrEMBL databases set for Viridiplantae (Green Plants) using Mascot (Matrix Science Ltd., London, UK, http://www.matrixscience.com) with the following settings: experimental and theoretical PMF patterns with a Dmass less than 100 ppm, trypsin as the digestion enzyme, one allowed missed cleavage, carbamidomethylation of cysteine as a fixed modification, and oxidation of methionine as a variable modification. The parameters used to accept identifications were the number of matched peptides, extent of sequence coverage, and probabilistic score. Only peptides with individual ion scores of $p < 0.05$ were significant.

3. Results

3.1. Morphological changes induced by metals are revealed by light and transmission electron microscopy in leaves of T. palustris and T. latifolia

Thelypteris palustris and *T. latifolia*, grown in the wetland apparatus tanks prepared as previously described, did not show alterations in macroscopical morphology and no differences were observed between control and treated plants. New leaves were produced by plants and no discoloration or chlorosis, due to photosynthetic activity alteration, was observed (Fig. S1; see Supplementary material). In addition, by rhizome expansion *T. latifolia* plants were able to vegetatively reproduce.

Plant exposure to metals induces cell responses which involve metabolism modifications and morphology remodeling (Arif et al., 2016; Molas et al., 2002; Oves et al., 2016; Sandalio et al., 2001; Todeschini et al., 2011). To reveal the morphological changes, leaves and rhizomes of *T. palustris* and *T. latifolia* plants, grown in the pilot wetland system, were analyzed by light and transmission electron microscope (TEM).

Histological observations showed that before metal exposure (T0), *T. latifolia* adult leaves showed large air chambers (Fig. S2A,a,c), located between two bilayered mesophylls located on the upper (adaxial) and lower (abaxial) leaf sides (Fig. S2A; see Supplementary material). In the mesophyll facing the monolayered epidermis, a multilayered palisade parenchyma (Fig. S2A, B, C, D; bracket) was observed with small cells rich in chloroplasts separated by small intracellular spaces. In the inner part of mesophyll, facing the large air chambers, parenchyma was formed by two layers of large isodiametric cells without chloroplasts and with large vacuoles. These cells were close to each other and extended to form the inner scaffold connecting the adaxial and abaxial leave sides (Fig. S2A and B). Vascular bundles were distributed in all the parenchymatic tissues (Fig. S2B and D, arrows).

A similar morphology of leaves was observed in T2 plants both in the control and treated samples, suggesting that exposure to metals did not lead to morphological changes in *T. latifolia* leaves (Fig. S2, compare A-D; E, F; H, I). TEM observations of chloroplasts showed thylakoids and starch granules in the control and treated plants, and did not show any alterations in organelle morphology after metal exposure (Fig. S2 G, J).

Thelypteris palustris leaves showed a different morphology in the control with respect to the treated plants (Fig. 1).

In fact, in T0, the leaf was thin and the mesophyll was formed by lacunose/spongy parenchyma with large intercellular spaces

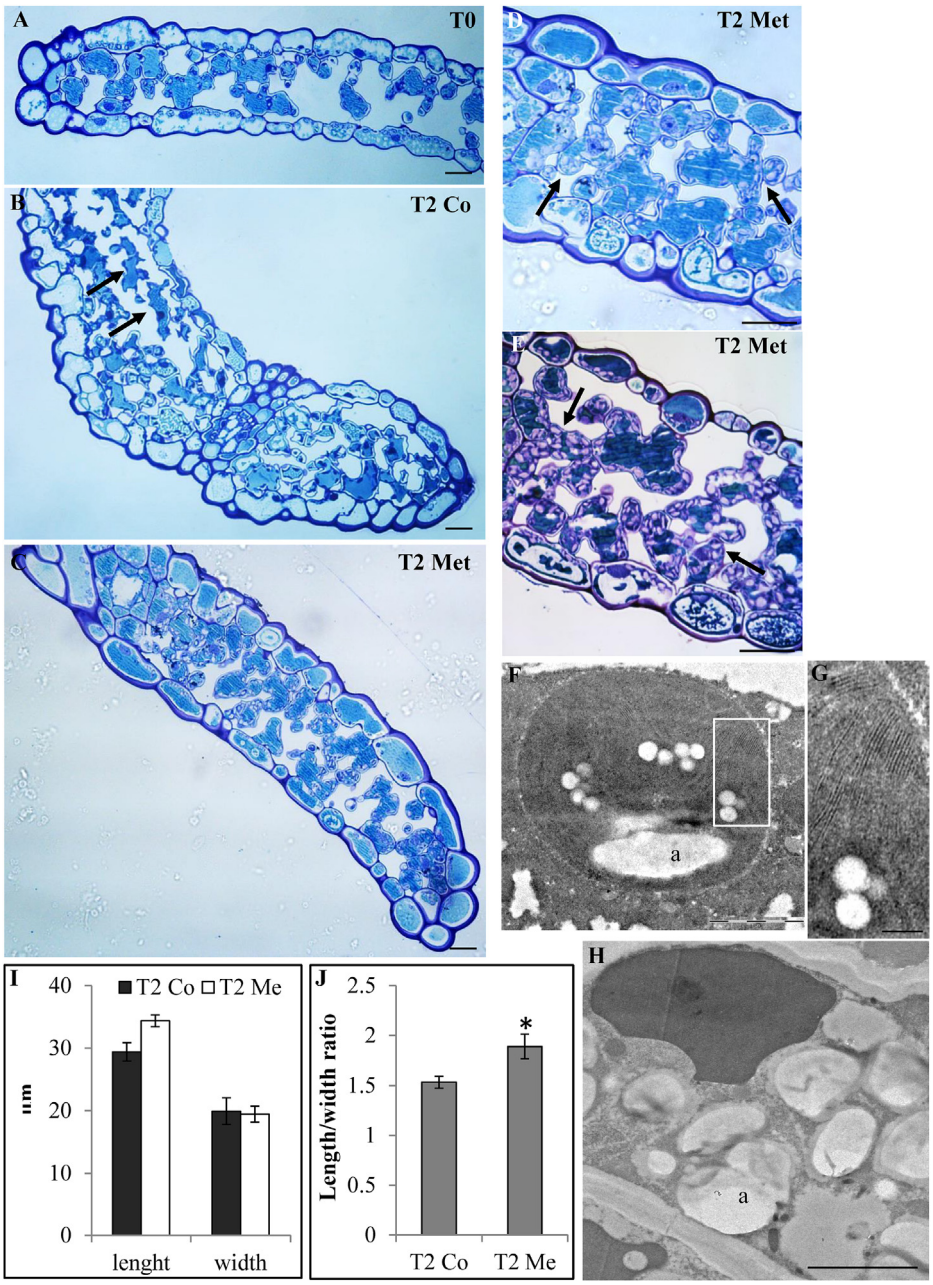

Fig. 1. (A) Histological observations of *T. palustris* leaves at T0. (B) Hystological observations of T2-Co *T. palustris* leaves; differentiated parenchymatic cells with a lobed profile are indicated by arrows. (C–E) Histological observations of T2-Met *T. palustris* leaves; amyloplasts accumulating in parenchyma and epidermal cells are indicated by arrows. Older leaves were showed in (E). (F–H) TEM observations showed that whereas in T2 Co cells chloroplasts showed well developed grana thylakoids (F, G), in T2-Met plants, a greater number of large starch grains was observed in mesophyll cells (H). Amyloplasts are indicated by: a. (I–J) Graphs reporting variations in parenchymatic cell shape occurring after metal exposure. Bars: (A–E) = 10 µm; (F, H) = 1 µm; (G) = 200 nm.

delimited by isodiametric or slight-lobated cells (Fig. 1A). In T2 control samples (T2-Co), parenchymatic cells were more differentiated with an extremely lobed/indented profile (Fig. 1B; arrows), while in T2 samples after metal treatment (T2-Met), the cells showed a linear profile and maintained a similar shape to that observed in T0 (Fig. 1C). In addition, there was a reduction in intracellular spaces with respect to T0.

To better define the cell shape variation, the cell size was calculated by measuring both their major (length) and minor axis (width), in sections obtained from three different leaf samples. Metal exposure led to an increase in cell length ($p = 0.053$) and thus a significant difference in length/width ratio ($p < 0.01$), confirming that there is a variation in parenchymatic cell shape after metal exposure (Fig. 1I and J). The similarity of T2-Met parenchyma cells with those of T0 leaves suggested that the metal treatment affected cell enlargement/differentiation, during the leaf development.

Microscopic analyses showed that in parenchymatic and epidermal cells, an accumulation of starch granules occurred in the chloroplast (Fig. 1D). In older leaves, this starch accumulation was enhanced and a great number of amyloplasts accumulated in the cells (Fig. 1E; arrows). The conversion of chloroplasts into amyloplasts was confirmed by TEM observation: in T2 control cells (Fig. 1F and G) chloroplasts showed well developed grana thylakoids, a few starch grains and some plastoglobules as observed in T0 (data not

shown). In treated plants, the mesophyll cells showed a greater number of large starch grains, while the thylakoid membrane systems disappeared (Fig. 1H), suggesting a transition from chloroplasts to amyloplasts.

3.2. Rhizome morphological alterations in response to metal treatment were similar in T. latifolia and T. palustris

Typha latifolia T0 rhizome was surrounded by a uniseriate epidermis (Fig. S3A; ep), and by a multiseriate hypodermis with large irregular cells (Fig. S3A; hp; see Supplementary material). The most significant characteristic was the presence of an outer cortical region and a central core showing different parenchymatic tissues (Fig. S3). The cortex was occupied by an aerial parenchyma (AP) formed by highly vacuolated large cells with different geometries, a thin cell wall and a few plastids (Fig. S3B). These cells were separated by large irregular intercellular spaces forming air ducts (see asterisks). Small vascular bundles (vb) were widespread in all the cortical areas (Fig. S3B).

In the inner rhizome, a storage parenchyma (SP; Fig. S3C) was found formed by isodiametric cells with numerous amyloplasts (Fig. S3C; see arrow) and small intercellular spaces. A ring of large vascular bundles defined the surface demarcating these two parenchyma (Fig. S3C; see bracket). In T2-Co and T2−Met plants, the morphology of AP and SP did not change (Fig. S3; compare F−I and E-H) and the cell dimension of SP was the same in both samples ($p > 0.05$). However, after metal treatment, in the SP there was a significant decrease in the number of amyloplasts in the treated samples compared to the control (Figs. S3F and I; see arrows). Staining with Sudan Black revealed starch grains. Although no significant differences were observed in starch grain content in the T0 and T2-Co samples (Fig. 2A and B; the amount of amyloplasts was calculated by counting them in sections obtained from rhizomes of three different plants; $p > 0.05$), after metal treatment, a significant decrease in amyloplasts was evident (Fig. 2C), suggesting the influence of metals in carbohydrate accumulation.

In T2 samples, AP and SP were separated by an endoderm-like layer (McManus et al., 2002), with cells showing thickening in the radial and inner tangential cell wall (Fig. S3E and H; arrow). Along the endoderm-like layer, in the SP, the ring of large vascular bundles was always present (Fig. S3E and H; bracket). After metal treatment (T2-Met), the endoderm cells showed a reduction in cell wall thickening compared to the T2-Co samples (Fig. S3E and H). T2-Met and T2-Co rhizomes were observed by TEM (Fig. 3A−F), thus confirming the differences in cell wall structure. In the AP of both treated and control samples, the cell wall was very thin and convolved. Cells were entirely occupied by large vacuoles and rare starch grains were observed (Fig. 3A, D).

The endoderm cells appeared very different in T2-Met and T2-Co rhizomes (Fig. 3B, E). In fact, the cell walls of the control samples showed a very think radial and inner tangential cell wall, showing a lamellate structure (Fig. 3B; cw). On the other hand, after metal treatment, cell walls were thinner (Fig. 3E), suggesting a different cell wall deposition and remodeling. In the SP, cell walls were thicker with respect to AP (Fig. 3C, F, I) and there were more starch grains in the control than in the treated cells (Fig. 3C, F), confirming the observations made with the light microscopy. The middle lamella in the cell corners was partially reabsorbed in the control samples creating intercellular spaces (Fig. 3G), while in the treated samples the middle lamella remained and cellular spaces did not form (Fig. 3H; arrow). Alterations in cell wall structure were also confirmed by analysis of the cell wall thickness (Fig. 3I). Both in AP and SP, the cell wall thickness significantly decreased by 45% and 60%, respectively, ($p < 0.01$) after metal treatment, suggesting an influence on the cell wall deposition and modification/remodeling.

In the rhizomes of *T. palustris*, both optical observations showed the presence of large vascular bundles (Fig. S4B, D, F; vb; see Supplementary material). In T0 and T2-Co samples, cortical and pith parenchymatic cells appeared isodiametric with small intercellular spaces and were rich in starch grains (Fig. S4A−D). In the large vacuoles, dense material was often observed (Fig. S4A and C; asterisks). Rhizomes in T2-Met plants appeared morphologically similar to Co (Fig. S4E and F) and the analysis of the cell dimension did not show significant differences in cell size ($p > 0.05$). However, Sudan black staining showed an increase in amyloplasts in parenchymatic T2-Co cells with respect to T0 (Fig. 2D, E) and a decrease in starch grains after metal treatment (Fig. 2F), as already observed in *T. latifolia*. This thus suggests that also in *T. palustris,* metals led to a modification in carbohydrate accumulation.

TEM observations showed that parenchymatic cell vacuoles were filled by dense material, and amyloplasts were present in higher amounts in T2-Co with respect to the treated sample (Fig. 3J-L). Similarly, *T. palustris* cell walls were different in the parenchymatic cells of T2-Co and T2-Met plants. In fact, metal treatment decreased the cell wall thickness by 40%, suggesting the influence of metals on cell wall remodeling (Fig. 3L). In roots, which have been reported to be involved in metal accumulation (Almeida et al., 2016; Klink, 2017; Klink et al., 2013), no difference in morphology was observed in treated plants with respect to controls, both in *T. latifolia* and *T. palustris* (data not shown).

3.3. Metals induce remodeling of cell walls in rhizomes of T. palustris but not in T. latifolia plants

To better define cell wall changes following metal treatment, two antibodies against high esterified (JIM7; high esterified pectins: HEPs) and low esterified pectins (LM19; low esterified pectins: LEPs) were used in indirect immunofluorescence assays. Control experiments performed without primary antibodies showed only a very low fluorescence signal in the rhizome tissues of both plants (Fig. S5; see Supplementary material).

In T2-Co *T. latifolia* plants, LM19/JIM7 antibodies showed that AP cells contained both low and high esterified pectins in the walls of rhizome cells (Figs. 4 and 5A, C, E, G respectively).

In particular, the distribution of HEPs was more discontinuous than the LEPs, as the HEPs were concentrated in small cell wall tracts (compare Figs. 4C and 5C). On the other hand, in the SP, HEPs were uniformly distributed in the cell wall, while LEPs were mainly located in the cell wall corners (Figs. 4G and 5G). The same distribution in the corner wall was observed in the hypodermis for both low and high esterified pectins (Figs. 4A and 5A). In the epidermis, both pectins were shown in outer cell wall (Figs. 4A and 5A; arrows), while in the endoderm, no pectins were recorded (Figs. 4E and 5E). In vascular bundles (Fig. 4; vb) pectins were distributed in the vascular and parenchymatic tissues and not in the sclerenchyma.

After metal treatment (T2-Met), AP, SP and endoderm did not show significant differences in LEP and HEP distribution (Figs. 4D, F, H and 5D, F, H). Interestingly, the most significant modification in the cell wall was observed in the epidermis where both pectins disappeared completely from the outer cell wall (Fig. 4A and B and. 5A and B), while only HEPs disappeared from the hypodermis cell walls.

Thelypteris palustris revealed a more extensive modification of LEPs and HEPs in the rhizomes. In T2-Co samples, LEPs were distributed in the cell wall of parenchyma and in the parenchymatic cells inside the vascular bundles (Fig. 6A, C, E).

In the epidermis and cortex, LEPs were located in the inner layer of the primary cell wall and in the middle lamella (Fig. 6A; arrows). The primary cell walls close to the middle lamella did not show

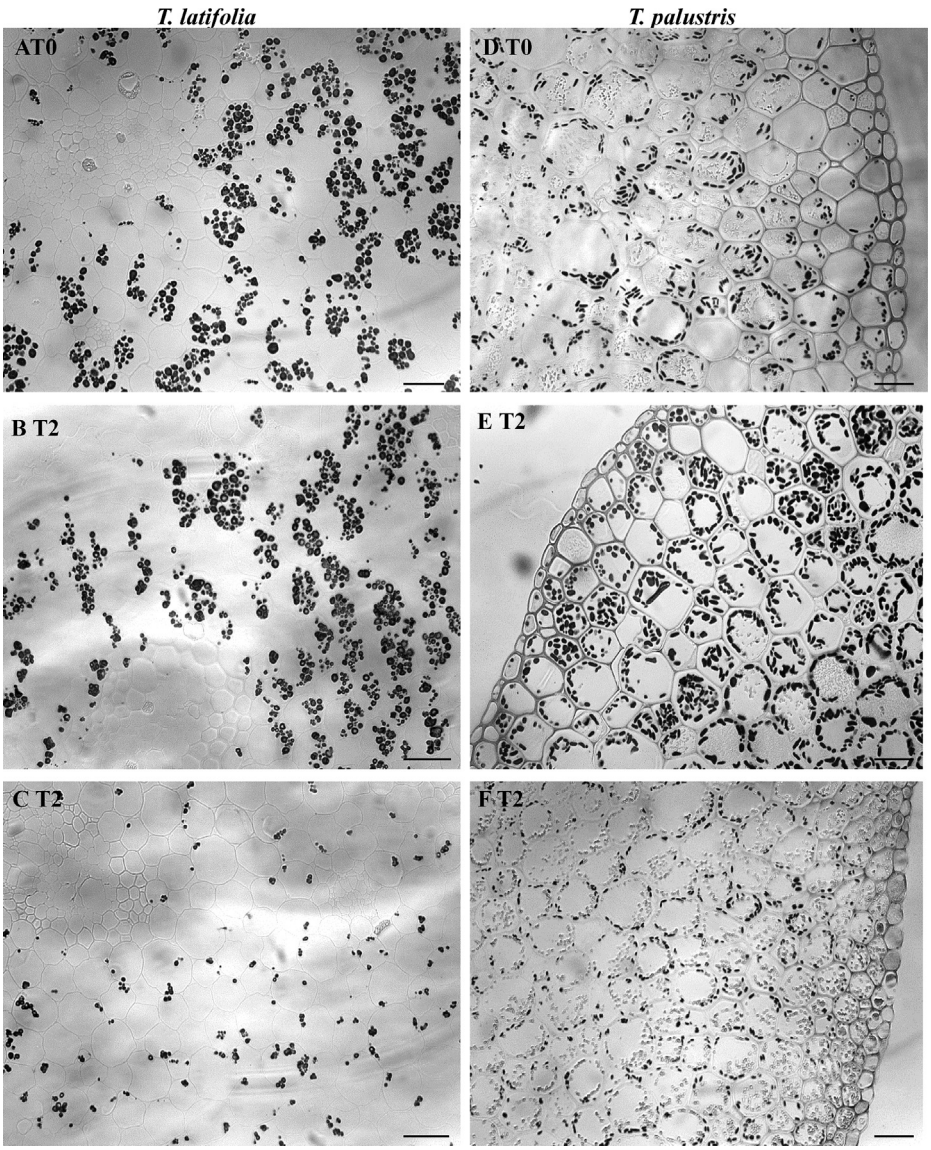

Fig. 2. Sudan Black staining of *T. latifolia* rhizomes (A–C) No differences were observed in starch grain content in rhizomes of T0 and T2-Co samples (A, B). After metals treatment a significant decrease in the number of amyloplasts was evident (C). Sudan Black staining of *Thelypteris palustris* rhizomes (D–F) parenchymatic T2-Co cells showed an increase of amyloplasts with respect to T0 (D, E). A decrease of starch grains was observed after metal treatment with respect to control (F). Bar = 20 μm.

LM19 staining (Fig. 6A). The low esterified pectins were uniformly distributed in the cell wall of pith cells and in the parenchymatic cells surrounding xylem (Fig. 6C, E). In the corners of cells, the middle lamella was reabsorbed creating intercellular spaces (Fig. 6E; arrows). After metal treatment, in the epidermis and cortex, LM19 stained only the middle lamella (Fig. 6B; arrows), while in the pith cells, LEPs were found in higher amounts in the corner of the cells, causing a reduction in intercellular spaces (Fig. 6F; arrow). No modifications were observed in the vascular systems (Fig. 6D).

HEP location also changed after metal treatment (Fig. 6G-L). In T2-Co samples, cortical cells showed a distribution of HEPs in the inner layer of the primary cell wall and in the middle lamella (Fig. 6G; arrows). Metal treatment led to the disappearance of HEPs from the middle lamella, thus only the inner layer of primary cell wall was stained by the JIM7 antibody (Fig. 6H; arrows). In T2-Co pith cells, the HEPs were uniform in the cell wall, excluding the corners of cells filled by intercellular spaces (Fig. 6K). In the vascular bundles all the cells showed a uniform HEP distribution (Fig. 6I). As observed for LEPs, in T2-Met cells, HEPs remained in the corners of cells, thus reducing the extent of intercellular spaces (Fig. 6L; arrow), while they maintained the same distribution inside the vascular bundle (Fig. 6J).

3.4. Protein analysis by 1D- and 2D-gel electrophoresis and protein identification

To investigate the molecular basis of cell walls and starch modification observed after metal treatment, we compared the protein profiles of leaves and rhizomes of the control and treated *T. latifolia* and *T. palustris* (T2-Me compared to T2-Co) by 1D-gel electrophoresis.

In the leaves of both plants, 1-D electrophoresis did not reveal qualitative and quantitative differences in the protein profile (compare Fig. 7A and B).

Similarly, control and treated rhizomes of *T. palustris* did not show differences in the 1-D gel electrophoresis protein profile

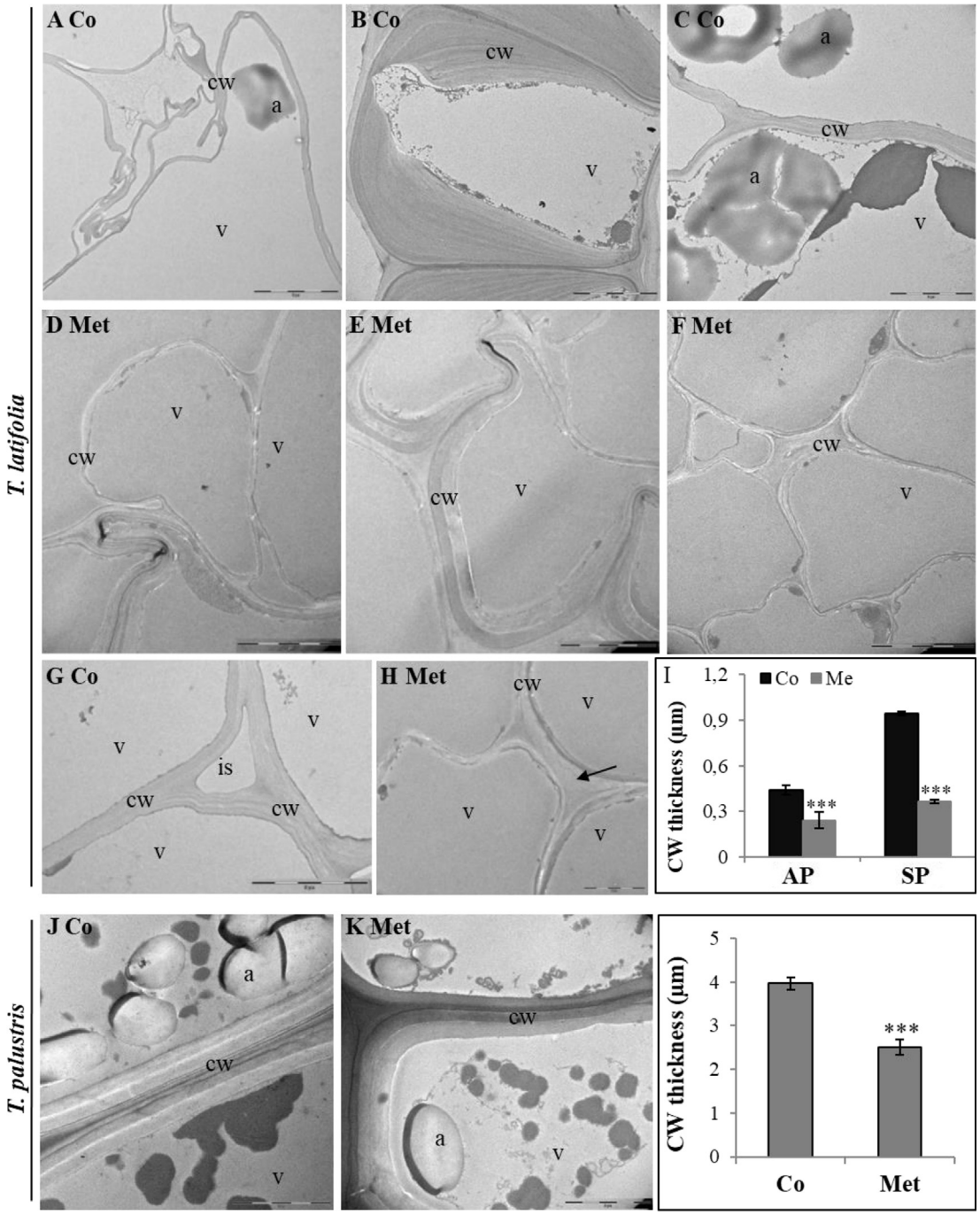

Fig. 3. TEM observation of *T. latifolia* T2-Co and T2-Met rhizomes. (A–C) In T2-Co, the AP cell wall (cw) is thin and convolved. Cells are mostly occupied by large vacuoles (v) and rare starch grains (a) are observed (A). The T2-Co endoderm cells showed radial and inner tangential thick cell wall, showing lamellate structure (B; cw). In the SP, cell walls were thicker with respect to AP (C; cw). (D–F) In T2-Met, SP cell walls were thinner (E) and a higher number of starch grains was observed in control with respect to treated cells (C, F). (G–I) The middle lamella in cell corners was partially reabsorbed in control samples creating intercellular spaces (G; is), while in treated samples the middle lamella persisted and cellular spaces did not form (H; arrow). The analysis of cell walls in AP and SP, showed that cell wall thickness significantly decreased ($p < 0.01$) after metal treatment (I). TEM observation of *T. palustris* T2-Co and T2-Met rhizomes. (J, K) Parenchymatic cell vacuoles (v) were filled with dense material in both samples while and amyloplasts (a) were present in higher amount in T2-Co with respect to T2-Met. (L) A decrease of cell wall (cw) thickness was observed in T2-Met with respect to T2-Co. Bar = 5 µm.

(Fig. 7A). On the other hand, in *T. latifolia* rhizomes exposed to metals, 1-D electrophoresis showed a decrease in proteins with a molecular mass of between 40 and 55 kDa (Fig. 7B; compare T2 Co and T2 Me; bands 1, 2, 3) and an increase in a 56 kDa protein (Fig. 7B; compare T2- Co and T2-Met; bands 4) in comparison to the controls. These polypeptides were excised from 1-D gels and subjected to MALDI TOF/TOF MS analysis (Fig. 7C).

Interestingly, mass spectrometry identified proteins belonging to the cytoskeletal system: β- and α-tubulin were identified in bands 1 and 2 respectively, and actin was identified in band 3, suggesting that metals induced a decrease in cytoskeletal proteins in treated plants (Fig. 7C). In the increased band 4, three different proteins were detected: cullin 3B; lysine-specific demethylase JMJ125 and pentatricopeptide repeat-containing protein (Fig. 7C).

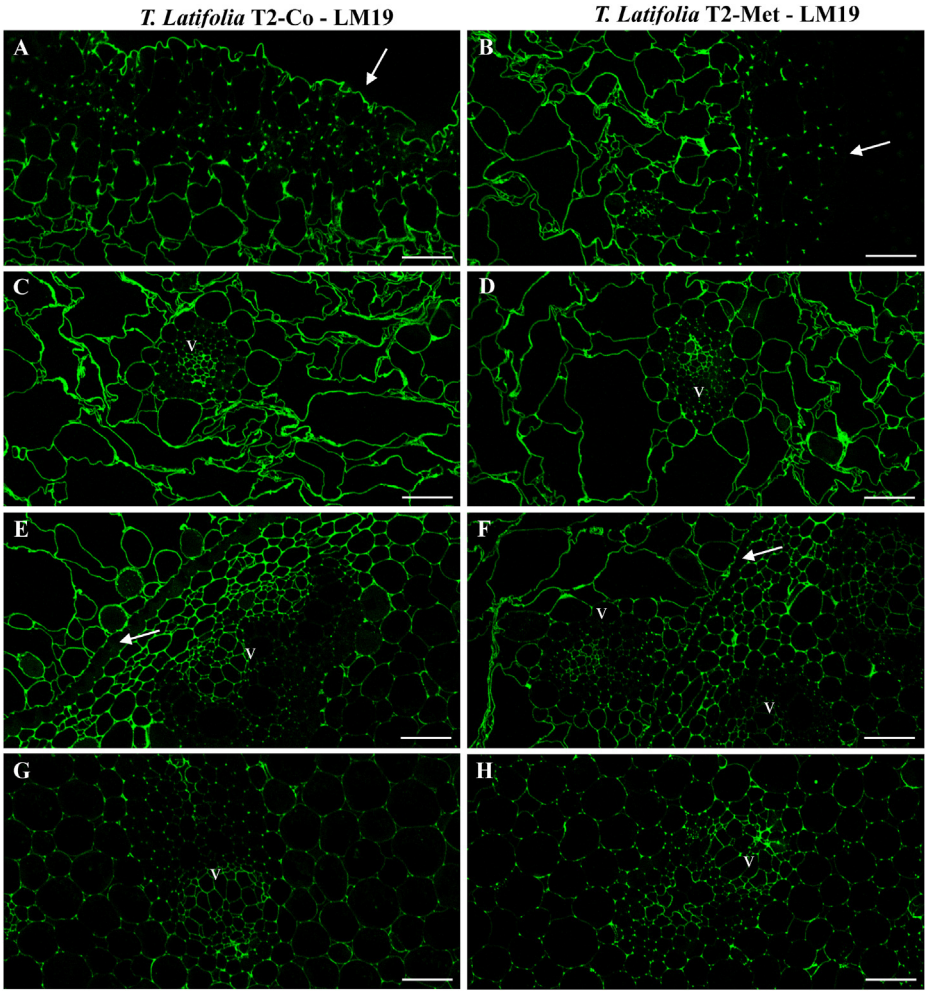

Fig. 4. Distribution of LEPs in T2-Co and T2-Met of *T. latifolia* rhizomes. (A, C, E, G) LEPs distribution appeared continuous (C). In the SP, LEPs appeared localized mostly at the cell wall corners (G). The same distribution at the corner wall was observed in the hypodermis (A). In the epidermis, LEPs decorated the outer cell wall (A; arrow). in the endoderm LEPs were nor detected (E; arrow). In vascular bundles (vb) pectins were distributed in the vascular and parenchymatic tissues and not in sclerenchyma. (B, D, F, H) In T2-Met, AP, SP and endoderm did not show relevant differences in LEPs with respect to control. The only modification of cell wall was observed in the epidermis where LEPs disappeared completely by the outer cell wall (B; arrows). Bar = 20 μm.

Although it is not possible to differentiate whether all or only one protein determined the increase in band 4 intensity, the molecular weight of pentatricopeptide repeat-containing protein was consistent with the band position in the gel (about 56 kDa). Cullin 3B and Lysine-specific demethylase JMJ125 proteins presented a lower molecular weight with respect to findings reported in the data bank.

4. Discussion

Animal production is a source of heavy metal contamination in the environment through the reuse of treated wastewaters for agricultural purposes. These waters contain substantial concentrations of metals, which are generally above the legal limits for irrigation. Innovative approaches are thus needed in order to make intensive livestock more sustainable.

Mechanisms based on tolerance and metal uptake/accumulation are species specific (Hasan et al., 2017; Kumar and Tivedi, 2016; Oves et al., 2016; Singh et al., 2016; Viehweger, 2014; Yadav, 2010). Through the integrated use of cell biological techniques, here we demonstrate that *T. palustris* and *T. latifolia,* deal in different ways with heavy metals with specific molecular responses.

4.1. Metal exposure induces alteration of T. palustris leaf ultrastructure and affects carbohydrate metabolism of both T. palustris and T. latifolia

Neither the leaf nor rhizome biomass of *T. palustris and T. latifolia,* were affected by the presence of metals (see accompayning paper, Hejna et al., 2019). Concerning *T. latifolia*, this result was expected since the Zn^{2+} and Cu^{2+} concentrations used in our experiment were below the tolerance thresholds identified by Manios et al. (2003).

In agreement with the lack of macroscopic alterations, no microscopic modifications occurred in the leaves of *T. latifolia* after 45 days of metal treatment. However, although symptomless in macroscopic morphology, *T. palustris* showed changes in mesophyll cell morphology. A similar cell shape to young T0 mesophyll leaf cells, was observed in *T. palustris* leaves after metal exposure (T2-Met), suggesting a delay in leaf cell differentiation. In bean (*Phaseolus vulgaris*), a low dose of heavy metals (Cd, Pb, Ni, Ti) was shown to induce a rejuvenating effect on leaves (Nyitrai et al., 2004). It was hypothesized that this process could be due to an increasing cytokinin concentration induced by low-dose stressors which generate a non-specific alarm reaction (Nyitrai et al., 2004).

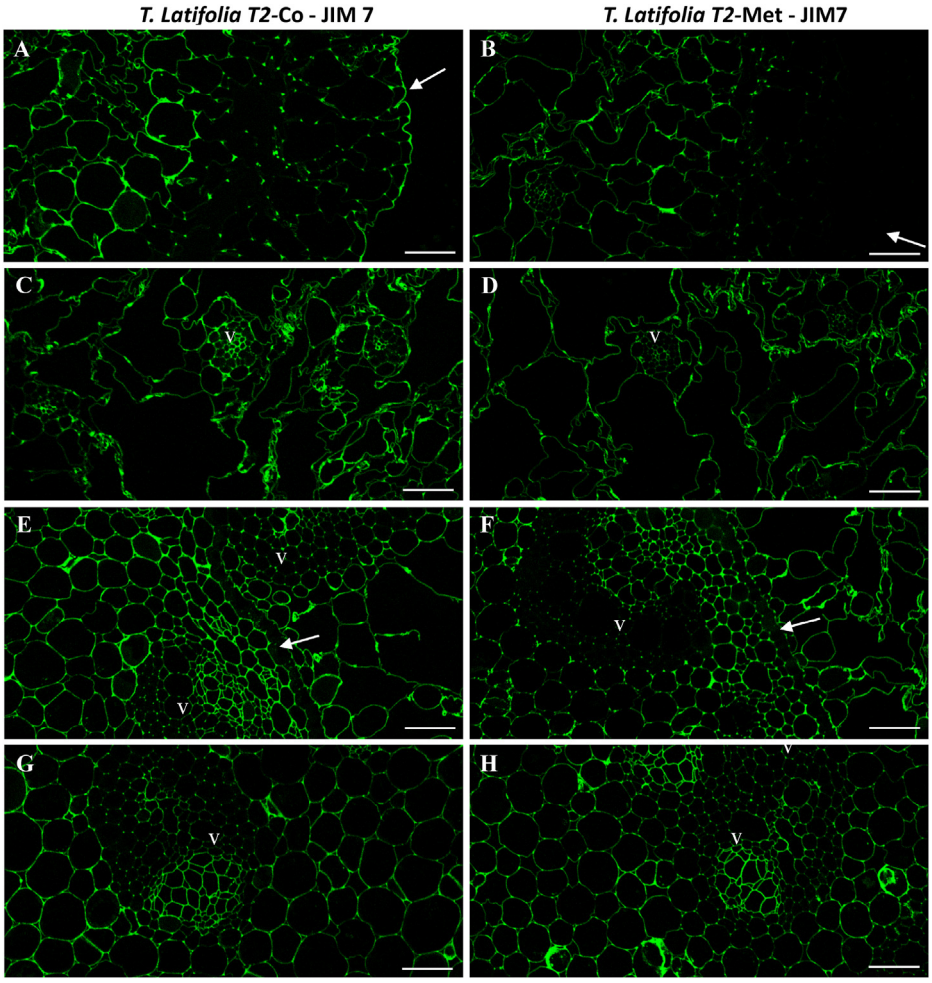

Fig. 5. Distribution of HEPs in T2-Co and T2-Met *T. latifolia* rhizomes. (A, C, E, G) HEPs distribution appeared discontinuous as they concentrated in small cell wall tracts (C). In the SP, HEPs were uniformly distributed in the cell wall (G). In the hypodermis HEPs were present at the corner of cell wall (A), while in the epidermis HEPs stained outer cell wall (A; arrow). In the endoderm no HEPs were detected (E; arrow). (B, D, F, H) Immunofluorescence by using JIM7 antibody in T2-Met showed that HEPs distribution was not altered in AP and SP with respect to T2-Co. On the contrary, HEPs disappeared from the epidermis and hypodermis cell wall (B; arrow). Bar = 20 μm.

In *T. palustris,* altered leaf cell shape was accompanied by an accumulation of starch grains which suggested a transformation of chloroplasts into amyloplasts.

All these data are supported by chemical analyses showing an increase in starch in the aerial organs (accompaying paper, Hejna et al., 2019). The accumulation of starch in the leaves could be due to changes in carbohydrate metabolism. In fact, in several plants, metal exposure causes a variation in photosynthetic process accompanied by significant alterations in plant biomass and leaf morphology/ultrastructure (Arif et al., 2016; Rufner and Barker, 1984; Stoláriková-Vaculíková et al., 2015; Todeschini et al., 2011). One of the mechanisms of metal tolerance has been shown to be the accumulation of metals in the ageing leaves (Małachowska-Jutsz and Gnida, 2015). The higher accumulation of amyloplasts in older with respect to younger leaves, also suggested that in *T. palustris,* such stress avoidance may occur. However, *T. palustris* did not show a decrease in biomass suggesting that, although chloroplasts were transformed into amyloplasts, the plants grew normally.

In most plants, high copper exposure disorganizes the chloroplast ultrastructure without starch accumulation (Maksymiec et al., 1996), while in screwbean mesquite, excess copper affects chloroplast development leading to starch accumulation in cotyledons (Zappala et al., 2014). However, this starch accumulation was induced by a much higher copper concentration (400 mg/L) than the one used in our model (8.63 mg/L). In addition, in detached bean leaves, a low-dose of Pb and Ni increased the starch content without significantly affecting photosynthetic activity (Nyitrai et al., 2004). In *T. palustris*, starch accumulation did not affect plant growth and did not induce discoloration or chlorosis in leaves.

An alternative hypothesis for the presence of amyloplasts in leaves could be due to a modification of carbohydrate translocation away from leaves. This hypothesis was supported by the decrease in starch granules in the rhizomes in treated plants with respect to the control, as also confirmed by chemical analyses (see accompayning paper, Hejna et al., 2019). In screwbean mesquite, the increase in copper was accompanied by a decrease in potassium concentration (Zappala et al., 2014). Interestingly, the alteration of Na and K homeostasis, disturbed phloem loading and translocation, leading to an accumulation of starch in Arabidopsis leaves (Tian et al., 2010). Further experiments would be necessary to better clarify this point in *T. palustris*.

In *T. latifolia*, no differences were observed in the leaves of T2-Met with respect to T2-Co plants. However, the starch accumulation in rhizome decreased, as also confirmed by chemical analyses (see accompayning paper, Hejna et al., 2019). Unlike *T. palustris*, the starch reduction could be due to different mechanisms not involving phloem translocation and loading. In *Cucurbita pepo,* a

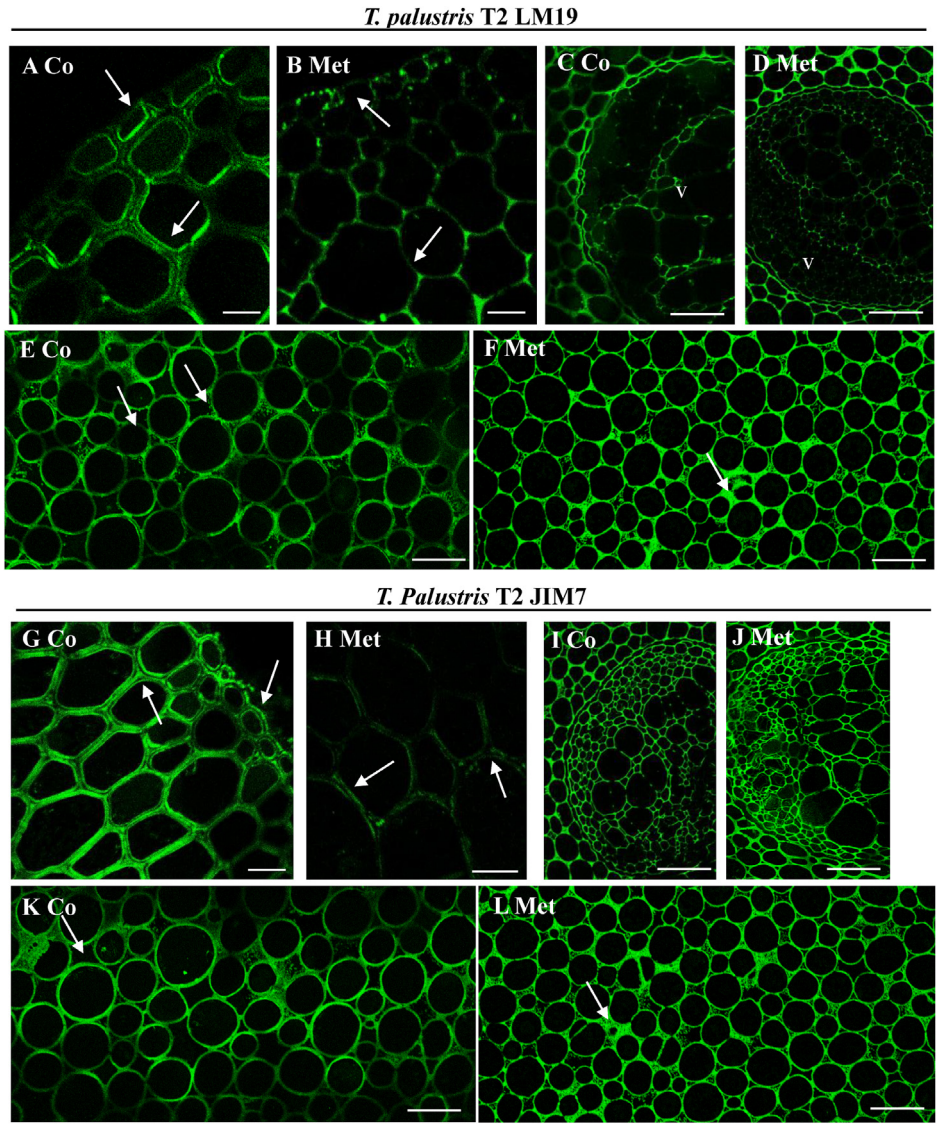

Fig. 6. Distribution of LEPs and HEPs in T2-Co and T2-Met of *T palustris* rhizomes. (A, C, E) LEPs were distributed in the cell wall of parenchyma and in the parenchymatic cells inside the vascular bundles. In the epidermis and cortex LEPs localized in the inner layer of the primary cell wall and in the middle lamella (A; arrow). LEPs appeared uniformly distributed in the cell wall of pith cells and in parenchymatic cells surrounding xylem (C; arrows; vb: vascular bundle). The middle lamella was reabsorbed in the corners among cells (E; arrows). (B, D, F) In T2-Met rhizomes LM19 stained only the middle lamella (B; arrows). In pith cells, LEPs localized in the corner among the cells, with a reduction of intercellular spaces (F; arrows). In vascular bundles the staining was similar to Co (D). (G, I, H) In T2-Co cortical cells HEPs were distributed in the inner layer of primary cell wall and in the middle lamella (A; arrows). In pith cells HEPs were uniformly distributed in the cell wall, excluding the corners, filled by intracellular spaces (K). In vascular bundles all the cells showed a uniform HEPs distribution (I; vb). (H, J, L) In T2-Met rhizomes HEPs disappeared from the middle lamella, so only the inner layer of primary cell wall was stained by JIM7 antibody (H; arrows). In the pith, HEPs persisted in the corners among cells, so reducing the extent of intercellular spaces (L; arrow), while they maintain a uniform distribution inside the vascular bundle (J; vb). Bars: (C–F, I-L) = 20 μm; (A, B; C, H) = 10 μm.

higher Zn^{2+} concentration was correlated with an increase in soluble sugars and a decrease in starch in roots and shoots (Ialelou et al., 2013). The increase in soluble sugars in stressed plants is considered to be important for preserving biological molecules and membranes (Gibson, 2005). In addition, although direct evidence of the effect of high Zn^{2+} concentration on the starch synthesis enzymes was lacking, zinc deficiency has been found to reduce the starch synthase activity (Ialelou et al., 2013). Further analyses could clarify whether the same inhibitory effect on starch synthesis enzymes also occur at high metal concentrations.

In *T. latifolia* and *T. palustris*, rhizome carbohydrate metabolism alterations therefore appeared to be caused by different mechanisms.

Although the carbohydrate metabolism was different in the control and metal treated cells, proteomic analysis did not show alterations in the polypeptides involved in carbohydrate metabolism or translocation. In addition, *T. palustris*, which changed above all in leaf morphology after metal exposure, did not show differences in the polypeptide profile in 1D-gel electrophoresis.

4.2. Cell wall remodeling in rhizomes was related to metal exposure of T. latifolia and T. palustris

In plants that accumulate metals, there are various strategies to prevent toxicity. One strategy is sequestration into extracytoplasmic compartments such as the cell wall. Cell wall polysaccharides play a major role in binding and accumulating metals in order to remove them from protoplasts (Jiang and Wang, 2008; Le

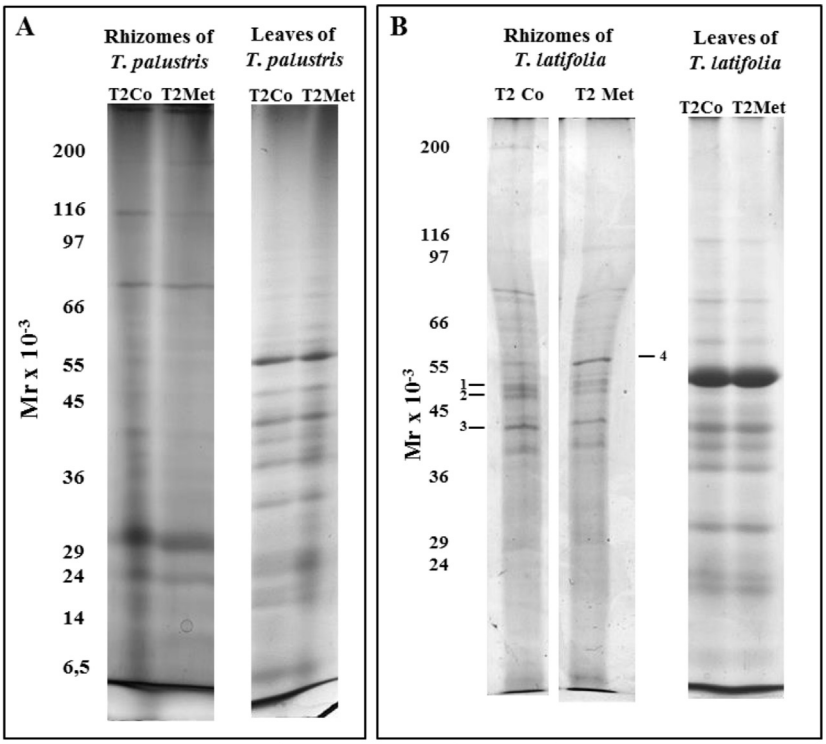

Band	Protein description	Accession number	Database	Mascot search results			Organism
				Score	Sequence coverage (%)	N. of matched peptides	
1	Tubulin beta-2 chain	TBB2_SOYBN	SwissProt	174	47	24/65	*Glycine max*
2	Tubulin alpha chain	TBA_DAUCA	SwissProt	203	46	20/40	*Daucus carota*
3	Actin-104 (Fragment)	ACT7_TOBAC	SwissProt	156	56	18/65	*Nicotiana tabacum*
4	Cullin-3B Lysine-specific demethylase JMJ25 Pentatricopeptide repeat-containing protein At2g36730	CUL3B_ARATH JMJ25_ARATH PP188_ARATH	SwissProt	98 61 58	31 26 34	28/114 23/114 15/114	*Arabidopsis thaliana*

Fig. 7. One-dimensional gel electrophoresis and mass spectrometry. (A) Electrophoretic profile of *T. palustris* T2-Co and T2-Met rhizome and leaves extracts. (B) Electrophoretic profile of *T. latifolia* T2-Co and T2-Met rhizome and leaves extracts. 20 μg of protein was loaded in each lane. (C) Proteins differentially expressed in T2-Co and T2-Met T. latifolia rhizomes.

Gall et al., 2015). In different plant phytoremediation models, metal exposure induces a thickening of the cell wall and pectin remodeling by modulating the degree of melthylesterification, thus affecting the ability of the cell wall to bind metals (Dronnet et al., 1996; Eticha et al., 2005; Krzeslowska, 2011; Le Gall et al., 2015). Previous studies have shown that Cu^{2+} and Zn^{2+} have a high affinity for low esterified pectins and replace Ca^{2+} ions in the pectin matrices (Dronnet et al., 1996). Metal exposure has been found to enhance cellulose, hemicellulose and pectin content in the cell walls and induce the up-regulation of CesA and XTH genes (Gao et al., 2013; Liu et al., 2014).

Unlike most plants used for phytoremediation, *T. latifolia* and *T. palustris* showed a significant reduction in cell wall thickening in rhizomes after metal exposure. This cell wall thinning could be associated with a dysfunction of cytoskeleton due, for instance, to a MT reduction as that observed in *T. latifolia* rhizomes after metal exposure. Microtubules (MTs) and actin filaments (AFs) were found to be involved in secretion processes necessary for plant cell wall building. Pectin, hemicellulose and cellulose synthase complex (CSC) were transported to and out of PM by Golgi-derived secretory vesicles. Both AFs and MTs play an important role in membrane trafficking and in the proper positioning of secretory vesicles carrying cell wall components (Gutierrez et al., 2009; Kim and Brandizzi, 2014; Onelli et al., 2015). The decrease in tubulin and actin revealed by electrophoretic analyses could be responsible for the thinning of the cell wall in *T. latifolia* rhizome parenchymatic cells.

It has been reported that cytoskeleton is affected by Zn^{2+} and Cu^{2+}: MTs and AFs can be targets of the metals, which leads to a disturbance of the organization and dynamics of cytoskeletal structures in the cells (Eagle et al., 1983; Gaskin and Kress, 1977; Horiunova, and Yemets, 2015; Kulikova et al., 2009). Both MTs and AFs are sensitive to Cu^{2+}, while Zn^{2+} only affects MTs: approximately 60 potential binding sites of tubulin with Zn^{2+} have been described (Horiunova et al., 2016).

Secretion is also important for the presence of pectin remodeling enzymes such as pectin methylesterase. In plants, during maturation in Golgi cisternae, pectins have been shown (Li et al.,

2002) to be high-methylesterified and secreted in this form by secretory vesicles. In the cell wall, pectin methylesterases could de-esterify pectins, allowing pectins to bind Ca^{2+} or other metals. The increase in LEPs was an important mechanism for metal tolerance (Eticha et al., 2005; Le Gall et al., 2015). In *T. latifolia* and *T. palustris* rhizomes, as expected the analyses of LEPs and HEPs revealed by the use of LM19 and JIM7 antibodies respectively, did not show an increase in LEPs concomitant with a decrease in HEPs.

In *T. latifolia*, the distribution of both pectins in the cell wall was similar in the control and metal treated samples in the inner tissues, while pectins disappeared completely from the outer epidermis cell wall. This slight effect of metal exposure on the extent of methyl esterification of pectins was probably due to the lower metal concentration in the water. Furthermore, in *T. latifolia* rhizomes, the reduction in cell wall thickness was also observed in the endodermis cells between AP and SP. Abiotic stresses induce suberin accumulation in the root endodermal cell wall (Andersen et al., 2015). The presence of suberin in the Casparian band was important to select the uptake of nutrients and to exclude potential phytotoxic compounds. The increase in endodermal cell wall suberification represents a physical barrier against the entry of metals into the symplastic compartment. Again, *T. latifolia* showed a different reaction, since in the endodermis, cell walls were thinner than the control. Presumably, suberin was still deposited in the cell wall, since the endodermis was never stained by antibodies against LEPs and HEPs.

T. palustris had a different distribution of HEPs and LEPs in the walls of parenchymatic cells. After metal treatment, HEPs were located in the inner part of the cell wall, while LEPs remained only in the middle lamellae. In addition, both LEPs and HEPs remained in the corner of the cells, which in control rhizomes were replaced by intercellular spaces. These data suggest that the cell wall remodeling was different after metal exposure with respect to the control, although no polypeptide modifications were revealed by 1D-gel electrophoresis. Modification of pectins cannot be explained by the need to bind excess metal ions to prevent their entry in the symplast, suggesting that these modifications are not part of a tolerance mechanism. Further analyses could better define the processes affected by the metal exposure which induced modifications of the cell wall in *T. palustris* rhizome.

In *T. latifolia*, proteomic analyses of polypeptides in 1D gel electrophoresis showed an increase in a band (band 4) containing three different proteins: cullin 3B; lysine-specific demethylase JMJ125 and pentatricopeptide repeat-containing protein. Pentatricopeptide repeat-containing protein is the only polypeptide with a molecular mass that is in line with the molecular weight of this band. It belongs to a superfamily of proteins involved in RNA editing, RNA stabilization, RNA cleavage, translational activation and RNA splicing in nuclei, chloroplast and mitochondria (Barkan and Small, 2014; Manna, 2015). This protein was shown to be involved in RNA modification in chloroplasts. A subclass of these proteins contains a domain with zinc-binding capabilities (Boussardon et. al 2014; Hayes et al., 2013). In *T. latifolia,* these proteins may perhaps have been susceptible to the Zn^{2+} concentrations used in our system. However, the modification of the content of this protein did not affect plant morphology or growth.

5. Conclusions

Typha. latifolia and *T. palustris* were able to grow and to significantly reduce the amount of Zn^{2+} and Cu^{2+} which are the main outputs of heavy metal from intensive livestock production. Metal concentrations which are fourteen times higher than Italian legal limits, were however too low to induce macroscopic morphological modifications in either of the plants. At these metal concentrations, which are in the range found in wastewaters generally used for field irrigation, both plants were successful in phytoremediation thanks to their capacity to accumulate metals within the rhizome and leaves. Our chemical analyses highlight that the two plants could be used in series to refine wastewater. However, although metal concentrations are below the toxicity limit already reported for *T. latifolia* (Klink, 2017), some tissue morphology alterations were observed in the rhizomes and leaves of both plants.

T. palustris and *T. latifolia* respond differently to the overall effect of the metals and show different cellular and biochemical characteristics, suggesting a different degree of tolerance. *T. palustris* was more sensitive than *T. latifolia*, since the modification in both the leaf and rhizome cells (cell shape, cell wall thickness and pectin distribution) and carbohydrate metabolism indicate that the marsh fern was affected the most by the presence of the two metals.

The early uptake of the metals in *T. palustris* revealed by chemical analyses (see the accompayning paper: Hejna et al., 2019) probably exposes the plants to metals for a longer period than *T. latifolia*. In fact, the accumulation of a large amount of Cu^{2+} and Zn^{2+} led to a slight toxic effect which was revealed by morphological observations without affecting plant growth.

However, it is interesting that the amount of metals in the marsh fern tissues were always higher than *T. latifolia*, also considering the increase in biomass from T0 to T2. It is possible that higher concentrations of metals or longer exposure times may cause macroscopical damage in the plants. Thus, in *T. palustris* the metal effects appeared to be due to a slight toxicity. On the other hand, in *T. latifolia*, changes in carbohydrate metabolism appeared to be part of a tolerance mechanism, while cell wall modifications are ascribable to a metal toxic effect.

In conclusion, although further analyses are needed to clarify whether some of the morphological and biochemical alterations are due to a toxic metal effect or are part of tolerance mechanisms, the data presented suggest that *T. latifolia* showed a higher tolerance to metals than *T. palustris* and seems to be more suitable for the long-term phytodepuration of livestock wastewaters, in series with marsh ferns.

We believe that our data also provide new insights into mechanisms that have evolved in plants and that belong to different evolutionary groups, in response to the presence of heavy metals in the environment.

Funding

This study was funded by the Italian Agricultural Ministry (MIPAAF grant - LOW METAL ID60, Italy).

Acknowledgment

We are very grateful to Prof. Sandra Citterio for the critical reading of the paper, Dr Enrico Sala and Valerio Parravicini for the wetland system building and for taking care of *Typha latifolia* and *Theliypteris palustris* plants. We tank also Prof. Marco Caccianiga for the helpful suggestion on wetland system management.

Appendix A. Supplementary data

Supplementary data to this article can be found online at https://doi.org/10.1016/j.chemosphere.2019.124915.

Author contributions

Conceptualization: Moscatelli A. Rossi L.; Data curation: Moscatelli A., Stroppa N., Onelli E.; Funding acquisition: Moscatelli A. Rossi L.; Methodology: Onelli E., Stroppa N., Gagliardi A., Bini L.;

Project administration: A. Moscatelli, Supervision: A. Moscatelli; Validation: E. Onelli, L. Rossi; Writing ± original draft: E. Onelli, A, Moscatelli; Editing: M. Hejna, L. Rossi.

References

Almeida, C.M.R., Santos, F., Ferreira, A.C., Gomes, C.R., Basto, M.C., Mucha, A.P., 2016. Constructed wetlands for the removal of metals from livestock wastewater - can the presence of veterinary antibiotics affect removals? Ecotoxicol. Environ. Saf. 137, 143–148. https://doi.org/10.1016/j.ecoenv.2016.11.021.

Andersen, T.G., Barberon, M., Geldner, N., 2015. Suberization - the second life of an endodermal cell. Curr. Opin. Plant Biol. 28, 9–15. https://doi.org/10.1016/j.pbi.2015.08.004.

Anning, A.K., Korsah, P.E., Addo-Fordjour, P., 2013. Phytoremediation of wastewater with *Limnocharis flava, Thalia geniculata* and *Typha latifolia* in constructed wetlands. Int. J. Phytoremediation 15, 452–464. https://doi.org/10.1080/15226514.2012.716098.

Arif, N., Yadav, V., Singh, S., Singh, S., Ahmad, P., Mishra, R.K., Sharma, S., Tripathi, D.K., Dubey, N.K., Chauhan, D.K., 2016. Influence of high and low levels of plant-beneficial heavy metal ions on plant growth and development. Front. Environ. Sci. 4, 69. https://doi.org/10.3389/fenvs.2016.00069.

Barkan, A., Small, I., 2014. Pentatricopeptide repeat proteins in plants. Annu. Rev. Plant Biol. 65, 415–442. https://doi.org/10.1146/annurev-arplant-050213-040159.

Boussardon, C., Avon, A., Kindgren, P., Bond, C.S., Challenor, M., Lurin, C., Small, I., 2014. The cytidine deaminase signature HxE (x) nCxxC of DYW1 binds zinc and is necessary for RNA editing of ndhD-1. New Phytol. 203, 1090–1095. https://doi.org/10.1111/nph.12928.

Bradford, M.M., 1976. A rapid and sensitive method for the quantitation of microgram quantities of protein utilizing the principle of protein-dye binding. Annal. Biochem. 72, 248–254. https://doi.org/10.1016/0003-2697(76)90527-3.

Collin, V.C., Eymery, F., Genty, B., Rey, P., Havaux, M., 2008. Vitamin E is essential for the tolerance of *Arabidopsis thaliana* to metal-induced oxidative stress. Plant Cell Environ. 31, 244–257. https://doi.org/10.1111/j.1365-3040.2007.01755.x.

Colzi, I., Arnetoli, M., Gallo, A., Doumett, S., Del Bubba, M., Pignattelli, S., Gabbrielli, R., Gonnelli, C., 2012. Copper tolerance strategies involving the root cell wall pectins in *Silene paradoxa* L. Environ. Exp. Bot. 78, 91–98. https://doi.org/10.1016/j.envexpbot.2011.12.028.

Doğanlar, Z.B., 2013. Metal accumulation and physiological responses induced by copper and cadmium in *Lemna gibba, L. minor* and *Spirodelan polyrhiza*. Chem. Speciat. Bioavailab. 25, 79–88. https://doi.org/10.3184/095422913X13706128469701.

Dronnet, V.M., Renard, C.M.G.C., Axelos, M.A.V., Thibault, J.F., 1996. Heavy metal binding by pectins: selectivity, quantification and characterization. Carbohydr. Polym. 30, 253–263. https://doi.org/10.1016/S0921-0423(96)80283-8.

Dubey, S., Shri, M., Misra, P., Lakhwani, D., Bag, S.K., Asif, M.H., Trivedi, P.K., Tripathi, R.D., Chakrabarty, D., 2014. Heavy metals induce oxidative stress and genome-wide modulation in transcriptome of rice root. Funct. Integr. Genom. 14, 401–417. https://doi.org/10.1007/s10142-014-0361-8.

Eagle, G.R., Zombola, R.R., Himes, R.H., 1983. Tubulin–zinc interactions: binding and polymerization studies. BMC Biochem. 22, 221–228. https://doi.org/10.1021/bi00270a032.

Eticha, D., Stass, A., Horst, W.J., 2005. Cell-wall pectin and its degree of methylation in the maize root apex: significance for genotypic differences in aluminium resistance. Plant Cell Environ. 28, 1410–1420. https://doi.org/10.1111/j.1365-3040.2005.01375.x.

Fediuc, E., Erdei, L., 2002. Physiological and biochemical aspects of cadmium toxicity and protective mechanisms induced in *Phragmites australis* and *Typha latifolia*. J. Plant Physiol. 159, 265–271. https://doi.org/10.1078/0176-1617-00639.

Gao, J., Sun, L., Yang, X., Liu, J.X., 2013. Transcriptomic analysis of cadmium stress response in the heavy metal hyperaccumulator *Sedum alfredii* Hance. PLoS One 8, e64643. https://doi.org/10.1371/journal.pone.0064643.

Gaskin, F., Kress, Y., 1977. Zinc ion induced assembly of tubulin. J. Biol. Chem. 252, 6918–6924.

Gibson, S., 2005. Control of plant development and gene expression by sugar signaling. J. Plant Biol. 8, 93–102. https://doi.org/10.1016/j.pbi.2004.11.003.

Gutierrez, R., Lindeboom, J.J., Paredez, A.R., Emons, A.M., Ehrhardt, D.W., 2009. Arabidopsis cortical microtubules position cellulose synthase delivery to the plasma membrane and interact with cellulose synthase trafficking compartments. Nat. Cell Biol. 11, 797–806. https://doi.org/10.1038/ncb1886.

Hasan, K., Cheng, Y., Kanwar, M.K., Chu, X.Y., Ahammed, G.J., Qi, Z.Y., 2017. Responses of plant proteins to heavy metal stress - a review. Front. Plant Sci. https://doi.org/10.3389/fpls.2017.01492.

Hayes, M.L., Giang, K., Berhane, B., Mulligan, R.M., 2013. Identification of two pentatricopeptide repeat genes required for RNA editing and zinc binding by C terminal cytidine deaminase-like domains. J. Biol. Chem. 288, 36519–36529. https://doi.org/10.1074/jbc.M113.485755.

Hellman, U., Wernstedt, C., Gonez, J., Heldin, C.H., 1995. Improvement of an "In-Gel" digestion procedure for the micropreparation of internal protein fragments for amino acid sequencing. Anal. Biochem. 224, 451–455. https://doi.org/10.1006/abio.1995.1070.

Hejna, M., Moscatelli, A., Stroppa, N., Onelli, E., Pilu, S., Baldi, A., Rossi, L., 2019. Bioaccumulation of Heavy Metals from Wastewater through *Typha Latifolia* and *Thelypteris palustris* Phytoremediation System. https://doi.org/10.1016/j.chemosphere.2019.125018. Submitted on the 19th of July to Chemosphere, Manuscript Number: CHEM64390.

Higuchi, K., Kanai, M., Tsuchiya, M., Ishii, H., Shibuya, N., Fujita, N., Nakamura, Y., Suzui, N., Fujimaki, S., Miwa, E., 2015. Common reed accumulates starch in its stem by metabolic adaptation under Cd stress conditions. Front. Plant Sci. 6, 138. https://doi.org/10.3389/fpls.2015.00138.

Horiunova, I.I., Yemets, A.I., 2015. Effect copper on actin filaments organization in Arabidopsis thaliana root cells. Fakt. Eksp. Evol. Organ. 16, 41–45.

Horiunova, I.I., Krasylenko, Y.A., Yemets, A.I., Blume, Y.B., 2016. Involvement of plant cytoskeleton in cellular mechanisms of metal toxicity. Cytol. Genet. 50, 47–59. https://doi.org/10.3103/S0095452716010060.

Ialelou, F.S., Shafagh-Kolvanagh, J., Fateh, M., 2013. Effect of various concentrations of zinc on chlorophyll, starch, soluble sugars and proline in Naked pumpkin (*Cucurbita pepo*). Int. J. Farm. Allied Sci. 24, 1198–1202. https://doi.org/10.12692/ijb/4.10.6-12.

Jiang, X., Wang, C., 2008. Zinc distribution and zinc-binding forms in *Phragmites australis* under zinc pollution. J. Plant Physiol. 165, 697–704. https://doi.org/10.1016/j.jplph.2007.05.011.

Kim, S.J., Brandizzi, F., 2014. The plant secretory pathway: an essential factory for building the plant cell wall. Plant Cell Physiol. 55, 687–693. https://doi.org/10.1093/pcp/pct197.

Klink, A., 2017. A comparison of trace metal bioaccumulation and distribution in *Typha latifolia* and *Phragmites australis*: implication for phytoremediation. Environ. Sci. Pollut. Res. Int. 24, 3843–3852. https://doi.org/10.1007/s11356-016-8135-6.

Klink, A., Maciol, A., Wislocka, M., Krawczyk, J., 2013. Metal accumulation and distribution in the ogans of Typha latifolia L. (cattail) and their potential use in bioindication. Limnologica 43, 164–168. https://doi.org/10.1016/j.limno.2012.08.012.

Krzeslowska, M., 2011. The wall cell in plant cell response to trace metals: polysaccharide remodeling and its role in defense strategy. Acta Physiol. Plant. 33, 35–51. https://doi.org/10.1007/s11738-010-0581-z.

Kulikova, A.L., Kholodova, V.P., Kuznetsov, V.V., 2009. Actin is involved in early plant responses to heavy metal stress and associates with molecular chaperons in stress environments. Russ. J. Rep. Dev. Biol. Sci. 424, 49–52. https://doi.org/10.1134/S0012496609010153.

Kumar, S., Trivedi, P.K., 2016. Heavy metal stress signaling in plants. In: Ahmad, P. (Ed.), Plant Metal Interaction- Emerging Remediation Techniques. Amsterdan: Elsevier, pp. 58–603. https://doi.org/10.1016/B978-0-12-803158-2.00025-4.

Laemmli, U.K., 1970. Cleavage of structural proteins during the assembly of the head of bacteriophage T4. Nature 227, 680–685. https://doi.org/10.1038/227680a0.

Le Gall, H., Philippe, F., Domon, J.M., Gillet, F., Pelloux, J., Rayon, C., 2015. Cell wall metabolism in response to abiotic stress. Plants 4, 112–166. https://doi.org/10.3390/plants4010112.

Li, Y.-Q., Mareck, A., Faleri, C., Moscatelli, A., Liu, Q., Cresti, M., 2002. Detection and localization of pectin methyl esterase isoforms in pollen tubes of *Nicotiana tabacum* L. Planta 214, 734–740.

Lingua, G., Bona, E., Todeschini, V., Cattaneo, C., Marsano, F., Berta, G., Cavaletto, M., 2012. Effects of heavy metals and arbuscular mycorrhiza on the leaf proteome of a selected poplar clone: a time course analysis. PLoS One 7, e38662. https://doi.org/10.1371/journal.pone.0038662.

Liu, T., Shen, C., Wang, Y., Huang, C., Shi, J., 2014. New insights into regulation of proteome and polysaccharide in cell wall of *Elsholtzia splendens* in response to copper stress. PLoS One 9, e109573. https://doi.org/10.1371/journal.pone.0109573.

Liu, Y., Espinosa, C.D., Abelilla, J.J., Casas, G.A., Lagos, L.V., Lee, S.A., Kwon, W.B., Mathai, J.K., Navarro, D.M.D.L., Jaworski, N.W., Stein, H.H., 2018. Non-antibiotic feed additives in diets for pigs: a review. Anim. Nutr. 4, 113–125. https://doi.org/10.1016/j.aninu.2018.01.007.

Maksymiec, W., Bednara, J., Baszynski, T., 1996. Different susceptibility of runner bean plants to excess copper as a function of the growth stages of primary leaves. J. Plant Physiol. 149, 217–221. https://doi.org/10.1016/S0176-1617(96)80198-2.

Małachowska-Jutsz, A., Gnida, A., 2015. Mechanisms of stress avoidance and tolerance by plants used in phytoremediation of heavy metals. Arch. Environ. Prot. 41, 104–114. https://doi.org/10.1515/aep-2015-0045.

Manios, T., Stentiford, E.I., Millner, P.A., 2003. The effect of heavy metals accumulation on the chlorophyll concentration of *Typha latifolia* plants, growing in a substrate containing sewage sludge compost and watered with metaliferus water. J. Ecolo. Eng. 20, 65–74. https://doi.org/10.1016/S0925-8574(03)00004-1.

Manna, S., 2015. An overview of pentatricopeptide repeat proteins and their applications. Biochimie 113, 93–99. https://doi.org/10.1016/j.biochi.2015.04.004.

McManus, H.A., Seago, J.L., Marsh, L.C., 2002. Epifluorescent and histochemical aspects of shoot anatomy of *Typha latifolia* L., *Typha angustifolia* L. and *Typha glauca*, Godr. Ann. Bot. 90, 489–493. https://doi.org/10.1093/aob/mcf211.

Meier, S., Alvear, M., Borie, F., Aguilera, P., Ginocchio, R., Cornejo, P., 2012. Influence of copper on root exudate patterns in some metallophytes and agricultural plants. Ecotoxicol. Environ. Saf. 75, 8–15. https://doi.org/10.1016/j.ecoenv.2011.08.029.

Molas, J., 2002. Changes of chloroplast ultrastructure and total chlorophyll concentration in cabbage leaves caused by excess of organic Ni(II) complexes. Environ. Exp. Bot. 47, 115–126. https://doi.org/10.1016/S0098-8472(01)00116-2.

Nicholson, F.A., Smith, S.R., Allowayc, B.J., Carlton-Smithd, C., Chambersa, B.J., 2003.

An inventory of heavy metals inputs to agricultural soils in England and Wales. Sci. Total Environ. 311, 205–219. https://doi.org/10.1016/S0048-9697(03)00139-6.
Nyitrai, P., Bóka, K., Gáspár, L., Sárvári, E., Keresztes, A., 2004. Rejuvenation of ageing bean leaves under the effect of low-dose stressors. Plant Biol. 6, 708–714. https://doi.org/10.1055/s-2004-830385.
Onelli, E., Idilli, A.I., Moscatelli, A., 2015. Emerging role for microtubules in angiosperm pollen tube growth highlight new research cues. Front. Plant Sci. 10, 51. https://doi.org/10.3389/fpls.2015.00051.
Oves, M., Saghir Khan, M., Huda Qari, A., Nadeen Felemban, M., Almeelbi, T., 2016. Heavy metals: biological importance and detoxification strategies. J. Biorem. Biodegrad. 7, 334. https://doi.org/10.4172/2155-6199.1000334.
Peterson, H.G., 1998. Use of constructed wetlands to process agricultural wastewater. Can. J. Plant Sci. 78, 199–210. https://doi.org/10.4141/P97-142.
Petraglia, A., De Benedictis, M., Degola, F., Pastore, G., Calcagno, M., Ruotolo, R., Mengoni, A., Sanità di Toppi, L., 2014. The capability to synthesize phytochelatins and the presence of constitutive and functional phytochelatin synthases are ancestral (plesiomorphic) characters for basal land plants. J. Exp. Bot. 65, 1153–1163. https://doi.org/10.1093/jxb/ert472.
Rao, K.P., Vani, G., Kumar, K., Wankhede, D.P., Misra, M., Gupta, M., Sinha, A.K., 2011. Arsenic stress activates MAP kinase in rice roots and leaves. Arch. Biochem. Biophys. 506, 73–82. https://doi.org/10.1016/j.abb.2010.11.006.
Rufner, R., Barker, A.V., 1984. Ultrastructure of zinc induced iron deficiency in mesophyll chloroplasts of spinach and tomato. J. Am. Soc. Hortic. Sci. 109, 164–168.
Sandalio, L.M., Dalura, H.C., Gomez, M., Romero-Puertas, M.C., Rio, L.A., 2001. Cadmium induced changes in the growth and oxidative metabolism of pea plants. J. Exp. Bot. 52, 2115–2126. https://doi.org/10.1093/jexbot/52.364.2115.
Singh, S., Parihar, P., Singh, R., Singh, V.P., Prasad, S.M., 2016. Heavy metal tolerance in plants: role of transcriptomics, proteomics, metabolomics, and ionomics. Front. Plant Sci. 6, 1143. https://doi.org/10.3389/fpls.2015.01143.
Sinha, P., Poland, J., Schnolzer, M., Rabilloud, T., 2001. A new silver staining apparatus and procedure for matrix-assisted laser desorption/ionization-time of flight analysis of proteins after two-dimensional electrophoresis. Proteomics 1, 835–840. https://doi.org/10.1002/1615-9861.
Soskic, V., Görlach, M., Poznanovic, S., Boehmer, F.D., Godovac Zimmermann, J., 1999. Functional proteomics analysis of signal transduction pathways of the platelet-derived growth factor beta receptor. Biochemistry 38, 1757–1764. https://doi.org/10.1021/bi982093r.
Stoláriková-Vaculíková, M., Romeo, S., Minnocci, A., Luxová, M., Vaculík, M., Lux, A., Sebastiani, L., 2015. Anatomical, biochemical and morphological responses of poplar *Populus deltoides* clone Lux to Zn excess. Environ. Exp. Bot. 109, 235–243. https://doi.org/10.1016/j.envexpbot.2014.07.001.
Tian, H., Baxter, I.R., Lahner, B., Reinders, A., Salt, D.E., Ward, J.M., 2010. Arabidopsis NPCC6/NaKR1 is a phloem mobile metal binding protein necessary for phloem function and root meristem maintenance. Plant Cell 22, 3963–3979. https://doi.org/10.1105/tpc.110.080010.
Tiwari, S., Lata, C., 2018. Heavy Metal stress, signaling, and tolerance due to plant-associated microbes: an overview. Front. Plant Sci. 9, 452. https://doi.org/10.3389/fpls.2018.00452.
Todeschini, V., Lingua, G., D'Agostino, G., Carniato, F., Roccotiello, E., Berta, G., 2011. Effects of high zinc concentration on poplar leaves: a morphological and biochemical study. Environ. Exp. Bot. 71, 50. https://doi.org/10.1016/j.envexpbot.2010.10.018.
Viehweger, K., 2014. How plants cope with heavy metals. Bot. Stud. 55, 35. https://doi.org/10.1186/1999-3110-55-35.
Yadav, S.K., 2010. Heavy metals toxicity in plants: an overview on the role of glutathione and phytochelatins in heavy metal stress tolerance of plants. South Afr. J. Bot. 76, 167–179. https://doi.org/10.1016/j.sajb.2009.10.007.
Yang, J., Ye, Z., 2009. Metal accumulation and tolerance in wetland plants. Front. Biol. China 4, 282–288. https://doi.org/10.1007/s11515-009-0024-7.
Yang, Y.Y., Jung, J.Y., Song, W.Y., Suh, H.S., Lee, Y., 2000. Identification of rice varieties with high tolerance or sensitivity to lead and characterization of the mechanism of tolerance. Plant Physiol. 124, 1019–1026. https://doi.org/10.1104/pp.124.3.1019.
Zappala, M.N., Ellzey, J.T., Bader, J., Peralta-Videa, J.R., Gardea-Torresdey, J., 2014. Effects of copper sulfate on seedlings of *Prosopis pubescens* (screwbean mesquite). Int. J. Phytoremediation 16, 1031–1041. https://doi.org/10.1080/15226514.2013.810582.

Chemosphere 241 (2020) 125018

Contents lists available at ScienceDirect

Chemosphere

journal homepage: www.elsevier.com/locate/chemosphere

Bioaccumulation of heavy metals from wastewater through a *Typha latifolia* and *Thelypteris palustris* phytoremediation system

Monika Hejna [a, *], Alessandra Moscatelli [b], Nadia Stroppa [b], Elisabetta Onelli [b], Salvatore Pilu [c], Antonella Baldi [a], Luciana Rossi [a]

[a] Department of Health, Animal Science and Food Safety, Università degli Studi di Milano, via Trentacoste 2, 20134, Milan, Italy
[b] Department of Biosciences, Università degli Studi di Milano, via Celoria 26, 20133, Milan, Italy
[c] Department of Agricultural and Environmental Sciences – Production, Land, Agroenergy, Università degli Studi di Milano, via Celoria 2, 20133, Milan, Italy

HIGHLIGHTS

- The increasing biomass showed that *T. latifolia* and *T. palustris* grew normally.
- The increase of Zn and Cu in plants was related by a decrease of metals in water.
- Both plants are able to phytoremediate Zn and Cu from contaminated wastewater.

ARTICLE INFO

Article history:
Received 19 July 2019
Received in revised form
28 September 2019
Accepted 29 September 2019
Available online 11 October 2019

Handling Editor: Martine Leermakers.

Keywords:
Phytoremediation
Heavy metals
Typha latifolia
Thelypteris palustris
Swine livestock
Environmental impact

ABSTRACT

Animal production is a source of heavy metals in livestock wastewater and also a key link in the food chain, with negative impacts on human and animal health. In intensive animal production systems, the most critical elements are zinc and copper. In order to development of innovative non-invasive strategies to reduce the environmental impact of livestock, this study assessed the ability of two plants, *Typha latifolia* and *Thelypteris palustris*, to bioaccumulate the heavy metals used in animal nutrition, from wastewater. Four mesocosms (width 2.0 m, length 2.0 m, 695 L of water, 210 kg of soil) were assembled outdoors at the Botanical Garden. Two of them were planted with *T. latifolia* (TL treated, n = 30; TL control, n = 30) and two with *T. palustris* (TP treated, n = 60; TP control, n = 60). In T0 a solution of a mineral additive premix (Zn 44.02 mg/L; Cu 8.63 mg/L) was dissolved in the treated mesocosms. At T0, d 15 (T1) and d 45 (T2) samples of roots, leaves, stems, soil and water were collected, dried, mineralized and analyzed using ICP-MS in order to obtain HMs content. We found that *T. latifolia* and *T. palustris* accumulate and translocate Zn, Cu from contaminated wastewater into plant tissues in a way that is directly related to the exposure time (T2 for Zn: 271.64 ± 17.70, 409.26 ± 17.70 for Cu: 47.54 ± 3.56, 105.58 ± 3.56 mg/kg of DM, respectively). No visual toxicity signs were observed during the experimental period. This phytoremediation approach could be used as an eco-sustainable approach to counteract the output of heavy metals.

1. Introduction

The contamination of wastewater with heavy metals and metalloids (HMs) has become a worldwide concern in areas of intensive agriculture (Bhargava et al., 2012). The long-term consequences of the accumulation of HMs can reduce the quality of cultivation and increase the pollution of agricultural lands (Gul et al., 2015; Jakubus et al., 2013; Liu et al., 2018; Lopez-Alonso et al., 2012; Rossi et al., 2013, 2014a,b). The major routes of HMs into the soil include atmospheric deposition, agrochemicals, inorganic fertilizers and also animal manure, the latter reflecting the content of HMs from animal feed (Nicholson et al., 2003).

Animal production is thus a possible source of HMs which can contaminate the food chain with a negative impact on human and

Abbreviations: DM, dry matter; f.w., fresh weight; ICP-MS, inductively coupled plasma mass spectrometry.

* Corresponding author.
E-mail addresses: monika.hejna@unimi.it (M. Hejna), alessandra.moscatelli@unimi.it (A. Moscatelli), nadia.stroppa@unimi.it (N. Stroppa), elisabetta.onelli@unimi.it (E. Onelli), salvatore.pilu@unimi.it (S. Pilu), antonella.baldi@unimi.it (A. Baldi), luciana.rossi@unimi.it (L. Rossi).

https://doi.org/10.1016/j.chemosphere.2019.125018
0045-6535/

animal health (Dumont et al., 2012; Jarup, 2003; Lyubenova et al., 2013; Ma et al., 2016; Hejna et al., 2019). HMs can enter the animals' diet both as contaminants or undesirable substances and as essential nutrients (Fink-Gremmels, 2012; Hejna et al., 2018). Elements such as cobalt (Co), copper (Cu), iron (Fe), iodine (I), manganese (Mn), molybdenum (Mo), selenium (Se) and zinc (Zn) are some of the numerous enzymes that coordinate biological processes, and consequently should be integrated into the animal diet as mineral additives by respecting the maximum admitted level (EC N° 1831/2003; Lopez-Alonso et al., 2012).

The previous study showed that the content of HMs in manure reflected their concentration in the diet (Hejna et al., 2019), and that Zn and Cu, widely used in high doses to control enteric bacterial infections as well as to enhance the integrity of the immune system (Liu et al., 2018) represent the most critical output from swine livestock.

The scenario of livestock have changed significantly in the last decade. In fact, after the antibiotics ban in 2006 in Europe (EC, Reg. 1831/2003), there was an increased use of high dosages of zinc salts, possible after veterinary prescription as an alternative to in-feed antibiotics to control the enteric disease in the growing phases. Despite the antibacterial activity of zinc salts, the use of zinc in feed might have contributed to the emergence of methicillin-resistant *Staphylococcus aureus* (MRSA). There is worldwide concern that MRSA has become a zoonotic pathogen in animal production. For these reasons together with the environmental issues, the EU has banned the inclusion of pharmacological levels of ZnO after 2022 (EMA/394961/2017; Commission Regulation EU 2016/1095, 2016).

Since the bioavailability of mineral sources is limited and they are partially absorbed by organisms, the excess is eliminated by excretion. In swine farms, wastewater-derived conventional techniques of civil and livestock waste, could be valuable for agricultural irrigation; however, HM contamination (Chardon et al., 2012; Hejna et al., 2018; Moral et al., 2005; Nicholson et al., 2003) drastically reduces their potential use in irrigation.

Since the use of contaminated irrigation water would be responsible for the distribution of large numbers of metallic ions in the environment, the removal of HMs from manure wastewaters is essential in order to improve the soil quality (Gul et al., 2015; Jakubus et al., 2013; Liu et al., 2018; Lopez-Alonso et al., 2012).

Thus, the aim of this study was to assess the ability of two aquatic species, *Typha latifolia* (Broadleaf cattail) and *Thelypteris palustris* (Marsh fern), to remove Zn and Cu from contaminated livestock wastewaters, given that these species have already been used to decontaminate water and soils from metals (Chandra and Yadav, 2010; Hazra et al., 2015; Manios et al., 2003a, b; Salem et al., 2017). Cattail is a wetland specie that can be grown under different climatic conditions such as brackish and polluted water and because of their rapid growth and easily harvesting they can be used in phytoremediation (Milam et al., 2004; Ahmad et al., 2017; Rodriguez-Hernandez et al., 2017). Marsh fern also could be ideal aquatic plant for phytoremediation due to its wide range of habitat and easy of cultivation in many environments including agricultural sites, endangered coastal wetlands and urban brownfield sites (Anderson and Walsh, 2007). A phytoremediation pilot mesocosms system was developed, which could be easily managed in animal production systems. In addition, to enable plants to work in the system for a long time and to reduce the amount of exhausted plants that need disposing of a mineral additive premix was dissolved in the wetland water to obtain a concentration of zinc fourteen times higher than the regulation limit.

2. Material and methods

2.1. Plant culture

A pilot wetland system containing four mesocosms (width: 2.0 m; length 2.0 m; depth 1.2 m) was assembled outdoors at the Botanical Garden of the University of Milan (Italy). The mesocosms were aligned in one row parallel to the sun's pathway to receive the same intensity of light radiation. Each mesocosm had a constant flow-through capacity by a horizontal submerged flow system, which was combined with the open input-output pipe.

Mesocosms were filled by waterproof cloths, two layers of stone chippings (1st gravel with diameter 1–3 cm; 2nd gravel with diameter 1 cm) and sand (diameter ˂1 cm) was poured into the basis. In order to create positive drainage, gravel was placed, and compacted on the bottom. This substratum was then induced to create a sediment upon water addition, and finally 210 kg of loam for plant culture composed of acid peat, pumice, clay and manure NPK (0.3 s/m of electric conductibility, 300 kg/m^3 dry density and 90% v/v total porosity; mature commercial compost Flox Containerpflanzez, Blumenerde VitaFlor) was layered on the substratum.

The commercial compost used in the experimental trial contained 45.45% of ashes as fresh weight (f.w.) with 8.57% humidity (Supplementary Table 1). Fresh water (650 L) was added to each mesocosm. Then young healthy plants (purchased from Centro Flora) were planted and were left in the substrate for one week for the adaptation. Two mesocosms were used for *T. latifolia* (TL control: control, n = 30; TL treated: treatment, n = 30) and two mesocosms were used to test *T. palustris* (TP control: control, n = 60; TP treated: treatment, n = 60).

After the adaptation (T0), 1.5 kg of a mineral commercial additive premix (feed Maxi CRC 0.5%, Alpha, Zn 20.400 mg/kg, Cu: 4.000 mg/kg, Mn: 5.020 mg/kg, Se 41 mg/kg, Vitamin K: 150 mg/kg; Vitamin B2: 440 (mg/kg); Vitamin A: 1.100.000 Ul/kg; Vitamin D3: 220.000 Ul/kg) was dissolved, more than 14 times higher concentration for Zn referring to the maximum admitted level established by Italian regulation (for Zn: 3 mg/L according D. 337 152/2006 and for Cu: 2 mg/L according 98/83/EC).) in the treatment mesocosms planted with *T. latifolia* (TL treated) and *T. palustris* (TP treated), respectively. The mineral commercial additive premix contain all essential trace elements and macronutrients for animal diet and it is normally added to the feed. The theoretical final concentrations were calculated: 44.02 mg/L of Zn; 8.63 mg/L of Cu (Fig. 1). The mineral premix was added carefully to the surface of the water taking care not to spill outside the mesocosm.

2.2. Plants, soil and water sampling

The experiment took place over a period of 10 weeks. Before the sampling procedure, each mesocosm was separated into three homogenous areas and plants were then collected from these three areas. At T0 and 15 d later (T1), and 45 d later (T2), samples of plants (aerial – leaves/stem and subaerial – rhizomes/roots organs), samples of water (5 ml) and soil (300 g) were collected. A total of 70% of each soil sample were collected near to the plants' roots, and the remaining 30% were collected from the different mesocosm parts. The water samples were derived from the horizontal submerged flow system, and were then combined with a special pipe in order to proceed with the sampling process. The plants were collected from three different mesocosm regions (n = 2–3 of *T. latifolia* and n = 4–6 of *T. palustris*; around 5–10% of total amount) at T0, T1 and T2. Each plant collected was rinsed twice with the distilled water in order to wash off any soil particles.

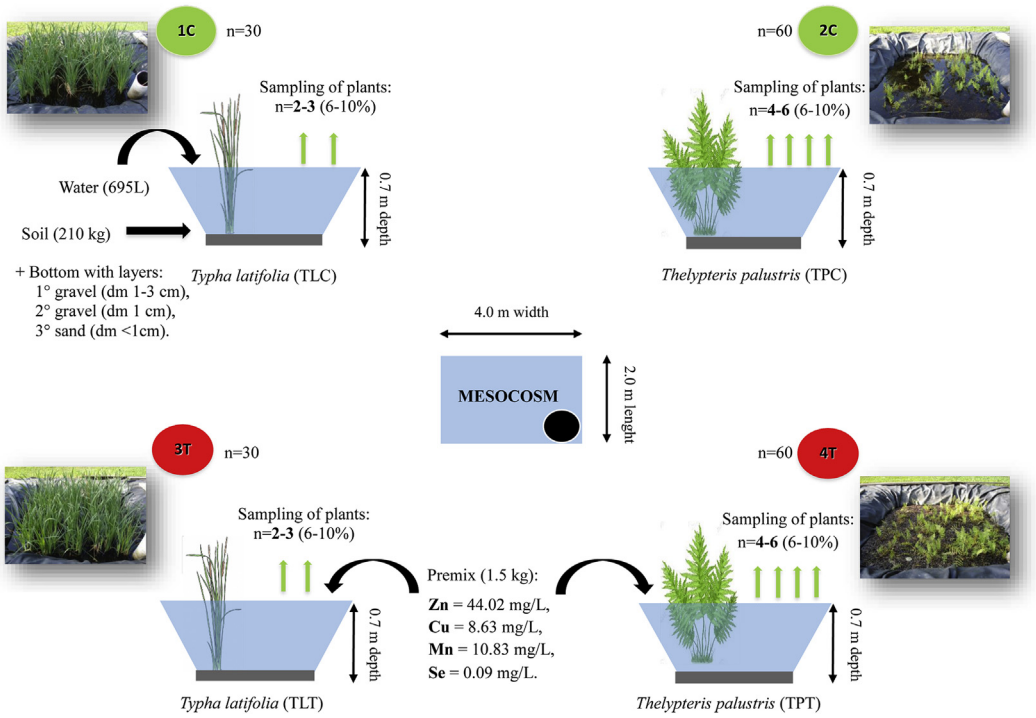

Fig. 1. The outdoor mesocosms with the amount of mineral additive premix dissolved on the first d of the experiment (T0). 1C: *T. latifolia* control mesocosm; 2C; *T. palustris* control mesocosm; 3T: *T. latifolia* treated mesocosm; 4T: *T. palustris* treated mesocosm.

2.3. Chemical composition of plant samples

The dry matter (DM) of plants (subaerial organs and aerial organs separately, TL control n = 14; TL treated n = 28; TP control n = 14; TP treated n = 28) was obtained by inserting the samples in preweighed aluminum bags which were dried in a forced-air oven at 80 °C for 72 h (AOAC 2005 method; proc. 930.15; CR No. 152/2009). All dried plants were ground with a laboratory mill to 0.5 mm (Cyclone Sample Mill, Model 3010-019, pbi International, Milan, Italy) and were evaluated from two time experimental points (T0 and T2). Crude protein (CP) was measured following the Kjeldahl method (AOAC 2005 method, proc. 2001.11). Crude fiber (CF) was determined by the Filter Bag technique (AOCS 2005 method, proc. Ba 6a-05). Lipid content (EE) was measured by the Soxhlet method, with prior hydrolysis (European Commission Regulation No. 152/2009). Ashes were measured using a muffle furnace at 550 °C (AOAC 2005 method; proc. 942.05). The amylose ratio in starch, on a dry weight basis (DW) was calculated (Megazyme total starch kit) by spectrophotometric evaluation at 510 nm.

2.4. Evaluations of HMs in plants, soil and water samples by inductively coupled plasma mass spectrometry (ICP-MS)

A total of 0.3 g of each dried plant (subaerial organs and aerial organs separately, TL control n = 14; TL treated n = 28; TP control n = 14; TP treated n = 28) and 0.3 g of dried soil (0.3 g/DM of each; TL control n = 6; TL treated n = 6; TP control n = 6; TP treated n = 6) were mineralized by an ultrawave single reaction chamber microwave digestion system (Anton Paar MULTIWAVE 3000) in Teflon tubes filled with 10 ml of HNO_3 (65% concentrated) by applying a one-step temperature ramp (at 120 °C in 10' and maintained for 10). The mineralized samples were cooled for 20 min and the homogenous samples solutions were transferred into polypropylene test tubes. Plant samples (250 μl) were then diluted 1:40 with a standard solution containing an internal standard (100 μl) and H_2O (9.75 ml). The soil samples (100 μl) were diluted 1:100 with a standard solution containing an internal standard (100 μl) and HNO_3 (0.3 M, 10 ml). Water samples were analyzed without dilution (0.5 ml; TL control n = 4; TL treated n = 4; TP control n = 4; TP treated n = 4).

An aliquot of 2 mgL^{-1} of an internal standard solution (^{72}Ge, ^{89}Y, ^{159}Tb) was added to the samples and calibration curve to obtain a final concentration of 20 μgL^{-1}. All samples were analyzed in triplicate by inductively coupled plasma mass spectrometry (ICP-MS; Bruker Aurora M90 ICP-MS, Bremen, Germany) in order to detect the following elements: Na, Mg, K, Ca, Cr, Mn, Fe, Co, Ni, Cu, Zn, As, Se, Mo, Cd, and Pb (Supplementary Tables 2 and 3). The accuracy of the results obtained using ICP-MS was evaluated using internal reference materials supplied by LGC Standards Company: sewage sludge (LGC 61812); poultry feed (LGC7173); and waste water (SPS-WW2 1). The typical polyatomical analysis interferences were removed using the collision-reaction interface (CRI) with an H_2 flow of 75ml/min^{-1} through a skimmer cone.

2.5. Statistical analysis

In order to evaluate any statistically significant differences among mean values, all data were analyzed using Glimmix of SAS software (9.4., SAS Inst. Inc., Cary, NC). The analysis accounted for the fixed effects of treatment, time, plant type and part, and associated two-way interactions and the random effect of plant (treatment). Repeated measures were used as the time (treatment). Means were considered different when $P < 0.05$ and tended to differ if $0.05 < P \leq 0.10$. Tukey-Kramer studentized adjustments were used to separate treatment means within the two-way interactions. Within significant two-way interactions, the slice option was used to separate means within a specific time and plant type. The results are reported as least squares means and standard errors of the means.

3. Results

3.1. Biomass and chemical composition of plants

In order to detect the effect of Zn and Cu exposure on plant growth, the amount of dry matter (DM)/plant was measured as an indicator of the biomass. *T. latifolia* and *T. palustris* plants grew normally in the control and metal-treated mesocoms from T0 to T2 as showed increasing trend of the plant biomass (Table 1). In fact, with respect to T0, the growth rate for TL treated and TP treated was higher (504.17% and 183.33%, respectively) comparing to TL control and TP control (329.63% and 131.58%, respectively). Interestingly, for both species, the biomass mostly increased in T2 treated with respect to control mesocosms.

The principal chemical components of the control and treated plants (aerial organs and subaerial organs) are presented in Table 1 for *T. latifolia* and *T. palustris*. For both plants, fiber and ash content increased from T0 to T2 in all the organs in parallel to the decrease in water content. However, slight differences were observed in plants grown in the control with respect to the treated mesocoms. On the other hand, there was a decrease in total lipids in *T. latifolia* and *T. palustris* after 45 d of metal exposure compared to the control (see T2 with respect to T0; 1). In the control leaves of both plants, lipids slightly increased from T0 to T2, while in treated samples there was a decrease of about 10% and 25% for *T. latifolia* and *T. palustris,* respectively. In rhizome, a decrease of total lipids was observed both in the control and treated plants particularly in marsh ferns (Table 1; compare T0 and T2). However, in T2 there was a greater decrease of lipids in the treated plants than in the control plants (Table 1).

Proteins showed different trends in *T. latifolia* and *T. palustris*, although they increased in both plants from T0 to T2. This increase was more pronounced in marsh ferns than in Monocot plants.

The quantification of starch showed that the amount of this polymer was different depending on the organ or the plant. In *T. latifolia*, no differences were observed for aerial organs in the treated and control samples (Table 1; see T2 with respect to T0). An opposite trend of starch content was observed in the aerial and subaerial organs of *T. palustris* after metal exposure with respect to the control. In fact, in the control, starch decreased in leaves and increased in rhizomes during plant growth (compare T0 and T2). On the other hand, in T2 treated plants, an increase of starch in leaves was accompanied by a decrease of starch in the subaerial organs with respect to T0 (Table 1).

3.2. Content of Cu^{2+} and Zn^{2+} in plants, soil and water from *T. latifolia* plants by ICP-MS

To evaluate the ability of *T. latifolia* to accumulate Zn and Cu and thus phytoremediate contaminated water, the concentrations of metals in plants, water and soil were measured in T0, T1 and T2.

In control mesocoms, whole *T. latifolia* plants showed the same concentration of Zn^{2+} and Cu^{2+} in samples collected in T0, T1 and T2 (Table 2). The same behavior was observed when subaerial and aerial organs were considered separately. However, there was an increase of Cu^{2+} in subaerial organs of T2 controls plants, although not significant ($p < 0.05$), showing that root and rhizomes can accumulate Cu^{2+}, which was naturally present in the soil and water. In treated samples, the plants began to accumulate Zn^{2+} and Cu^{2+} after 15 d of metal exposure, since there was only a significant increase in metal concentration in T2 (Zn: $p < 0.001$; TL treated $= 271.64 \pm 17.71$ vs. TL control $= 55.79 \pm 17.71$ mg/kg; Cu: $p < 0.001$; TL treated $= 47.54 \pm 3.56$ vs. TL control $= 15.20 \pm 3.56$ mg/kg; Table 2).

However, even if no significantly different was observed for the Zn and Cu concertation in aerial and subaerial organs, Zn was

Table 1
The chemical composition (on DM basis) and the biomass of *T. latifolia* and *T. palustris* plants (for aerial organs and subaerial organs) in time points (T0 and T2) for control (TL control) and treatment (TL treated) mesocosms.

Chemical composition								
Part of plants	Treatment	Time points	Humidity (%)	Crude protein (g/100g)	Crude fiber (g/100 g)	Lipids (g/100 g)	Ash (g/100 g)	Starch (g/100 g)
T. latifolia								
Aerial organs	Control	T0	21.04	5.34	17.42	2.19	9.41	19.43
		T2	10.05	8.56	32.71	2.52	9.75	10.81
	Treated	T0	13.86	10.78	17.92	2.93	9.36	19.90
		T2	8.83	11.54	29.04	2.60	10.70	10.12
Subaerial organs	Control	T0	12.53	2.97	26.43	0.94	7.27	–
		T2	8.33	4.96	26.01	0.91	9.82	–
	Treated	T0	9.53	4.49	26.31	1.05	7.73	–
		T2	6.55	5.62	26.78	0.78	10.54	–
T. palustris								
Aerial organs	Control	T0	24.85	7.69	24.51	1.68	6.75	8.90
		T2	16.03	7.92	27.08	1.84	8.87	8.09
	Treated	T0	23.88	7.26	24.25	1.76	7.23	6.02
		T2	22.20	10.20	29.26	1.27	9.01	12.53
Subaerial organs	Control	T0	18.72	5.48	20.93	1.23	6.68	18.07
		T2	14.92	6.81	23.26	0.55	9.06	20.67
	Treated	T0	15.31	4.46	21.54	3.66	8.71	22.32
		T2	13.34	11.46	27.01	0.72	10.61	16.30
Biomass of *T. latifolia* (kg DM/Plant)								
Control		T0	0.027 ± 0.010					
		T2	0.089 ± 0.054					
Treated		T0	0.024 ± 0.010					
		T2	0.121 ± 0.075					
Biomass of *T. palustris* (kg DM/Plant)								
Control		T0	0.019 ± 0.011					
		T2	0.025 ± 0.018					
Treated		T0	0.018 ± 0.011					
		T2	0.033 ± 0.014					

T0: first d of the experiment, T2: 45 d later.

Table 2
The average Zn and Cu concentration in *T. latifolia* (TL) plants in the control and treatment mesocosms (TL control; TL treated) at the three time points (T0, T1, T2).

Experimental groups	Time point	Concentrations of heavy metals (mg/kg DM)	
		Zn	Cu
TL control	T0	56.35 ± 17.70^{aA}	12.64 ± 3.56^{aA}
	T1	57.61 ± 17.70^{aA}	10.47 ± 3.56^{aA}
	T2	55.79 ± 17.70^{aA}	15.20 ± 3.56^{aA}
TL treated	T0	81.14 ± 17.70^{aA}	13.81 ± 3.56^{aA}
	T1	105.80 ± 17.70^{aA}	25.92 ± 3.56^{aA}
	T2	271.64 ± 17.70^{bB}	47.54 ± 3.56^{bB}

TL control: *T. latifolia* control mesocosm; TL treated: *T. latifolia* treated mesocosm; T0: first d of the experiment, T1: 15 d later, T2: 45 d later.
a-b: the obtained values are expressed as means ± SE; means with different superscriptions (ab) are significantly different within the same time points (T0, T1, T2) between TL control and TL treated ($p < 0.001$); means with different superscriptions (AB) are significantly different among different time points (T0, T1, T2) in TL control and TL treated ($p < 0.001$).

accumulated in TL treated subaerial organs, with the maximum concentration at T2 (177.28 ± 30.66 mg/kg). At the same time, TL control showed a concentration of zinc of about 77.16 ± 30.66 mg/kg. Similarly, the Zn concentration of aerial organs was higher in T2-TL treated than T2-TL control (59.29 ± 30.66 vs. 31.26 ± 30.66 mg/kg, respectively).

Higher Cu concentrations were also observed in aerial and subaerial organs of metal treated plants with respect to the control. In addition, rhizomes/roots showed a higher Cu content compared with aerial organs (33.29 ± 6.16 vs. 14.73 ± 6.16 mg/kg, respectively.

The increase of Zn^{2+} and Cu^{2+} concentrations in plant organs was related by a decrease of these metals in water (Table 3). Zn^{2+} and Cu^{2+} were higher in the water of T0 treated mesocoms with respect to the controls due to the addition of the commercial mineral additive premix containing metals used in the experimental trial. The metals in the water had already decreased after two weeks (T1, Table 3) remaining constant for Zn, and slightly decreasing for Cu in T2 water. The decrease of metals in water was in parallel with the increase of metals in soil, particularly in T2 samples (Table 3; $p < 0.001$).

Since the bioavailability of metals depends on the pH in the environment, the pH values has been measured. During the experiment, the pH of water varied from neutral to slightly alkaline. However, even if no significantly different, in TL control the pH values remained higher with respect to TL treated mesocosm (Table 3). Moreover, the mineral additive premix inclusion led to a reduction of pH at the beginning of the experiment (T0 7.36 vs 7.00).

Table 3
The average Zn and Cu concentration in soil and water and pH of water of *T. latifolia* (TL) mesocosms in the control and treatment mesocosms (TL control; TL treated) in the three time points (T0, T1, T2).

Experimental groups	Time points	Concentration of heavy metals (mg/kg)	
		Zn	Cu
TL control soil	T0	59.19 ± 30.66^{aA}	8.88 ± 6.16^{aA}
	T1	46.01 ± 30.66^{aA}	6.10 ± 6.16^{aA}
	T2	58.94 ± 30.66^{aA}	6.71 ± 6.16^{aA}
TL treated soil	T0	87.18 ± 30.66^{aA}	12.14 ± 6.16^{aA}
	T1	179.72 ± 30.66^{aA}	29.97 ± 6.16^{aA}
	T2	578.36 ± 30.66^{bB}	94.59 ± 6.16^{bB}
		Concentration of heavy metals (mg/L)	
		Zn	**Cu**
TL control H_2O	T0	0.001	0.009
	T1	0.001	0.004
	T2	0.005	0.007
TL treated H_2O	T0	0.187	0.204
	T1	0.023	0.033
	T2	0.022	0.024
			pH of H_2O
TL control	T0	7.36 ± 0.07^{a}	
	T1	7.14 ± 0.07^{a}	
	T2	7.58 ± 0.07^{a}	
TL treated	T0	7.00 ± 0.07^{a}	
	T1	7.07 ± 0.07^{a}	
	T2	7.25 ± 0.07^{a}	

TL control: *T. latifolia* control mesocosm; TL treated: *T. latifolia* treated mesocosm; T0: first d of the experiment, T1: 15 d later, T2: 45 d later.
a-b: the obtained values are expressed as means ± SE; means with different superscriptions (ab) are significantly different within the same time points (T0, T1, T2) between TL control and TL treated ($p < 0.001$); means with different superscriptions (AB) are significantly different among different time points (T0, T1, T2) in TL control and TL treated ($p < 0.001$); for pH: $p < 0.05$.

3.3. Content of Cu^{2+} and Zn^{2+} in plants, soil and water from *T. palustris* plant by ICP-MS

As observed in *T. latifolia*, whole plants of *T. palustris* were also able to accumulate Zn^{2+} and Cu^{2+} in their organs. In fact, higher concentrations of metals were detected in TP treated than in the control already 15 d (T1) after metal addition (Table 4; $p < 0.001$) and there was a slight decrease in T2 plants.

There was a similar trend in the aerial and subaerial organs separately, in which high concentrations of Zn^{2+} and Cu^{2+} were reached in T1-TP treated samples (Table 5). Zn was mostly accumulated in TP treated subaerial organs, with the maximum concentration at T2 (Table 5). At T2, the Zn concentration of aerial organs was higher in TP treated than TP control (Table 5).

Cu concentration also significantly increased in T1 and T2-TP treated subaerial organs compared with TP control (Table 5; $p < 0.001$), and likewise for T1-TP treated aerial organs. Surprisingly, 45 d after metal addition, Cu decreased significantly in leaves of *T. palustris* (Table 5, T2). Translocation of metals from subaerial organs to leaves was higher with respect to *T. latifolia,* however, *T. palustris* accumulated Zn^{2+} and Cu^{2+} preferentially in subaerial organs (Table 5).

The increase of metals in plants was related by a decrease of Zn^{2+} and Cu^{2+} in water (Table 6). As observed in *T. latifolia* mesocoms, Zn^{2+} and Cu^{2+} were higher in T0 treated water than in the controls; during the experimental proceed the metal concentration decreased both in T1 and T2 samples (Table 6). Unlike the *T. latifolia*

Table 4
The average Zn and Cu concentration in *T. palustris* (TP) plants in the control and the treatment mesocosms (TP control; TP treated) in the three time points (T0, T1, T2).

Experimental groups	Time point	Concentrations of heavy metals (mg/kg DM)	
		Zn	Cu
TP control	T0	113.33 ± 17.70^{aA}	11.30 ± 3.56^{aA}
	T1	85.62 ± 17.70^{aA}	18.25 ± 3.56^{aA}
	T2	88.36 ± 17.70^{aA}	16.50 ± 3.56^{aA}
TP treated	T0	89.11 ± 17.70^{aA}	12.46 ± 3.56^{aA}
	T1	414.67 ± 17.70^{bB}	136.12 ± 3.56^{bB}
	T2	409.26 ± 17.70^{bB}	105.58 ± 3.56^{bB}

TP control: *T. palustris* control mesocosm; TP treated: *T. palustris* treated mesocosm; T0: first d of the experiment, T1: 15 d later, T2: 45 d later.
a-b: the obtained values are expressed as means ± SE; means with different superscriptions (ab) are significantly different within the same time points (T0, T1, T2) between TL control and TL treated ($p < 0.001$); means with different superscriptions (AB) are significantly different among different time points (T0, T1, T2) in TL control and TL treated ($p < 0.001$).

Table 5
The average Zn and Cu concentration in *T. palustris* (TP) subaerial organs and the average Zn and Cu concentration in *T. palustris* aerial organs in the control and in the treatment mesocosms (TP control; TP treated) in the three time points (T0, T1, T2).

Experimental groups	Time point	Concentrations of heavy metals (mg/kg DM)	
		Zn	Cu
T. palustris aerial organs			
TP control	T0	35.49 ± 30.66^{aA}	7.08 ± 6.16^{aA}
	T1	43.95 ± 30.66^{aA}	8.94 ± 6.16^{aA}
	T2	22.04 ± 30.66^{aA}	8.98 ± 6.16^{aA}
TP treated	T0	$22.32 \pm 30.66b^{aA}$	6.59 ± 6.16^{aA}
	T1	235.08 ± 30.66^{bB}	119.48 ± 6.16^{bB}
	T2	201.63 ± 30.66^{bB}	33.03 ± 6.16^{aA}
T. palustris subaerial organs			
TP control	T0	191.96 ± 30.66^{aA}	$15,21 \pm 6.16^{aA}$
	T1	93.94 ± 30.66^{aA}	31.79 ± 6.16^{aA}
	T2	134.51 ± 30.66^{aA}	24.19 ± 6.16^{aA}
TP treated	T0	175.79 ± 30.66^{aA}	18.12 ± 6.16^{aA}
	T1	527.37 ± 30.66^{bAB}	204.70 ± 6.16^{bB}
	T2	786.49 ± 30.66^{bB}	235.10 ± 6.16^{bB}

TP control: *T. palustris* control mesocosm; TP treated: *T. palustris* treated mesocosm; T0: first d of the experiment, T1: 15 d later, T2: 45 d later.
a-b: the obtained values are expressed as means ± SE; means with different superscriptions (ab) are significantly different within the same time points (T0, T1, T2) between TL control and TL treated ($p < 0.001$); means with different superscriptions (AB) are significantly different among different time points (T0, T1, T2) in TL control and TL treated ($p < 0.001$).

Table 6
The average Zn and Cu concentration in soil and water and pH of water of *T. palustris* (TP) mesocosms in the control and treatment mesocosms (TL control; TL treated) in the three time points (T0, T1, T2).

Experimental groups	Time points	Concentration of heavy metals (mg/kg)	
		Zn	Cu
TP control soil	T0	112.53 ± 30.66^{aA}	11.60 ± 6.16^{aA}
	T1	118.97 ± 30.66^{aA}	14.02 ± 6.16^{aA}
	T2	108.55 ± 30.66^{aA}	16.34 ± 6.16^{aA}
TP treated soil	T0	69.24 ± 30.66^{aA}	12.66 ± 6.16^{aA}
	T1	481.55 ± 30.66^{bB}	84.17 ± 6.16^{bB}
	T2	239.65 ± 30.66^{aA}	48.60 ± 6.16^{aA}
		Concentration of heavy metals (mg/L)	
		Zn	**Cu**
TP control H_2O	T0	0.001	0.007
	T1	0.001	0.003
	T2	0.002	0.005
TP treated H_2O	T0	0.381	0.240
	T1	0.053	0.025
	T2	0.036	0.013
			pH of H_2O
TP control	T0	7.18 ± 0.03^{a}	
	T1	7.12 ± 0.03^{a}	
	T2	7.29 ± 0.03^{a}	
TP treated	T0	6.99 ± 0.03^{a}	
	T1	7.27 ± 0.03^{b}	
	T2	7.41 ± 0.03^{a}	

TP control: T. palustris control mesocosm; TP treated: T. palustris treated mesocosm; T0: first d of the experiment, T1: 15 d later, T2: 45 d later.
a-b: the obtained values are expressed as means ± SE; means with different superscriptions (ab) are significantly different within the same time points (T0, T1, T2) between TL control and TL treated ($p < 0.001$); means with different superscriptions (AB) are significantly different among different time points (T0, T1, T2) in TL control and TL treated ($p < 0.001$); for pH: $p < 0.05$.

mesocoms, both Zn^{2+} and Cu^{2+} were present at significantly higher concentrations in soil two weeks after the metals had been added (Table 6; $p < 0.001$). There was then a significant decrease in the Zn^{2+} and Cu^{2+} concentration in T2 soil samples (Table 6; $p < 0.001$), confirming the idea that the uptake of metals by plants occurs preferentially by soil.

During the experiment, water pH varied from neutral to slightly alkaline both in the control and in treated mesocoms. After the premix had been added in T0 the pH decreased in TP treated compared with TP control. However, even if later pH mostly increased in T1-TP treated and T2-TP treated with respect to T1-TL treated T2-TL treated mesocoms (Table 6, $p < 0.05$ in T1).

4. Discussion

The intensive animal production system is a source of HM input into environment and also a key link in the food chain. This has led to the development of approaches to increase the sustainability of intensive livestock farming. Animal manure reflects the composition of their diet and is frequently used as an organic fertilizer given that it contains a broad range of nutrients such as nitrogen, phosphorus, potassium, as well as micronutrients and HMs. Although the maximum permitted levels are well defined by EU regulations (EC N° 1831/2003), they are often above the physiological requirements.

In line with the major topics of agroecology, multidisciplinary strategies are required that take into account the needs of animals (health, welfare and nutrition productivity) and farmers (profitability and productivity) together with the environment. Phytoremediation system is used to refine pre-treated wastewaters before they are used for irrigation (Peterson, 1998).

The tolerance threshold for HM accumulation in the tissues in each plant differs from species to species and is determined by genetical, environmental and physiological features (Ali et al., 2013; Lone et al., 2008; Mukhopadhyay and Maiti, 2010; Thangavel and Subbhuraam, 2004). However, our approach showed that both *T. palustris* and *T. latifolia* removed Zn and Cu from pilot wetland systems contaminated by a mineral additive premix normally used in animal diets.

4.1. *T. latifolia and T. palustris could work in series to refine wastewater by Cu and Zn phytoremediation*

The ability of *T. latifolia* to accumulate metals is well known (Fediuc and Erdei, 2002; Hemmati and Yazdi Nezhad, 2012; Klink et al., 2013; Klink et al., 2016; Klink, 2017; Kumari and Tripathi, 2015; Lyubenova and Schröder, 2011; Manios et al., 2002, 2003a,b; Maric et al., 2013; Peralta et al., 2001; Rafati et al., 2011; Rai et al., 1995; Ye et al., 1997). On the other hand, the potential of *T. palustris* in phytoremediation systems has only been tested for arsenic (Anderson et al., 2011).

In order to mimic the condition of wastewater refining systems in the livestock, an outdoor pilot wetland system was used. In this system, *T. latifolia* and *T. palustris* showed different capability to accumulated Cu and Zn contained after the mineral additive premix has been added to the water in the TL treated and TP treated mesocosms. The decreasing trend for Zn and Cu in the water and soil was accompanied by an increase of metal concentration in the TL treated and TP treated plants. Our phytoremediation pilot system decontaminated the wastewater from the toxic elements in line with Petroselli et al., (2015).

Analyses of HM concentrations in plants (in the whole plants or in the aerial and subaerial organs) suggested that *T. palustris* was more effective than *T. latifolia* in accumulating metals in subaerial organs and in translocating them to leaves in a short time. The low capacity of *T. latifolia* to translocate metals is already reported and is considered a metal tolerance strategy (Fediuc and Erdei, 2002; Klink et al., 2013, 2017).

Already after 15 d of exposure to metals, *T. palustris* was able to

efficiently uptake Zn and Cu, while *T. latifolia* started the accumulation process later. This difference could be due to the high metal concentration in the soil. When we added metals to the water in the treatment mesocoms, Zn and Cu concentrations were higher in the water than in the soil. The concentrations of the metals then decreased in water and increased in soil. It has been reported that in wetlands, the binding of metals to substrate is the major process for water to remove metals (Almeida et al., 2017; Yadav et al., 2012). Our data suggest that metal uptake occurs preferentially by the soil rather than by the water. In addition, the concentrations of Zn and Cu increased earlier in the soil of *T. palustris* compared to *T latifolia* mesocoms.

It is possible to hypothesize that marsh ferns modify the chemical features of soil by increasing the adsorption capacity of the matrix. In fact, several molecules were released by the roots into the rhizosphere and could thus modify the availability of nutrients and the matrix composition (Dakora and Phillips, 2002; Lyubenova et al., 2013). The significant decrease of metal concentrations in the soil in T2 samples suggested that *T. palustris* was more efficient in short-term phytoremediation processes. The co-presence of two species which work in series could increase the efficiency of the phytoremediation wetland systems.

In wetland systems, the degree of metal translocation by soil to plants depends on several environmental conditions (Yang and Ye, 2009). The pH influences the bioavailability of metal ions, and low pH promotes metal accumulation in rooted wetland plants (Emamverdian et al., 2015; Yang and Ye, 2009). The optimal condition for the uptake of several nutrients in *T. latifolia* is a pH value of 6.5 (Brix et al., 2002; Dyhr-Jensen and Brix, 1996). The addition of mineral additive led to a decrease in water pH, which during the experiment subsequently increased to slightly alkaline values. This trend has been observed in other phytoremediation systems (Barakat, 2011; Han et al., 2015; Kumari and Tripathi, 2015) and could be due to the ability of plants to modify the pH condition in the rhizosphere (Brix et al., 2002; Dyhr-Jensen and Brix, 1996). The increase in water pH to slightly alkaline values did not seem to affect plant uptake.

4.2. *T latifolia and T. palustris differently respond to metal exposure in a pilot wetland system*

Our results showed that the metal concentrations used in the pilot system were not toxic for the two plants, in fact the biomass increased over time. Biomass is a relevant factor for metal exchange and an important aspect of the health status of plants. In fact, according to Maric et al. (2013) the ideal plant for removing HMs should have a very large biomass and a rapid growth. Although *T. latifolia* showed a lower capacity to absorb metals in a short period of time, it may be better than hyperaccumulator plants because it produces more biomass and has a higher growth rate (Ali et al., 2013). Interestingly, in our treated plants the biomass increase was higher with respect to the control suggesting that although the metal concentrations used were fourteen times higher than that permitted by Italian regulations, they stimulate plant growth.

Zn^{2+} and Cu^{2+} are essential trace metals involved in many physiological processes in plants (Arif et al., 2016; Emamverdian et al., 2015; Manios et al., 2002). It is possible to hypothesize that these concentrations provide an amount of heavy metals which accelerates the growth of *T. palustris* and *T. latifolia*. Alternatively, the increase in biomass could be a tolerance mechanism of plants which grow in order to increase the number of tissues where metals could be accumulated or diluted.

Despite the increase of biomass, some chemical variations were recorded by ICP-analyses. Most relevant alterations in treated with respect to T2 control plants were detected for proteins, lipids and starch. The different behaviors of protein content observed in T2-TL treated and T2-TP treated with respect to the control suggested that the early uptake of metals by *T. palustris*, could activate stress and tolerance mechanisms that enabled plants to grow in the contaminated mesocoms. It is known that HMs trigger the expression of those genes that codify for proteins involved in stress responses (Hasan et al., 2017), such as phytochelatins and metallothioneins or enzymes with antioxidant activities to scavenge active oxygen species (REF). These tolerance mechanisms could also be activated in *T. palustris* during metal exposure.

After metal treatment, in T2 samples, the amount of lipid decreased with respect to the control in both plants. This difference was similar in subaerial organs and in leaves, but appeared more pronounced in marsh ferns compared to *T. latifolia*. This effect could be due to a lower *T. palustris* metal tolerance or to a rapid accumulation of metals in this plant (accompanying paper Stroppa et al., 2019). The ability of metals to induce a decrease in lipids and changes in lipid composition has been reported in other plants (Elloumi et al., 2014; Oves et al., 2016). The reduction of lipids that we detected in T2 metal exposed plants, particularly in *T. palustris*, could also be due to an alteration in the carbohydrate metabolisms. In fact, in *T. palustris*, the increase of starch in aerial organs suggests an evolution of chloroplasts into amyloplasts, as also observed in microscopical analyses (accompanying paper Stroppa et al., 2019). Plastids transformation could trigger a reduction in thylakoid and thus a reduction of lipid content. The decrease of starch in roots and rhizomes of both plants was different from what has been reported elsewhere for other plants in phytoremediation systems since in this case the starch content in roots and rhizomes increased (Frossard et al., 1989; Higuchi et al., 2015; Todeschini et al., 2011). The modification of carbohydrate metabolisms was considered a response of plants to metal accumulation. In L. *perenne*, the increase in Zn induced a fructan accumulation, while the increase in Cu induced an increase of starch (Frossard et al., 1989). In our study, the presence of high amounts of starch in the leaves of *T. palustris*, suggests that it has greater sensitivity to metal exposure than *T. latifolia*. (12.53 vs 10.12 g/100 g in T2 treated mesocosms, respectively).

Since these modifications occurred in the absence of visible symptoms of phytotoxicity, it appears that in *T. latifolia* and *T. palustris*, some mechanisms of metal tolerance have been present. However, it is not possible to exclude that some effects to metal exposure could also be due to the toxicity of metals. Further analyses could better clarify this point.

Moreover, tested plants after the bioaccumulation process can be used as eco-material for building constructions (Melià et al., 2014). Contemporary building materials (cement concrete, steel) require high energy for their production and are responsible for the emission of greenhouse gases (Morel et al., 2001; Venkatarama Reddy and Prasanna Kumar, 2010). The use of natural materials is encouraged by its availability, large quantities, affordable cost and less energy needed during the production process (Melià et al., 2014); Thus, once at the end of life the natural material is recyclable with no impact on the environment (Delgado and Guerrero, 2006).

5. Conclusions

The mesocosms treated with *T. latifolia* and *T. palustris* in our experiment were highly contaminated with a heavy metal mineral additive premix widely used in swine nutrition. *T. latifolia* and *T. palustris* exhibited relatively high Zn and Cu accumulation and translocation abilities. In addition, *T. latifolia* and *T. palustris* tolerated high levels of Zn and Cu, with no visual toxicity signs and no

significant visual effect on their development throughout the experimental period. To conclude, both *T. latifolia* and *T. palustris* can accumulate and translocate the Zn and Cu form contaminated wastewater. However, in order to decrease critical amounts of Zn and Cu in swine livestock output, when its level is critical, *T. palustris* can be used to reduce the Zn and Cu content in a short period of time. On the other hand, the wastewater phytoremediation for a long time could be achieved by *T. latifolia* working in series with respect *T. palustris*.

The results suggest that the ability of the two plants to survive different concentrations of Zn and Cu indicates that they could be used in a phytoremediation strategy to counteract the output of zinc and copper, and possibly other HMs from the livestock industry.

Author contributions

Conceptualization: Moscatelli A., Rossi L., Onelli E., Baldi A.

Data curation: Rossi L., Hejna. M., Moscatelli A.Formal analysis: Hejna M., Pilu S.Funding acquisition: Moscatelli A., Rossi L.

Investigation: Hejna M., Rossi L., Moscatelli A., Onelli E., Stroppa N.

Methodology: Hejna M., Moscatelli A., Onelli E., Pilu S. Rossi L.Project administration: Rossi L., Hejna M. Resources: Hejna M., Rossi L., Stroppa N., Pilu S. Software: Hejna M., Pilu S. Supervision: Rossi L., Moscatelli A. Validation: Hejna M., Rossi L., Onelli E. Visualization: Baldi A., Hejna M., Rossi L., Onelli E.Roles/writing - original draft: Hejna M., Moscatelli A., Onelli E., Rossi L.Writing - review&editing: Hejna M., Moscatelli A., Rossi L., Pilu S., Onelli E., Stroppa N., Baldi A.

Declaration of competing interest

The authors declare no competing financial interests.

Acknowledgments

This work was supported by the Ministry of Agriculture Food and Forestry Policies (MIPAAF 2015_ID60_Low Metal project). The funders had no role in study design, data collection and analysis, decision to publish, or preparation of the manuscript.

Appendix A. Supplementary data

Supplementary data to this article can be found online at https://doi.org/10.1016/j.chemosphere.2019.125018.

References

Ahmad, M.S., Mehmood, M.A., Taqvi, S.T.H., Elkamel, A., Liu, C.G., Xu, J., Rahimuddin, S.A., Gull, M., 2017. Pyrolysis, kinetics analysis, thermodynamics parameters and reaction mechanism of *Typha latifolia* to evaluate its bioenergy potential. Bioresour. Technol. 491–501. https://doi.org/10.1016/j.biortech.2017.08.162.

Ali, H., Khan, E., Anwar Sajad, M., 2013. Phytoremediation of heavy metals - concepts and applications. Chemosphere 869–881. https://doi.org/10.1016/j.chemosphere.2013.01.075.

Almeida, C.M.R., Santos, F., Ferreira, A.C., Gomes, C.R., Basto, M.C., Mucha, A.P., 2017. Constructed wetlands for the removal of metals from livestock wastewater - can the presence of veterinary antibiotics affect removals? Ecotoxicol. Environ. Saf. 143–148. https://doi.org/10.1016/j.ecoenv.2016.11.021.

Anderson, L.S., Walsh, M.M., 2007. Arsenic uptake by common marsh fern *Thelypteris palustris* and its potential for phytoremediation. Sci. Total Environ. 263–265.

Anderson, L.L., Walsh, M., Roy, A., Bianchetti, C.M., Merchan, G., 2011. The potential of *Thelypteris palustris* and *Asparagus sprengeri* in phytoremediation of arsenic contamination. Int. J. Phytoremediation 177–184. https://doi.org/10.1080/15226511003671346.

AOCS, 2005. Official Methods of the American Oil Chemists Society, " fifth ed. American Oil Chemists Society, Champaign.

Arif, N., Yadav, V., Singh, S., Singh, S., Ahmad, P., Mishra, R.K., et al., 2016. Influence of high and low levels of plant-beneficial heavy metal ions on plant growth and development. Front. Environ. Sci. https://doi.org/10.3389/fenvs.2016.00069.

Barakat, M.A., 2011. New trends in removing heavy metals from industrial wastewater. Arab. J. Chem. 361–377. https://doi.org/10.1016/j.arabjc.2010.07.019.

Bhargava, A., Carmona, F.F., Bhargava, M., Srivastava, S., 2012. Approaches for enhanced phytoextraction of heavy metals. J. Environ. Manag. 103–120. https://doi.org/10.1016/j.jenvman.2012.04.002.

Brix, H., Dyhr-Jensen, K., Lorenzen, B., 2002. Root-zone acidity and nitrogen source affects *Typha latifolia* L. growth and uptake kinetics of ammonium and nitrate. J. Exp. Bot. 2441–2450. https://doi.org/10.1093/jxb/erf106.

Chandra, R., Yadav, S., 2010. Potential of *Typha angustifolia* for phytoremediation of heavy metals from aqueous solution of phenol and melanoidin. Ecol. Eng. 1277–1284. https://doi.org/10.1016/j.ecoleng.2010.06.003.

Chardon, X., Rigolot, C., Baratte, C., Espagnol, S., Raison, C., Martin-Clouaire, R., et al., 2012. MELODIE: a whole-farm model to study the dynamics of nutrients in dairy and pig farms with crops. Animal 1711–1721. https://doi.org/10.1017/S1751731112000687.

Commission Regulation (EU) 2016/1095, 2016. Concerning the authorization of Zinc acetate dihydrate, Zinc chloride anhydrous, Zinc oxide (…) as feed additive for all animal species. Off J. L: 182/7.

Dakora, F.D., Phillips, D.A., 2002. Root exudates as mediators of mineral acquisition in low-nutrient environment. Plant Soil 35–47. https://doi.org/10.1023/A:1020809400075.

Delgado, M.C.J., Guerrero, I.C., 2006. Earth building in Spain. Constr. Build. Mater. 679–690. https://doi.org/10.1016/j.conbuildmat.2005.02.006.

Dumont, B., Fortun-Lamothe, L., Jouven, M., Thomas, M., Tichit, M., 2012. Prospects from agroecology and industrial ecology for animal production in the 21st century. Animal 1028–1043. https://doi.org/10.1017/S1751731112002418.

Dyhr-Jensen, K., Brix, H., 1996. Effects of pH on ammonium uptake by *Typha latifolia L.* Plant Cell Environ. 1431–1436. https://doi.org/10.1111/j.1365-3040.1996.tb00022.x.

Elloumi, N., Zouari, M., Chaari L, L., Jomni, C., Marzouk, B., Abdallah, F.B., 2014. Effects of cadmium on lipids of almond seedlings (*Prunus dulcis*). Bot. Stud. 55, 61. https://doi.org/10.1186/s40529-014-0061-7.

Emamverdian, A., Ding, Y., Mokhberdoran, F., Xie, Y., 2015. Heavy metal stress and some mechanisms of plant defense response. Sci. World J. https://doi.org/10.1155/2015/756120.

European Medicine Agency (EMA) N° 394961/2017. Questions and Answers on Veterinary Medicinal Products Containing Zinc Oxide to Be Administered Orally to Food-Producing Species.

European Parliament and the Council. Regulation (EC) no 1831/2003 of 22 September 2003 on additives for use in animal nutrition. Off J. L: 268/29.

Fediuc, E., Erdei, L., 2002. Physiological and biochemical aspects of cadmium toxicity and protective mechanisms induced in *Phragmites australis* and *Typha latifolia*. J. Plant Physiol. 265–271. https://doi.org/10.1078/0176-1617-00639.

Fink-Gremmels, J., 2012. Animal Feed Contamination, 1st Edition. Effects on Livestock and Food Safety. Woodhead Publishing Limited, Cambridge.

Frossard, R., Stadelmann, F.X., Niederhauser, J., 1989. Effects of different heavy metals on fructan, sugar and starch content of ryegrass. J. Plant Physiol. 180–185. https://doi.org/10.1016/S0176-1617(89)80052-5.

Gul, S., Naz, A., Fareed, I., Khan, A., Irshad, M., 2015. Speciation of heavy metals during co-composting of livestock manure. Pol. J. Chem. Technol. 19–23. https://doi.org/10.1515/pjct-2015-0044.

Han, J., Chen, F., Zhou, Y., Wang, C., 2015. High Pb concentration stress on *Typha latifolia* growth and Pb removal in microcosm wetlands. Water Sci. Technol. 71 (11), 1734–1741. https://doi.org/10.2166/wst.2015.163.

Hasan, K., Cheng, Y., Kanwar, M.K., Chu, X.Y., Ahammed, G.J., Qi, Z.Y., 2017. Responses of plant proteins to heavy metal stress - a review. Front. Plant Sci. https://doi.org/10.3389/fpls.2017.01492.

Hazra, M., Avishek, K., Pathak, G., 2015. Phytoremedial potential of *Typha latifolia, Eichornia crassipes* and *Monochoria hastata* found in contaminated water bodies across Ranchi City (India). Int. J. Phytoremediation 835–840. https://doi.org/10.1080/15226514.2014.964847.

Hejna, M., Gottardo, D., Baldi, A., Dell'Orto, V., Cheli, F., Zaninelli, M., et al., 2018. Review: nutritional ecology of heavy metals. Animal 1–15. https://doi.org/10.1017/S175173111700355X.

Hejna, M., Moscatelli, A., Onelli, E., Baldi, A., Pilu, S., Rossi, 2019. Evaluation of concentration of heavy metals in animal rearing system. Ital. J. Anim. Sci. https://doi.org/10.1080/1828051X.2019.1642806.

Hemmati, F., Yazdi Nezhad, M., 2012. Survey of *Typha Latifolia* for phytoremediation of cadmium in international shadegan wetland. Adv. Environ. Biol. 6 (12), 4041–4044.

Higuchi, K., Kanai, M., Tsuchiya, M., Ishii, H., Shibuya, N., Fujita, N., et al., 2015. Common reed accumulates starch in its stem by metabolic adaptation under Cd stress conditions. Front. Plant Sci. 138 https://doi.org/10.3389/fpls.2015.00138.

Jakubus, M., Dach, J., Starmans, D., 2013. Bioavailability of copper and zinc in pig and cattle slurries. Fresenius Environ. Bull. 22 (4), 995–1002. https://doi.org/10.2527/jas.53895.

Jarup, L., 2003. Hazards of heavy metal contamination. Br. Med. Bull. 167–182. https://doi.org/10.1093/bmb/ldg032.

Klink, A., 2017. A comparison of trace metal bioaccumulation and distribution in *Typha latifolia* and *Phragmites australis*: implication for phytoremediation. Environ. Sci. Pollut. Res. Int. 3843–3852. https://doi.org/10.1007/s11356-016-8135-6.

Klink, A., Macioł, A., Wisłocka, M., Krawczyk, J., 2013. Metal accumulation and distribution in the organs of *Typha latifolia L.* (cattail) and their potential use in bioindication. Limnologica 164–168. https://doi.org/10.1016/j.limno.2012.08.012.

Klink, A., Polechońska, L., Cegłowska, A., Stankiewicz, A., 2016. *Typha latifolia* (broadleaf cattail) as bioindicator of different types of pollution in aquatic ecosystems-application of self-organizing feature map (neural network). Environ. Sci. Pollut. Res. Int. 14078–14086. https://doi.org/10.1007/s11356-016-6581-9.

Kumari, M., Tripathi, B.D., 2015. Effect of *Phragmites australis* and *Typha latifolia* on biofiltration of heavy metals from secondary treated effluent. Int. J. Environ. Sci. Technol. 1029–1038. https://doi.org/10.1007/s13762-013-0475-x.

Liu, Y., Espinosa, C.D., Abelilla, J.J., Casas, G.A., Lagos, L.V., Lee, S.A., Kwon, W.B., Mathai, J.K., Navarro, D.M.D.L., Jaworski, N.W., Stein, H.H., 2018. Non-antibiotic feed additives in diets for pigs: a review. Anim. Nutr. 1–13. https://doi.org/10.1016/j.aninu.2018.01.007.

Lone, M.I., He, Z., Stoffella, P.J., Yang, X., 2008. Phytoremediation of heavy metal polluted soils and water: progresses and perspectives. J. Zhejiang Univ. - Sci. 210–220.

Lopez-Alonso, M., Garcia-Vaquero, M., Benedito, J.L., Castillo, C., Miranda, M., 2012. Trace mineral status and toxic metal accumulation in extensive and intensive pigs in NW Spain. Livest. Sci. 47–53. https://doi.org/10.1016/j.livsci.2012.02.019.

Lyubenova, L., Schröder, P., 2011. Plants for wastewater treatment - effects of heavy metals on the detoxification system of *Typha latifolia*. Bioresour. Technol. 996–1004. https://doi.org/10.1016/j.biortech.2010.09.072.

Lyubenova, L., Kuhn, A.J., Höltkemeier, A., Schröder, P., 2013. Root exudation pattern of *Typha latifolia* L. plants after copper exposure. Plant Soil 187. https://doi.org/10.1007/s11104-013-1634-z.

Ma, Y., Egodawatta, P., McGree, J., Liu, A., Goonetilleke, A., 2016. Human health risk assessment of heavy metals in urban stormwater. Sci. Total Environ. 557–558, 764–772. https://doi.org/10.1016/j.scitotenv.2016.03.067.

Manios, T., Stentiford, E.I., Millner, P., 2002. The effect of heavy metals on the total protein concentration of *Typha latifolia* plants, growing in a substrate containing sewage sludge compost and watered with metaliferus wastewater. J. Environ. Sci. Health A Tox. Hazard Subst. Environ. Eng. 1441–1451. https://doi.org/10.1081/ESE-1200013268.

Manios, T., Stentiford, E.I., Millner, P., 2003a. Removal of heavy metals from a metaliferous water solution by *Typha latifolia* plants and sewage sludge compost. Chemosphere 487–494. https://doi.org/10.1016/S0045-6535(03)00537-X.

Manios, T., Stentiford, E.I., Millner, P.A., 2003b. The effect of heavy metals accumulation on the chlorophyll concentration of *Typha latifolia* plants, growing in a substrate containing sewage sludge compost and watered with metaliferus water. Ecol. Eng. 65–74. https://doi.org/10.1016/S0925-8574(03)00004-1.

Maric, M., Antonijevic, M., Alagic, S., 2013. The investigation of the possibility for using some wild and cultivated plants as hyperaccumulators of heavy metals from contaminated soil. Environ. Sci. Pollut. Res. 1181–1188. https://doi.org/10.1007/s11356-012-1007-9.

Melià, P., Ruggieri, G., Sabbadini, S., Dotelli, G., 2014. Environmental impacts of natural and conventional building materials: a case study on earth plasters. J. Clean. Prod. 179–186. https://doi.org/10.1016/j.jclepro.2014.05.073.

Milam, C.D., Bouldin, J.L., Farris, J.L., Schulz, R., Moore, M.T., Bennett, E.R., Cooper, C.M., Smith Jr., S., 2004. Evaluating acute effect of methyl parathionapplication in constructed wetland mesocosms. Environ. Toxicol. 471–479. https://doi.org/10.1002/tox.20052.

Moral, R., Moreno Caselles, J., Perez-Murcia, M.D., Perez-Espinosa, A., Rufete, B., Paredes, C., 2005. Characterisation of the organic matter pool in manures. Bioresour. Technol. 96, 153–158. https://doi.org/10.1016/j.biortech.2004.05.003.

Morel, J.C., Mesbah, A., Oggero, M., Walker, P., 2001. Building houses with local materials: means to drastically reduce the environmental impact of construction. Build. Environ. 1119–1126. https://doi.org/10.1016/S0360-1323(00)00054-8.

Mukhopadhyay, S., Maiti, S.K., 2010. Phytoremediation of metal enriched mine waste: a review. Glob. J. Environ. Res. 135–150.

Nicholson, F.A., Smith, S.R., Allowayc, B.J., Carlton-Smithd, C., Chambersa, B.J., 2003. An inventory of heavy metals inputs to agricultural soils in England and Wales. Sci. Total Environ. 205–219. https://doi.org/10.1016/S0048-9697(03)00139-6.

Oves, M., Saghir Khan, M., Huda Qari, A., Nadeen, et al., 2016. Heavy metals: biological importance and detoxification strategies. J. Biorem. Biodegrad. 334 https://doi.org/10.4172/2155-6199.1000334.

Peralta, J.R., Gardea-Torresdey, J.R., Tiemann, K.J., Gomez, E., Arteaga, S., Rascon, E., et al., 2001. Uptake and effects of five heavy metals on seed germination and plant growth in Alfalfa (*Medicago sativa L.*). Bull. Environ. Contam. Toxicol. 727–734. https://doi.org/10.1007/s001280069.

Peterson, H.G., 1998. Use of constructed wetlands to process agricultural wastewater. Can. J. Plant Sci. 199–210. https://doi.org/10.4141/P97-142.

Petroselli, A., Giannotti, M., Allegrini, E., Marras, T., 2015. Integrated system of phytodepuration for agroindustrial wastewater: three different case studies. Int. J. Phytoremediation 1227–1236. https://doi.org/10.1080/15226514.2015.1045138.

Rafati, M., Khorasani, N., Moattar, F., Shirvany, A., Moraghebi, F., Hosseinzadeh, S., 2011. Phytoremediation potential of *Populus Alba* and *Morus alba* for cadmium, chromuim and nickel absorption from polluted soil. Int. J. Environ. Res. 961–970. https://doi.org/10.22059/ijer.2011.453.

Rai, U.N., Sinha, S., Tripathi, R.D., Chandra, T.P., 1995. Wastewater treatability potential of some aquatic macrophytes: removal of heavy metals. Ecol. Eng. 5–12. https://doi.org/10.1016/0925-8574(95)00011-7.

Rodriguez-Hernandez, M.C., García De la-Cruz, R.F., Leyva, E., Navarro-Tovar, G., 2017. *Typha latifolia* as potential phytoremediator of 2,4-dichlorophenol: analysis of tolerance, uptake and possible transformation processes. Chemosphere 190–198. https://doi.org/10.1016/j.chemosphere.2016.12.043.

Rossi, L., Di Giancamillo, A., Reggi, S., Domeneghini, C., Baldi, A., Sala, V., et al., 2013. Expression of verocytotoxic *Escherichia coli* antigens in tobacco seeds and evaluation of gut immunity after oral administration in mouse model. J. Vet. Sci. 263–270. https://doi.org/10.4142/jvs.2013.14.3.263.

Rossi, L., Pinotti, L., Agazzi, A., Dell'Orto, V., Baldi, A., 2014a. Plant bioreactors for the antigenic hook-associated flgK protein expression. Ital. J. Anim. Sci. 2939 https://doi.org/10.4081/ijas.2014.2939.

Rossi, L., Dell'Orto, V., Vagni, S., Sala, V., Reggi, S., Baldi, A., 2014b. Protective effect of oral administration of transgenic tobacco seeds against verocytotoxic *Escherichia coli* strain in piglets. Vet. Res. Commun. 39, 49. https://doi.org/10.1007/s11259-013-9583-9.

Salem, Z.B., Laffray, X., Al-Ashoor, A., Ayadi, H., Aleya, L., 2017. Metals and metalloid bioconcentrations in the tissues of *Typha latifolia* grown in the four interconnected ponds of a domestic landfill site. J. Environ. Sci. 56–68. https://doi.org/10.1016/j.jes.2015.10.039.

Stroppa, N., Onelli, E., Hejna, M., Rossi, L., Gagliardi, A., Bini, L., Baldi, A., Moscatelli, A., 2019. *Typha latifolia* and *Thelypteris palustris* behavior in a pilot system for the refinement of livestock wastewaters: a case of study. Chemosphere 124915. https://doi.org/10.1016/j.chemosphere.2019.124915.

Thangavel, P., Subbhuraam, C., 2004. Phytoextraction: role of hyperaccumulators in metal contaminated soils. Proc. Natl. Acad. Sci. 109–130.

Todeschini, V., Lingua, G., D'Agostino, G., Carniato, F., Roccotiello, E., Berta, G., 2011. Effects of high zinc concentration on poplar leaves: a morphological and biochemical study. Environ. Exp. Bot. 50–56. https://doi.org/10.1016/j.envexpbot.2010.10.018.

Venkatarama Reddy, B.V., Prasanna Kumar, P., 2010. Embodied energy in cement stabilised rammed earth walls. Energy Build. 380–385. https://doi.org/10.1016/j.enbuild.2009.10.005.

Yadav, A.K., Abbassi, R., Kumar, N., Satya, S., Sreekrishnan, T.R., Mishra, B.K., 2012. The removal of heavy metals in wetland microcosms: effects of bed depth, plant species, and metal mobility. Chem. Eng. J. 501–507. https://doi.org/10.1016/j.cej.2012.09.039.

Yang, J., Ye, Z., 2009. Metal accumulation and tolerance in wetland plants. Front. Biol. China 282–288. https://doi.org/10.1007/s11515-009-0024-7.

Ye, Z.H., Baker, A.J.M., Wong, M.H., Willis, A.J., 1997. Copper and nickel uptake, accumulation and tolerance in *Typha latifolia* with and without iron plaque on the root surface. New Phytol. 481–488.

International Journal of
Environmental Research and Public Health

MDPI

Review

Heavy-Metal Phytoremediation from Livestock Wastewater and Exploitation of Exhausted Biomass

Monika Hejna [1], Elisabetta Onelli [2,*], Alessandra Moscatelli [2], Maurizio Bellotto [3], Cinzia Cristiani [3], Nadia Stroppa [2] and Luciana Rossi [1]

[1] Department of Health, Animal Science and Food Safety, Università degli Studi di Milano, 20133 Milan, Italy; monika.hejna@unimi.it (M.H.); luciana.rossi@unimi.it (L.R.)
[2] Department of Biosciences, Università degli Studi di Milano, 20133 Milan, Italy; alessandra.moscatelli@unimi.it (A.M.); nadia.stroppa@unimi.it (N.S.)
[3] Department of Chemistry, Materials and Chemical Engineering "G. Natta", Politecnico di Milano, 20133 Milan, Italy; maurizio.bellotto@opigeo.eu (M.B.); cinzia.cristiani@polimi.it (C.C.)
* Correspondence: elisabetta.onelli@unimi.it

Abstract: Sustainable agriculture is aimed at long-term crop and livestock production with a minimal impact on the environment. However, agricultural practices from animal production can contribute to global pollution due to heavy metals from the feed additives that are used to ensure the nutritional requirements and also promote animal health and optimize production. The bioavailability of essential mineral sources is limited; thus, the metals are widely found in the manure. Via the manure, metallic ions can contaminate livestock wastewater, drastically reducing its potential recycling for irrigation. Phytoremediation, which is an efficient and cost-effective cleanup technique, could be implemented to reduce the wastewater pollution from livestock production, in order to maintain the water conservation. Plants use various strategies for the absorption and translocation of heavy metals, and they have been widely used to remediate livestock wastewater. In addition, the pollutants concentrated in the plants can be exhausted and used as heat to enhance plant growth and further concentrate the metals, making recycling a possible option. The biomass of the plants can also be used for biogas production in anaerobic fermentation. Combining phytoremediation and biorefinery processes would add value to both approaches and facilitate metal recovery. This review focuses on the concept of agro-ecology, specifically the excessive use of heavy metals in animal production, the various techniques and adaptations of the heavy-metal phytoremediation from livestock wastewater, and further applications of exhausted phytoremediated biomass.

Keywords: sustainable agriculture; phytoremediation techniques; heavy metals; wastewater; exhausted biomass reuse

Citation: Hejna, M.; Onelli, E.; Moscatelli, A.; Bellotto, M.; Cristiani, C.; Stroppa, N.; Rossi, L. Heavy-Metal Phytoremediation from Livestock Wastewater and Exploitation of Exhausted Biomass. *Int. J. Environ. Res. Public Health* **2021**, *18*, 2239. https://doi.org/10.3390/ijerph18052239

Academic Editors: Luís Novo and Rui S. Oliveira

Received: 11 January 2021
Accepted: 18 February 2021
Published: 24 February 2021

1. Sustainability in Animal Production

Sustainability is aimed at the best use of environmental services without any negative or harmful impact [1]. Sustainable agriculture, which is focused on long-term crop and livestock production with a minimal impact on the environment, is thus an immediate global priority in order to ensure a balance between food production and the preservation of the environment. In addition, many goals related to sustainable agriculture and the modern principles of agro-ecology need to be effectively implemented in food production. These include (i) water conservation, (ii) a reduction in the use of fertilizers and pesticides, and (iii) promotion of biodiversity throughout the entire agro-ecosystem, as well as (iv) the continued economic profitability of farms [2,3]. Products, processes, and business models therefore need to be redesigned to maximize the value and utility of natural resources, while at the same time reducing adverse health and environmental impacts and climate changes [4].

Swine production is one of the most important branches of food production, and pork is the most consumed meat worldwide. The fast growth of the swine production sector has contributed to high economic gain due to the relatively short life cycle of pigs that have a high feed conversion ratio and reproductive rate. In animal production, nutrition, where animals are fed in line with the nutritional ecology strategy, and management are thus crucial in order to improve swine rearing, maintain animal well-being, meet the sustainable livestock production goals, and reduce water contamination, including heavy-metals (HMs) pollution from livestock-related activities [5].

2. The Importance of Heavy-Metals Use in Intensive Animal Production

Heavy metals (HMs) are metallic elements that have a high density compared to water and induce toxicity at low exposure levels [6–10]. Some heavy metals are essential to maintain biochemical and physiological functions, although excessive exposure has been linked with cellular or systemic disorders, acute and chronic toxicity, and sources of pollution [11]. Different HMs can enter animal diets both as contaminants/undesirable substances and as essential nutrients (Table 1) [12,13]. In the farming industry, essential trace elements are usually used as feed additives in order to not only satisfy the nutritional requirements and prevent nutritional deficiencies but also to promote health and welfare, optimize production, and improve food safety [14]. These elements are included within animal diets as mineral additives (Table 1) in compliance with the maximum admitted levels [15].

Table 1. Heavy metals in animal nutrition [6,9].

Essential Elements (authorized in animal nutrition according to EC N°1831/2003)								
Co (cobalt)	Cr (chromium)	Cu (copper)	Fe (iron)	Mn (manganese)	Mo (molybdenum)	Ni (nickel)	Se (selenium)	Zn (zinc)
Nonessential elements (undesirable elements according to 2002/32/EC)								
	As (arsenic)		Cd (cadmium)		Hg (mercury)		Pb (lead)	

Heavy metals can also enter animal diets as contaminants with no established biological functions [16]. Arsenic (As), cadmium (Cd), chrome (Cr), lead (Pb), nickel (Ni), and mercury (Hg), which are a major risk to public health, are highly toxic and can induce organ damage even at low exposure levels. In line with previous research [17], swine and cattle were not affected by high amounts of these undesirable elements in the animal feed.

3. The Importance of Zinc and Copper as Alternative to Antibiotics in Animal Feeding

In intensive livestock, weaning is the most critical stage associated with low feed intake, influencing the growth performance, and with fluctuations in gut function, making piglets sensitive to digestive disorders. Weaning stress is a major cause of diarrhea and is often associated with many pathotypes of *Escherichia coli* infection of the intestine [18]. Previously, antibiotic growth promoters (AGPs) were used to reduce the instance of diarrhea at weaning. However, antibiotic resistance is a global concern, and restricting the use of antimicrobials in food-producing animals has reduced the prevalence of antimicrobial resistance in bacteria isolated from farm animals [19]. In the last decade in the EU, the state of livestock has thus changed significantly due to the ban on antibiotics [20], which has led to the study of alternative compounds. The first adopted alternative to feed antibiotics was the application of high doses of zinc and copper salts in the form of a premix to control enteric diseases in the growing phase.

Zinc is toxic to animals, bacteria, and plants when encountered in high concentrations; however, it is also essential in the maintenance and restoration of barrier integrity, protec-

tion against pathogens, and modulation of the immune system by promoting antibody production against pathogens [11]. Today, zinc oxide (ZnO), which is the most common form of Zn, is widely used (up to 150 ppm in complete feed) to maintain the nutritional requirements of weaning [21]. In addition, Zn is applied in pharmacological doses (from 1000 to 3000 mg/kg feed) as an alternative to antibiotics in order to promote growth performance [22,23] and to control enteric intestinal bacterial disorders as well as enhancing the immune system for diarrhea prevention in pigs [22].

Copper (Cu) is also an important mineral that is widely used as a supplement in the diet of weaning pigs due to its role in increasing growth performance and favoring a better feed conversion ratio [24]. In pigs, dietary concentrations from 150 to 250 mg of Cu/kg can maximize growth performance without any risk of poisoning. The routine inclusion of $CuSO_4$, which is the most common form of Cu, in diets was found to reduce intestinal diseases and to be a cost-effective solution to the replacement of growth-promoting antimicrobials in pig diets [25].

4. Heavy Metals and Their Impact on the Environment

Despite the antibacterial and anti-inflammatory activities of zinc and copper salts, their wide use has raised many concerns related to environmental pollution, especially soil and groundwater contamination [6]. Mainly because the bioavailability and digestibility of Zn and Cu sources are limited, the metals are thus partially digested by animals, and the excess is eliminated by excretion in feces and found in the manure [26]. Several studies indicated that Zn and Cu are widely found in pig manure [17,27–30], cattle [30], and poultry livestock manure [27,28] as a result of their high doses in swine diets (Table 2).

Table 2. Concentration of Zn and Cu in livestock manures [27–30].

Area	Heavy Metal			Source of Heavy Metals		
				Swine Slurry	Cattle Slurry	Poultry Slurry
England	Zn	mg/kg d.w.		650.0	170.0	217.0
	Cu			470.0	45.0	32.0
Netherlands	Zn	$mg \cdot kg^{-1}$		186.2	73.7	-
	Cu			644.7	296.3	-
China	Zn	mg/kg d.w.		843.3	151.9	308.9
	Cu			472.6	46.5	102.0
China	Zn	mg/kg d.w.	[a] S	119.1	674.7	268.2
			[b] M	126.3	476.0	241.7
			[c] L	136.1	691.6	384.2
	Cu		S	30.8	958.8	51.6
			M	31.0	420.4	57.2
			L	31.4	612.2	87.1

[a] S—small animal population (head): cattle <100, chicken <2000, swine <200. [b] M—middle animal population (head): cattle 100–300, chicken >2000, swine 200–800. [c] L—large animal population (head): cattle >300, chicken >20,000, swine >800. d.w.—dry weight.

The HMs content in manure is therefore its reflection of the feed [27,31–33]. Through the manure, large amounts of metallic ions may enter to the livestock soil (Table 3) [6,7,28,34]. Moreover, through the animal manure, large amounts of metals may also enter to livestock wastewater and may drastically reducing their potential use for agricultural irrigation [27–30,35,36].

Table 3. Annual input of Zn and Cu in soil for 1 mln of ha [27,28,34].

Region		China	France	Germany	United Kingdom	Netherlands
Total land area (mln ha)		122.0	29.0	17.0	11.1	2.0
Heavy metals	Zn (g/ha^{-1})	1538.9	523.8	1249.2	453.9	684.5
	Cu (g/ha^{-1})	588.7	167.9	269.2	146.0	294.0

Moreover, the use of zinc and copper in animal feed may also have contributed to the emergence of methicillin-resistant *Staphylococcus aureus* (MRSA) due to the potential increase in the prevalence of antibiotic-resistant bacteria [11,37–39]. MRSA is rarely a clinically significant pathogen in pigs; however, it is one of leading causes of opportunistic infection in humans due to the increased burden on healthcare systems and treatment failures associated with antimicrobial therapy. Some recent evidence suggests that the use of zinc, copper, and metals in pigs is a risk factor for MRSA, as these compounds are associated with the co-selection of resistance genes to antibiotics [38]. Resistance determinants for zinc and copper are wide-spread among MRSA of pig origin and provide selective pressure on antimicrobial-resistant bacteria, which is why the implementation of high doses of these metals may play a role in maintaining antimicrobial resistance. In addition, copper can impose selective pressure on the bacterial community's of its tolerance during manure composting. In light of this, exposure to trace metals may also contribute to antibiotic resistance, even in the absence of antibiotics themselves. Consequently, antibiotic resistance due to Zn and Cu may expose a zoonotic pathogen in animal production [11,37,38,40,41].

The anthropogenic contamination of the environment with HMs is thus a serious problem, and their long-term accumulation in the environment has led to their propagation in the food chain by accidental ingestion of soil, contamination of edible plants through the soil, or the consumption of contaminated animal-derived food products (Figure 1) [12].

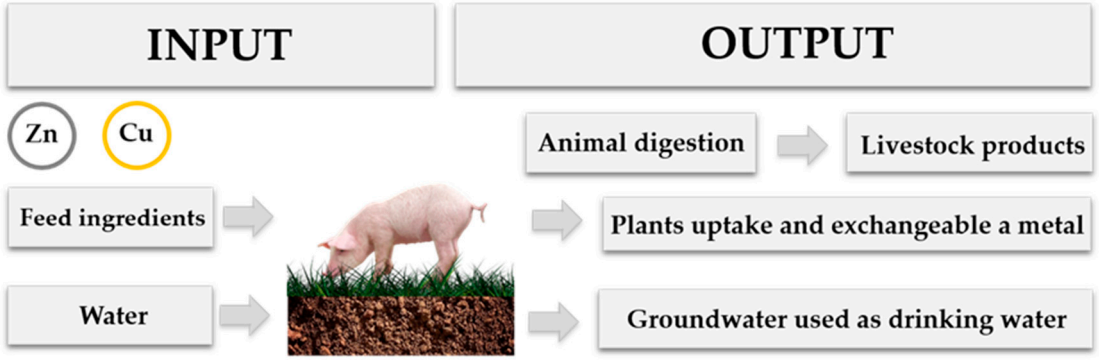

Figure 1. Possible routes of HMs entrance to the food chain and the consequences of their output.

The focus of EU environmental protection policies is on promoting economic growth together with the reduction in the impact of HMs [42]. Animals require essential minerals in their diets to meet the animals' physiological needs and maintain various metabolic functions; hence, they are included in the European register of feed additives. European authorities have thus adopted various measures to control the HMs in the environment which are the result of human activities such as farming and industry. The comprehensive regulations on the maximum authorized admissible concentrations of essential and undesirable trace elements in additives have been established for animal nutrition [16,20]. The EU also recently decided to ban the inclusion of pharmacological levels of zinc oxide in animal feed after 2022 [43], because the overall balance between the benefits and risks remains negative for feed additives containing zinc oxide. Similarly, the new maximum admissible Cu content (for different Cu sources) was also established in complete feed for different animal species [44] in order to protect feed and food safety and ultimately human health.

5. How Can Plants Remove Metals from Livestock Wastewater?

Animals should be fed in accordance with nutritional ecology strategies because livestock nutrition plays a pivotal role in controlling environmental pollution [5]. However, if the nutritional ecology strategy is not sufficient to reduce the wastewater pollution from livestock production and to ensure water conservation, then efficient, cost-effective, reliable, and apt materials and methods need to be developed and locally implemented.

This can be achieved through multidisciplinary research aimed at studying water pollution for the appropriate management of water resources [6,7], because in swine farms, HMs contamination of wastewater considerably reduces its potential for being recycled in irrigation [12,27,31,35]. Traditional wastewater treatment technologies [27] are ineffective in providing adequate safe water due to the increasing demand for water, coupled with stringent health guidelines and emerging contaminants. New materials and methods are therefore needed in order to obtain considerable potable water savings through the reuse of wastewater.

Over the last few years, plants have been widely used to remediate wastewater from livestock induced pollution [45–50], due to their ability to remove HMs and other contaminants from the soil and water [51,52]. The most useful method for phytoremediation of livestock manure and wastewater can be achieved through constructed wetlands (CWs), which uptake metals and organic matter from water and mimic natural wetland processes at biological, chemical, and physiological levels [47,53–55]. CWs are mainly used for treating municipal, industrial, storm and agricultural waters, landfill leachate, and mine drainage wastewater, thus facilitating the recovery of both organic and inorganic compounds [53–55]. CWs can recover contaminants mainly due to the removal capability of microorganisms and to the pollutants' adsorption from the substrate. Plants are able to extract contaminants through the root system and improve pollutant removal by providing an appropriate environment for rhizosphere microorganism growth or by modifying chemicals by improving their biological availability [51–55].

5.1. How Plants Function in the Phytoremediation of Heavy Metals

Some plants are able to uptake HMs from soil or water, due to the roots' ability to adsorb and translocate these compounds in plant cells. Plants adopt both avoidance and tolerance to deal with the toxicity of HMs [52,56]. Avoidance is the first line of defense, and plants limit the uptake of HMs and their entry in the root tissues [57]. The mechanisms of avoidance work at different levels and involve (i) cell wall modification through callose, suberin, or lignin deposition [58]; (ii) the sequestration of metals into the cell wall [59–63]; (iii) the secretion of a root extracellular matrix which binds ions, stabilizing HMs in the rhizosphere and limiting their assimilation [57,64]; and (iv) the removal of excess metals by leaf glands [56]. Mycorrhizae could also function as avoidance mechanisms since fungi are able to uptake and immobilize metals into the mycelium, inhibiting translocation to the root tissues. In addition, fungi activate detoxification or chelation, thus reducing metal uptake from plants [65,66].

Rhizosphere microorganisms also support plants phytoremediation because they increase metal tolerance by enhancing metal bioavailability and their translocation in root tissues [67–69]. Tolerance mechanisms enable plant cells to accumulate metal ions in cell walls and vacuoles after chelation by amino acids, phytochelatins, metallothioneins, pectins, and phenols [70–76]. In addition, tolerance strategies involve proteins in metal detoxification metabolism, signal transduction, stress, and ROS signaling [77–80].

The ability to persist in HM-polluted environments enables some plants to be used for phytoremediation. Several phytoremediation strategies are applied for different substrates and different contaminants, most of which are used for both HMs-polluted soil and water. Phytostabilization uses plants to immobilize metals in the substrate or in the rhizosphere, preventing their leaching to groundwater. Microorganisms from the rhizosphere are also involved, which cooperate with plants, thus improving phytostabilization [52,56]. Phytoextraction, on the other hand, is exploited by plants to uptake metals inside the roots or underground organs, and to translocate and accumulate them in aboveground tissues. The evaporation of assimilated metals through leaves is defined as phytoevaporation [52,56].

For contaminated waters, the most common strategy used is phytofiltration, which includes the use of plant roots (rhizofiltration), shoots (caulofiltration), and seedlings (blastofiltration). In rhizofiltration, metals are adsorbed on the root or rhizome surface or accumulated in root or rhizome tissues. Most of the metals remain in the aboveground

organs and only a small amount is translocated to the shoots. For this reason, plants with an extensive root system and high aboveground biomass are used [51,53,56,81]. This strategy, as well as phytoextraction and phytostabilization, is applied extensively in CWs.

5.2. CWs in the Phytoremediation of Heavy Metals from Livestock Wastewater

Pig manure is processed by separating the liquid and solid fractions. Waters obtained by sedimentation need to be refined in order to be reused for field irrigation. In the secondary or tertiary treatment, CWs are widely used, particularly for nitrogen and phosphorous recovery [45,53,82]. However, recent data have highlighted the use of CWs for HMs remediation [46,48,51,83–85]. In particular, both horizontal-vertical and surface-subsurface flow of CWs (S-CWs and SF-CWs, respectively) are used for treating HM-polluted water [46,54,86,87].

In the S-CW system, water flows above the substrate, while in SF-CWs, water flows inside the porous substrate (Figure 2) [53,54]. The S-CWs is effective for the removal of suspended solid, biochemical oxygen demand (BOD_5), nitrogen, and HMs, while phosphorous removal is limited. The flow of water in SF-CWs can be horizontal or vertical. In the horizontal SF-CWs, the improvement in microorganism growth conditions in the rhizosphere enhances the removal of organic matter. On the other hand, in vertical SF-CWs, nitrogen and phosphorous removal also occurs. For this reason, the combination of different CWs are used in order to improve the efficiency of the remediation system [53,54]. More complex hybrid CWs were extensively described in Stefanakis et al. [54]. Usually, plants in the CWs accumulate HMs in their aboveground biomass [88,89]. This feature is considered important for a good bioremediation together with the limited translocation ability of HMs in the shoot and the tolerance to high level of HMs [90,91].

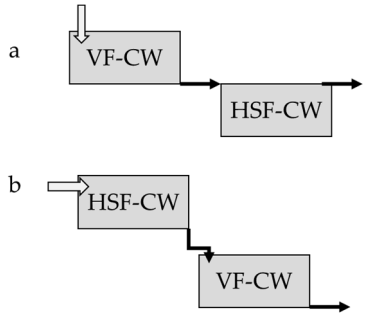

Figure 2. Diagram of hybrid constructed wetland where, (**a**) is vertical flow SF-CWs followed by horizontal flow SF-CWs and (**b**) is horizontal flow SF-CWs followed by vertical flow SF-CWs.

One of the most efficient plants used to reduce HMs in wetlands is the water hyacinth (*Eichhornia crassipes)*. This plant accumulates metals, such as Cd, Cr, Ni, Fe, and also Cu and Zn, in the root system and reduces their concentration in municipal and industrial wastewater, thus facilitating water reuse in agricultural systems [84,92,93]. *Eichhornia crassipes* is also efficient in CWs designed for pretreated swine effluent [45]. However, these SF-CWs are mostly able to efficiently remove suspended solids (96–99%), chemical oxygen demand (COD; 77–84%), total phosphorous (47–59%), and total nitrogen (10–24%). In terms of HMs, macrophytes have been found to be more effective for treating the liquid fraction of municipal wastewater or pig manure [46,85,86]. In fact, CWs with *Phragmites australis* reduce Cu and Zn levels, as well as COD, phosphorous, and nitrogen. However, while in these systems the sediment or belowground biomass plays a major role in Cu retention, plant uptake, and translocation accounts for about 30% of Zn retention [46]. A more recent study showed that *Phragmites australis* accumulates metals in the roots and rhizomes, and at lower levels, in the stems and leaves, and thus *Phragmites australis* efficiently removed Cu, Fe, Mn, and Zn from livestock wastewater in the CWs [48]. In wetland microcosms, also *Canna indica* L., *Typha angustifolia* L., and *Cyperus alternifolius* L. were very efficient for HMs removal in vertical CWs [89,94,95]. All these species with features described above fit for

plants useful in CWs, because they showed (i) developed rhizomes and root system able to accumulate and retain HMs, (ii) low translocation ability of HMs in aboveground biomass, (iii) mechanisms of HMs tolerance, being able to growth in contaminated environment, and (iv) mechanisms able to growth in wetland environment [49,50].

While different publications documented the ability of plants in HMs remediation in CWs, only a few papers reported the biological mechanisms allowing plants to live in high-HMs-contaminated wet environment. In plants which are suitable for CWs, tolerance mechanisms include (i) synthesis of phytochelatins, peptides, and exudates to chelate-free metal ions, (ii) the increasing of antioxidant enzyme activities, and (iii) the sequestration of HMs in organs or subcellular compartments [96–99]. Among plants with those features, *Typha latifolia* is a macrophyte which accumulates HMs in its tissues and has therefore been used in the phytoremediation of wastewater for irrigation reuse [49,50,86]. *Typha latifolia* was found to accumulate Mn, B, Pb, Zn, and Cu in the root system. However, as *Phragmites australis*, it had a limited ability to translocate metals in the shoots. This plant therefore plays an important role in both rhizofiltration and phytostabilization in CWs [86].

Typha latifolia also works in smaller systems, such as nonintensive pig farms [49,50]. In a pilot system for the refinement of the liquid fraction of manure, *Typha latifolia*, associated with the marsh fern (*Thelypteris palustris)* was effective in the uptake of Zn and Cu [49]. In this system, the contribution to metal stabilization of both the substrate and rhizosphere was found to be relevant. Both plants contribute to the phytoremediation of metals. *Typha latifolia* activates various tolerance mechanisms, making it more suitable for the long-term phytodepuration of livestock wastewater. On the other hand, marsh fern was more sensitive but accumulated metals more efficiently within a short time. Thus, the use of both plants in this phytoremediation system was significantly effective [50]. Moreover, although neither plant showed macroscopical alterations, microscopical observations revealed that both rhizome and leaf morphology were affected by the exposure to Zn and Cu. *Thelypteris palustris* was more sensitive than *Typha latifolia*, because the modification in both the leaf and rhizome cells (cell shape, cell wall thickness, and pectin distribution) and carbohydrate metabolism indicated that the marsh fern was affected more by the presence of the two metals. On the other hand, the accumulation of amyloplasts instead of chloroplasts during leaf senescence in *Typha latifolia*, together with the decrease in starch in rhizomes, could be considered as part of a tolerance mechanism [50]. The altered carbohydrate metabolism in this plant [45,46] could be due to the requirement of soluble sugars, which is important in preserving biological molecules and membranes while a plant is in stressed condition [100].

In several plant phytoremediation models, one tolerance strategy is sequestration into the cell wall, because cell-wall polysaccharides play a major role in binding and accumulating HMs in order to remove them from protoplasts [62,101]. In these plants, the tolerance mechanism induces a thickening of the cell wall and pectin remodeling by modulating the degree of melthyl-esterification, thus affecting the ability of the cell wall to bind metals [60,62,102,103]. Unlike most plants used for phytoremediation, *Typha latifolia* and *Thelypteris palustris* showed a significant reduction in cell wall thickening in rhizomes after metal exposure [50]. In addition, changes in the balance between esterified and de-esterified pectins did not follow the phytoremediation model, suggesting that these modifications are part of a toxic response rather than a tolerance mechanism. These modifications were related to alteration of cytoskeleton protein induced by metals exposures. Proteomic analysis showed a decrease of both actin and microtubules. Actin filaments and microtubules are needed for secretion processes during cell wall building suggesting that these modifications are not part of a tolerance mechanism [50].

Plants used for metals uptake are numerous, and Sandoval et al. [104] summarized some natural and ornamental plants for phytoremediation in CWs. However, the use of *Typha latifolia* and *Thelypteris palustris* in a pilot system suggested that macrophytes could be useful in CWs for HMs remediation of livestock wastewater, thanks to their ability to produce higher underground biomass able to accumulate HMs without translocating them

in belowground organs. Toleration or avoiding mechanisms allowed plants to grow and act in CWs for long time.

6. Plant Reuse after Phytoremediation

After a successful phytoremediation, every part of the plant contains heavy-metal pollutants due to the transport processes. Phytoremediation may thus result in potentially hazardous biomass. The downstream processing of the biomass is therefore an integral part of the remediation approach. Phytoremediation techniques have several advantages over physical or chemical processes for treating wastewater. Physical processes involve the precipitation of the HMs as insoluble salts or hydroxides, followed by flocculation and separation. Chemical processes involve HMs adsorption onto a substrate, which is subsequently regenerated by ion exchange or disposed by landfilling.

Both approaches need a significant surface area for the installations, use of chemicals (for pH control, flocculation, adsorption, and regeneration), and energy for pumping and stirring. The quality of the landscape is preserved or even improved by phytoremediation, which also has a limited environmental impact given that it uses mostly solar energy. However, life-cycle assessments (LCAs) have shown that if the produced biomass is not enhanced, the sustainability of phytoremediation is questionable compared to landfilling [105].

During phytoremediation, the pollutants are concentrated in the plants, and ashing of the exhaust harvested plants further concentrates the metals, making recycling possible. Moreover, the recovery of the ashing-generated heat may be used for enhancing plant growth [106,107]. Alternatively, the plants biomass may be used for biogas production in anaerobic fermentation processes [108–110].

6.1. Incineration

Phytoremediation biomass can be treated thermochemically, through gasification, pyrolysis or combustion, achieving a valorization to provide fuel gas that can be used for electricity generation or to produce heat [111]. The volume of the ashes is substantially reduced compared to the volume of the biomass. The HMs content in processed ash from the thermochemical process is further concentrated compared to the original biomass. The process conditions need to be selected so that they minimize HMs volatilization and concentrate them in the solid ashes. Reuse of the ash or recovery of the HMs is cost-effective, avoiding the disposal cost for toxic materials. This thermal treatment is used when the volumes produced are sufficient to operate an efficient large-scale efficient combustion. Heat generated directly through combustion or from the fuel gas can be used to foster plant growth and for the supply of ancillary items of the phytoremediation plant.

The resulting ash may be used as a pozzolanic addition to hydraulic binders in the formulation of composite Portland cement [112] and geopolymers [113]. This exploits the hydraulic activity of the calcined phytoliths as a source of reactive silica. To prevent the captured metals from leaching and being redispersed into the environment, they need to be fixed in the hardened hydrated structure. The fixation of the captured metals is more efficient for geopolymeric binders than Portland cement, due to the different pH of the interstitial solution and the different hydrated mineral phases [114], thus making geopolymers more attractive than Portland cement stabilization.

Metal enrichment in the ashes could also impact metal recovery and recycling of metals, particularly those included in the critical raw materials list [115]. Recovery has great potential when a limited number of metals are present in relatively high concentrations. Among others, some examples are Cu and Zn, present in swine wastewater, as a result of their addition to the animal feed for their antibacterial and anti-inflammatory activities. Another example is the recovery and recycling of the nickel, whose demand is increasing for the production of batteries, to replace cobalt both for political and environmental issues [116].

The recovery of HMs from phytoremediation biomass ashes can be performed through pyrometallurgical processes [117], however these energy-intensive treatments are not suited to the low volumes of ashes produced. A more suitable approach is the recovery of metals via solid–liquid adsorption and desorption processes [118]. This process is suitable for treating small volumes of ashes, which are first treated with a digestion process in order to solubilize the HMs, and then processed to adsorb the valuable metals on a properly designed solid. The adsorbed metals are then selectively desorbed and the solid regenerated [119].

6.2. Biotechnological Process

Fermentation of the exhaust biomass has demonstrated its potential for the degradation of lignocellulose to produce sugars and organic molecules of industrial interest. Anaerobic digestion refers to how organic materials are decomposed by microorganisms to produce biogas under anaerobic conditions [120]. The biogas mixture obtained contains on average 60% methane, which can be used as a substitute for fuel in boilers. As it has high N, P, and K contents, the associated liquid fraction can be used in agriculture [121].

Few studies have been conducted on the production of biogas by anaerobic fermentation from plant biomass used for the phytoremediation of industrial waste. The quantitative and qualitative increase in biogas generation from water hyacinths and water chestnuts grown in brass and electroplating industry effluent has been observed by Verma et al. [122]. The positive role of the waste stream, enhancing biogas production, is due to the presence of various pollutants that act as micronutrients for aquatic macrophytes/methanogens, especially at lower concentrations. Biomass grown in higher effluent concentrations severely reduced the methane content in the biogas owing to the methanogenesis inhibition caused by toxic effects due to the higher concentrations of metals. The production of biogas from plant biomass used for phytoremediation of a Cu-contaminated mine site was studied by Cao et al. [123]. In this case, 100 mg kg^{-1} Cu also promoted the anaerobic digestion and shortened the digestion times compared to the control group with a low Cu content. On the other hand, the presence of 500, 1000, and 5000 mg kg^{-1} Cu decreased cumulative biogas production by 12.5%, 14.9%, and 41.2%, respectively. Even higher Cu concentrations (>1000 mg kg^{-1}) significantly hampered the anaerobic digestion of plants.

Sotenko et al. [124] showed that nickel extracted from plants (*Sinapis alba* and *Helianthus annuus*) grown in contaminated soil can be easily extracted by aqueous extraction under mild conditions. The biomass was then subjected to solid-state fermentation as a downstream process. The plants that accumulated 11.9–15.1 ppm of nickel were degraded by the fungus *P. chrysosporium*. The contamination worsened the degradation of *H. annuus* by 10% but not that of *S. alba*. The pretreatment by aqueous extraction prior to fermentation increased the degradation yield by 14–15% for *S. alba*. Extraction was also found to significantly reduce the amount of soluble sugars from 56–106 to 18–24 mg g_{dw}. This led to the deficiency of available sugars and phenols and to the enhancement of the degrading fungus growth for *S. alba* but not for *H. annuus*. The degradation of lignocellulose that underwent pretreatment led to a higher final amount of sugars (ca. 50 mg g_{dw}) and phenols (5–6 mg g_{dw}) in the extracts.

7. Discussion and Conclusions

This review has focused on animal production as a possible source of HMs in the water which have negative effects on human and animal health. The concept of agro-ecology has been highlighted by describing phytoremediation strategies for HMs recovery from livestock wastewater and by the reuse of exhausted phytoremediated biomass.

Agricultural activity is a significant global concern in terms of its negative impact on the environment and on food chain [17,42,125,126]. Animal production and pig livestock in particular are a key link in the food chain and in the spread of heavy metals. Arsenic, cadmium, chrome, lead, and mercury are considered priority hazards to public health due to their high toxicity even at low exposure levels [16]. However, in general, they are

well controlled in the field. Conversely, many heavy metals (cobalt, copper, chromium, iron, manganese, molybdenum, selenium, zinc, and nickel) are essential nutrients with a wide array of vital physiological functions and which are usually added as additives in feed to satisfy the daily requirements [20]. Furthermore, in commercial conditions, feeding piglets with high doses of Zn and/or Cu stimulates piglets' daily gain and decreases the feed conversion factor. Until now, Zn and Cu have been widely used as growth promoters, although Europe is now adopting strategies for their reduction. Considering the low bioavailability of the mineral additives, which are more concentrated in feces that are usually used as soil organic fertilizers, Cu and Zn represent the most critical HMs in intensive pig production. Sustainable approaches that consider both input and output HMs are urgently needed to guarantee the reduction of the environmental pollution from livestock-related activities. Firstly, levels of Cu and Zn in diets for growing pigs should be reduced without detrimental effects on the production and mineral status. Secondly, higher dietary bioavailable organic complexes of these metals lead to a substantial reduction in the dietary inclusion rate, which should have a positive outcome for pig health and environmental sustainability. Thirdly, the potential sources of HMs outputs from livestock wastewater to the environment should be controlled. Integrated plant-based strategies such as CWs are thus a valuable tool for phytoremediation in order to reduce the high content metals from livestock wastewater.

Constructed wetlands are largely used for pollutant recovery of wastewater from different sources, and their efficiency of CWs in recovering HMs critically depends on the differences in uptake and translocation of HMs and other pollutants among plants used for phytoremediation. However, it is difficult to quantitatively define the performance of plants since the environment created in the CWs heavily shapes the pollutant removal efficiencies. Yadav et al. [89] showed that the wetland bed depth has direct significant effect on HMs removal efficiencies in vertical flow CWs. In fact, the removal of Cr, Ni, Cu, Zn and Co increased by 16.6%, 22.9%, 20.4%, 21.5%, and 21.8%, respectively, when the gravel bed depth of CWs was increased from 0.3 to 1.5 m. In addition, the presence of various microorganisms and the initial concentration of HMs also affect plant performance [127]. The higher HMs concentration in water induces the higher uptake by plants [95]. The pattern of CWs is also critical in conditioning the efficiency of plants in pollutant uptake. Sandoval et al. [104] presented a synthesis which could be used in the design of new CWs and suggested "there is no clear pattern in the use of a specific plant species for a certain type of wastewater", thus making it difficult to associate specific plants with a specific pollutant uptake. Compared to chemical and physical approaches, phytoremediation is thus more effective in counteracting Zn, Cu, and other sources of metal pollution. It also offers new means for metal recovery, leading to innovative high-value raw materials and valuable organic compounds.

Despite the potential of phytoremediation to result in hazardous biomass, the application of a proper downstream processing of the biomass can transform waste into a high-value material. If the downstream processing of the exhausted harvested plants is carefully designed, landfilling of the biomass itself or even of its ashes can be prevented, thus contributing to its benefits. Several downstream approaches are possible, and between other incineration and anaerobic digestion, are probably those of choice, considering the amount of waste to be treated. After phytoremediation, biomass can be treated thermochemically, through gasification, pyrolysis, or combustion, thereby providing fuel gas that can be used for electricity generation or to produce heat and a reduced volume of the ashes compared to the volume of the biomass. Heat generated directly through combustion or from the fuel gas can be used to foster plant growth and for the supply of ancillary items of the phytoremediation plant. The resulting ash could also be used as a pozzolanic addition to hydraulic binders, in the formulation of composite Portland cement and geopolymers. The production of biogas by anaerobic fermentation of the plant biomass used for the phytoremediation is also a possible circular approach. The biogas mixture obtained on average contains 60% methane, which can be used as a substitute for fuel in boilers. As it

has high N, P, and K contents, the associated liquid fraction could also be used in agriculture. Combining phytoremediation and biorefinery could therefore be developed into a sustainable strategy which would add value to both approaches, enabling metal recovery and producing valuable sugars and organic compounds.

In conclusion, in order to move toward a more resource efficient and sustainable food system, it is essential to find more efficient ways to improve the technical knowledge on the environmental impacts of food, stimulating sustainable livestock production. Regarding soil and water quality, livestock production systems have the highest impact on agricultural pollution, particularly in terms of the animal-manure management by farms. There is currently a great interest in new ways to manage the water contamination and manure management within farms.

Author Contributions: Conceptualization, M.H., E.O., A.M., L.R.; methodology, M.H., E.O., A.M., L.R.; investigation, M.H., E.O., A.M., L.R.; resources, L.R.; writing—original draft preparation, M.H., E.O., A.M., M.B., L.R.; writing—review and editing, M.H., E.O., A.M., C.C., M.B., N.S., L.R.; visualization, M.H.; supervision, A.M., L.R.; project administration, L.R.; funding acquisition, L.R. All authors have read and agreed to the published version of the manuscript.

Funding: The research study was conducted in the frame of FOODTECH PROJECT (ID 203370), this project is co-funded by European Regional Development Fund (ERDF). The funders had no role in study design, data collection and analysis, decision to publish, or preparation of the manuscript.

Institutional Review Board Statement: Not applicable.

Informed Consent Statement: Not applicable.

Conflicts of Interest: The authors declare no conflict of interest.

References

1. Kesavan, P.C.; Swaminathan, M.S. Strategies and models for agricultural sustainability in developing Asian countries. *Philos. Trans. R. Soc. B Biol. Sci.* **2008**, *363*, 877–891. [CrossRef]
2. Pretty, J. Agricultural sustainability: Concepts, principles and evidence. *Philos. Trans. R. Soc. B Biol. Sci.* **2008**, *363*, 447–465. [CrossRef]
3. Velten, S.; Leventon, J.; Jager, N.; Newig, J. What Is Sustainable Agriculture? A Systematic Review. *Sustainability* **2015**, *7*, 7833–7865. [CrossRef]
4. Hysa, E.; Kruja, A.; Rehman, N.U.; Laurenti, R. Circular Economy Innovation and Environmental Sustainability Impact on Economic Growth: An Integrated Model for Sustainable Development. *Sustainability* **2020**, *12*, 4831. [CrossRef]
5. Raubenheimer, D.; Simpson, S.J.; Mayntz, D. Nutrition, ecology and nutritional ecology: Toward an integrated framework. *Funct. Ecol.* **2009**, *23*, 4–16. [CrossRef]
6. Bhargava, A.; Carmona, F.F.; Bhargava, M.; Srivastava, S. Approaches for enhanced phytoextraction of heavy metals. *J. Environ. Manag.* **2012**, *105*, 103–120. [CrossRef]
7. Govind, P.; Madhuri, S. Heavy metals causing toxicity in animals and fishers. *J. Anim. Sci.* **2014**, *2*, 17–23.
8. Dai, S.Y.; Jones, B.; Lee, K.-M.; Li, W.; Post, L.; Herrman, T.J. Heavy metal contamination of animal feed in Texas. *JRS* **2016**, *1*, 21–32.
9. Giromini, C.; Rebucci, R.; Fusi, E.; Rossi, L.; Saccone, F.; Baldi, A. Cytotoxicity, apoptosis, DNA damage and methylation in mammary and kidney epithelial cell lines exposed to ochratoxin A. *Cell Biol. Toxicol.* **2016**, *32*, 249–258. [CrossRef]
10. Santos, D.; Luzio, R.V.A.; Félix, L. Chapter five—Zebrafish early life stages for toxicological screening: Insights from molecular and biochemical markers. *Adv. Mol. Toxicol.* **2018**, *12*, 151–179.
11. Rossi, L.; Dell'Orto, V.; Vagni, S.; Sala, V.; Reggi, S.; Baldi, A. Protective effect of oral administration of transgenic tobacco seeds against verocytotoxic Escherichia coli strain in piglets. *Vet. Res. Commun.* **2014**, *38*, 39–49. [CrossRef]
12. Hejna, M.; Gottardo, D.; Baldi, A.; Dell'Orto, V.; Cheli, F.; Zaninelli, M.; Rossi, L. Review: Nutritional ecology of heavy metals. *Animal* **2018**, *12*, 2156–2170. [CrossRef]
13. Fink-Gremmels, J. *Animal Feed Contamination. Effects on Livestock and Food Safety*; Woodhead Publishing Series in Food Science, Technology and Nutrition; Woodhead Publishing: Cambridge, UK, 2012.
14. Suttle, N.F. *Mineral Nutrition of Livestock*, 4th ed.; CABI: Oxfordshire, UK, 2010.
15. López-Alonso, M.; García-Vaquero, M.; Benedito, J.L.; Castillo, C.; Miranda, M. Trace mineral status and toxic metal accumulation in extensive and intensive pigs in NW Spain. *Livest. Sci.* **2012**, *146*, 47–53. [CrossRef]
16. European Commission. European Parliament and of the Council. Directive 2002/32/EC of 7 May 2002 on Undesirable Substances in Animal Feed. *Off. J. Eur. Commun.* **2002**, *L140*, 10–21.

17. Hejna, M.; Moscatelli, A.; Onelli, E.; Baldi, A.; Pilu, S.; Rossi, L. Evaluation of concentration of heavy metals in animal rearing system. *Ital. J. Anim. Sci.* **2019**, *18*, 1372–1384. [CrossRef]
18. Kim, K.; He, Y.; Xiong, X.; Ehrlich, A.; Li, X.; Raybould, H.; Atwill, E.R.; Maga, E.A.; Jørgensen, J.; Liu, Y. Dietary supplementation of Bacillus subtilis influenced intestinal health of weaned pigs experimentally infected with a pathogenic E. coli. *J. Anim. Sci. Biotechnol.* **2019**, *10*, 52. [CrossRef]
19. WHO. *Guidelines on Use of Medically Important Antimicrobials in Food-Producing Animals*; World Health Organization: Geneva, Switzerland, 2017.
20. European Parliament and the Council. Regulation (EC) No. 1831/2003 of 22 September 2003 on Additives for Use in Animal Nutrition. *Off. J. Eur. Union* **2003**, *268*, 29–43. Available online: https://eur-lex.europa.eu/legal-content/EN/TXT/?uri=CELEX%3A32003R1831 (accessed on 6 September 2020).
21. Commission Regulation (EC) No. 1334/2003 of 25 July 2003 Amending the Conditions for Authorisation of a Number of Additives in Feedingstuffs Belonging to the Group of Trace Elements. *Off. J. Eur. Union* **2003**, *187*, 11–15. Available online: https://eur-lex.europa.eu/legal-content/EN/TXT/?uri=CELEX%3A32003R1334 (accessed on 10 September 2020).
22. Sales, J. Effects of Pharmacological Concentrations of Dietary Zinc Oxide on Growth of Post-weaning Pigs: A Meta-analysis. *Biol. Trace Elem. Res.* **2013**, *152*, 343–349. [CrossRef]
23. Walk, C.L.; Wilcock, P.R.; Magowan, E. Evaluation of the effects of pharmacological zinc oxide and phosphorus source on weaned piglet growth performance, plasma minerals and mineral digestibility. *Animal* **2015**, *9*, 1145–1152. [CrossRef]
24. Polen, T.; Voia, O.S. Copper effect of feed supplementation on growth performance in fattening pigs. *Anim. Sci. J.* **2015**, *48*, 28–30.
25. Suleiman, N.; Ibitoye, E.B.; Jimoh, A.A.; Sani, Z.A. Assessment of heavy metals in chicken feeds available in Sokoto, Nigeria. *Sokoto J. Vet. Sci.* **2015**, *13*, 17–21.
26. Adewole, D.; Kim, I.H.; Nyachoti, C.M. Gut Health of Pigs: Challenge Models and Response Criteria with a Critical Analysis of the Effectiveness of Selected Feed Additives—A Review. *Asian Australas. J. Anim. Sci.* **2015**, *29*, 909–924. [CrossRef]
27. Nicholson, F.A.; Smith, S.R.; Alloway, B.J.; Carlton-Smith, C.; Chambers, B.J. An inventory of heavy metals inputs to agricultural soils in England and Wales. *Sci. Total Environ.* **2003**, *311*, 205–219. [CrossRef]
28. Luo, L.; Ma, Y.; Zhang, S.; Wei, D.; Zhu, Y.-G. An inventory of trace element inputs to agricultural soils in China. *J. Environ. Manag.* **2009**, *90*, 2524–2530. [CrossRef]
29. Zhang, F.; Li, Y.; Yang, M.; Li, W. Content of Heavy Metals in Animal Feeds and Manures from Farms of Different Scales in Northeast China. *Int. J. Environ. Res. Public Health* **2012**, *9*, 2658–2668. [CrossRef]
30. Jakubus, M.; Dach, J.; Starmans, D. Biovailability of copper and zinc in pig and cattle slurries. *Fresenius Environ. Bull.* **2013**, *22*, 995–1002.
31. Chardon, X.; Rigolot, C.; Leterme, P.; Paillat, J.; Delaby, L.; Garcia, F.; Peyraud, J.; Poupa, J.; Morvan, T.; Faverdin, P.; et al. MELODIE: A whole-farm model to study the dynamics of nutrients in dairy and pig farms with crops. *Animal* **2012**, *6*, 1711–1721. [CrossRef]
32. Ingelmo, F.; Molina, M.J.; Soriano, M.D.; Gallardo, A.; Lapeña, L. Influence of organic matter transformations on the bioavailability of heavy metals in a sludge based compost. *J. Environ. Manag.* **2012**, *95*, S104–S109. [CrossRef]
33. Wang, H.; Dong, Y.; Yang, Y.S.; Toor, G.S.; Zhang, X. Changes in heavy metal contents in animal feeds and manures in an intensive animal production region of China. *J. Environ. Sci.* **2013**, *25*, 2435–2442. [CrossRef]
34. Belon, E.; Boisson, M.; Deportes, I.; Eglin, T.; Feix, I.; Bispo, A.; Galsomies, L.; Leblond, S.; Guellier, C. An inventory of trace elements inputs to French agricultural soils. *Sci. Total Environ.* **2012**, *439*, 87–95. [CrossRef]
35. Moral, R.; Moreno-Caselles, J.; Perez-Murcia, M.; Pérez-Espinosa, A.; Rufete, B.; Paredes, C. Characterisation of the organic matter pool in manures. *Bioresour. Technol.* **2005**, *96*, 153–158. [CrossRef]
36. Gul, S.; Naz, A.; Fareed, I.; Khan, A.; Irshad, M. Speciation of heavy metals during co-composting of livestock manure. *Pol. J. Chem. Technol.* **2015**, *17*, 19–23. [CrossRef]
37. Lyubenova, L.; Schreoder, P. Plants for wastewater treatment—Effects of heavy metals on the detoxification system of Typha latifolia. *Bioresour. Technol.* **2011**, 996–1004. [CrossRef]
38. Yazdankhah, S.; Rudi, K.; Bernhoft, A. Zinc and copper in animal feed-development of resistance and co-resistance to antimicrobial agents in bacteria of animal origin. *Microb. Ecol. Health Dis.* **2014**, *25*. [CrossRef]
39. Seiler, C.; Berendonk, T.U. Heavy metal driven co-selection of antibiotic resistance in soil and water bodies impacted by agriculture and aquaculture. *Front. Microbiol.* **2012**, *3*, 399. [CrossRef]
40. Aarestrup, F.M.; Cavaco, L.; Hasman, H. Decreased susceptibility to zinc chloride is associated with methicillin resistant Staphylococcus aureus CC398 in Danish swine. *Vet. Microbiol.* **2010**, *142*, 455–457. [CrossRef]
41. Cavaco, L.M.; Hasman, H.; Stegger, M.; Andersen, P.S.; Skov, R.; Fluit, A.C.; Ito, T.; Aarestrup, F.M. Cloning and Occurrence of czrC, a Gene Conferring Cadmium and Zinc Resistance in Methicillin-Resistant Staphylococcus aureus CC398 Isolates. *Antimicrob. Agents Chemother.* **2010**, *54*, 3605–3608. [CrossRef]
42. Järup, L. Hazards of heavy metal contamination. *Br. Med. Bull.* **2003**, *68*, 167–182. [CrossRef]

43. European Medicine Agency (EMA). *Questions and Answers on Veterinary Medicinal Products Containing Zinc Oxide to Be Administered Orally to Food-Producing Species*; EMA No. 394961; EMA: Amsterdam, The Netherlands, 2017.
44. Commission Implementing Regulation (EU) 2018/1039 of 23 July 2018 concerning the authorisation of Copper(II) diacetate monohydrate, Copper(II) carbonate dihydroxy monohydrate, Copper(II) chloride dihydrate, Copper(II) oxide, Copper(II) sulphate pentahydrate, Copper(II) chelate of amino acids hydrate, Copper(II) chelate of protein hydrolysates, Copper(II) chelate of glycine hydrate (solid) and Copper(II) chelate of glycine hydrate (liquid) as feed additives for all animal species and amending Regulations (EC) No 1334/2003, (EC) No 479/2006 and (EU) No. 349/2010 and Implementing Regulations (EU) No. 269/2012, (EU) No. 1230/2014 and (EU) 2016/2261. *Off. J. Eur. Union* **2018**, *186*, 3–24. Available online: https://eur-lex.europa.eu/eli/reg_impl/2018/1039/oj (accessed on 5 September 2020).
45. Lee, C.-Y.; Lee, C.-C.; Lee, F.-Y.; Tseng, S.-K.; Liao, C.-J. Performance of subsurface flow constructed wetland taking pretreated swine effluent under heavy loads. *Bioresour. Technol.* **2004**, *92*, 173–179. [CrossRef]
46. Meers, E.; Rousseau, D.P.L.; Blomme, N.; Lesage, E.; Du Laing, G.; Tack, F.M.G.; Verloo, M.G. Tertiary treatment of the liquid fraction of pig manure with Phragmites australis. *Water Air Soil Pollut.* **2005**, *160*, 15–26. [CrossRef]
47. Knight, R.L.; Payne, V.W.; Borer, R.E.; Clarke, R.A.; Pries, J.H. Constructed wetlands for livestock wastewater management. *Ecol. Eng.* **2000**, *15*, 41–55. [CrossRef]
48. Almeida, C.M.R.; Santos, F.; Ferreira, A.C.F.; Gomes, C.R.; Basto, M.C.P.; Mucha, A.P. Constructed wetlands for the removal of metals from livestock wastewater—Can the presence of veterinary antibiotics affect removals? *Ecotoxicol. Environ. Saf.* **2016**, *137*, 143–148. [CrossRef]
49. Hejna, M.; Moscatelli, A.; Stroppa, N.; Onelli, E.; Pilu, S.; Baldi, A.; Rossi, L. Bioaccumulation of heavy metals from wastewater through a Typha latifolia and Thelypteris palustris phytoremediation system. *Chemosphere* **2020**, *241*, 125018. [CrossRef]
50. Stroppa, N.; Onelli, E.; Hejna, M.; Rossi, L.; Gagliardi, A.; Bini, L.; Baldi, A.; Moscatelli, A. Typha latifolia and Thelypteris palustris behavior in a pilot system for the refinement of livestock wastewaters: A case of study. *Chemosphere* **2020**, *240*, 124915. [CrossRef]
51. Ali, S.; Abbas, Z.; Rizwan, M.; Zaheer, I.E.; Yavaş, I.; Ünay, A.; Abdel-Daim, M.M.; Bin-Jumah, M.; Hasanuzzaman, M.; Kalderis, D. Application of Floating Aquatic Plants in Phytoremediation of Heavy Metals Polluted Water: A Review. *Sustainability* **2020**, *12*, 1927. [CrossRef]
52. Yan, A.; Wang, Y.; Tan, S.N.; Yusof, M.L.M.; Ghosh, S.; Chen, Z. Phytoremediation: A Promising Approach for Revegetation of Heavy Metal-Polluted Land. *Front. Plant Sci.* **2020**, *11*, 359. [CrossRef]
53. Kadlec, R.H.; Knight, R.L.; Vymazal, J.; Brix, H.; Cooper, P.; Haberl, R. *Constructed Wetlands for Pollution Control: Processes, Performance, Design and Operation*; Scientific and Technical Report; IWA Publishing: London, UK, 2000; Volume 8, pp. 1–15.
54. Stefanakis, A.; Akratos, C.; Tsihrintzis, V. Constructed Wetlands Classification. In *Vertical Flow Constructed Wetlands*; Elsevier: Amsterdam, The Netherlands, 2014; pp. 17–25.
55. Fitch, M.W. Constructed Wetlands. *Compr. Water Qual. Purif.* **2014**, *3*, 268–295. [CrossRef]
56. Jutsz, A.M.; Gnida, A. Mechanisms of stress avoidance and tolerance by plants used in phytoremediation of heavy metals. *Arch. Environ. Prot.* **2015**, *41*, 104–114. [CrossRef]
57. Dalvi, A.A.; Bhalerao, S.A. Response of plants towards heavy metal toxicity: An overview of avoidance, tolerance and uptake mechanism. *Ann. Plant Sci.* **2013**, *2*, 362–368.
58. Miransari, M. Hyperaccumulators, arbuscular mycorrhizal fungi and stress of heavy metals. *Biotechnol. Adv.* **2011**, *29*, 645–653. [CrossRef]
59. Memon, A.R.; Schröder, P. Implications of metal accumulation mechanisms to phytoremediation. *Environ. Sci. Pollut. Res.* **2009**, *16*, 162–175. [CrossRef]
60. Krzeslowska, M. The wall cell in plant cell response to trace metals: Polysaccharide remodeling and its role in defense strategy. *Acta Physiol. Plant.* **2011**, *33*, 35–51. [CrossRef]
61. Colzi, I.; Arnetoli, M.; Gallo, A.; Doumett, S.; Del Bubba, M.; Pignattelli, S.; Gabbrielli, R.; Gonnelli, C. Copper tolerance strategies involving the root cell wall pectins in *Silene paradoxa* L. *Environ. Exp. Bot.* **2012**, *78*, 91–98. [CrossRef]
62. Le Gall, H.; Philippe, F.; Domon, J.-M.; Gillet, F.; Pelloux, J.; Rayon, C. Cell Wall Metabolism in Response to Abiotic Stress. *Plants* **2015**, *4*, 112–166. [CrossRef]
63. Oves, M.; Saghir Khan, M.; Huda Qari, A.; Nadeen Felemban, M.; Almeelbi, T. Heavy metals: Biological importance and detoxification strategies. *J. Biorem. Biodegrad.* **2016**, *7*, 334. [CrossRef]
64. Meier, S.; Alvear, M.; Borie, F.; Aguilera, P.; Ginocchio, R.; Cornejo, P. Influence of copper on root exudate patterns in some metallophytes and agricultural plants. *Ecotoxicol. Environ. Saf.* **2012**, *75*, 8–15. [CrossRef]
65. Bradley, R.; Burt, A.J.; Read, D.J. The biology of mycorrhiza in the ericaceae. VIII. The role of mycorrhizal infection in heavy metal resistance. *New Phytol.* **1982**, *91*, 197–209. [CrossRef]
66. Tiwari, S.; Lata, C. Heavy Metal Stress, Signaling, and Tolerance Due to Plant-Associated Microbes: An Overview. *Front. Plant Sci.* **2018**, *9*, 452. [CrossRef]
67. Göhre, V.; Paszkowski, U. Contribution of the arbuscular mycorrhizal symbiosis to heavy metal phytoremediation. *Planta* **2006**, *223*, 1115–1122. [CrossRef]

68. Cicatelli, A.; Torrigiani, P.; Todeschini, V.; Biondi, S.; Castiglione, S.; Lingua, G. Arbuscular mycorrhizal fungi as a tool to ameliorate the phytoremediation potential of poplar: Biochemical and molecular aspects. *iForest* **2014**, *7*, 333–341. [CrossRef]
69. Fasani, E.; Manara, A.; Martini, F.; Furini, A.; DalCorso, G. The potential of genetic engineering of plants for the remediation of soils contaminated with heavy metals. *Plant, Cell Environ.* **2018**, *41*, 1201–1232. [CrossRef]
70. Doganlar, Z.B. Metal accumulation and physiological responses induced by copper and cadmium in Lemna gibba, L. minor and Spirodela polyrhiza. *Chem. Speciat. Bioavailab.* **2013**, *25*, 79–88. [CrossRef]
71. Hasan, K.; Cheng, Y.; Kanwar, M.K.; Chu, X.-Y.; Ahammed, G.J.; Qi, Z.-Y. Responses of Plant Proteins to Heavy Metal Stress—A Review. *Front. Plant Sci.* **2017**, *8*, 1492. [CrossRef]
72. Petraglia, A.; De Benedictis, M.; Degola, F.; Pastore, G.; Calcagno, M.; Ruotolo, R.; Mengoni, A.; Di Toppi, L.S. The capability to synthesize phytochelatins and the presence of constitutive and functional phytochelatin synthases are ancestral (plesiomorphic) characters for basal land plants. *J. Exp. Bot.* **2014**, *65*, 1153–1163. [CrossRef]
73. Yadav, S.K. Heavy metals toxicity in plants: An overview on the role of glutathione and phytochelatins in heavy metal stress tolerance of plants. *S. Afr. J. Bot.* **2010**, *76*, 167–179. [CrossRef]
74. Singh, S.; Parihar, P.; Singh, R.; Singh, V.P.; Prasad, S.M. Heavy Metal Tolerance in Plants: Role of Transcriptomics, Proteomics, Metabolomics, and Ionomics. *Front. Plant Sci.* **2016**, *6*, 1143. [CrossRef]
75. Kumar, S.; Trivedi, P.K. Heavy Metal Stress Signaling in Plants. In *Plant Metal Interaction-Emerging Remediation Techniques*; Ahmad, P., Ed.; Elsevier: Amsterdam, The Netherlands, 2016; pp. 585–603.
76. Dubey, S.; Shri, M.; Misra, P.; Lakhwani, D.; Bag, S.K.; Asif, M.H.; Trivedi, P.K.; Tripathi, R.D.; Chakrabarty, D. Heavy metals induce oxidative stress and genome-wide modulation in transcriptome of rice root. *Funct. Integr. Genom.* **2014**, *14*, 401–417. [CrossRef]
77. Collin, V.C.; Eymery, F.; Genty, B.; Rey, P.; Havaux, M. Vitamin E is essential for the tolerance of Arabidopsis thaliana to metal-induced oxidative stress. *Plant Cell Environ.* **2008**, *31*, 244–257. [CrossRef]
78. Lingua, G.; Bona, E.; Todeschini, V.; Cattaneo, C.; Marsano, F.; Berta, G.; Cavaletto, M. Effects of Heavy Metals and Arbuscular Mycorrhiza on the Leaf Proteome of a Selected Poplar Clone: A Time Course Analysis. *PLoS ONE* **2012**, *7*, e38662. [CrossRef]
79. Rao, K.P.; Vani, G.; Kumar, K.; Wankhede, D.P.; Misra, M.; Gupta, M.; Sinha, A.K. Arsenic stress activates MAP kinase in rice roots and leaves. *Arch. Biochem. Biophys.* **2011**, *506*, 73–82. [CrossRef]
80. Viehweger, K. How plants cope with heavy metals. *Bot. Stud.* **2014**, *55*, 1–12. [CrossRef]
81. Seth, C.S. A Review on Mechanisms of Plant Tolerance and Role of Transgenic Plants in Environmental Clean-up. *Bot. Rev.* **2012**, *78*, 32–62. [CrossRef]
82. Harrington, R.; McInnes, R. Integrated Constructed Wetlands (ICW) for livestock wastewater management. *Bioresour. Technol.* **2009**, *100*, 5498–5505. [CrossRef]
83. Sukumaran, D. Phytoremediation of Heavy Metals from Industrial Effluent Using Constructed Wetland Technology. *Appl. Ecol. Environ. Sci.* **2013**, *1*, 92–97. [CrossRef]
84. Mora-Ravelo, S.G.; Alarcón, A.; Rocandio-Rodríguez, M.; Vanoye-Eligio, V. Bioremediation of wastewater for reutilization in agricultural systems: A review. *Appl. Ecol. Environ. Res.* **2016**, *15*, 33–50. [CrossRef]
85. Rai, P.K. Heavy metals/metalloids remediation from wastewater using free floating macrophytes of a natural wetland. *Environ. Technol. Innov.* **2019**, *15*, 100393. [CrossRef]
86. Morari, F.; Ferro, N.D.; Cocco, E. Municipal Wastewater Treatment with Phragmites australis L. and Typha latifolia L. for Irrigation Reuse. Boron and Heavy Metals. *Water Air Soil Pollut.* **2015**, *226*, 1–4. [CrossRef]
87. Cortes-Esquivel, J.A.; Giácoman-Vallejos, G.; Barceló-Quintal, I.D.; Méndez-Novelo, R.; Ponce-Caballero, M.C. Heavy Metals Removal from Swine Wastewater Using Constructed Wetlands with Horizontal Sub-Surface Flow. *J. Environ. Prot.* **2012**, *3*, 871–877. [CrossRef]
88. Weis, J.S.; Weis, P. Metal uptake, transport and release by wetland plants: Implications for phytoremediation and restoration. *Environ. Int.* **2004**, *30*, 685–700. [CrossRef]
89. Yadav, A.K.; Abbassi, R.; Kumar, N.; Satya, S.; Sreekrishnan, T.; Mishra, B. The removal of heavy metals in wetland microcosms: Effects of bed depth, plant species, and metal mobility. *Chem. Eng. J.* **2012**, *211*, 501–507. [CrossRef]
90. Salt, E.; Blaylock, M.; Kumar, N.P.B.A.; Dushenkov, V.; Ensley, D.; Chet, I.; Raskin, I. Phytoremediation: A novel strategy for the removal of toxic metals from the environment using plants. *Biotechnology* **1995**, *13*, 468–474.
91. Brisson, J.; Cogliastro, A.; Robert, M. Controlling Speckled Alder (Alnus incana ssp. rugosa) Invasion in a Wetland Reserve of Southern Québec. *Nat. Areas J.* **2006**, *26*, 78–83. [CrossRef]
92. Lissy, P.N.M.; Madhu, G. Removal of heavy metals from wastewater using water hyacinth. *ACEEE Int. J. Transp. Urb. Dev.* **2011**, *1*, 48–52.
93. Ajayi, T.O.; Ogunbayio, A.O. Achieving Environmental Sustainability in Wastewater Treatment by Phytoremediation with Water Hyacinth (Eichhornia Crassipes). *J. Sustain. Dev.* **2012**, *5*, 80–90. [CrossRef]
94. Barya, M.P.; Gupta, D.; Shukla, R.; Thakur, T.K.; Mishra, V.K. Phytoremediation of heavy metals from mixed domestic sewage through vertical-flow constructed wetland planted with Canna Indica and Acorus Calamus. *Curr. World Environ.* **2020**, *15*. Available online: https://www.cwejournal.org/vol15no3/phytoremediation-of-heavy-metals-from-mixed-domestic-sewage-through-vertical--flow-constructed-wetland-planted-with-canna-indica-and-acorus-calamus/ (accessed on 19 October 2020).

95. Soda, S.; Hamada, T.; Yamaoka, Y.; Ike, M.; Nakazato, H.; Saeki, Y.; Kasamatsu, T.; Sakurai, Y. Constructed wetlands for advanced treatment of wastewater with a complex matrix from a metal-processing plant: Bioconcentration and translocation factors of various metals in Acorus gramineus and Cyperus alternifolius. *Ecol. Eng.* **2012**, *39*, 63–70. [CrossRef]
96. Fediuc, E.; Erdei, L. Physiological and biochemical aspects of cadmium toxicity and protective mechanisms induced in Phragmites australis and Typha latifolia. *J. Plant Physiol.* **2002**, *159*, 265–271. [CrossRef]
97. Higuchi, K.; Kanai, M.; Tsuchiya, M.; Ishii, H.; Shibuya, N.; Fujita, N.; Nakamura, Y.; Suzui, N.; Fujimaki, S.; Miwa, E. Common reed accumulates starch in its stem by metabolic adaptation under Cd stress conditions. *Front. Plant Sci.* **2015**, *6*, 138. [CrossRef]
98. Yang, J.; Ye, Z. Metal accumulation and tolerance in wetland plants. *Front. Biol. China* **2009**, *4*, 282–288. [CrossRef]
99. Yang, Y.-Y.; Jung, J.-Y.; Song, W.-Y.; Suh, H.-S.; Lee, Y. Identification of Rice Varieties with High Tolerance or Sensitivity to Lead and Characterization of the Mechanism of Tolerance. *Plant Physiol.* **2000**, *124*, 1019–1026. [CrossRef]
100. Gibson, S.I. Control of plant development and gene expression by sugar signaling. *Curr. Opin. Plant Biol.* **2005**, *8*, 93–102. [CrossRef]
101. Jiang, X.; Wang, C. Zinc distribution and zinc-binding forms in Phragmites australis under zinc pollution. *J. Plant Physiol.* **2008**, *165*, 697–704. [CrossRef]
102. Dronnet, V.M.; Renard, C.M.G.C.; Axelos, M.A.V.; Thibault, J.F. Heavy metals binding by pectins: Selectivity, quantification and characterization. *Carbohydr. Polym.* **1996**, *30*, 253–263. [CrossRef]
103. Eticha, D.; Stass, A.; Horst, W.J. Cell-wall pectin and its degree of methylation in the maize root-apex: Significance for genotypic differences in aluminium resistance. *Plant Cell Environ.* **2005**, *28*, 1410–1420. [CrossRef]
104. Sandoval, L.; Zamora-Castro, S.A.; Vidal-Álvarez, M.; Marín-Muñiz, J.L. Role of Wetland Plants and Use of Ornamental Flowering Plants in Constructed Wetlands for Wastewater Treatment: A Review. *Appl. Sci.* **2019**, *9*, 685. [CrossRef]
105. Vigil, M.; Pérez, M.F.M.; Huerta, G.M.M.; Cabal, J.V. Álvarez Is phytoremediation without biomass valorization sustainable? Comparative LCA of landfilling vs. anaerobic co-digestion. *Sci. Total Environ.* **2015**, *505*, 844–850. [CrossRef]
106. Anderson, C.W.N.; Brooks, R.; Chiarucci, A.; Lacoste, C.; Leblanc, M.; Robinson, B.H.; Simcock, R.; Stewart, R.B. Phytomining for nickel, thallium and gold. *J. Geochem. Explor.* **1999**, *67*, 407–415. [CrossRef]
107. Novo, L.A.B.; Castro, P.M.L.; Alvarenga, P.; Da Silva, E.F. Phytomining of Rare and Valuable Metals. *Phytoremediation* **2017**, *13*, 469–486. [CrossRef]
108. Weyens, N.; van der Lelie, D.; Taghavi, S.; Newman, L.; Vangronsveld, J. Exploiting plant–microbe partnerships to improve biomass production and remediation. *Trends Biotechnol.* **2009**, *27*, 591–598. [CrossRef]
109. Gomes, H.I. Phytoremediation for bioenergy: Challenges and opportunities. *Environ. Technol. Rev.* **2012**, *1*, 59–66. [CrossRef]
110. Bauddh, K.; Singh, B.; Korstad, J. *Phytoremediation Potential of Bioenergy Plants*; Springer Nature: Singapore, 2017.
111. Bridgwater, A.V.; Meier, D.; Radlein, D. An overview of fast pyrolysis of biomass. *Org. Geochem.* **1999**, *30*, 1479–1493. [CrossRef]
112. Salvo, M.; Rizzo, S.; Caldirola, M.; Novajra, G.; Canonico, F.; Bianchi, M.; Ferraris, M. Biomass ash as supplementary cementitious material (SCM). *Adv. Appl. Ceram.* **2015**, *114* (Suppl. 1), S3–S10. [CrossRef]
113. Rajamma, R.; Labrincha, J.A.; Ferreira, V.M. Alkali activation of biomass fly ash–metakaolin blends. *Fuel* **2014**, *98*, 265–271. [CrossRef]
114. Luukkonen, T.; Heponiemi, A.; Runtti, H.; Pesonen, J.; Yliniemi, J.; Lassi, U. Application of alkali-activated materials for water and wastewater treatment: A review. *Rev. Environ. Sci. Biotechnol.* **2019**, *18*, 271–297. [CrossRef]
115. European Commission. *Study on the EU's List of Critical Raw Materials (2020)*; Final Report; Publications Office of the European Union: Brusseles, Belgium, 2020; ISBN 978-92-76-21049-8. [CrossRef]
116. Edmondson, J.; Holland, A. Materials for Electric Vehicles: Electric Motors, Battery Cells & Packs, HV Cabling 2020–2030. Available online: https://www.idtechex.com/en/research-report/materials-for-electric-vehicles-2020-2030/770 (accessed on 11 October 2020).
117. Ebin, B.; Isik, M. Pyrometallurgical Processes for the Recovery of Metals from WEEE. In *WEEE Recycling Research, Development, and Policies*; Chagnes, A., Cote, G., Ekberg, C., Nilsson, M., Retegan, T., Eds.; Elservier: Amsterdam, The Netherlands, 2016. [CrossRef]
118. Iannicelli-Zubiani, E.M.; Stampino, P.G.; Cristiani, C.; Dotelli, G. Enhanced lanthanum adsorption by amine modified activated carbon. *Chem. Eng. J.* **2018**, *341*, 75–82. [CrossRef]
119. Iannicelli-Zubiani, E.M.; Cristiani, C.; Dotelli, G.; Stampino, P.G. Recovery of valuable metals from electronic scraps by clays and organo-clays: Study on bi-ionic model solutions. *Waste Manag.* **2017**, *60*, 582–590. [CrossRef]
120. Mata-Alvarez, J.; Macé, S.; Llabrés, P. Anaerobic digestion of organic solid wastes. An overview of research achievements and perspectives. *Bioresour. Technol.* **2000**, *74*, 3–16. [CrossRef]
121. Tafdrup, S. Centralized biogas plants combine agricultural and environmental benefits with energy production. *Water Sci. Technol.* **1994**, *30*, 133–141. [CrossRef]
122. Verma, V.; Singh, Y.; Rai, J. Biogas production from plant biomass used for phytoremediation of industrial wastes. *Bioresour. Technol.* **2007**, *98*, 1664–1669. [CrossRef]

123. Cao, Z.; Wang, S.; Wang, T.; Chang, Z.; Shen, Z.; Chen, Y. Using Contaminated Plants Involved in Phytoremediation for Anaerobic Digestion. *Int. J. Phytoremediation* **2015**, *17*, 201–207. [CrossRef]
124. Sotenko, M.; Coles, S.; Barker, G.; Song, L.; Jiang, Y.; Longhurst, P.J.; Romanova, T.; Shuvaeva, O.; Kirwan, K. Phytoremediation-biorefinery tandem for effective clean-up of metal contaminated soil and biomass valorisation. *Int. J. Phytoremediation* **2017**, *19*, 965–975. [CrossRef]
125. Dumont, B.; Fortun-Lamothe, L.; Jouven, M.; Thomas, M.A.; Tichit, M. Prospects from agroecology and industrial ecology for animal production in the 21st century. *Animal* **2012**, *7*, 1028–1043. [CrossRef]
126. Lyubenova, L.; Kuhn, A.J.; Höltkemeier, A.; Schröder, P. Root exudation pattern of Typha latifolia L. plants after copper exposure. *Plant Soil* **2013**, *370*, 187–195. [CrossRef]
127. Calheiros, C.S.C.; Pereira, S.I.A.; Franco, A.R.; Castro, P.M.L. Diverse Arbuscular Mycorrhizal Fungi (AMF) Communities Colonize Plants Inhabiting a Constructed Wetland for Wastewater Treatment. *Water* **2019**, *11*, 1535. [CrossRef]

Protoplasma
https://doi.org/10.1007/s00709-020-01553-6

ORIGINAL ARTICLE

The aquatic carnivorous plant *Aldrovanda vesiculosa* (Droseraceae) exhibits altered developmental stages in male gametophyte

Elisabetta Onelli[1] · Mario Beretta[2] · Alessandra Moscatelli[1] · Marco Caccianiga[1,2] · Michele Pozzi[1] · Nadia Stroppa[1] · Lubomír Adamec[3]

Received: 26 May 2020 / Accepted: 31 August 2020

Abstract

Aldrovanda vesiculosa (Droseraceae) is a rare aquatic carnivorous plant, distributed in Europe, Asia, Africa, and Australia. *Aldrovanda* populations can flower prolifically under favourable conditions, but seed set is very limited. We studied the structure of *Aldrovanda* pollen collected from flowers in different developmental stages (opened and non-opened anthers) from both European and Australian populations to elucidate pollination traits and the basis of poor seed set on the basis of microscopic observation of pollen and anther structure. Microscopic analyses of *Aldrovanda* pollen showed that this plant has pollen arranged in tetrads like other species in the Droseraceae family. In hydrated pollen, cytoplasmic protrusions originate from pores located along the equatorial wall of monads, and can develop into pollen tubes. Interestingly, pollen development from microspores occurs in open anthers, suggesting a delay of the developmental stages. In addition, pollen development displays altered sperm cell formation and precocious pollen germination. Precocious germination may characterize recalcitrant pollen, which naturally do not undergo dehydration before anthesis and remain partially hydrated, particularly in aquatic and wetland plants. These alterations of male gametophyte development could affect fertilization processes, and be the reason for the low reproductive capability of *Aldrovanda* observed both in the field and in cultures. Generally, reduced pollen longevity and very quick germination are considered an adaptation to aquatic or wet environments.

Keywords *Aldrovanda vesiculosa* · Pollen development · Pollen structure · Generative cell · Pollination · Anther structure

Introduction

Aldrovanda vesiculosa L. (Waterwheel plant, Droseraceae) is a rare and endangered aquatic carnivorous plant exhibiting spectacular, rapid movement of its snapping traps. *Aldrovanda* grows on a vast range of territories in Europe, Asia, Africa, and Australia and across various climatic zones—from temperate to tropical and subtropical ones—but its recent natural spread includes only around 50 known sites worldwide (Cross 2012; Adamec 2018). Plants are perennial, rootless, submerged, and free-floating below the water surface, growing in shallow, standing humic waters (Adamec 1995, 2018; Weber 1995; Cross 2012; Fleischmann et al. 2018). Its poorly branched linear shoots have a highly modular structure and are usually ca. 6–20 cm long, including a shoot apex and ca. 14–24 mature leaf whorls. *Aldrovanda* also exhibits distinct and steep morphological, growth, and physiological polarity (Adamec 2000, 2018; Cross 2012). The main feature of this polarity is the permanent, rapid apical shoot growth of 1–1.5 new leaf whorls a day, whereas the basal shoot segments continuously senesce and decay at a similar rate so that shoot length is generally constant ("conveyer belt"–like shoot growth system). New biomass is allocated only to branching and flowering (Adamec 2018). High frequency of branching indicates plant vigour and optimal ecological conditions and is the principal prerequisite for a high relative growth rate. New study on *Aldrovanda vesiculosa* has detailed some aspects of its anatomical structure and novel lifestyle (Atsuzawa et al. 2020).

Handling Editor: Handling Editor: Peter Nick

✉ Lubomír Adamec
lubomir.adamec@ibot.cas.cz

[1] Department of Biosciences, University of Milano, Via Celoria 26, 20133 Milan, Italy

[2] "Città Studi" Botanical Garden, Department of Biosciences, University of Milano, Via Celoria 26, 20133 Milan, Italy

[3] Institute of Botany of the Czech Academy of Sciences, Dukelská 135, CZ-379 82 Třeboň, Czech Republic

Published online: 11 September 2020

All temperate and (sub)tropical *Aldrovanda* populations can flower prolifically under favourable natural conditions and even set fertile seed (e.g. Adamec and Tichý 1997; Adamec 1999; Okada 2008; Cross 2012; Cross et al. 2016). Nevertheless, the plants mainly propagate vegetatively by apical formation of new branches, which may be fairly regular within each successive 5–7 leaf whorl (Adamec 2018). Generally, clonal aquatic plants with frequent branching of the mother shoot exhibit some of the lowest rates of generative reproduction (Herben et al. 2014), which applies well for flowering and seed set of mainly temperate *Aldrovanda* populations. Although several dozens of ecophysiological, biophysical, or genetic studies on *Aldrovanda* have been published so far (for the review, see Cross 2012; Adamec 2018), fewer studies have focused on morphological or ecological aspects of flowering and seed set or germination (e.g. Adamec and Tichý 1997, Adamec 1999; Cross et al. 2015, 2016), and only Sahashi and Ikuse (1973) and Okada (2008) addressed pollen morphology and/or pollination traits.

A single flower bud is initiated at the shoot apex underwater, but near the water surface (Okada 2008; Cross 2012; Adamec 2018). Its erect flower stalk develops on a modified leaf whorl without traps, gradually growing to 12–16 mm length, and at maturity, reaches the water surface. *Aldrovanda* flowers emerge slightly above the water only during anthesis, when they open. The open flower has a subglobose, superior ovary bearing five styles radially, alternating to five slender stamens with yellow anthers. As described by Okada (2008) and Cross (2012), it is important for pollination that some flowers have straight styles (with no contact with anthers), while in others, some styles are bent laterally towards the anthers. The estimated pollen to ovule ratio of 28.5 ± 4.6 indicates a strictly autogamous or self-fertilizing character, which was confirmed both experimentally (Okada 2008) and in closed aquaria without any insects (Adamec 2018). *Aldrovanda* has two different types of flowers which can be distinguished by the stage of floral development: autogamous (opened) and cleistogamous (closed; Adamec and Tichý 1997; Okada 2008; Cross 2012; Cross et al. 2016; Adamec 2018). Under suboptimal ecological conditions, only cleistogamous flowers are formed. All recorded observations confirm that pollination and seed set are only possible in opened flowers, but in temperate populations, both at natural sites and in outdoor cultures, full flower opening is only a few hours (2.5–3), mostly on afternoons when water temperature is highest (Adamec and Tichý 1997; Okada 2008; Cross 2012; Cross et al. 2016; Adamec 2018). High afternoon water temperature ca. > 27 °C is considered a crucial habitat factor, regulating flower opening and thus successful pollination and seed set (Cross 2012). It follows from various studies that the percentage of fertile capsules (floral success of individual flowers) with ripe seeds is extremely variable: from 0 to 53% (*cf.* Adamec and Tichý 1997; Adamec 1999; Okada 2008; Cross et al. 2016). The anthers open immediately after the petals opened and each anther (per stamen) contains 12–22 pollen tetrads (Okada 2008). Sahashi and Ikuse (1973) estimated the individual pollen grain diameter to be ca. 35 × 45 μm and the diameter of a pollen tetrad ca. 66 μm. The pollen grains are three-operculate and have echinate ornamentations (Chanda 1965; Sahashi and Ikuse 1973; Takahashi and Sohma 1982). Neither the longevity of *Aldrovanda* pollen nor pollen germination traits have been observed. It may be hypothesized, however, that it is very short pollen longevity that strongly limits the pollination and thus, the seed set. From 1 to 14 seeds are produced in each capsule (Adamec and Tichý 1997; Okada 2008; Cross 2012; Cross et al. 2016; Adamec 2018).

Our aim was to study *Aldrovanda* pollen structure in pollen collected from flowers of different ages and development stages (opened and non-opened anthers) in plants of several world populations, to elucidate the conserved pollination traits of *Aldrovanda* and the reason for its poor seed set. We show that several steps of pollen development that are altered, including pollen grains in which the generative cell/sperm cells (GC/SCs) are not internalized within the vegetative cell (VC), leading to a hypothesis that pollen tubes could not transport SCs to the embryo sac for fertilization. In addition, early pollen germination was detected within anthers, before pollen delivery. These results, together with the short duration of receptivity, could explain the reasons for low seed production and the high level of autogamy observed in *A. vesiculosa*.

Material and methods

Plant origin and sampling

Plants of several *Aldrovanda* populations were used for studying pollen structure. Opened flowers of temperate *Aldrovanda* (originated in SW Hungary; Elansary et al.

Fig. 1 *Aldrovanda vesiculosa* pollen morphology. **a, b, c**: pollen obtained from squashed anthers and observed by light microscopy. Pollen was organized in permanent tetrads of about 65 μm in diameter and arranged in tetrahedral (**a**) or tetragonal (**b**) arrangement. Pollen surface was covered by many drops of pollenkit (**a**; arrows). In dried pollen, the pores were locked by an operculum (**c**; arrows). **d, e, f**: autofluorescence analysis of dried anthers. Few tetrads were presents in the pollen sacs (about 5; **d**, **e**) and both tetrahedral and tetragonal tetrads were present in the same theca (**d**, **e**). The pores of two neighbouring monads appeared aligned along the equator of pollen grains (**e**, **f**; arrows). **g, h, i**: Anthers stained by Aniline Blue. Callose was not present in the tetrads (**g**, **i**). Hydrated pollen showed operculum retraction (**i**; arrow) and distal wall showed intectate and echinate exine (**i**; arrowhead). Callose-stained cell-wall ribs in endothecium cells (**g**, **h**; arrows). **j, k**: squashed anthers observed by LM. The ribs in endothecium cell walls were observed (arrows). Three pores were evident in monads (**j**; numbered as 1, 2, 3). **l**: Anther section showed thickness in endothecium cell wall (arrow) and pollen tetrads with baculae of echinate exine (arrowheads). Tg, tetragonal tetrad; Te, tetrahedral tetrad. Magnification bars: **a**, **b**, **f**: 10 μm; **d**, **e**, **g**, **h**: 50 μm; **c**, **i**, **j**, **k**: 20 μm; and **l**: 30 μm

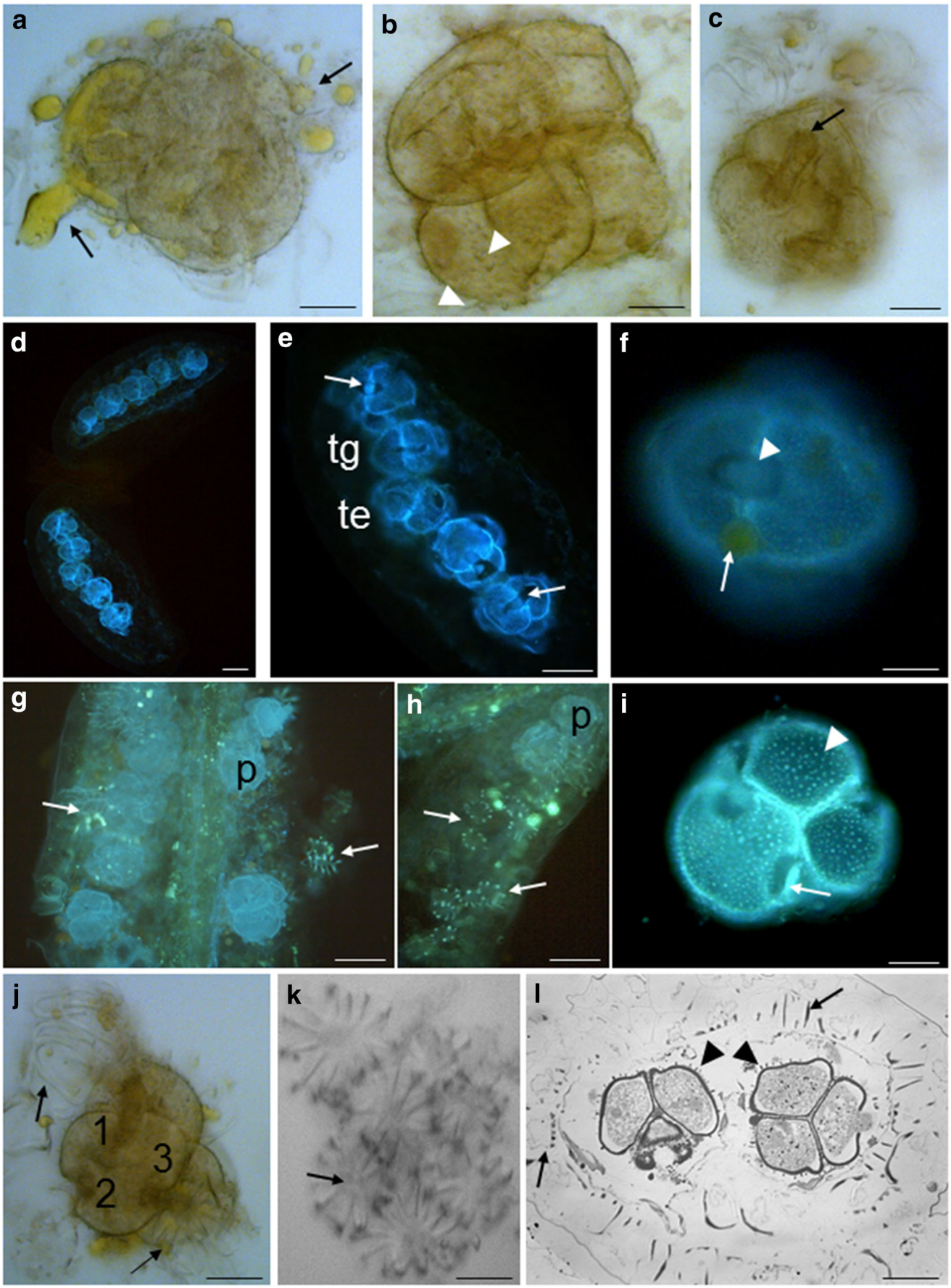
a
b
c
d
e
tg
te
f
g
p
h
p
i
j
1
2
3
k
l

2010) were collected from a pool in a sand-pit Cep I near Suchdol nad Lužnicí, South Bohemia, Czech Republic, in August 2016 (see Cross et al. 2016). The flowers were dried at ca. 25 °C and kept above silica gel before processing. Flowers of different stages of an *Aldrovanda* population (originated from E Poland; Elansary et al. 2010) were also collected from a fen pool at Karštejn, South Bohemia, Czech Republic (Cross et al. 2016) in July 2017. Tropical *Aldrovanda* plants from Leach Lagoon near Katherine, N.T., N Australia, and subtropical plants from Esperance Bay, W.A., SW Australia (see Elansary et al. 2010), were grown indoors in 3-litre aquaria (Sirová et al. 2003). The litter of robust sedges was used as the main cultivation substrate in these aquaria and the water was considered humic and oligotrophic.

Light and transmission electron microscopy

Flowers from cultivated N and SW Australian and naturalized E Polish populations were collected during June and July 2017, then immediately put in a HEM buffer (0.05-M HEPES, 1-mM $MgCl_2$, 5-mM EDTA, pH 7.4) and kept at 4 °C until processing. Six to 10 flowers were always collected for each flower category (opened or closed). Anthers were squashed and observed in a light microscope Leica DMRB equipped with a MC170HD camera.

To detect callose in the cell walls, dried flowers were stained with 0.1% decolorized Aniline Blue in 100-mM K_2HPO_4/KOH, pH 11, and observed with a Leica DMRB fluorescence microscope equipped with filter set A (Ex BP: 340–380, DM: 400, Em LP 425) and with a MC170HD camera. To observe sections of *A. vesiculosa* pollen, anthers were fixed in 4% formaldehyde in the HEM buffer. Afterwards, they were rinsed with HEM buffer and postfixed in 1% osmium tetroxide. After several rinses by the HEM buffer, samples were dehydrated in ethanol and embedded in LR White resin. Anthers were also fixed in a hypertonic concentration of HEM buffer (with 0.5-M HEPES) to induce plasmolysis. Samples were embedded in the LR White resin as described above.

Semi-fine sections (2 μm) and ultra-thin sections (80 nm) were obtained using a Reichert-Jung microtome. Semi-fine sections were stained by 1% Toluidine Blue and observed with a Leica DMRB light microscope. Ultrathin sections were stained with 3% uranyl acetate and observed with an EFTEM LEO 912AB transmission electron microscope (TEM; Zeiss) working at 100 kV.

Scanning electron microscopy

For SEM analysis, we used open *Aldrovanda* flowers from SW Australian and Hungarian populations and closed flowers from SW and N Australian populations. Pollen grains were acetolyzed according to Erdtman (1960), air dried, sputtered with 25 nm layer of gold in argon plasma (AGAR Automatic Sputter Coater B7341 equipped with a quartz crystal thickness monitor), and then studied using a Leo 1430 scanning electron microscope.

Results

Aldrovanda pollen is organized in permanent tetrads

It has been reported that *Aldrovanda* flowers remain opened only for very short time (about 3 h) and anther dehiscence occurs only after the petals open (Okada 2008; Adamec 2018). Opened flowers were collected at different stages during the short flowering period, since they contained closed anthers (suggesting flowers were collected immediately after opening) or open anthers (suggesting they were collected later; Figs. 1 and 3). Pollen was organized in permanent tetrads of about 65 μm in diameter and arranged in tetrahedral or tetragonal orientations (Fig.1a, b, respectively). This organization of *Aldrovanda* pollen was confirmed also by fluorescence analysis (Fig. 1d–i). The autofluorescence analysis of dried flowers showed that several tetrads were present in the anthers (about 5; Fig. 1d, e). Both tetrahedral and tetragonal tetrads were present in the same theca (Fig. 1e).

The pollen surface was covered by many drops, probably representing pollenkit produced by the tapetum (Fig. 1a, f; arrows). The high amount of this material, the most common adhesive material covering pollen grains (Pacini and Hesse 2005), could explain the difficulty of pollen release from the anthers; in fact, pollen had to be scraped off from the anther envelope. Like other members of the Droseraceae, *Aldrovanda* pollen displayed three equatorial apertures (Figs. 1 j and 3 d), and as also confirmed by SEM analyses (Fig. 2a, e), pores of two neighbouring monads involve the outline of both the distal and proximal sides of pollen grains (Fig. 1c, e, f). In dried pollen, the pores were locked in by an operculum (Fig. 1f, i) and they opened in hydrated pollen by operculum retraction (Fig. 2c).

Anther staining by Aniline Blue showed that callose was not present in tetrads, as expected. On the contrary, callose seemed to be present in the cell wall of anther endothecium cells (Fig. 1g, h). Aniline Blue staining suggested that callose

Fig. 2 SEM micrographs of acetolyzed pollen grains. **a**: tetrad with tetrahedral arrangement of pollen grains with equatorial apertures (o = operculum). **b**: pollen grain showing echinate features on distal face (g = granules, sp = spinules, S = spines). **c**: tetrad with equatorial apertures and retracted opercula (o). **d**: echinate features on distal face and irregular perforations (arrows). **e**: two equatorial apertures of two different pollen grains. **f**: broken pollen grain showing the thickness of the pollen wall. Magnification bars—**a**, **c**: 10 μm; **b**, **f**: 2 μm; and **d**, **e**: 1 μm

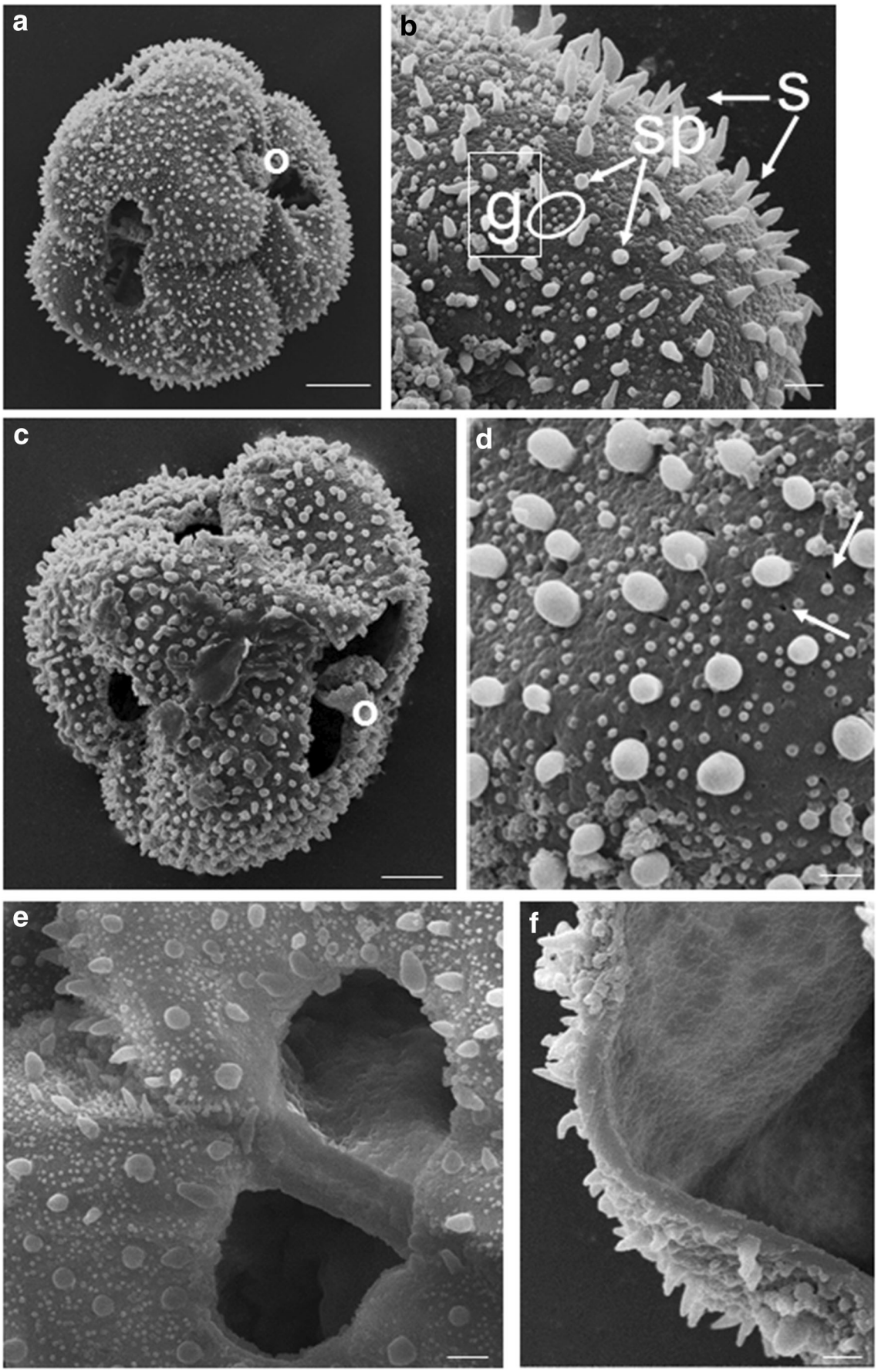
a
o
b
S
sp
go
c
o
d
e
f

was deposited in these wall bars. On the contrary, a solid plate formed in the inner periclinal wall, from which the bars originate, did not contain callose (Fig. 1g, h). In *Aldrovanda*, cell-wall bars were also revealed in the endothecium cells of squashed anthers (Fig. 1j, k) and in anther sections (Figs. 1 l and 3 a, c, g). Autofluorescence and light microscopy (LM) of distal pollen cell walls and tetrad sections revealed that the exine appeared intectate and echinate for the presence of different spinae (Fig. 1b, i, l).

Using SEM analysis, we observed exine ornamentation which revealed that there are no relevant morphological differences between pollen grains of opened and closed flowers (Fig. 2a, c). As already reported for other Droseraceae (Rodondi et al. 2004), there are three main different echinate features on the distal face of each *grain* of the tetrad: spines, spinules, and granules (Fig. 2b). Granules (around 0.1–0.2 μm long, 0.1–0.2 μm wide at the base) are the most numerous and are about three times the sum of spines and spinules, very short, and constant in shape. Spines are around 3 μm long, 1 μm wide at the base and are numerous, with a regular distribution, variable in shape and length, whereas their width remains quite constant. Spinules (around 1 μm long and 1 μm wide at the base) are the least frequent features. The spinules appear like blunt spines and are randomly distributed. Their shapes are similar to granules, but are bigger and sometimes as wide as spines. On the pollen wall, some sporadic and irregular perforations are also present (Fig. 2d). In some broken pollen grains and in some grains without the operculum, it was also possible to measure the exine thickness of 0.7–1.0 μm (Fig. 2e, f).

Inside closed and opened anthers: *Aldrovanda* pollen showed different morphologies

Sections of closed anthers showed tapetum degeneration and cell-wall bands in endothecium cell walls (Fig. 3a). Mature pollen grains, as observed both by LM and TEM, appeared full of amyloplasts (Fig. 3a, b) and no cytoplasmic protrusions were observed at the pollen apertures (Fig. 3a). Observation of pollen obtained by squashed opened anthers and by opened anther sections revealed that in mature pollen, each monad displayed cytoplasmic protrusions originating from each pore (Fig. 3c–g). In *Aldrovanda*, unlike *Dionaea* (Halbritter et al. 2012), the protrusions did not show the persistence of the operculum. LM and TEM analyses showed that only intine covered the cytoplasmic papillae (Figs. 3 e–g and 4 a–c). At the protrusions, the intine appeared thick and was formed with three layers. The innermost region consisted of an inner thin compact layer, a middle layer showing microchannels, and an outer fibril layer (Fig. 4b, layers 1, 2, and 3, respectively). In the area where the exine was present, the fibrillar layer was not observed (Fig. 4a, d) and microchannels disappeared or were reduced considerably in the middle layer (Fig. 4d, arrow).

TEM analyses showed that the exine was organized in a homogenous electron-dense layer from which spinae/spinulae protrude (Fig. 4d–f), as described above, and where fibrillar matrix was observed (Fig. 4f). The presence of spinae/spinulae also characterized the wall between two adjacent monads (Fig. 3 b and 4 e, f). Intine microchannels were also observed in pollen inside closed anthers (Fig. 3b). In relation to the operculum, when the pore is still locked, the inner homogenous layer of sporopollenin was missing and only the thick sculptured cell wall was observed (Fig. 3b).

Aldrovanda pollen displayed different developmental stages in opened anthers

In *Aldrovanda* anthers at anthesis, the vegetative and generative cells (VC and GC) were observed but the GC was not yet internalized within the VC (Fig. 5a, b). In this phase, cytoplasmic protrusions were not observed. TEM revealed that at anthesis, pollen grains showed a vegetative cell with dense cytoplasm, a prominent lobed vegetative nucleus and a stacked rough ER (Fig. 6). In addition, dark lipid drops and small vacuoles were also observed inside the vegetative cell (Figs. 3 e–g; 4 a, d, e; and 6 b). Clusters of vesicles characterized both cytoplasmic protrusions and vegetative cells (Figs. 4 a, d; 5 d; and 6 c). The GC inclusion into the VC appeared delayed with respect to the timing of anthesis. In addition, after the first microspore mitosis, before the GC inclusion, VC did not show a large vacuole but dispersed small vacuoles (Fig. 5 b–d and 6 a, c). In *Aldrovanda*, the GC was also observed inside the VC (Fig. 5a, c), suggesting that GC internalization and subsequent pollen development can occur correctly (Fig. 5c, d). In the same anthers, pollen with either GC included in VC or not included was observed (Fig. 5a–c). The generative cell was surrounded by a thin cell wall and showed some organelles as ER and vesicles and, intriguingly, the GC seldom appeared lobed (Fig. 5d, e).

Moreover, germinated pollen with long pollen tubes were sometimes observed in the old opened anther (Fig. 7). The pollen tubes, which reached a remarkable length (about 300 μm), started by a cytoplasmic protrusion (Fig. 7a) and originated by more monads belonging to the same tetrad (Fig. 7b, c). Inside the anther, some algae with a large nucleus and chloroplasts characterized by single organized thylakoids (Fig. 3g, h) were observed, suggesting the entry of ambient water into the opened flower.

The opened anther sections also showed the presence of two sperm cells in the pollen grain, confirming that *Aldrovanda* possesses tricellular pollen (Fig. 8), as do other Droseraceae (Rodondi et al. 2004). Sperm cells revealed a prominent nucleus surrounded by dense cytoplasm containing small vacuoles and a smooth ER (Fig. 8c–e). Interestingly, plasmolysis of cells highlighted that the two SCs were not included inside the VC, since no cytoplasm was observed

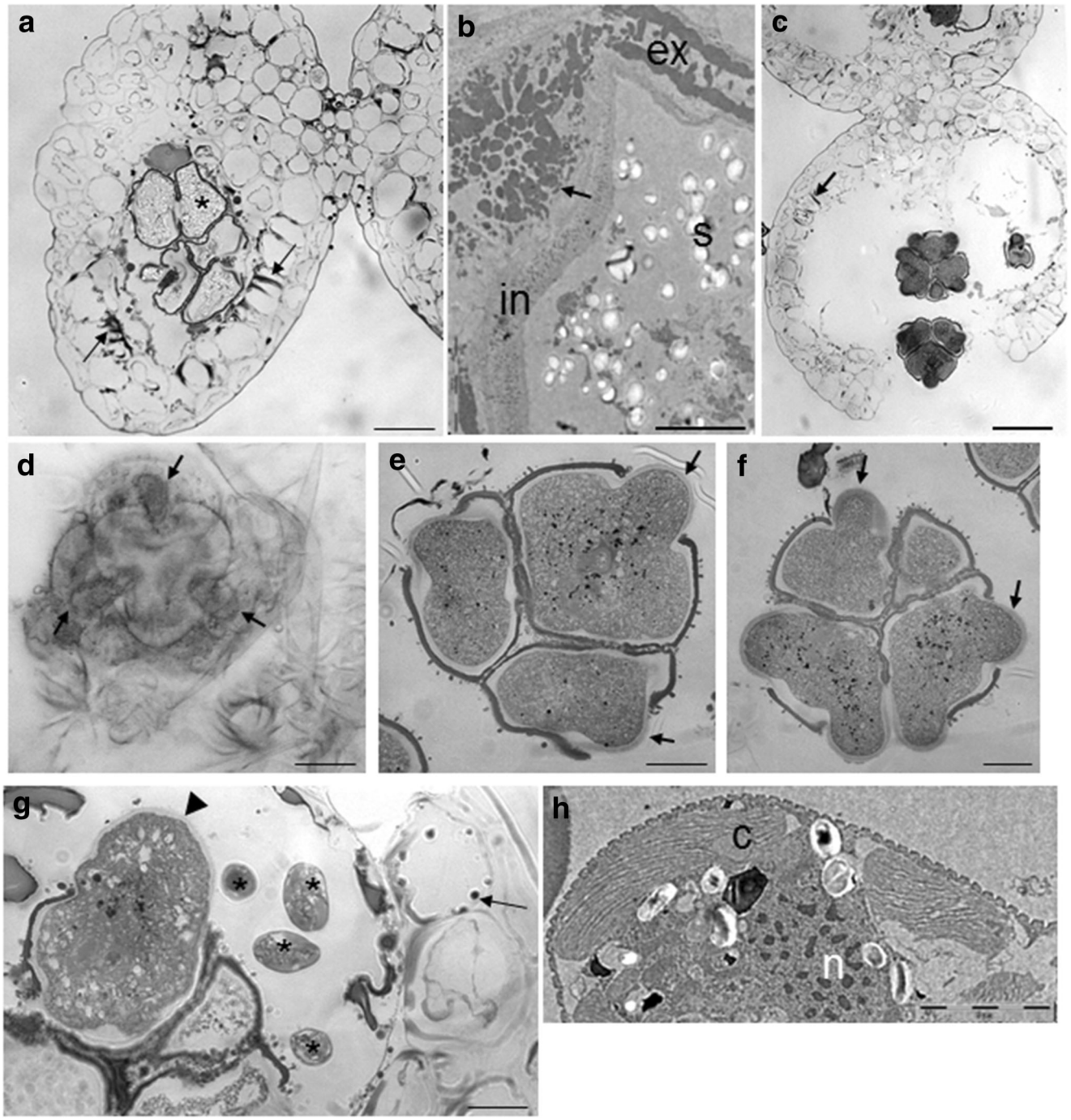

Fig. 3 Pollen morphology in closed and open anthers. **a**, **b**: sections of closed anthers. Tapetum undergoes to degeneration and wall bands in endothecium cell walls were observed (**a**, arrows). Pollen grains appeared filled with amyloplasts (**a**; asterisks) and no cytoplasmic protrusions were observed at pollen apertures (**a**). TEM observations confirmed the presence of numerous small starch granules inside pollen (**b**). Intine (**b**) and exine (**b**) were present. Between two adjacent monads, exine was organized in a homogenous electron-dense layer from which spinae/spinulae protrude (**b**). The operculum showed only the thick sculptured cell wall while the inner homogenous layer of sporopollenine was missing (**b**; arrow). **c-h**: sections of open anthers. Open anthers showed tetrads in which monads display cytoplasmic protrusions that originate from each pore (**c**, **e**, **f**). Protrusions were also observed in squashed anthers (**d**; arrows). In correspondence of protrusion, exine disappeared for the retraction of operculum and only a tick intine was observed (**e**, **f**, **g**; arrows). Starch granules were not present in hydrated pollen and some osmiophilous dark granules were observed as dark spots inside the pollen grains (**e**, **f**, **g**). Inside the pollen sac, some algae were present (**g**; asterisks). These algae were unicellular and displayed a large nucleus and chloroplasts characterized by single thylakoids (**h**); in, intine; ex, exine; s, starch; n, nucleus; c, chloroplast. Magnification bars—**a**: 50 μm; **c**: 40 μm; **d**, **e**, **f**: 10 μm; and **g**, **h**, **b**: 5 μm

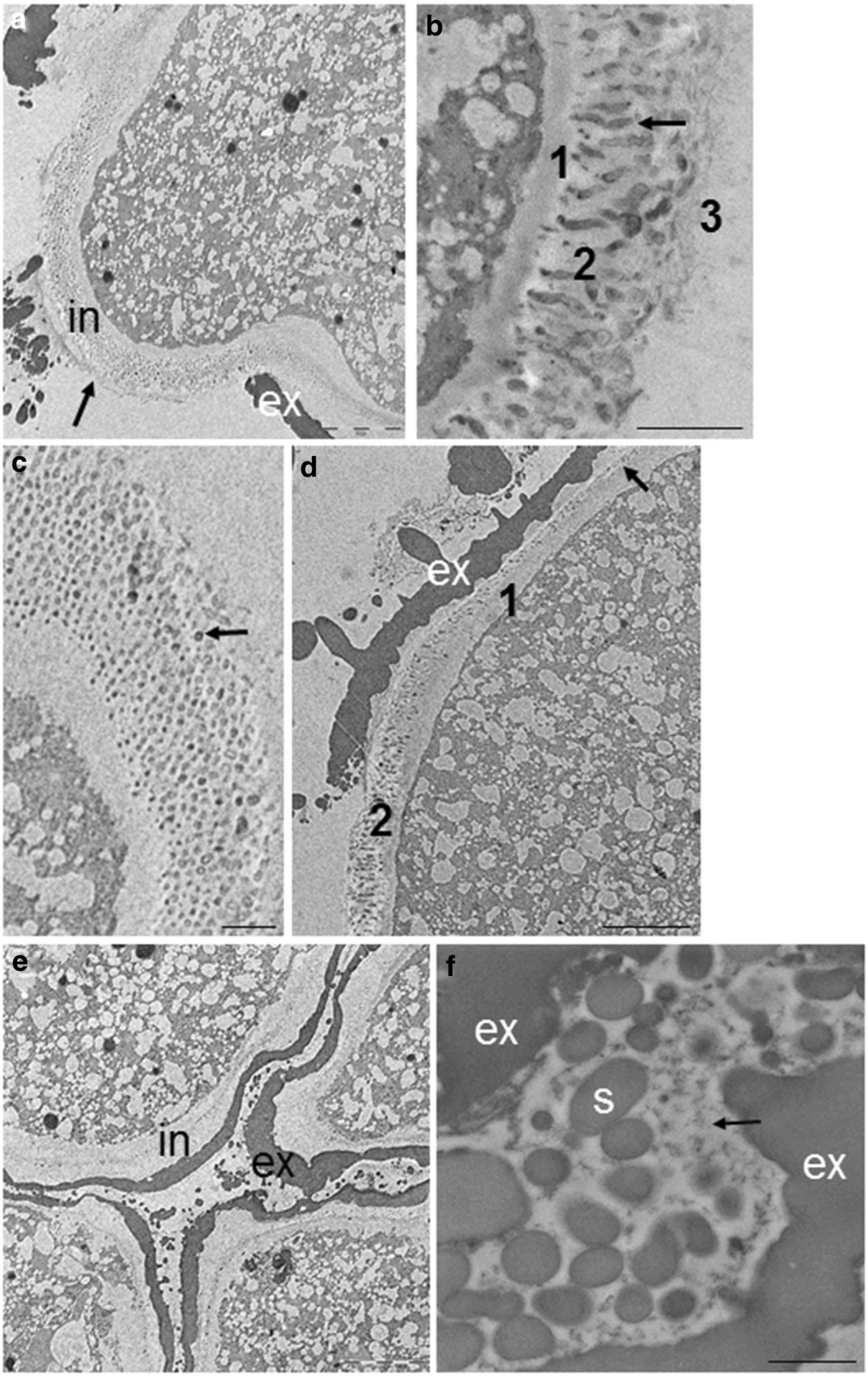
a
in
ex
b
1
2
3
c
d
ex
1
2
e
in
ex
f
ex
s
ex

◀ **Fig. 4** TEM analyses of pollen cell wall in open anthers. **a-c**: intine structure at the protrusions. Protrusion showed a thick intine organized in three layers: an inner thin compact layer (**b**; 1), a middle layer showing microchannels (**b**, 2; **b** longitudinal/**c** transversal sections; arrows) and an outer fibrillar layer (**b**; 3). **d–f**: cell wall around pollen grains. In the exine, spinae/spinulae protrude from a homogenous electron-dense layer (**d**) also at two adjacent monads (**e**). In this area, microchannels (**d**; 2) disappeared from intine or were reduced considerably (**d**, **e**; arrow) allowing only the persistence of the homogenous layer (**d**; **e**). Fibril matrix, probably derived by tapetum degeneration, was observed in the intercellular space between two adjacent monads (**f**; arrow). The VC cytoplasm showed numerous clusters of vesicles and little vacuoles (**a**, **d**, **e**); in, intine; ex, exine; s, spinae. Magnification bars—**a**, **d**, **e**: 5 μm; **b**, **c**, **f**: 1 μm

around the two SCs and the periplasmic space due to plasmolysis was observed between the cells and the pollen wall (Fig. 8b, c). These data suggest that the GC was not included in the VC, and thus, the mitosis II occurred outside the VC.

Discussion

Aldrovanda vesiculosa displays both cleistogamous and autogamous flowers (Adamec and Tichý 1997; Okada 2008; Adamec 1999; Cross et al. 2016); however, cleistogamous flowers fail to produce seeds and in autogamous flowers, when pollen grains reach the stigma, they are able to form pollen tubes that reach the ovule through a mucilaginous path in the style (Atsuzawa et al. 2020). However, it was observed that in *Aldrovanda*, the number of fertile fruits produced is highly variable and often scarce (Cross 2012; Adamec 2018). In addition, genetic uniformity was observed among different populations of *Aldrovanda*, suggesting that low mutation rates, dominant asexual reproduction, and autogamous reproduction occur (Elansary et al. 2010; Adamec 2018). Data presented in this study were performed on closed and opened flowers, thus on potentially fertile flowers. LM and TEM observations showed altered development of male gametophyte, which could explain the failure of the fertilization process and the rarity of seed set.

Aldrovanda pollen morphology shares some features with other Droseraceae

The morphology of *Aldrovanda* pollen is poorly known (Sahashi and Ikuse 1973; Okada 2008), but it shares some features with other Droseraceae (Kuprianova 1973; Rodondi et al. 2004; Halbritter et al. 2012). In fact, optical and electron microscopy observations of pollen in plants from European and Australian populations showed tetrahedral/tetragonal organization of tetrads, echinate pollen walls, and as reported in species that naturally form permanent tetrads (Blackmore and Crane 1988; Scott et al. 2004; Copenhaver 2005) and produce little or no callose in the intersporal cross-walls of the tetrad. It is not clear which mechanisms allowed monads to remain close to each other. Between monads, some fibrillar materials were observed which could represent pollenkit or tapetum debris. In *Annona*, different species with monad and permanent tetrad pollen were observed. In tetrads of different *Annona* species, several mechanisms for monads adhesion were observed involving both intine and exine bridges or cohesion. In some plants, also callose and cellulose participate in monads adhesion (Copenhaver 2005; Lora et al. 2014). Further analyses could clarify this mechanisms also in Droseraceae.

Instead, callose was present in ribs observed in endothecial cells. In other species, just before anthesis and during the pollen maturation, cell walls of endothecium cells develop characteristic thickened bars which are reported to consist mainly of cellulose and lignin (De Fossard 1969; Whatley 1982; Manning 1996). In *Aldrovanda*, these wall thickenings of the endothecium resemble the palmate ribs described in the Solanaceae (Carrizo García 2002) and have an essential role in anther dehiscence. In fact, in some male sterile *Arabidopsis thaliana* mutants, endothecial wall thickening is affected, resulting in failure of anther opening and pollen release (Dawson et al. 1999; Wilson et al. 2011).

Microscopic observations of *Aldrovanda* pollen also show the presence of cytoplasmic protrusions at pores, a distinctive trait of Droseraceae pollen. In fact, in both *Drosera* and *Dionaea*, cytoplasmic protrusions can emerge from numerous apertures localized in the equatorial area of monads (Rodondi et al. 2004; Halbritter et al. 2012). As already suggested for *Drosera* and *Dionaea* (Halbritter et al. 2012), protrusions in *Aldrovanda* pollen resulted from hydration because in its dry state, pores were occluded by the operculum. Regions of cytoplasmic protrusions showed the presence of microchannels in the intine as well. This microchannelled intine has been reported in pollen of the *Drosera* genus, Poaceae, and other plants as well (Kuprianova 1973; Takahashi 1988; Marquez et al. 1997; Vega-Maray et al. 2003; Eliseu and Dinis 2008). It was suggested that this wall layer plays a role in pollen hydration and activation (Eliseu and Dinis 2008).

A very interesting feature was the presence of tricellular pollen in *Aldrovanda*. In Angiosperms, pollen could be delivered in two different states, depending on the species. In bicellular pollen, the microspore completes only the first asymmetric mitosis prior to pollination giving rise to a large VC and a small GC. Then, after cytokinesis, the GC is internalized into the VC. In tricellular pollen, the internalized GC divides into two sperm cells (SCs) before pollen dispersal giving rise to tricellular pollen (Angold 1968; Pacini and Juniper 1984). Droseraceae is in the latter group, forming tricellular pollen, with two sperm cells within the VC (Rodondi et al. 2004). Similar to other tricellular pollen species, *Drosera* was also described as partially hydrated pollen/

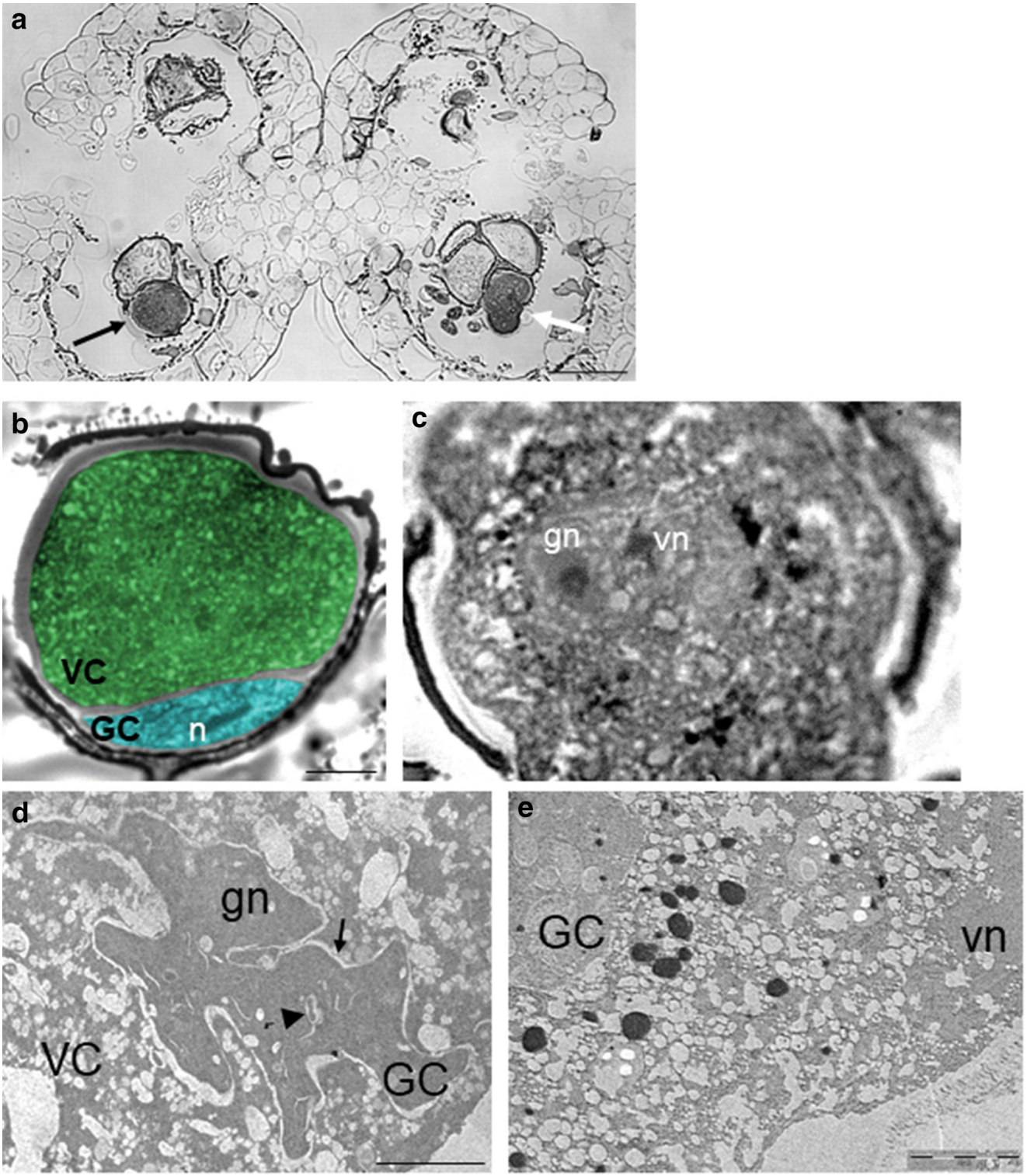

Fig 5 Generative cell formation in open anthers. **a, b, c**: light microscopy of open anther sections. Vegetative and generative cell were observed (**a**, **b**, **c**: VV green, GC blue) but the GC was not yet internalized into the VC (**a**, black arrow; **b**). Cytoplasmic protrusions were not observed even when the operculum was already retracted (arrow) and only the intine was present at the pore (**a**, arrow; **b**). Dispersed vesicles and small vacuoles were observed in the VC (**b**). In the same anther, pollen with GC including in VC was observed (**a**, white arrow; C). **d**, **e**: GC was internalized into VC. GC appeared lobed and surrounded by a thin cell wall (**d**, arrow). Some organelles such as ER (**d**, arrowhead) and vesicles were observed (**d**, **e**). GC, generative cell; VC, vegetative cell; n, nucleus; gn, generative cell nucleus; vn, vegetative cell nucleus. Magnification bars—**a**, 50 μm; **b**, 10 μm; and **c**, **d**, 5 μm

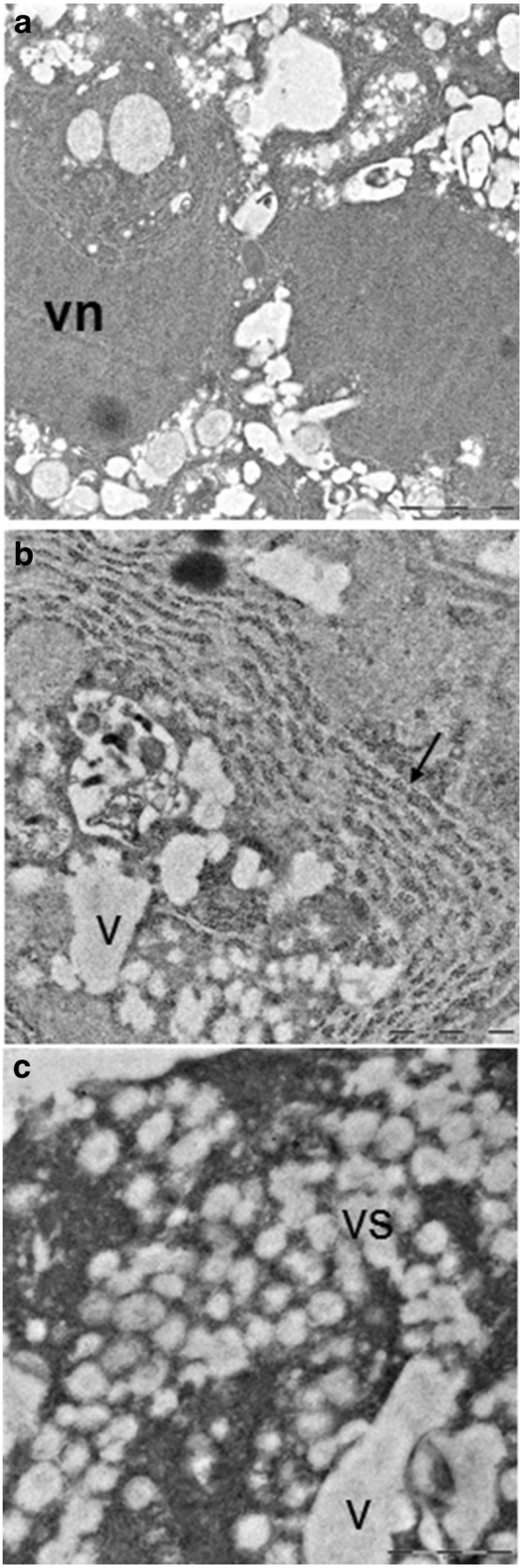

◀ **Fig. 6** Ultrastructure of the vegetative cell at anthesis. **a**: vegetative cell shows a prominent lobed nucleus and dense cytoplasm. **b**: rough ER was arranged in well-ordered thick stacks. **c**: numerous small vacuoles and cluster of vesicles were also observed. vn, vegetative cell nucleus; v, vacuole; vs, vesicles. Magnification bars—**a**, **b**, **d**: 1 μm; **c**: 2 μm

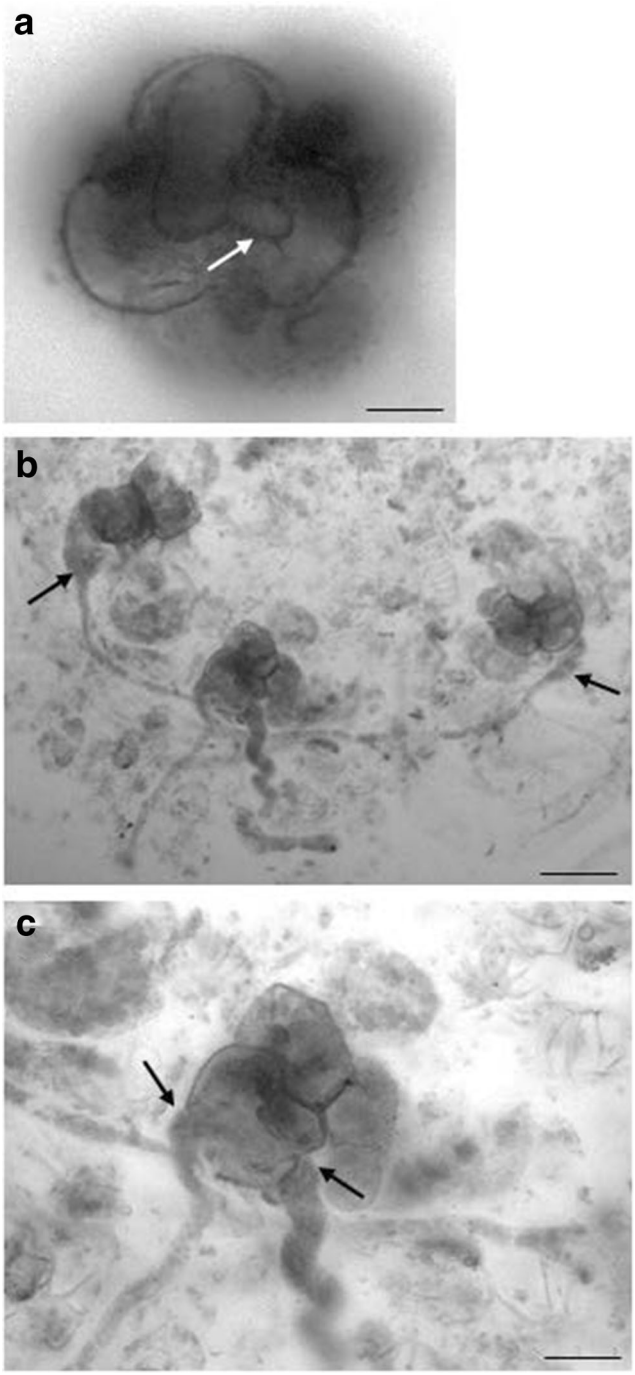

Fig. 7 Germinated pollen tube inside the open anthers. **a**, **b**, **c**: light microscopy of squashed old anthers. Pollen tube germinated by cytoplasmic protrusion (**a**, arrow). Pollen tube reached a remarkable extension (about 300 μm in length; **b**, arrows) and originated simultaneously from more pollen grains belonging to the same tetrad (**c**, arrows). Magnification bars: **a**, 15 μm; **b**, 50 μm; and **c**, 30 μm

recalcitrant plant (Gardner 1975; Franchi et al. 2002). Recalcitrant pollen is dehydration sensitive, and when dispersed, it has reduced longevity and very quick germination (Franchi et al. 2011; Pacini and Dolferus 2019). This feature is also found in different taxa and is considered an adaptation to underwater or wet environments (Brewbaker 1967; Lora et al. 2009; Franchi et al. 2011). In *Aldrovanda*, the short pollen longevity, because of the very short exposure of pollen to air together with a very short flowering time (Adamec and Tichý 1997; Okada 2008; Adamec 2018), could negatively affect fertilization. On the other hand, very rapid pollen germination could be correlated with very short flowering time, facilitating the fertilization process if the time necessary to reach a pollination target is short enough. The density of pollinating targets

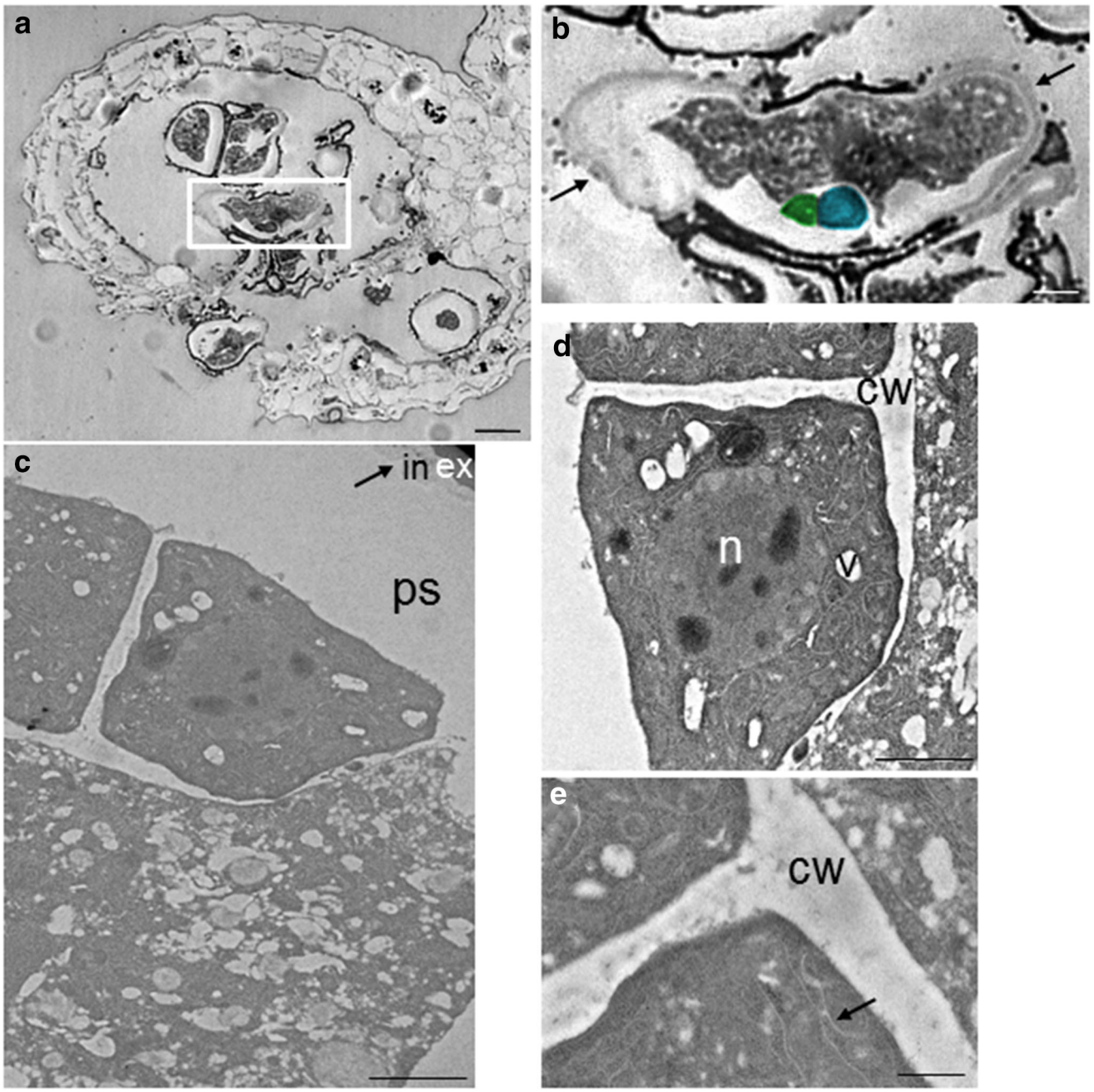

Fig. 8 *Aldrovanda vesiculosa* pollen was tricellular. **a**, **b**: light microscopy of open plasmolysed anthers. Pollen showed cytoplasmic protrusions but not pollen tubes (**b**; arrows). Magnification of pollen in the box of panel **a** showed that sperm cells (**b**; blue and green cells) were not included inside the vegetative cell. **c**, **d**, **e**: TEM analyses of sperm cells in plasmolysed pollen. Plasmolysis creates a periplasmic space between sperm cells and pollen cell wall and no cytoplasm was observed around sperms (**c**; arrow). Sperm cells were surrounded by a thin cell wall and showed a prominent nucleus with dense cytoplasm containing little vacuoles and smooth ER (**d**, **e**; arrow); ps, periplasmic space; in, intine; ex, exine; cw, cell wall; n, nucleus; v, little vacuole. Magnification bars: **a**, 25 μm; **b**, 10 μm; **c**, 3 μm; **d**, 2 μm; and **e**, 0,5 μm

in the area and the number of receptive flowers/inflorescences per plant also determine the success of pollination (Pacini and Dolferus 2019).

However, pollen longevity after dispersal strongly depends on environmental conditions and high temperature could affect hydrated/recalcitrant pollen (Pacini and Dolferus 2019). High water temperature during flowering is crucial for the floral success in *Aldrovanda* (Cross 2012; Adamec 2018); the recent climate change could thus be an important factor for reproductive success of *Aldrovanda*, at least in some parts of its distribution range. Because metabolite homeostasis is important for cell protection during pollen dehydration, further studies could also better characterize this process in *Aldrovanda*.

Aldrovanda showed an altered pattern of pollen development

In order to better understand the origin of the low reproductive success of *A. vesiculosa*, we investigated the development of male gametophyte. Pollen grains usually complete their development before anthesis and pollen presentation (Pacini and Dolferus 2019). In *Arabidopsis thaliana*, a plant with tricellular pollen, the first mitotic division of microspores starts during the tapetum degeneration, whereas the second division forming the two sperms occurs when endothecium lignification is completed and anthesis has not yet occurred (Nagpal et al. 2005; Cecchetti et al. 2008). Auxin and jasmonic acid are involved in the coordination of pollen maturation and anther dehiscence (Nagpal et al. 2005; Cecchetti et al. 2008) and several genes were identified to control pollen/anther ripening (Gómez et al. 2015).

Interestingly, in *Aldrovanda*, these later pollen maturation steps occurred after anther dehiscence. In fact, in open anthers, pollen displayed different developmental stages, from the end of mitosis I, when GC and VC formed, to germinated pollen. This suggests a delay of pollen maturation or premature anther opening. However, the presence of pollen showing GC inclusion in VC or pollen without CG inclusion in the same anther together with the presence of a differentiated endothecium layer with lignified wall thickening in closed anthers suggested that anther dehiscence occurred as expected. Moreover, because the anther dehiscence occurred immediately after the flower opening and in the opened flower, both open and closed anthers were collected; a delay in pollen developmental pattern was hypothesized.

Through microscopic analysis, we found evidence that *Aldrovanda* pollen also showed both normal and altered developmental pattern. Generally, it was reported for other plant species that during pollen development, water was stored in large vacuole and starch was accumulated, while in mature pollen, large vacuole disappeared and numerous vesicles or little vacuoles contained soluble carbohydrates derived by hydrolysis of starch in order to protect pollen from osmotic stress (Pacini et al. 2011; Firon et al. 2012; Carrizo García et al. 2017; Pacini and Dolferus 2019). In *Aldrovanda* VC, starch hydrolysis and large vacuole disappearance seemed to occur early, before the GC inclusion, suggesting a modification of water/carbohydrate pattern which could affect water homeostasis and then pollen viability.

Another modification of *Aldrovanda* pollen development related to sperm formation: In most pollen grains, the GC was included in the VC and sometimes the GC appeared lobed. As reported for the pollen grains of other species (e.g. see Cresti et al. 1979; Heslop-Harrison et al. 1988), during pollen maturation and pollen tube formation, the GC undergoes progressive changes in shape and GC microtubules play a role in cell reshaping (cf. Heslop-Harrison et al. 1988). However, the presence of two sperm cells outside the VC in several pollen grains suggested that GC was not included in the VC, and thus, the mitosis II occurs outside the VC. In this case, if pollen germinates, two sperms cannot be transmitted to the female gametophyte through the pollen tube, which could be one mechanism of fertilization failure. Overall, these data revealed a delay of pollen maturation and severe modifications of developmental patterns so that when pollen is exposed to the environment, it can be immature and not ready for the fertilization process. In this case, the availability of functional pollen is further restricted in flowers with a very short opening time as for *Aldrovanda* (Adamec and Tichý 1997; Okada 2008; Adamec 1999, 2018).

Aldrovanda pollen development in open anthers stopped during the phase of pollen tube formation and growth. It is possible that the presence of very sticky pollenkit trapped mature pollen into the anthers preventing them to reach the stigma and thus avoiding or reducing fertilization. Nevertheless, germination of pollen inside the anthers is a feature of cleistogamous species (Lord 1979; Pacini and Franchi 1982); however, numerous autogamous species also show this pollen behaviour (Pacini and Franchi 1982; Kaur et al. 2005; Sahai et al. 2016). The precocious germination may characterize recalcitrant pollen, which naturally do not undergo dehydration before anthesis and remain partially hydrated, particularly in plants living in aquatic or wet habitats (Pacini and Franchi 1982), as for the aquatic plant *Aldrovanda*. The entry of ambient water into the opened flower, indicated by the presence of algae in the loculi, might affect the hydration status of pollen and induce germination. However, precocious pollen germination inside the anthers was also observed in various *A. thaliana* mutants (Johnson and McCormick 2001; Xie et al. 2010; Wang et al. 2012), suggesting that pollen dormancy is not controlled exclusively by the dehydration level but also by genetic mechanisms. As reported in *A. thaliana*, the presence of gametes is not necessary for pollen tube growth (Glöckle et al. 2018). Similarly, it is possible to assume that also in *Aldrovanda*, pollen tube growth is independent of the correct development of the male gametophyte (Glöckle et al. 2018).

Conclusions

In *Aldrovanda*, as observed for recalcitrant pollen, transport on a compatible stigma is a prerequisite for successful fertilization, or alternatively, autogamy occurs. The reason for the high level of autogamy observed in *Aldrovanda* could be the precocious pollen germination inside the anthers. In addition, the low level of seed production observed could also be ascribed to an alteration of pollen development because in some cases, the presence of sperm cells outside the VC was observed as a consequence of lack of GC internalization. For this reason, although the *Aldrovanda* pollen tube grows, it could often be unable to deliver sperm to the embryo sac for double fertilization. Knowledge of molecular mechanisms regulating the GC internalization could help us understand the alteration in *Aldrovanda* pollen development. Unfortunately, no mutants have yet been described with this defect. The assessment of the frequency of such an alteration within and among different populations growing in different geographic areas and under different environmental conditions could shed light on the reproductive behaviour of *Aldrovanda* throughout its wide distribution range.

Acknowledgements Sincere thanks are due to Mr. Curtis Lubbe (Institute of Botany CAS, Třeboň, Czech Rep.) for English correction. Thanks are also due to two anonymous reviewers for correcting the manuscript and valuable comments.

Funding This research was partly supported by the Czech Long-term research development project No. RVO 67985939 (for LA).

Compliance with ethical standards

Conflict of interest The authors declare that they have no conflict of interest.

References

Adamec L (1995) Ecological requirements and the European distribution of the aquatic carnivorous plant *Aldrovanda vesiculosa* L. Folia Geobot Phytotax 30:53–61

Adamec L (1999) Further notes on flowering and seed set of *Aldrovanda vesiculosa*. Flytrap News (Sydney) 12(4):9–12

Adamec L (2000) Rootless aquatic plant *Aldrovanda vesiculosa*: physiological polarity, mineral nutrition, and importance of carnivory. Biol Plant 43:113–119

Adamec L (2018) Biological flora of Central Europe: *Aldrovanda vesiculosa* L. Perspect Plant Ecol Evol Syst 35:8–21

Adamec L, Tichý M (1997) Flowering of *Aldrovanda vesiculosa* in outdoor culture in the Czech Republic and isozyme variability of its European populations. Carniv Plant Newsl 26:99–103

Angold RE (1968) The formation of the generative cell in the pollen grain of *Endymion non-scriptus* (L). J Cell Sci 3:573–578

Atsuzawa K, Kanaizumi D, Ajisaka M, Kamada T, Sakamoto K, Matsushima H, Kaneko K (2020) Fine structure of *Aldrovanda vesiculosa* L.: the peculiar lifestyle of an aquatic carnivorous plant elucidated by electron microscopy using cryo-techniques. Microscopy (in press):dfaa019. https://doi.org/10.1093/jmicro/dfaa019

Blackmore S, Crane PR (1988) The systematic implications of pollen and spore ontogeny. In: Humphries CJ (ed) Ontogeny and systematics. Columbia University Press, New York, USA, pp 83–115

Brewbaker JL (1967) The distribution and phylogenetic significance of binucleate and trinucleate pollen grains in the angiosperms. Am J Bot 9:1069–1083

Carrizo García C (2002) An approach to the diversity of endothecial thickenings in Solanaceae. Flora 197:214–223

Carrizo García C, Nepi M, Pacini E (2017) It is a matter of timing: asynchrony during pollen development and its consequences on pollen performance in angiosperms—a review. Protoplasma 254: 57–73

Cecchetti V, Altamura MM, Falasca G, Costantino P, Cardarelli M (2008) Auxin regulates *Arabidopsis* anther dehiscence, pollen maturation and filament elongation. Plant Cell 20:1760–1774

Chanda S (1965) The pollen morphology of Droseraceae with special reference to taxonomy. Pollen Spores 7:509–528

Copenhaver GP (2005) A compendium of plant species producing pollen tetrads. J N Carol Acad Sci 121:17–35

Cresti M, Ciampolini F, Pacini E, Sarfatti G, Donini B (1979) Ultrastructural features of *Prunus avium* L. pollen tube in vivo. Caryologia 32:433–440

Cross A (2012) *Aldrovanda*. The waterwheel plant. Redfern Natural History Productions, Poole

Cross AT, Skates LM, Adamec L, Hammond CM, Sheridan PM, Dixon KW (2015) Population dynamics of the endangered aquatic carnivorous macrophyte *Aldrovanda vesiculosa* at a naturalised site in North America. Freshw Biol 60:1772–1783

Cross AT, Adamec L, Turner SR, Dixon KW, Merritt DJ (2016) Seed reproductive biology of the rare aquatic carnivorous plant *Aldrovanda vesiculosa* (Droseraceae). Bot J Linn Soc 180:515–529

Dawson J, Sozen E, Vizir I, Van Waeyenberge S, Wilson ZA, Mulligan BJ (1999) Characterization and genetic mapping of a mutation (ms35) which prevents anther dehiscence in *Arabidopsis thaliana* by affecting secondary wall thickening in the endothecium. New Phytol 144:213–222

De Fossard RA (1969) Development and histochemistry of the endothecium in the anthers of in vitro grown *Chenopodium rubrum* L. Bot Gaz 130:10–22

Elansary HOM, Adamec L, Štorchová H (2010) Uniformity of organellar DNA in *Aldrovanda vesiculosa*, an endangered aquatic carnivorous species, distributed across four continents. Aquat Bot 92:214–220

Eliseu SA, Dinis AM (2008) Ultrastructure and cytochemistry of *Eucalyptus globulus* (Myrtaceae) pollen grain. Grana 47:39–51

Erdtman G (1960) The acetolysis method, a revised description. Sven Bot Tidskr 54:561–564

Firon N, Nepi M, Pacini E (2012) Water status and associated processes mark critical stages in pollen development and functioning. Ann Bot 109:1201–1213

Fleischmann A, Cross AT, Gibson R, Gonella PM, Dixon KW (2018) Systematics and evolution of Droseraceae. In: Ellison AM, Adamec L (eds) Carnivorous plants: physiology, ecology, and evolution. Oxford University Press, Oxford, pp 45–57

Franchi GG, Nepi M, Dafni A, Pacini E (2002) Partially hydrated pollen: taxonomic distribution, ecological and evolutionary significance. Plant Syst Evol 234:211–227

Franchi GG, Piotto B, Nepi M, Baskin CC, Baskin JM, Pacini E (2011) Pollen and seed desiccation tolerance in relation to degree of developmental arrest, dispersal, and survival. J Exp Bot 62:5267–5281

Gardner RO (1975) A survey of the distribution of binucleate and trinucleate pollen in the New Zealand flora. New Zealand J Bot 13:361–366

Glöckle B, Urban WJ, Nagahara S, Andersen ED, Higashiyama T, Grini PE, Schnittger A (2018) Pollen differentiation as well as pollen tube

guidance and discharge are independent of the presence of gametes. Development 145:e152645
Gómez JF, Talle B, Wilson ZA (2015) Anther and pollen development: a conserved developmental pathway. J Integr Plant Biol 57:876–891
Halbritter H, Hesse M, Weber M (2012) The unique design of pollen tetrads in *Dionaea* and *Drosera*. Grana 51:148–157
Herben T, Šerá B, Klimešová J (2014) Clonal growth and sexual reproduction: tradeoffs and environmental constraints. Oikos 124:469–476
Heslop-Harrison J, Heslop-Harrison Y, Cresti M, Tiezzi A, Moscatelli A (1988) Cytoskeletal elements, cell shaping and movement in the angiosperm pollen tube. J Cell Sci 91:49–60
Johnson SA, McCormick S (2001) Pollen germinates precociously in the anthers of raring-to-go, an *Arabidopsis* gametophytic mutant. Plant Physiol 126:685–695
Kaur S, Nayyar H, Bhanwra RK, Kumar S (2005) Precocious germination of pollen grains in anthers of soybean (*Glycine max* (L.) Merr.). Soybean Genet Newsl 32:1–10
Kuprianova LA (1973) Pollen morphology within the genus *Drosera*. Grana 13:103–107
Lora J, Herrero M, Hormaza JI (2009) The coexistence of bicellular and tricellular pollen in *Annona cherimola* (Annonaceae): implications for pollen evolution. Am J Bot 96:802–808
Lora J, Herrero M, Hormaza JI (2014) Microspore development in *Annona* (Annonaceae): differences between monad and tetrad pollen. Am J Bot 101:1508–1518
Lord E (1979) The development of cleistogamous and chasmogamous flowers in *Lamium amplexicaule* (Labiatae); an example of heteroblastic inflorescence development. Bot Gaz 140:39–50
Manning JC (1996) Diversity of endothecial patterns in the angiosperms. In: D'Arcy WG, Keating RC (eds) The anther, form, function and phylogeny. Cambridge University Press, Cambridge, pp 136–158
Marquez J, Seoane-Camba JA, Suarez-Cervera M (1997) The role of the intine and cytoplasm in the activation and germination processes of Poaceae pollen grains. Grana 36:328–342
Nagpal P, Ellis CM, Weber H, Ploense SE, Barkawi LS, Guilfoyle TJ, Hagen G, Alonso JM, Cohen JD, Farmer EE, Ecker JR, Reed JW (2005) Auxin response factors ARF6 and ARF8 promote jasmonic acid production and flower maturation. Development 132:4107–4118
Okada H (2008) Pollination system of *Aldrovanda vesiculosa* (Droseraceae), a critically endangered aquatic plant in Japan. Makinoa New Ser (Kochi) 7:93–100
Pacini E, Dolferus R (2019) Pollen developmental arrest: maintaining pollen fertility in a world with a changing climate. Front Plant Sci 10:e679
Pacini E, Franchi GG (1982) Germination of pollen inside anthers in some non-cleistogamous species. Caryologia 35:205–215
Pacini E, Hesse M (2005) Pollenkitt – its composition, forms and functions. Flora 200:399–415
Pacini E, Juniper B (1984) The ultrastructure of pollen grain development in *Lycopersicum peruvianum*. Caryologia 37:21–50
Pacini E, Jacquard C, Clément C (2011) Pollen vacuoles and their significance. Planta 234:217–227
Rodondi G, Beretta M, Andreis C (2004) The genus *Drosera* L. in northern Italy: pollen morphology as a taxonomic tool. Plant Biosyst 138:157–164
Sahai K, Rawat KK, Gupta D (2016) A note on precocious pollen germination in *Woodfordia fruticosa* (L.) Kurz. Trop Plant Res 3:606–610
Sahashi N, Ikuse M (1973) Pollen morphology of *Aldrovanda vesiculosa*. J Jap Bot 48:374–379
Scott RJ, Spielman M, Dickinson HG (2004) Stamen structure and function. Plant Cell 16(Suppl 1):S46–S60
Sirová D, Adamec L, Vrba J (2003) Enzymatic activities in traps of four aquatic species of the carnivorous genus *Utricularia*. New Phytol 159:669–675
Takahashi H (1988) Ontogenetic development of pollen tetrads of *Drosera capensis* L. Bot Gaz 149:275–282
Takahashi H, Sohma K (1982) Pollen morphology of the Droseraceae and its related taxa. Sci Rep Res Inst Tohoku Univ (Biol) 38:81–156
Vega-Maray A, Fernández-González D, Valencia-Barrera R, Seoane-Camba J, Suárez-Cervera M (2003) Ultrastructural modifications in the apertural intine of *Parietaria judaica* L. (Urticaceae) pollen during the early stages of hydration. Grana 42:220–226
Wang Y, Chu YJ, Xue HW (2012) Inositol polyphosphate 5-phosphatase-controlled Ins(1,4,5)P3/Ca2+ is crucial for maintaining pollen dormancy and regulating early germination of pollen. Development 139:2221–2233
Weber HE (1995) *Aldrovanda*. In: Hegi G (ed) Illustrierte Flora von Mitteleuropa, Band IV, Teil 2A, 3. Auflage. Blackwell Wissenschafts, Berlin, pp 34–37
Whatley JM (1982) Fine structure of the endothecium and developing xylem in *Phaseolus vulgaris*. New Phytol 91:561–570
Wilson ZA, Song J, Taylor B, Yang C (2011) The final split: the regulation of anther dehiscence. J Exp Bot 62:1633–1649
Xie B, Wang X, Hong Z (2010) Precocious pollen germination in *Arabidopsis* plants with altered callose deposition during microsporogenesis. Planta 231:809–823

ACKNOWLEDGEMENTS

Sono molte le persone a cui sono grata e che vorrei ufficialmente ringraziare alla (quasi) fine di questo percorso.

In primis, la Prof.ssa Alessandra Moscatelli e la Prof.ssa Elisabetta Onelli, per essere state sempre guide e punti di riferimento importanti in questi anni, nonché modelli di dedizione e tenacia sulla, a volte ardua, strada della Ricerca. Le ringrazio anche per aver compreso (o tollerato!) il mio essere un po'naïf, facendomi sentire accolta al 2C sin dai tempi della laurea triennale.

Ringrazio inoltre la Prof.ssa Morena Casartelli per essere stata la mia tutor ufficiale negli ultimi due anni; la Prof.ssa Simona Masiero per l'entusiasmo e la curiosità stimolante con cui ha sempre accolto i miei risultati sperimentali durante i report annuali; il Prof. Marco Caccianiga per i suoi suggerimenti che ogni volta mi hanno fatto abbandonare la "visione da biologa", giusto il tempo di osservare e cercare di comprendere da un altro punto di vista, per le pazienti consulenze in statistica e per l'ironia diffusa in laboratorio.

Ringrazio il Prof. Patrick Moreau e la Prof.ssa Lilly Maneta-Peyret, del Laboratoire de Biogenèse Membranaire dell'Università Bordeux Segalen, per aver collaborato al progetto, per la sempre tempestiva analisi lipidica delle membrane e per gli spunti per l'interpretazione dei risultati. Devo ringraziare il Prof. Moreau anche per i preziosi suggerimenti ricevuti durante la fase di prima revisione della tesi.

Ringraziamenti anche alla Prof.ssa Caterina Mencarelli per l'aiuto e la paziente ed accurata revisione.

Grazie a Valeria Berno, del centro ALEMBIC (Advanced Light and Electron Microscopy BioImaging Center) per la sua gentile disponibilità e per la consulenza in microscopia confocale e analisi delle immagini.

Ringrazio il Dr. Stefano Santabarbara per averci permesso di utilizzare la strumentazione del CNR - ultracentrifuga e particle bombardment device – e per le chiacchierate d'aggiornamento in materia di fotosintesi!

Grazie a Mario e Valerio del nostro Orto Botanico, per la cura delle mie *Nicotiane* e per avermi trasformata in una perfetta coltivatrice di tabacco…e una seconda professione non può che fare comodo!

Infine ringrazio tutte quelle persone con cui ho la fortuna di condividere i "pensieri belli" e le avventure di ogni giorno. In particolare Alessandro, Anastasia, Chiara, Marina e Valentina, per l'affetto, per la presenza costante e perché mi accompagnano sempre a "riveder le stelle".